Stochastic Modeling and Simulation of Ground Motions for Performance-Based Earthquake Engineering

Sanaz Rezaeian

and

Armen Der Kiureghian

University of California, Berkeley

Stochastic Modeling and Simulation of Ground Motions for Performance-Based Earthquake Engineering

Sanaz Rezaeian

Department of Civil and Environmental Engineering
University of California, Berkeley

Armen Der Kiureghian

Department of Civil and Environmental Engineering
University of California, Berkeley

ABSTRACT

A fully nonstationary stochastic model for strong earthquake ground motion is developed. The model employs filtering of a discretized white-noise process. Nonstationarity is achieved by varying the filter properties and modulating the intensity of the process in time. Separation of the spectral and temporal nonstationary characteristics of the process allows flexibility and ease in modeling and parameter estimation. The evolving intensity and time-varying frequency content of the process are characterized by a set of statistical measures including the mean-square intensity, the mean zero-level up-crossing rate, and a measure of the bandwidth. Model parameters are identified by matching these measures with those of a target accelerogram. Post-processing of simulated ground motions by a second filter assures zero residual velocity and displacement, and improves the response spectral ordinates for long periods.

By identifying the parameters of the stochastic model for a large sample of recorded accelerograms drawn from the NGA database, predictive equations are developed that empirically relate the model parameters to a set of earthquake and site characteristics. For specified earthquake and site characteristics, sets of the model parameters are generated that are used in the stochastic model to generate an ensemble of synthetic ground motions. The resulting synthetic acceleration, as well as corresponding velocity and displacement time-histories, captures the main features of real earthquake ground motions, including the evolving intensity, duration, spectral content, natural variability, and peak values. Furthermore, the statistics of their resulting elastic response spectra, i.e., the median and logarithmic standard deviation, closely agree with the values predicted by the NGA ground motion prediction equations. The synthetic motions can be used with or in place of recorded motions in seismic design and analysis, particularly in the context of performance-based earthquake engineering.

The proposed method is extended to simulate the orthogonal horizontal components of ground motion for specified earthquake and site characteristics. This is achieved by taking advantage of the notion of principal axes directions, along which the two components are statistically independent, and by properly accounting for the correlations among the model parameters of the two components.

ACKNOWLEDGMENTS

CONTENTS

LIST OF FIGURES

x

LIST OF TABLES

1   Introduction

1.1   INTRODUCTION

In the past decade, a major advancement in earthquake engineering research and practice has been the development of the concept and tools for performance-based earthquake engineering (PBEE) (Bozorgnia and Bertero 2004). While traditional building design codes are prescriptive and assure only minimum safety and serviceability requirements, PBEE attempts to consider the entire range of seismic hazards and structural behaviors in the context of minimizing overall risk and life-cycle cost. This range includes nonlinear behavior and even collapse of structures. Development of tools for such analysis (e.g., OpenSees; see http://opensees.berkeley.edu for the software and documentation by Mazzoni et al. [2006], or nonlinear structural analysis methods presented by Filippou and Fenves in Chapter 6 of Bozorgnia and Bertero [2004]) has been the focus of much research and development during the past decade.

Two approaches are available for nonlinear dynamic analysis of structures subjected to earthquakes: (1) nonlinear response-history analysis by use of a selected set of ground motion time-histories (either recorded or synthetic) and (2) nonlinear stochastic dynamic analysis by use of a stochastic representation of the ground motion. Well-developed methods and tools are available for nonlinear response-history analysis, including the OpenSees software mentioned above. Stochastic methods are not as developed, but research in that direction is continuing (e.g., Li and Der Kiureghian [1995]; Au and Beck [2001a, 2003]; Franchin [2004]; Fujimura and Der Kiureghian [2007]; and Der Kiureghian and Fujimura [2009]).

In the current PBEE practice, the input ground motion time-histories are selected from a database of ground motions recorded during past earthquakes, which are often modified to fit desired conditions. However, for many regions of the world and for many design scenarios of interest, the database of recorded motions is sparse or lacking. As a result, in practice, one is forced to significantly alter recorded motions, e.g., scale them by factors as large as 10 or 20 or

modify their frequency contents, in order to achieve the desired intensity or frequency characteristics. These modifications have raised concern about the validity of the approach, as the modified motions may not accurately represent real earthquake ground motions. As a result of this shortcoming, there has been increasing interest in methods for generation of synthetic ground motions for specified design scenarios.

For stochastic dynamic analysis, there is need for a random process model of the earthquake ground motion. Many such models have been developed in the past (see the review in Section 1.4). However, for nonlinear stochastic dynamic analysis, it is essential that the stochastic model accurately reflects the evolving intensity and time-varying frequency content of the motion. Furthermore, the model should be of a form that facilitates nonlinear stochastic dynamic analysis. While several previously developed models provide adequate representation of the characteristics of real earthquake ground motions, for the most part they are of a form that makes their use in nonlinear stochastic dynamic analysis cumbersome. Moreover, for PBEE analysis, it is desirable to have a stochastic model that is parameterized in terms of information that is available to an engineer for a given design scenario. Such a model currently does not exist.

This study attempts to fill the above-described gaps in PBEE. Specifically, it develops a stochastic model of earthquake ground motions that possesses the characteristics of real ground motions and that is described in terms of parameters that typically define a design scenario. The model can be used to generate realistic synthetic ground motions for nonlinear response-history analysis, or can be used directly for nonlinear stochastic dynamic analysis. The specific features and uses of the model are described in the following section.

1.2   MAJOR RESULTS AND SIGNIFICANCE OF RESEARCH

In this study, a stochastic model for characterization and simulation of earthquake ground motion time-histories is developed. Three potential applications of the proposed model in research and engineering practice are (1) generation of samples of synthetic ground motion components with specified statistical characteristics defining their evolving intensities and frequency contents; (2) generation of samples of synthetic ground motion components for a given design earthquake scenario defined in terms of a set of earthquake and site characteristics that are typically

available to a practicing engineer; and (3) representation of the components of earthquake ground motion as a vector random process in a form that facilitates nonlinear stochastic dynamic analysis by existing methods. The following paragraphs elaborate on these applications of the model developed in this study.

The model developed in this study facilitates generation of synthetic earthquake ground motions with specified statistical characteristics. The specific statistical characteristics considered include the time-varying intensity of the motion as defined by the variance of the acceleration time-history, the effective duration of the motion measured between the time points at 5% and 95% of cumulative energy, and the evolving predominant frequency and bandwidth of the motion. These characteristics are key features of earthquake ground motions that are known to have significant influences on structural response, particularly in the nonlinear range, and on determination of damage induced by earthquakes. By generating synthetic motions with specified statistical characteristics and estimating the corresponding structural response, various parametric studies that investigate the effects of ground motion characteristics on structural response may be conducted. Furthermore, studies that determine the statistics of structural response to earthquake ground motions with specified statistical characteristics may be of interest. This is useful, for example, in the construction of structural fragility models, which defines the conditional probability of exceeding a given limit state as a function of a measure of the ground motion intensity. Another possibility is to generate synthetic motions with statistical characteristics similar to those of a recorded motion. One may view a recorded ground motion as one sample observation of all the possible ground motions with the specified statistical characteristics. An ensemble of ground motions consisting of a recorded motion and samples of synthetic motions with similar statistical characteristics may be used to determine the statistics of structural response to the ground motion process.

The main advancement of the present study is to provide the capability to generate a suite of synthetic ground motion components for a future seismic event with specified earthquake and site characteristics, i.e., for a specified design scenario. The earthquake and site characteristics considered are the type of faulting, the earthquake magnitude, the source-to-site distance, and the shear-wave velocity of the local soil at the site. Most importantly, the variability exhibited by the suite of synthetic ground motions for the given set of earthquake and site characteristics is consistent with the variability observed in recorded ground motions for the same design scenario.

3

This consistency is essential for accurate estimation of the statistics of structural response and damage in the context of PBEE analysis. This capability is particularly useful for predicting future seismic loading in regions where recorded ground motions are lacking, as there is no need for previously recorded motions for generating the synthetics. This independence from recorded ground motions is achieved by developing predictive equations for the parameters of the stochastic ground motion model in terms of the earthquake and site characteristics. The predictive equations are developed empirically using a large data set of recorded earthquake ground motions taken from the widely used PEER NGA (Pacific Earthquake Engineering Research Center, Next Generation Attenuation of Ground Motions Project; see http://peer.berkeley.edu/smcat/) database.

The model proposed in this study facilitates nonlinear stochastic dynamic analysis by several existing methods. Stochastic dynamic analysis provides the means for probabilistic assessment of seismic demand on structures when the input excitation is defined as a stochastic process. This type of analysis allows determination of various statistics of the structural response, such as the probability distributions of peak values, level-crossings, or the first-passage probability. Since failure usually occurs in the nonlinear range of structural behavior, nonlinear stochastic dynamic analysis methods are of particular interest in assessing the safety of structures and in PBEE. Recently, Fujimura and Der Kiureghian (2007) have developed a new method for nonlinear stochastic dynamic analysis, known as the Tail-Equivalent Linearization Method (TELM), that is computationally more efficient than a Monte Carlo simulation method and provides superior accuracy compared to the conventional equivalent linearization method. In a more recent paper, Der Kiureghian and Fujimura (2009) have demonstrated the utility of TELM for PBEE analysis. An essential step in TELM is discrete representation of the input excitation in terms of a set of standard normal random variables. The stochastic ground motion model proposed in this study has a form that satisfies this requirement so that it can be used in conjunction with TELM for nonlinear stochastic dynamic analysis. Of course the model can also be used with a number of other methods for nonlinear stochastic dynamic analysis as described, e.g., in Lutes and Sarkani (2004).

The following section discusses the current practice in seismic load prediction and the role of the present study in advancing the field and in overcoming some of the shortcomings and challenges of the existing methods.

1.3 CURRENT PRACTICE OF SEISMIC LOAD PREDICTION

One of the major obstacles in seismic assessment of structures is identification of future seismic loading. Problems arise from the limited number of previously recorded ground motions and the lack of such recordings for many earthquake scenarios and site locations. The problem of predicting appropriate ground motions for future seismic events is currently receiving a great deal of attention. Extensive research is being conducted on developing and evaluating ground motion prediction equations (GMPEs), also known as attenuation models, and on developing and evaluating methods for selecting and scaling (in both time and frequency domains) previously recorded ground motions. A recent study by Douglas and Aochi (2008) provides a survey of techniques for predicting earthquake ground motions for engineering purposes.

Existing GMPEs (attenuation models), e.g., Campbell and Bozorgnia (2008), Abrahamson and Silva (2008), Boore and Atkinson (2008), Chiou and Youngs (2008), and Idriss (2008), are designed to predict measures of ground motion intensity for specified earthquake and site characteristics. Typical measures considered are peak ground motion values (i.e., peak ground acceleration, velocity, and displacement) and elastic response spectra as functions of the oscillator period and damping. More recently, GMPEs for inelastic response spectra have also been developed (Bozorgnia et al. 2010). These GMPEs are useful for linear response-spectrum analysis or crude nonlinear analysis, but not for response-history analysis, as they do not predict ground motion time-histories. Such simplified analysis methods have proven to be adequate for code-based design purposes. However, they are not adequate for PBEE analysis, which aims at accurately predicting structural behavior in grossly nonlinear domains and even collapse. With increasing computing power and the advent of nonlinear response-history dynamic analysis tools for PBEE, such as OpenSees, the need for predicting ground motion time-histories for specified design scenarios has become urgent. This issue is addressed in the present study. In this sense, the present study complements GMPEs by providing models for predicting ground motion time histories for specified design scenarios.

In the current PBEE practice, real recorded ground motions are used to perform response-history dynamic analysis. Ground motion properties vastly vary for different earthquake and site characteristics, but recorded motions are not available for all types of earthquakes and in all regions. Due to scarcity of recorded motions, engineers are often forced to select records from

locations other than the project site and modify them by scaling or spectrum matching methods, see, e.g., Watson-Lamprey (2007), Bommer and Acevedo (2004), Hancock et al. (2006). These methods are often controversial as, without careful processing, they may easily render motions with unrealistic characteristics. On the other hand, because nonlinear structural response is sensitive to the characteristics of the seismic loading, care should be taken in realistic representation of the ground motion. To avoid selection of ground motions from inappropriate locations, with unreasonable scaling and spectrum matching, an alternative approach is to use synthetic motions with or in lieu of recorded motions. The trick, of course, is to make sure that these motions have characteristics that are representative of real earthquake ground motions. The present study develops a method for generating synthetic ground motions, which incorporate realistic representation of those features of the ground motion that are known to be important to the structural response. The proposed method is ideal for use in practice, since it is computationally straightforward and it requires information only on earthquake and site characteristics, which are readily available to the practicing engineer.

1.4   EXISTING MODELS OF EARTHQUAKE GROUND MOTION

There are two main categories of models for generating synthetic ground motions: models that describe the occurrence of fault ruptures at the source and propagation of the resulting seismic waves through the ground medium, and models that describe the ground motion for a specific site by fitting to a recorded motion with known earthquake and site characteristics. We refer to the first category as "source-based" models and to the second category as "site-based" models. Source-based models can produce realistic accelerograms at low frequencies (typically <1 Hz), but often need to be adjusted for high frequencies by combining with a stochastic or empirical component, resulting in "hybrid" models (Douglas and Aochi 2008). An early review of source-based models is presented by Zerva (1988). In general, these models tend to heavily employ seismological principles to describe the source mechanism and wave travel path, and as pointed out by Stafford et al. (2009), they depend on physical parameters that vary significantly from region to region. This limits their use in regions where seismological data are lacking — exactly in places where there is an increased need for generation of synthetic ground motions. In the current practice, most engineers prefer using methods of scaling and spectrum matching of

recorded motions instead of incorporating source-based models. This is partly due to lack of understanding the seismological principles underlying these models, and that the models require a thorough knowledge of the source, wave path, and site characteristics, which typically are not available to a design engineer. In this study, we focus on developing a site-based stochastic model, which has advantages over existing models of this type, as described below. Furthermore, with the aim of developing a method that uses information readily available to the practicing engineer, the model parameters are directly related to the earthquake and site characteristics that define a design scenario.

A large number of site-based stochastic ground motion models have been developed in the past. Formal reviews are presented by Liu (1970), Ahmadi (1979), Shinozuka and Deodatis (1988), and Kozin (1988). The paper by Conte and Peng (1997) presents a brief but comprehensive review of more recent work. To categorize the existing site-based stochastic models and to develop a model that overcomes their disadvantages, the following criteria are recognized. A good stochastic ground motion model must represent both the temporal and the spectral nonstationary characteristics of the motion. Temporal nonstationarity refers to the variation in the intensity of the ground motion over time, while spectral nonstationarity refers to the variation in the frequency content of the motion over time. Whereas temporal nonstationarity can be easily modeled by time-modulating a stationary process, spectral nonstationarity is not as easy to model. Nevertheless, this spectral nonstationarity is of particular importance in nonlinear response analysis because of the moving resonant effect (Papadimitriou 1990) of nonlinear structures and cannot be ignored. In addition, for a stochastic model to be of practical use in earthquake engineering, it should be parsimonious, i.e., it must have as few parameters as possible. Preferably, the model parameters should provide physical insight into the characteristics of the motion. Furthermore, the model should refrain from complicated analysis, involving extensive processing of recorded motions for parameter identification.

Existing site-based stochastic ground motion models can be classified into four categories: (1) Processes obtained by passing a white noise through a filter, e.g., Bolotin (1960), Shinozuka and Sato (1967), Amin and Ang (1968), Iyengar and Iyengar (1969), Ruiz and Penzien (1971), with subsequent modulation in time to achieve temporal nonstationarity. These processes have essentially time-invariant frequency content. (2) Processes obtained by passing a train of Poisson pulses through a linear filter, e.g., Cornell (1960), Lin (1965). Through

modulation in time, these processes can possess both temporal and spectral nonstationarity (Lin, 1986). However, matching with recorded ground motions is difficult. (3) Auto-regressive moving average (ARMA) models, e.g., Jurkevics and Ulrych (1978), Hoshiya and Hasgur (1978), Polhemus and Cakmak (1981), Kozin (1988), Chang et al. (1982), Conte et al. (1992), Mobarakeh et al. (2002). By allowing the model parameters to vary with time, these models can have both temporal and spectral nonstationarity. However, it is difficult to relate the model parameters to any physical aspects of the ground motion. (4) Various forms of spectral representation, e.g., Saragoni and Hart (1974), Der Kiureghian and Crempien (1989), Conte and Peng (1997), Wen and Gu (2004). The focus in these models is in developing a time-varying spectral representation by matching to a target recorded ground motion. These models require extensive processing of the target motion. Virtually all these models assume the ground motion to be a zero-mean Gaussian process.

With the goal to achieve efficiency and convenience in modeling and simulation, similar to the models of the first category, the stochastic ground motion model developed in this study is based on a modulated filtered white-noise process. However, unlike previous models, the filter used in this study has time-varying properties, adjusted to capture the time-varying predominant frequency and bandwidth of a target accelerogram, thus allowing variation of the spectral content with time. Temporal nonstationarity is achieved by modulation in time, as is done in most previous studies.

Two previous models are particularly relevant to the present study. One is the model by Yeh and Wen (1990), which is also a filtered white-noise process. They use a time-invariant filter; however, to achieve spectral nonstationarity, they modify the time scale through a nonlinear transformation. The model parameters are identified by matching the cumulative energy and zero-level up-crossings of the target motion. This approach for parameter identification is also used in the present work. The second is a model developed by Papadimitriou (1990), which is based on a second-order differential equation with time-varying properties and subjected to a modulated white-noise process (essentially a filtered white-noise process). Papadimitriou derives approximate expressions for the second-moment statistics of the process under conditions of slowly varying coefficients and wide bandwidth. This model can be seen as a special case of the model presented in this study (the filter in the present formulation can be more general). However, in the present work no approximations are made (other than

8

presenting the model in a discrete form) in deriving the model statistics, and no assumptions are made regarding the rate of change of the filter parameters or the bandwidth. Furthermore, the approaches to parameterization and fitting of the model are entirely different. In particular, the present model has the important advantage that the temporal and spectral nonstationary characteristics are completely decoupled, thus facilitating modeling and parameter identification.

In general, site-based stochastic ground motion models fail to match the response spectrum associated with the target accelerogram in the long-period range, typically beyond 2 to 4 s, e.g., see the review by Douglas and Aochi (2008). This is because a stochastic model developed for an acceleration process cannot guarantee zero velocity and displacement residuals (final values at the end of the record) upon integration of a sample realization. The model proposed in this study is no exception because it yields motions with non-zero velocity and displacement residuals and hence overestimates the response spectrum of a target motion at long-period ranges. This shortcoming of site-based models has also been recognized by Papadimitriou (1990) and by Liao and Zerva (2006), who have extended baseline correction methods used for recorded accelerograms to simulated motions. Following a similar approach, we post-process the ground motion obtained from our stochastic model by high-pass filtering through a critically damped oscillator. In this way, we obtain zero velocity and displacement residuals and appropriate response spectrum values for periods as long as 5 to 10 s.

Most existing site-based stochastic models limit their scope to generating synthetic motions similar to a target recorded ground motion and make no attempt in selecting an appropriate set of model parameters for a specified earthquake and site of interest. One of the few works that has addressed this issue is by Sabetta and Pugliese (1996). They relate their model parameters to the earthquake magnitude, source-to-site distance, and soil conditions, using empirical data from the Italian strong-motion database. They simulate nonstationary accelerograms by summation of Fourier series with random phases and time-dependent coefficients. The major shortcoming of their model is that the only source of variability considered is that inherent in the random phases. As a result, their model underestimates the variability inherent in real ground motions for specified earthquake and site characteristics. A more recent study by Stafford et al. (2009) also addresses the issue of developing relations between the model parameters and the earthquake and site characteristics, using the PEER NGA strong-motion database. However, this study models only the temporal nonstationarity of the

ground motion and is not suitable for nonlinear analysis in its current form. One of the novel aspects of our approach is that we relate the parameters of our model to earthquake and site characteristics. Furthermore, by accounting for the uncertainty in the model parameters, we capture the natural variability of real ground motions in the synthetics. This variability is explained in more detail below.

A major problem with the current practice of seismic hazard analysis and generation of synthetic ground motions is related to underestimation of the ground motion variability. Abrahamson et al. (1990) divided the uncertainty in numerical simulation procedures into two categories: (1) modeling plus random uncertainty and (2) parametric uncertainty. Parametric uncertainty, which refers to the uncertainty in source parameters of future earthquakes, is often ignored in source-based models, causing underestimation of the total variability in the synthetic ground motions. Even though the focus of Abrahamson et al. is on source-based models, the same problem applies to site-based models, which, as pointed out by Douglas and Aochi (2008), "can underestimate the true ground motion variability." This underestimation is mainly due to neglecting the uncertainty in the parameters of the stochastic model. Exceptions are the work by Pousse et al. (2006), in which the parameters of an improved version of the model by Sabetta and Pugliese (1996) are fitted to the K-Net Japanese database, and the work by Alamilla et al. (2001), in which the parameters of a model similar to that proposed by Yeh and Wen (1989) are fitted to a database of ground motions corresponding to the subduction zone lying along the southern coast of Mexico. In these cases, the model parameters are randomized to achieve the variability. It is noted that several recent seismological source-based models properly account for the variability in ground motions. Typically, this is done by varying the source parameters, as in Liu et al. (2006), Hutchings et al. (2007), Causse et al. (2008) and Ameri et al. (2009). In the present study, parametric uncertainty is accounted for by random generation of the model parameters from probability distributions conditioned on earthquake and site characteristics. Therefore, we are able to reproduce in the synthetics the variability present in real ground motions, which has been lacking in a majority of previous models.

For proper dynamic analysis of complex structural systems, it is necessary to consider the ground motion at a site in three orthogonal directions. The vast majority of previous site-based models are restricted to single-component motions. In some studies, two horizontal components have been developed independently, using the same set of model parameters (e.g., Yeh and Wen

10

[1989]). In the present study, the stochastic ground motion model is developed for two horizontal components of the ground motion, properly accounting for the cross-correlations between the model parameters that control the intensities and the frequency contents of the two components. Although not considered, the proposed model can also be extended to the vertical component of the ground motion following the same techniques that are used for the horizontal components. To our knowledge, this is the first multi-component stochastic ground motion model for specified earthquake and site characteristics that properly accounts for the statistical characteristics of the component processes.

Finally, comparisons against empirical data and trusted models in engineering practice provide a means for model validation and aid in identifying the limitations of the proposed model. Additionally, such comparisons may encourage implementation of the proposed model in engineering practice. One validation approach used in the present study is through comparing the statistics of synthetic elastic response spectra with their corresponding values predicted by the recently developed and widely used Next Generation Attenuation (NGA) models (Abrahamson et al. 2008). Similar comparison is performed by Frankel (2009), where a seismological physics-based model is employed to generate synthetic ground motions and comparisons with NGA models are conducted in terms of elastic response spectra. Because NGA models are based on empirical data, this type of comparison indirectly validates synthetic ground motions against real ground motions.

1.5   OBJECTIVES AND SCOPE OF THE STUDY

The research described in this study has two main objectives: (1) developing a stochastic model for strong ground motions, (2) generating synthetic ground motions for specified earthquake and site characteristics.

The first half of this report focuses on developing a fully nonstationary stochastic ground motion model that is based on a modulated filtered white-noise process with time-varying parameters. Compared to the existing models, the proposed model has the following advantages: (a) the temporal and spectral nonstationary characteristics are completely decoupled, facilitating identification and interpretation of the model parameters; (b) the model has a small number of parameters with physical interpretations; (c) there is no need for complicated analysis, such as

11

Fourier analysis or estimation of evolutionary power spectral density, to process the target accelerogram for identifying the model parameters; (d) simulation of a synthetic ground motion for specified model parameters is simple and requires little more than generation of standard normal random variables; (e) the long-period content of the motion is corrected by high-pass filtering to achieve zero velocity and displacement residuals and avoid overestimation of response spectral values at long periods; (f) the model and simulation method are developed for two horizontal components of the ground motion and can easily be extended to include the vertical component; (g) the model facilitates nonlinear random vibration analysis by TELM. Innovative and efficient parameter identification methods are developed to fit the stochastic model to a target accelerogram. Examples of simulated motions having statistical characteristics similar to target recorded accelerograms are presented.

The second half of this report employs the proposed stochastic ground motion model to develop and validate a method for generating an ensemble of synthetic ground motion time-histories for specified earthquake and site characteristics. This is achieved by fitting the stochastic model to a database of strong-motion records. Identification of the model parameters for many recorded motions allows development of predictive relations that empirically relate the model parameters to a selected set of earthquake and site characteristics. These predictive relations facilitate random generation of the model parameters, which is the key to realistically representing the natural variability of ground motions, for a given set of earthquake and site characteristics. The predictive models are validated by comparing the statistics of the elastic response spectra of synthetic ground motions with predicted statistics generated from the NGA database. The stochastic model and the simulation method are then extended to generation of two horizontal components of ground motion by proper accounting of the cross-correlations between the model parameters.

The database of ground motions employed in this study is a subset of the widely used PEER NGA strong-motion database. At their present form, the results are applicable to shallow crustal earthquakes in active tectonic regions such as the Western United States, to moment magnitudes greater than 6.0, to source-to-site distances of at least 10 km, and to sites with shear-wave velocity exceeding 600 m/s.

This research helps advance the practice of PBEE by providing a means for generation of realistic synthetic ground motions for specified earthquake and site characteristics, which can be

used in lieu of or in conjunction with recorded motions, when the latter are lacking or nonexistent for specified design scenarios.

1.6 ORGANIZATION OF REPORT

This report is organized into eight chapters. The first objective as described in the previous section is addressed in Chapters 2 and 3, where a stochastic model for synthetic ground motions is derived and a method for parameter identification by fitting to a target recorded motion is developed. The second objective is addressed in Chapters 4 through 6, where a method for generating synthetic ground motions for specified earthquake and site characteristics is proposed and validated. In Chapter 7, the stochastic model and simulation method are extended to generate bi-directional ground motions. More details on the specific subjects covered in each chapter are presented below.

Chapter 2 describes the development of a new site-based stochastic ground motion model. It begins with a modified formulation of the filtered white-noise process, which through a normalization decouples the temporal and spectral characteristics of the process. The model is then extended by allowing the filter parameters to vary with time, while maintaining complete separation of the time-varying temporal and spectral characteristics. A discrete representation of the process is then developed, whereby the process is defined as the summation of standard normal random variables with time-varying coefficients. This form is of particular interest for nonlinear random vibration analysis by TELM (Fujimura and Der Kiureghian 2007). This is followed by parameterization of the model and high-pass filtering to assure zero residual velocity and displacement. This chapter results in a stochastic model that captures the important characteristics of strong earthquake ground motions, while maintaining a mathematical form that is appropriate and efficient for modeling, digital simulation, and for use in nonlinear random vibration analysis.

Chapter 3 develops a parameter identification method by fitting the statistical characteristics of the stochastic model to those of a target accelerogram. It also describes in detail the simulation procedure for generating synthetic ground motions once the model parameters are specified. By fitting the evolutionary statistical characteristics of the stochastic model proposed in Chapter 2 to those of a recorded motion, the model parameters are identified and synthetic

13

ground motions with characteristics similar to the recorded accelerogram are generated. Several examples of recorded ground motions, their identified parameters, and corresponding synthetic motions are presented. A condensed version of the materials in Chapters 2 and 3 has appeared in the journal publication Rezaeian and Der Kiureghian (2008).

Chapter 4 begins the discussion on simulating synthetic motions for specified earthquake and site characteristics. In this chapter, the model proposed in Chapter 2 is fitted to a database of recorded ground motions by using a simplified version of the methods proposed in Chapter 3. The database of strong ground motions is created by selecting recordings from a larger PEER NGA database. Fitting the model to the records of this database provides a data set of model parameters versus variables describing the selected set of earthquake and site characteristics. Statistical data analysis is then performed to develop predictive equations for the model parameters in terms of the earthquake and site characteristic variables. The details and the results of the data analysis, such as distribution fitting for each model parameter, regression analysis, and correlation analysis are presented. The results in this chapter allow prediction of the stochastic model parameters without a need for recorded accelerograms.

Chapter 5 employs the results of Chapter 4 to generate an ensemble of synthetic ground motions for specified earthquake and site characteristics. A method for random simulation of stochastic model parameters is presented that accounts for the cross-correlations between the parameters. Then the methods of Chapter 3 are used to generate synthetic ground motions for the simulated model parameters. Methods for conditional simulation of ground motions, where one or more of the model parameters (e.g., those defining the intensity or duration of the motion) are prescribed, are also developed. In simulation, the natural variability of real ground motions is preserved. Examples are presented and applications of the proposed method in PBEE are discussed.

In Chapter 6, the proposed method of generating synthetic ground motions for specified earthquake and site characteristics is validated through examination of elastic response spectra. Elastic response spectra of simulated motions are compared against real recorded motions. Furthermore, the statistics of elastic response spectra of simulated motions at given periods are compared with those predicted by the NGA models. The methods incorporated in this chapter allow quantitative comparison between the variability among synthetic and real ground motions. It is concluded that, in general, the median and variability of the response spectra of simulated

14

motions agree with those predicted by the NGA models. A condensed version of the materials in Chapters 4, 5, and 6 has appeared in a journal publication by Rezaeian and Der Kiureghian (2010).

Chapter 7 presents a method for simulating the orthogonal horizontal components of ground motion with correlated parameters for specified earthquake and site characteristics. The stochastic model parameters are identified for a database of recorded horizontal ground motion pairs that are rotated to their principal axes, along which the two components are statistically independent. New predictive equations are developed for the stochastic model parameters in terms of earthquake and site characteristics, and correlation coefficients between model parameters of the two components are estimated empirically. An extension of the simulation method proposed in Chapters 4 and 5 is then utilized to generate pairs of synthetic ground motion components along the principal axes.

Finally, Chapter 8 provides a summary of the main results and conclusions of the study. Recommendations for future studies are presented.

2 Stochastic Model of Earthquake Ground Motion

2.1 INTRODUCTION

For many years, stochastic processes have been used to model earthquake ground motions. One class of stochastic process models for earthquake ground motion is based on the interpretation of ground acceleration as a filtered white-noise process, i.e., a process obtained by passing a white-noise process through a filter. Due to efficient digital simulation of sample functions for a filtered white-noise process, this class of models is appealing when it comes to simulating earthquake ground motions. One of the earliest efforts in this area is the work done by Tajimi (1959). His model does not account for the nonstationarity that is present in earthquake ground motions. Other early representative works that have employed the filtered white-noise model with alternative filters and subsequent modulation in time to achieve temporal nonstationarity include Bolotin (1960), Shinozuka and Sato (1967), Amin and Ang (1968), Iyengar and Iyengar (1969), and Ruiz and Penzien (1971). Unlike real ground motions, these models have essentially time-invariant frequency content. As a result, other types of stochastic models such as those based on filtered Poisson processes (e.g., Cornell [1960]; Lin [1965]), auto-regressive moving average models (e.g., Jurkevics and Ulrych [1978]; Hoshiya and Hasgur [1978]; Polhemus and Cakmak [1981]; Kozin [1988]; Chang et al. [1982]; Conte et al. [1992]; Mobarakeh et al. [2002]); and various forms of spectral representations (e.g., Saragoni and Hart [1974]; Der Kiureghian and Crempien [1989]; Conte and Peng [1997]; Wen and Gu [2004]) became popular for modeling earthquake ground motions. These models are in general difficult to match with recorded ground motions and complicated to simulate. This chapter introduces a new formulation of the filtered white-noise process for modeling earthquake ground motions. While this model takes advantage of the efficiency of the filtered white-noise process in modeling and simulation, it adequately represents the nonstationary characteristics of real earthquake ground

motions both in time and frequency domains. Hence, we refer to it as a fully nonstationary stochastic model.

We start by developing a new formulation of the filtered white-noise process. Temporal and spectral nonstationarities are achieved through modulation in time and by varying the filter parameters over time. Through a normalization, the temporal and spectral characteristics of the process are completely separated, which greatly simplifies the modeling procedure. A discrete representation of the process, defined as the summation of standard normal random variables with time-varying coefficients, is then presented. This form is of particular interest for digital simulation and for nonlinear random vibration analysis. This is followed by interpreting the characteristics of real ground motions (e.g., evolutionary intensity and time-varying frequency content) as the statistical characteristics of a stochastic process (e.g., mean-square intensity, mean zero-level up-crossing rate, and bandwidth of the process). The model is then parameterized such that a few parameters control the main statistical characteristics of the ground motion. Finally, the last section describes a post-processing procedure that is required in order to assure zero residuals in the velocity and displacement time-histories. This post-processing corrects the long-period content of the resulting response spectrum, which has been overestimated by most stochastic ground motion models in the past.

The main goal of this chapter is to develop a stochastic model that captures important characteristics of strong earthquake ground motions while ensuring a mathematical form that is adequate and efficient for modeling, digital simulation, and for use in nonlinear random vibration analysis.

2.2   FORMULATION OF THE MODEL

Earthquake ground motions have nonstationary characteristics both in the time and the frequency domains. The temporal nonstationarity (nonstationarity in the time domain) refers to the variation of the intensity of the ground motion in time. The spectral nonstationarity (nonstationarity in the frequency domain) refers to the variation of the frequency content of the motion in time. It is important to accurately model both these nonstationarities when simulating ground motions. A fully nonstationary filtered white-noise process can properly represent both the temporal and spectral nonstationary characteristics of earthquake ground motions. This

18

process is obtained by time-modulating a filtered white-noise process with the filter having time-varying parameters. Whereas time-modulation provides the temporal nonstationarity, variation of filter parameters over time achieves the spectral nonstationarity.

2.2.1 Filtered White-Noise Process

White noise refers to a stationary random process that has a zero mean and a constant spectral density for all frequencies. The word *white* refers to the equal distribution of power among all the frequencies and comes from an analogy with white light, which is known to have equal contributions from all visible frequency components. Let $w(t)$ represent a white-noise process in the time domain with power spectral density (PSD) function $S_{ww}(\omega) = S$, where ω is the angular frequency and ranges from $-\infty$ to ∞. This process has an infinite variance (sometimes referred to as the total power), $\sigma_w^2 = \int_{-\infty}^{\infty} S_{ww}(\omega)d\omega = \infty$, and hence is purely theoretical. Even though the white-noise process is not a physically meaningful entity by itself, it can be used to approximate meaningful processes in real-world situations. One example is the use of a filtered white-noise process to model earthquake ground acceleration.

The conventional *filtered white-noise process* is the stationary response of a linear time-invariant filter subjected to a white-noise excitation. The response of a linear filter may be calculated by using the Duhamel convolution integral. Hence, the filtered white-noise process is formulated as

$$f(t) = \int_{-\infty}^{t} h(t - \tau, \boldsymbol{\lambda})\, w(\tau) d\tau \tag{2.1}$$

where $h(t, \boldsymbol{\lambda})$ denotes the impulse response function (IRF)[1] of the linear filter, with $\boldsymbol{\lambda}$ representing a set of parameters used to "shape" the filter response. Specifically, $\boldsymbol{\lambda}$ may include the natural frequency and damping of the filter, which control the predominant frequency and bandwidth of the resulting process. We assume the filter is causal so that $h(t, \boldsymbol{\lambda}) = 0$ for $t < 0$, and that it is stable so that $\int_{0}^{\infty} h(t, \boldsymbol{\lambda})dt < \infty$, which also implies $\lim_{t\to\infty} h(t, \boldsymbol{\lambda}) = 0$. We also assume $h(t, \boldsymbol{\lambda})$ is at least once differentiable for all t. Note that this requires $h(t, \boldsymbol{\lambda})$ to start from zero at $t = 0$ and not have any discontinuities. (The reason for this requirement will become

---

[1] IRF is the response of a linear system (i.e., the filter) to a unit impulsive excitation with zero initial conditions. It uniquely characterizes a linear system for a specified input-output pair (see Figure 2.1a).

evident in Section 2.3.) More details on the choice of the linear filter are presented in Section 2.4.2. As previously mentioned, $w(t)$ represents a white-noise process, which is the input excitation to the linear filter. The white-noise process and, therefore, the filter response are assumed to be Gaussian. Figure 2.1 schematically shows the input-output pairs for a linear filter.

The standard deviation of the filtered white-noise process in (2.1) is represented by σ_f. Since the response of a stable filter to a white-noise excitation becomes stationary after sufficient time, and since the white-noise process is assumed to have started in the infinite past (the lower limit of the integral is $-\infty$), the filter response at any finite time point is stationary and, therefore, σ_f is a constant and is given by

$$\sigma_f^2 = 2\pi S \int_{-\infty}^{t} h^2(t - \tau, \boldsymbol{\lambda}) \mathrm{d}\tau \qquad (2.2)$$

where S is the constant PSD, commonly referred to as the intensity of the white-noise process.

A filtered white-noise process may be physically interpreted as a seismic ground motion process by virtue of the superposition principle of the Duhamel integral. The white-noise may be regarded as a train of random pulses (as explained later in Section 2.2.4) that represent intermittent ruptures at the source of generation of the earthquake (i.e., the fault). The filter may represent the medium through which seismic waves travel with the characteristics of the filter controlling the frequency content and bandwidth of the process. The sketch in Figure 2.2 demonstrates this concept.

Unlike real seismic ground motions, the filtered white-noise process defined by (2.1) lacks nonstationarity in both the time and frequency domains. In subsequent sections, this stochastic model is modified in ways to accommodate for this shortcoming. In particular, the filtered white-noise process will be multiplied by a deterministic time modulating function to achieve temporal nonstationarity; furthermore, a linear filter with time-varying parameters is used to achieve spectral nonstationarity.

2.2.2   Modulated Filtered White-Noise Process: Achieving Temporal Nonstationarity

After normalization by its standard deviation, the filtered white-noise process in (2.1) is time-modulated to obtain temporal nonstationarity. The resulting process is called a *modulated filtered*

white-noise process. When representing earthquake ground motions, the modulation over time represents the evolution of the ground motion intensity in time.

The modulated filtered Gaussian white-noise process is formulated as

$$x(t) = q(t, \boldsymbol{\alpha}) \left[\frac{1}{\sigma_f} \int_{-\infty}^{t} h(t - \tau, \boldsymbol{\lambda}) \, w(\tau) \mathrm{d}\tau \right] \tag{2.3}$$

where $q(t, \boldsymbol{\alpha})$ is the deterministic, non-negative modulating function with $\boldsymbol{\alpha}$ denoting a set of parameters used to control the shape and intensity of the function. Due to the normalization by σ_f, the process inside the square brackets in (2.3) has unit variance. As a result, the function $q(t, \boldsymbol{\alpha})$ defines the standard deviation of the process $x(t)$, i.e.,

$$\sigma_x(t) = q(t, \boldsymbol{\alpha}) \tag{2.4}$$

Thus, the function $q(t, \boldsymbol{\alpha})$ completely defines the temporal nonstationarity of the process. Figure 2.3 represents a typical realization of the stationary process inside the square brackets in (2.3), and Figure 2.4 represents the same process modulated over time.

The disadvantage of the modulated filtered white-noise process defined by (2.3) is that it lacks spectral nonstationarity. (Note the time-invariant frequency content of the process in Fig. 2.4.) This causes the frequency content of the process, as represented by the instantaneous power spectral density, to have a time-invariant shape that is scaled in time uniformly over all frequencies according to the variance of the process, $q^2(t, \boldsymbol{\alpha})$. For this reason, this class of processes is known as uniformly modulated.

2.2.3   Modulated Filtered White-Noise Process with Spectral Nonstationarity

As mentioned earlier, earthquake ground motions have nonstationary characteristics in both the time and frequency domains. The temporal nonstationarity arises from the transient nature of the earthquake event. The intensity of a typical strong ground motion gradually increases from zero to achieve a nearly constant intensity during a "strong shaking" phase, and then gradually decays to zero with a total duration of about 10-60 seconds. This temporal nonstationarity is achieved by multiplying the stochastic process with a deterministic function that varies over time as done in Section 2.2.2.

The spectral nonstationarity of the ground motion arises from the evolving nature of the seismic waves arriving at a site. Typically, high-frequency (short wavelength) P waves tend to

dominate the initial few seconds of the motion. These are followed by moderate-frequency (moderate wavelength) S waves, which tend to dominate the strong-motion phase of the ground motion. Towards the end of the shaking, the ground motion is dominated by low-frequency (long wavelength) surface waves. The complete ground motion is an evolving mixture of these waves with a dominant frequency that tends towards lower values with time. This evolving frequency content of the ground motion can be critical to the response of degrading structures, which have resonant frequencies that also tend to decay with time as the structure responds to the excitation. Thus, in modeling earthquake ground motions, it is crucial that both the temporal and spectral nonstationary characteristics are properly represented. As described below, one convenient way to achieve spectral nonstationarity with the filtered white-noise process is to allow the filter parameters to vary with time.

Generalizing the form in (2.3), we define the fully nonstationary filtered white-noise process as

$$x(t) = q(t, \boldsymbol{\alpha}) \left\{ \frac{1}{\sigma_f(t)} \int_{-\infty}^{t} h[t - \tau, \boldsymbol{\lambda}(\tau)] w(\tau) d\tau \right\} \qquad (2.5)$$

where the parameters $\boldsymbol{\lambda}$ of the filter are now made dependent on τ, the time of application of the load increment. Figure 2.5 illustrates the idea behind this formulation. The figure shows the responses of a linear filter to two unit load pulses at times $\tau = 1$ s, and $\tau = 3$ s, with the filter having a higher frequency at the earlier time. The superposition of such incremental responses to a sequence of random load pulses produces a process that has a time-varying frequency content, as formulated by the integral process inside the braces in (2.5) and illustrated in Figure 2.6.

Naturally, the response of such a filter may not reach a stationary state. Indeed, the standard deviation $\sigma_f(t)$ of the process defined by the integral in (2.5) in general is a function of time and is given by

$$\sigma_f^2(t) = 2\pi S \int_{-\infty}^{t} h^2[t - \tau, \boldsymbol{\lambda}(\tau)] d\tau \qquad (2.6)$$

However, owing to the normalization by the standard deviation, the process inside the braces in (2.5) has unit variance. Hence, the identity in (2.4) still holds. However, the normalized process inside the braces now has a time-varying frequency content (Fig. 2.6). Thus, in addition to temporal nonstationarity, the formulation in (2.5) provides spectral nonstationarity. By proper

22

selection of the filter parameters and their evolution in time, one can model the spectral nonstationarity of a ground motion process.

2.2.4   Discretization of the Fully Nonstationary Process

In order to digitally simulate a stochastic process, some sort of discretization is necessary. Furthermore, a discretized form that facilitates nonlinear random vibration analysis by use of the Tail-Equivalent Linearization Method (TELM) (Fujimura and Der Kiureghian 2007), is desirable. The following describes a discretized form of the process in (2.5) that meets these objectives.

The modulating function $q(t, \boldsymbol{\alpha})$ used in modeling ground motions usually starts from a zero value and gradually increases over a period of time. Furthermore, the damping value of the filter used to model ground motions is usually large so that the IRF, $h[t - \tau, \boldsymbol{\lambda}(\tau)]$, quickly diminishes with increasing $t - \tau$. Under these conditions, the lower limit of the integral in (2.5) and (2.6), which is $-\infty$, can be replaced with zero (or a finite negative value) without loss of accuracy. This replacement offers a slight computational convenience, allowing the discretized time points to start from zero.

We select a discretization in the time domain. Let the duration of the ground motion be discretized into a sequence of equally spaced time points $t_i = i \times \Delta t$ for $i = 0,1, \dots, n$, where Δt is a small time step. The discretization time steps must be sufficiently small to capture the critical points of a complete cycle. Figure 2.7 shows a complete symmetrical cycle with stars indicating the critical points. If ω_{max} denotes the largest frequency to be considered, then $\Delta t \leq \pi / (2\omega_{max})$ (i.e., quarter of the complete cycle) must be selected. In most earthquake engineering applications $\Delta t = 0.01$ s is adequate.

At a time t, $0 < t \leq t_n$, letting $k = \text{int}\left(\frac{t}{\Delta t}\right)$, where $0 \leq k \leq n$, the process in (2.5) can be written as

$$
\begin{aligned}
x(t) &= q(t, \boldsymbol{\alpha}) \left\{ \frac{1}{\sigma_f(t)} \int_{t_k}^{t} h[t - \tau, \boldsymbol{\lambda}(\tau)] w(\tau) d\tau \right\} \quad \text{if } k = 0 \\
&= q(t, \boldsymbol{\alpha}) \left\{ \frac{1}{\sigma_f(t)} \sum_{i=1}^{k} \int_{t_{i-1}}^{t_i} h[t - \tau, \boldsymbol{\lambda}(\tau)] w(\tau) d\tau + \frac{1}{\sigma_f(t)} \int_{t_k}^{t} h[t - \tau, \boldsymbol{\lambda}(\tau)] w(\tau) d\tau \right\} \quad \text{if } 0 < k
\end{aligned}
$$

(2.7)

Neglecting the integral over the time duration between t_k and t, which is an integral over a fraction of the small time step, and assuming that $h[t - \tau, \boldsymbol{\lambda}(\tau)]$ remains essentially constant during each small time interval $t_{i-1} \leq t \leq t_i$, one obtains

$$
\begin{aligned}
\hat{x}(t) &= q(t, \boldsymbol{\alpha}) \left\{ \frac{1}{\hat{\sigma}_f(t)} \sum_{i=1}^{k} h[t - t_i, \boldsymbol{\lambda}(t_i)] \int_{t_{i-1}}^{t_i} w(\tau) \mathrm{d}\tau \right\} \\
&= q(t, \boldsymbol{\alpha}) \left\{ \frac{1}{\hat{\sigma}_f(t)} \sum_{i=1}^{k} h[t - t_i, \boldsymbol{\lambda}(t_i)] W_i \right\}; \quad t_k \leq t < t_{k+1}
\end{aligned}
\tag{2.8}
$$

where

$$
W_i = \int_{t_{i-1}}^{t_i} w(\tau) \mathrm{d}\tau \tag{2.9}
$$

Integrals of the white-noise process, W_i, $i = 1, \dots, n$, are statistically independent and identically distributed Gaussian random variables having zero mean and the variance $2\pi S \Delta t$. Introducing the standard normal random variables $u_i = W_i / \sqrt{2\pi S \Delta t}$, (2.8) is written as

$$
\hat{x}(t) = q(t, \boldsymbol{\alpha}) \left\{ \frac{\sqrt{2\pi S \Delta t}}{\hat{\sigma}_f(t)} \sum_{i=1}^{k} h[t - t_i, \boldsymbol{\lambda}(t_i)] u_i \right\}; \quad t_k \leq t < t_{k+1} \tag{2.10}
$$

We have used superposed hats on two terms in the above expressions. The one on $\hat{x}(t)$ is to highlight the fact that the expressions (2.8) and (2.10) are for the discretized process and employ the approximations involved in going from (2.7) to (2.8). The hat on $\hat{\sigma}_f(t)$ is used to signify that this function is the standard deviation of the discretized process represented by the sum inside the braces in (2.8), so that the process inside the braces in (2.10) is properly normalized. Since W_i in (2.8) are statistically independent random variables, one has

$$
\hat{\sigma}_f^2(t) = 2\pi S \Delta t \sum_{i=1}^{k} h^2[t - t_i, \boldsymbol{\lambda}(t_i)]; \quad t_k \leq t < t_{k+1} \tag{2.11}
$$

This equation is the discretized form of (2.6).

The discretized representation in (2.10) has the compact form:

$$
\hat{x}(t) = q(t, \boldsymbol{\alpha}) \sum_{i=1}^{k} s_i[t, \boldsymbol{\lambda}(t_i)] u_i; \quad t_k \leq t < t_{k+1} \tag{2.12}
$$

where

24

$$s_i[t, \boldsymbol{\lambda}(t_i)] = \frac{\sqrt{2\pi S \Delta t}}{\hat{\sigma}_f(t)} h[t - t_i, \boldsymbol{\lambda}(t_i)]$$

$$= \frac{h[t - t_i, \boldsymbol{\lambda}(t_i)]}{\sqrt{\sum_{j=1}^{k} h^2[t - t_j, \boldsymbol{\lambda}(t_j)]}} \; ; \quad t_k \le t < t_{k+1} \; ; \;\; 1 \le i \le k \tag{2.13}$$

Note that $s_i[t, \boldsymbol{\lambda}(t_i)]$ is a function of the filter parameters at time t_i; therefore each $s_i[t, \boldsymbol{\lambda}(t_i)]$, $i = 1, \dots, k$, may correspond to a different set of values of the filter parameters. For simplicity in notation, hereafter $s_i[t, \boldsymbol{\lambda}(t_i)]$ is referred to as $s_i(t)$.

The discretized stochastic ground motion process in (2.12) not only facilitates digital simulation but is of a form that can be employed for nonlinear random vibration analysis by use of the TELM. Furthermore, it has interesting geometric interpretations as described in Der Kiureghian (2000). In particular, the zero-mean Gaussian process $\hat{x}(t)$ can be seen as the scalar product of a deterministic, time-varying vector of magnitude $q(t, \boldsymbol{\alpha})$ along the unit vector of the deterministic basis functions $\mathbf{s}(t) = [s_1(t), \dots, s_k(t)]^{\mathrm{T}}$ and a vector of time-invariant, standard normal random variables $\mathbf{u} = [u_1, \dots, u_k]^{\mathrm{T}}$:

$$\hat{x}(t) = q(t, \boldsymbol{\alpha})[\mathbf{s}(t)^{\mathrm{T}} \mathbf{u}]; \quad t_k \le t < t_{k+1} \tag{2.14}$$

Furthermore, the model form in (2.14) has interesting physical interpretations. Standard normal random variables, u_i, provide the randomness that exists in real ground motions. The deterministic basis functions, $s_i(t)$, control the evolving frequency content of the process, capturing the spectral nonstationarity of real ground motions. Finally, the modulating function, $q(t, \boldsymbol{\alpha})$, controls the time evolution of the intensity of the process, hence capturing the temporal nonstationarity of real ground motions.

2.2.5 Remark: Complete Separation of Temporal and Spectral Nonstationarities

An important advantage of the proposed model is the complete separation of the temporal and spectral nonstationarities. The key to this separation is the normalization by $\sigma_f(t)$ in (2.5). Owing to this normalization, the segment inside the braces in (2.5) is a unit-variance process, which causes the modulating function, $q(t, \boldsymbol{\alpha})$, to be the standard deviation of the overall process, $x(t)$, as seen in (2.4). This way, the evolving intensity of the process is solely controlled by the modulating function, while the selected filter (the form of the IRF) and its time-varying

parameters completely control the spectral nonstationarity. Figure 2.8 illustrates this concept graphically.

Normalization by $\sigma_f(t)$, and separation of temporal and spectral nonstationarities provide several noteworthy advantages of the proposed model. First, due to normalization by $\sigma_f(t)$, the intensity of the white-noise process cancels out and S can be assigned any arbitrary positive value. Second, selection of the modulating function is completely independent from the selection of the linear filter, providing flexibility in modeling. Finally, the separation of temporal and spectral nonstationarities provides ease in parameter identification and simulation procedures (see Chapter 3).

2.3 STATISTICAL CHARACTERISTICS OF THE GROUND MOTION PROCESS

In the time domain, a ground motion can be characterized by its evolving intensity. The intensity of a zero-mean Gaussian process (employed in this study to model ground motions) is completely characterized by its time-varying standard deviation. In the proposed ground motion model, this time-varying standard deviation is identical to the modulating function $q(t, \boldsymbol{\alpha})$.

In the frequency domain, a ground motion process can be characterized by its evolving frequency content. In particular, the frequency content may be characterized in terms of a predominant frequency and a measure of the bandwidth of the process as they evolve in time. These properties of the process are influenced by the selection of the filter, i.e., the form of the IRF, $h[t - \tau, \boldsymbol{\lambda}(\tau)]$, and its time-varying parameters $\boldsymbol{\lambda}(\tau)$.

As a surrogate for the predominant frequency of the process, we employ the mean zero-level up-crossing rate, $\nu(0^+, t)$, i.e., the mean number of times per unit time that the process crosses the level zero from below (see Fig. 2.9). Since the scaling of a process does not affect its zero-level crossings, $\nu(0^+, t)$ for the process in (2.12), which is the discretized equivalent of the process (2.5), is identical to that for the unmodulated process:

$$y(t) = \sum_{i=1}^{k} s_i(t)\, u_i\,; \quad t_k \le t < t_{k+1}\,, \quad k = 1, \dots n \tag{2.15}$$

It is well known (Lutes and Sarkani 2004) that for a zero-mean Gaussian process $y(t)$

$$v(0^+, t) = \frac{\sqrt{1 - \rho_{y\dot{y}}^2(t)}}{2\pi} \frac{\sigma_{\dot{y}}(t)}{\sigma_y(t)} \qquad (2.16)$$

where $\sigma_y(t)$, $\sigma_{\dot{y}}(t)$, and $\rho_{y\dot{y}}(t)$ are, respectively, the standard deviations and cross-correlation coefficient of $y(t)$ and its time derivative, $\dot{y}(t) = dy(t)/dt$, at time t. For the process in (2.15), these are given by

$$\sigma_y^2(t) = \sum_{i=1}^{k} s_i^2(t) = 1 ; \quad t_k \leq t < t_{k+1} \qquad (2.17)$$

$$\sigma_{\dot{y}}^2(t) = \sum_{i=1}^{k} \dot{s}_i^2(t) ; \quad t_k \leq t < t_{k+1} \qquad (2.18)$$

$$\rho_{y\dot{y}}(t) = \frac{1}{\sigma_y(t)\sigma_{\dot{y}}(t)} \sum_{i=1}^{k} s_i(t)\dot{s}_i(t) ; \quad t_k \leq t < t_{k+1} \qquad (2.19)$$

where $\dot{s}_i(t) = ds_i(t)/dt$. Using (2.13) and letting $h_i(t) = h[t - t_i, \lambda(t_i)]$, one can easily show that

$$\dot{s}_i(t) = \left[\dot{h}_i(t) - \frac{\sum_{j=1}^{k} h_j(t)\dot{h}_j(t)}{\sum_{j=1}^{k} h_j^2(t)} h_i(t)\right] \frac{1}{\sqrt{\sum_{j=1}^{k} h_j^2(t)}} ; \quad t_k \leq t < t_{k+1} , 1 \leq i \leq k \qquad (2.20)$$

The second equality in (2.17) is a direct result of the normalization explained in Section 2.2. Since $y(t)$ is a zero-mean process and, therefore, $\sigma_y^2 = E[y^2]$, the equality $d(E[y^2])/dt = 0$ is obtained by taking the derivative of (2.17) with respect to time. Reversing the orders of differentiation and expectation results in $E[y\dot{y}] = 0$, which implies zero correlation between y and its derivative, i.e., $\rho_{y\dot{y}}(t) = 0$. Thus, (2.16) can be simplified to

$$v(0^+, t) = \frac{\sigma_{\dot{y}}(t)}{2\pi} \qquad (2.21)$$

It is clear from (2.18) and (2.20) that the filter should be selected so that its IRF is differentiable at all times. For any given differentiable IRF and filter parameter functions, the mean zero-level up-crossing rate is computed from (2.21) by use of the relations in (2.18) and (2.20). Naturally, one can expect that the fundamental frequency of the filter will have a dominant influence on the predominant frequency of the resulting process.

Several alternatives are available for characterizing the time-varying bandwidth of the process. In this paper we use the mean rate of negative maxima or positive minima as a surrogate for the bandwidth (see Fig. 2.9 for examples of negative maxima and positive minima). This measure has the advantage that it is not affected by the modulating function. As is well known, in a zero-mean narrow-band process, almost all maxima are positive and almost all minima are negative (see Fig. 2.10a). With increasing bandwidth, the rate of occurrence of negative maxima or positive minima increases (see Fig. 2.10b). Thus, by determining the rate of negative maxima or positive minima, a time-varying measure of bandwidth can be developed. An analytical expression of this rate for the theoretical model can be derived in terms of the well-known distribution of local peaks (Lutes and Sarkani 2004). However, the resulting expression is cumbersome, since it involves the variances and cross-correlations of $y(t)$, $\dot{y}(t)$, and $\ddot{y}(t)$ and, therefore, the second derivative of $s_i(t)$. For this reason, in this paper the mean rate of negative maxima or positive minima for the selected model process are computed by counting and averaging them in a sample of simulated realizations of the process. As we will shortly see, the damping ratio of the filter has a dominant influence on the bandwidth of the process.

2.4   PARAMETERIZATION OF THE MODEL

The parameters of the proposed stochastic ground motion model defined by (2.5) can be categorized into two independent groups: (1) the parameters $\boldsymbol{\alpha}$ of the modulating function and (2) the time-varying parameters of the linear filter, $\boldsymbol{\lambda}(\tau)$. The model is completely defined by specifying the forms and parameters of the modulating function and the IRF of the linear filter. This section describes the possible forms and constraints of these functions and identifies the model parameters.

2.4.1   Modulating Function and Its Parameters

In general, any function that gradually increases from zero to achieve a nearly constant intensity that represents the "strong shaking" phase of an earthquake and then gradually decays back to zero is a valid modulating function. Several models have been proposed in the past. These include piece-wise modulating functions proposed by Housner and Jennings (1964) and Amin

and Ang (1968), a double-exponential function proposed by Shinozuka and Sato (1967), and a gamma function proposed by Saragoni and Hart (1974). Two modulating functions that are employed in this study are presented below.

Piece-wise modulating function:

A modified version of the Housner and Jennings (1964) model that hereafter will be referred to as the "piece-wise" modulating function is defined by

$$
\begin{aligned}
q(t, \boldsymbol{\alpha}) &= 0 && \text{if} \quad t \le T_0 \\
&= \alpha_1 \left(\frac{t - T_0}{T_1 - T_0} \right)^2 && \text{if} \quad T_0 \le t \le T_1 \\
&= \alpha_1 && \text{if} \quad T_1 \le t \le T_2 \\
&= \alpha_1 \exp[-\alpha_2 (t - T_2)^{\alpha_3}] && \text{if} \quad T_2 \le t
\end{aligned}
\tag{2.22}
$$

This model has the six parameters $\boldsymbol{\alpha} = (\alpha_1, \alpha_2, \alpha_3, T_0, T_1, T_2)$, which obey the conditions $T_0 < T_1 \le T_2$, and $0 < \alpha_1, \alpha_2, \alpha_3$. (The Housner and Jennings model has $\alpha_3 = 1$.) T_0 denotes the start time of the process; T_1 and T_2 denote the start and end times of the "strong shaking" phase, which has intensity α_1; and α_2 and α_3 control the shape of the decaying end of the function. Figure 2.11 shows a piece-wise modulating function for selected parameter values.

Gamma modulating function:

Another model used in this study is the "gamma" modulating function, defined by the formula:

$$
\begin{aligned}
q(t, \boldsymbol{\alpha}) &= 0 && \text{if} \quad t \le T_0 \\
&= \alpha_1 (t - T_0)^{\alpha_2 - 1} \exp[-\alpha_3 (t - T_0)] && \text{if} \quad T_0 \le t
\end{aligned}
\tag{2.23}
$$

This function is proportional to the gamma probability density function, thus the reason for its name. The model has four parameters $\boldsymbol{\alpha} = (\alpha_1, \alpha_2, \alpha_3, T_0)$, where $0 < \alpha_1, \alpha_3$, and $1 < \alpha_2$. Again, T_0 denotes the start time of the process. Of the other three parameters, α_1 controls the intensity of the process, α_2 controls the shape of the modulating function, and α_3 controls the duration of the motion. Figure 2.12 shows a gamma modulating function for selected parameter values.

2.4.2 Linear Filter and Its Parameters

In the frequency domain, the properties of the model process are influenced by the selection of the filter, i.e., the form of the IRF $h[t - \tau, \lambda(\tau)]$, and its time-varying parameters $\lambda(\tau)$ that are used to "shape" the filter response. In particular, for a second-order filter (employed in this study), the time-varying frequency content of the process may be controlled by the natural frequency and damping of the filter, as they evolve in time.

As stated in Section 2.2.1, in choosing the linear filter, certain constraints must be followed to make sure that the choice of the IRF is acceptable:

- The filter should be causal so that $h(t, \lambda)=0$ for $t < 0$.

- The filter should be stable so that $\int_0^\infty h(t, \lambda)dt < \infty$, which requires $\lim_{t\to\infty} h(t, \lambda) = 0$.

- The filter must have an IRF that is at least once differentiable so that (2.20) can be evaluated.

Any damped single or multi-degree-of-freedom linear system that follows the above constraints can be selected as the filter.

In this study, we select

$$h[t - \tau, \lambda(\tau)] = \frac{\omega_f(\tau)}{\sqrt{1 - \zeta_f^2(\tau)}} \exp\left[-\zeta_f(\tau)\omega_f(\tau)(t - \tau)\right] \times \sin\left[\omega_f(\tau)\sqrt{1 - \zeta_f^2(\tau)}(t - \tau)\right]; \ \tau \le t$$

$$= 0 \quad \text{otherwise} \tag{2.24}$$

which represents the pseudo-acceleration response of a single-degree-of-freedom linear oscillator subjected to a unit impulse, in which τ denotes the time of the pulse (see Fig. 2.5) and $\lambda(\tau) = [\omega_f(\tau), \zeta_f(\tau)]$ is the set of parameters of the filter with $\omega_f(\tau)$ denoting the natural frequency and $\zeta_f(\tau)$ denoting the damping ratio, both dependent on the time of application of the pulse. We expect $\omega_f(\tau)$ to influence the predominant frequency of the resulting ground motion process, whereas $\zeta_f(\tau)$ to influence its bandwidth.

Aiming for a simple model and based on analysis of a large number of accelerograms, we adopt a linear form for the filter frequency:

$$\omega_f(\tau) = \omega_0 - (\omega_0 - \omega_n)\frac{\tau}{t_n} \tag{2.25}$$

In the above expression, t_n is the total duration of the ground motion, ω_0 is the filter frequency at time $t_0 = 0$, and ω_n is the frequency at time t_n. Thus, the two parameters ω_0 and ω_n describe

30

the time-varying frequency content of the ground motion. The predominant frequency of a typical earthquake ground motion tends to decay with time; hence, it is expected that $\omega_0 > \omega_n$ for a typical motion. Of course any other two parameters that describe the linear function in (2.25) may be used in place of ω_0 and ω_n (as is done later in Chapter 4).

Investigations of several accelerograms revealed that the variation of their bandwidth measure with time is relatively insignificant. Thus, as a first approximation, the filter damping is considered a constant:

$$\zeta_f(\tau) = \zeta_f \tag{2.26}$$

A more refined model for the filter damping ratio that accounts for the observed variation in the bandwidth of some recorded motions is considered later in this study (see Section 3.2.3). The refined model is a piece-wise constant function of the form:

$$\zeta_f(\tau) = \begin{cases} \zeta_1 & \text{if} \quad 0 \le \tau \le T_1 \\ \zeta_2 & \text{if} \quad T_1 < \tau \le T_2 \\ \zeta_3 & \text{if} \quad T_2 < \tau \le t_n \end{cases} \tag{2.27}$$

with parameters ζ_1, ζ_2, ζ_3, T_1, and T_2 that must be identified for a target motion. The function in (2.27) may have fewer or more than three pieces, as required.

One disadvantage of using a single-degree-of-freedom filter, as in (2.24), is that such a filter can characterize only a single dominant frequency in the ground motion. One can select a multi-degree-of-freedom filter instead to simulate ground motions with multiple dominant frequencies, in which case additional parameters will need to be introduced and identified. This is possible with the proposed model, but is not pursued in the present study.

2.4.3 Model Parameters

With the above parameterization, the stochastic ground motion model is completely defined by specifying the forms of the modulating and IRF functions, and the parameters that define them. Specifically, the parameters $\boldsymbol{\alpha} = (\alpha_1, \alpha_2, \alpha_3, T_0, \dots)$ define the modulating function and completely control the temporal nonstationarity of the process (six parameters $(\alpha_1, \alpha_2, \alpha_3, T_0, T_1, T_2)$ if a "piece-wise" formulation as in (2.22) is selected, four parameters $(\alpha_1, \alpha_2, \alpha_3, T_0)$ if a "gamma" formulation as in (2.23) is selected). With a linearly varying filter frequency and a constant filter damping ratio, the three parameters $(\omega_0, \omega_n, \zeta_f)$ define the filter

31

IRF and completely control the spectral nonstationarity of the process. Therefore, the total number of the model parameters may be as few as six if $T_0 = 0$ is selected: $(\alpha_1, \alpha_2, \alpha_3, \omega_0, \omega_n, \zeta_f)$.

2.5   POST-PROCESSING BY HIGH-PASS FILTERING

In general, site-based stochastic ground motion models tend to overestimate the structural response at long periods (as also recognized by Papadimitriou [1990] and Liao and Zerva [2006]), and the model presented in this study is not an exception. Furthermore, the proposed stochastic ground motion model does not guarantee that the first and second integrals of the acceleration process over time vanish as time goes to infinity. As a result, the variances of the velocity and displacement processes usually keep on increasing even after the acceleration has vanished, resulting in non-zero residuals. This is contrary to base-line-corrected accelerograms, which have zero residual velocity and displacement at the end of the record. To overcome these problems, a high-pass filter is used to adjust the low-frequency content of the stochastic model. Furthermore, this high-pass filter is selected to be the critically damped, second-order oscillator to guarantee zero residuals in the acceleration, velocity, and displacement time-histories. The corrected acceleration record, denoted $\ddot{z}(t)$, is obtained as the solution of the differential equation:

$$\ddot{z}(t) + 2\omega_c \dot{z}(t) + \omega_c^2 z(t) = \hat{x}(t) \tag{2.28}$$

where ω_c is the frequency of the high-pass filter and $\hat{x}(t)$ is the discretized acceleration process as defined in (2.12). Due to high damping of the oscillator, it is clear that $z(t)$, $\dot{z}(t)$, and $\ddot{z}(t)$ will all vanish shortly after the input process $\hat{x}(t)$ has vanished, thus assuring zero residuals for the simulated ground motion. This filter, which was also used by Papadimitriou (1990), is motivated by Brune's (1970, 1971) source model, based on which ω_c, also known as the "corner frequency," can be related to the geometry of the seismic source and the shear-wave velocity. Most ground motion databases, e.g., http://peer.berkeley.edu/nga/index.html, provide the corner frequency for a recorded motion.

An example of a simulated ground motion before and after post-processing is shown in Figure 2.13. The left-hand side of this figure shows one realization of the fully nonstationary stochastic process (representing acceleration time-history) before and after post-processing by

the filter in (2.28), and their integrals over time (representing velocity and displacement time-histories). The right-hand side shows the same motions after post-processing, drawn in a different scale. Observe that even though the difference between the acceleration processes is insignificant, the integration over time results in unacceptably high nonzero velocity and displacement residuals for the acceleration process that is not high-pass filtered. The velocity and displacement traces after post-processing are shown to have zero residual values.

Figure 2.14 shows 5% damped pseudo-acceleration response spectra of the ground motions in Figure 2.13. As expected, the pre-processed motion causes high spectral intensities at long periods.

It is noted that for stochastic dynamic analysis by TELM (Fujimura and Der Kiureghian 2007), the high-pass filter can be included as a part of the structural model so that the discretized form of the input process in (2.12) is preserved.

2.6   SUMMARY

The response of a linear filter with time-varying parameters subjected to a white-noise process is normalized by its standard deviation and is multiplied by a deterministic time-modulating function to obtain the ground acceleration process. Normalization by the standard deviation separates the spectral (achieved by time-variation of the filter parameters) and temporal (achieved by multiplying the process with a time-modulating function) nonstationary characteristics of the process. This model is formulated in the continuous form by (2.5) and in the discrete form by (2.12). The discrete form is ideal for digital simulation and for use in nonlinear random vibration analysis by the tail-equivalent linearization method. The model is completely defined by the form of the filter IRF and the modulating function and their parameters. Suggested models for the IRF and the modulating function and their parameters are provided in Section 2.4. The stochastic model may have as few as six parameters that control the statistical characteristics of the ground motion. The simulated acceleration process according to (2.12) is then high-pass filtered in accordance with (2.28) to assure zero residual velocity and displacement, as well as to produce reliable response spectral values at long periods. Figure 2.15 illustrates the steps involved in simulating a single ground acceleration time-history for a given set of model parameters.

Fig. 2.1 **Schematic of input-output relationship for a linear filter. (a) Response of the linear filter to the unit impulse centered at $t = \tau$, indicated by the shifted Dirac delta function $\delta(t - \tau)$, is the impulse response function $h(t - \tau)$. (b) Response of the linear filter to the white-noise excitation, $w(t)$, is the filtered white-noise process, $f(t)$.**
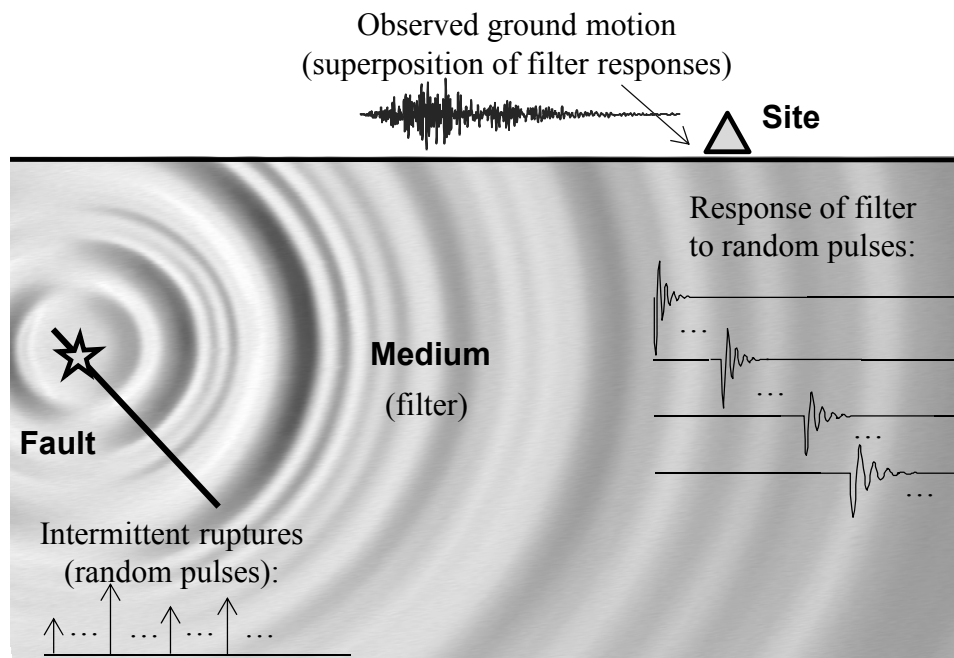
Fig. 2.2 Representation of earthquake excitation as a filtered white-noise process.
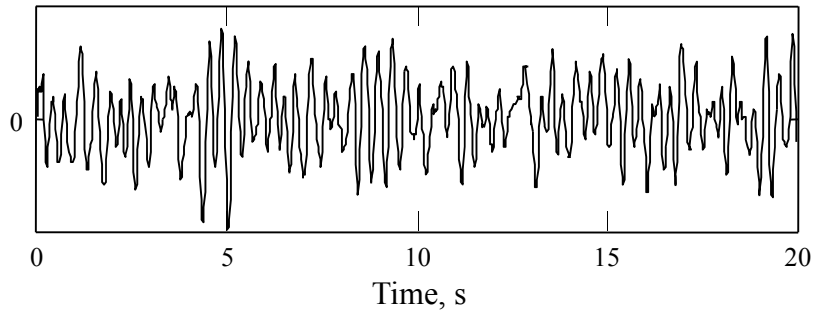
Fig. 2.3 Realization of a stationary filtered white-noise process.
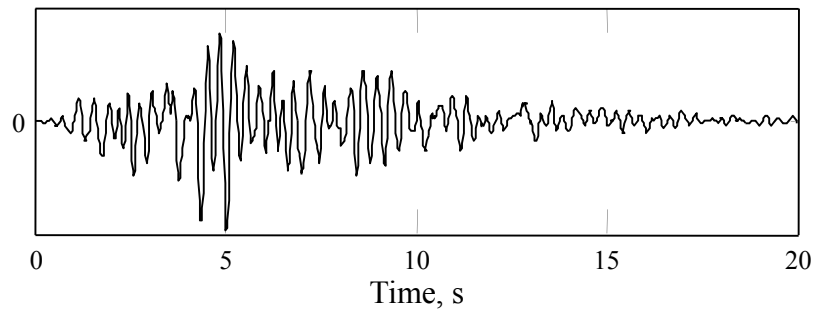
Fig. 2.4 Realization of a time-modulated filtered white-noise process.

36
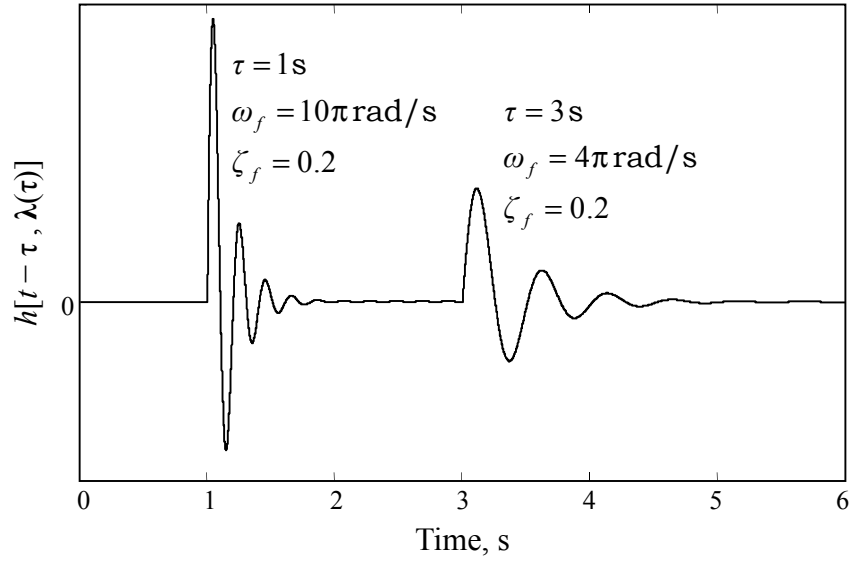
Fig. 2.5 **Responses of a filter with time-varying parameters (ω_f denoting the filter frequency, ζ_f denoting the filter damping ratio) to unit pulses at two time points.**
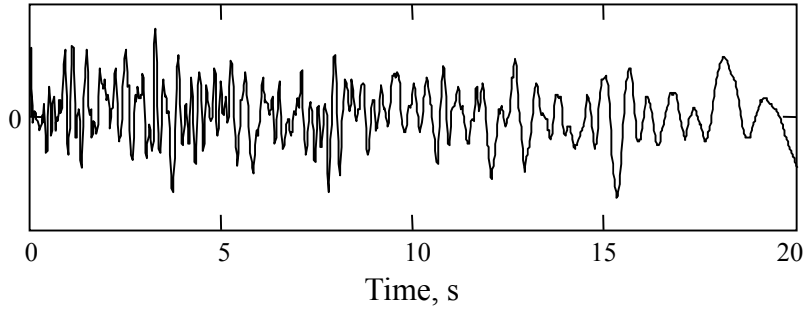
Fig. 2.6 Realization of a process with time-varying frequency content.
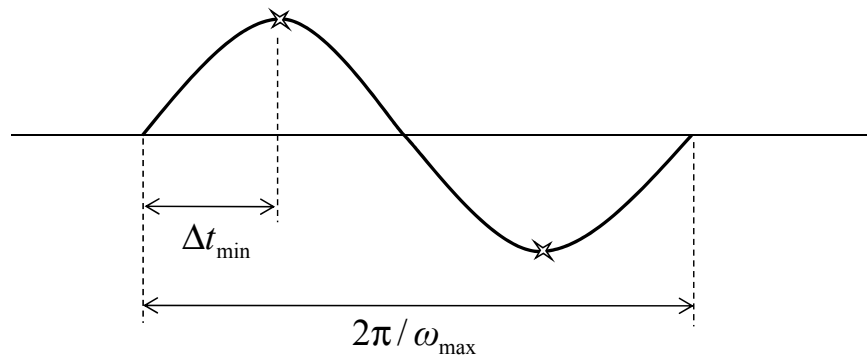
Fig. 2.7 Minimum acceptable discretization step, Δt.

$$x(t) = q(t, \boldsymbol{\alpha}) \left\{ \frac{1}{\sigma_f(t)} \int_{-\infty}^{t} h[t - \tau, \lambda(\tau)] w(\tau) d\tau \right\}$$

Time modulating function

Controls temporal nonstationarity

Unit-variance process

Controls spectral nonstationarity

×

Fully-nonstationary process
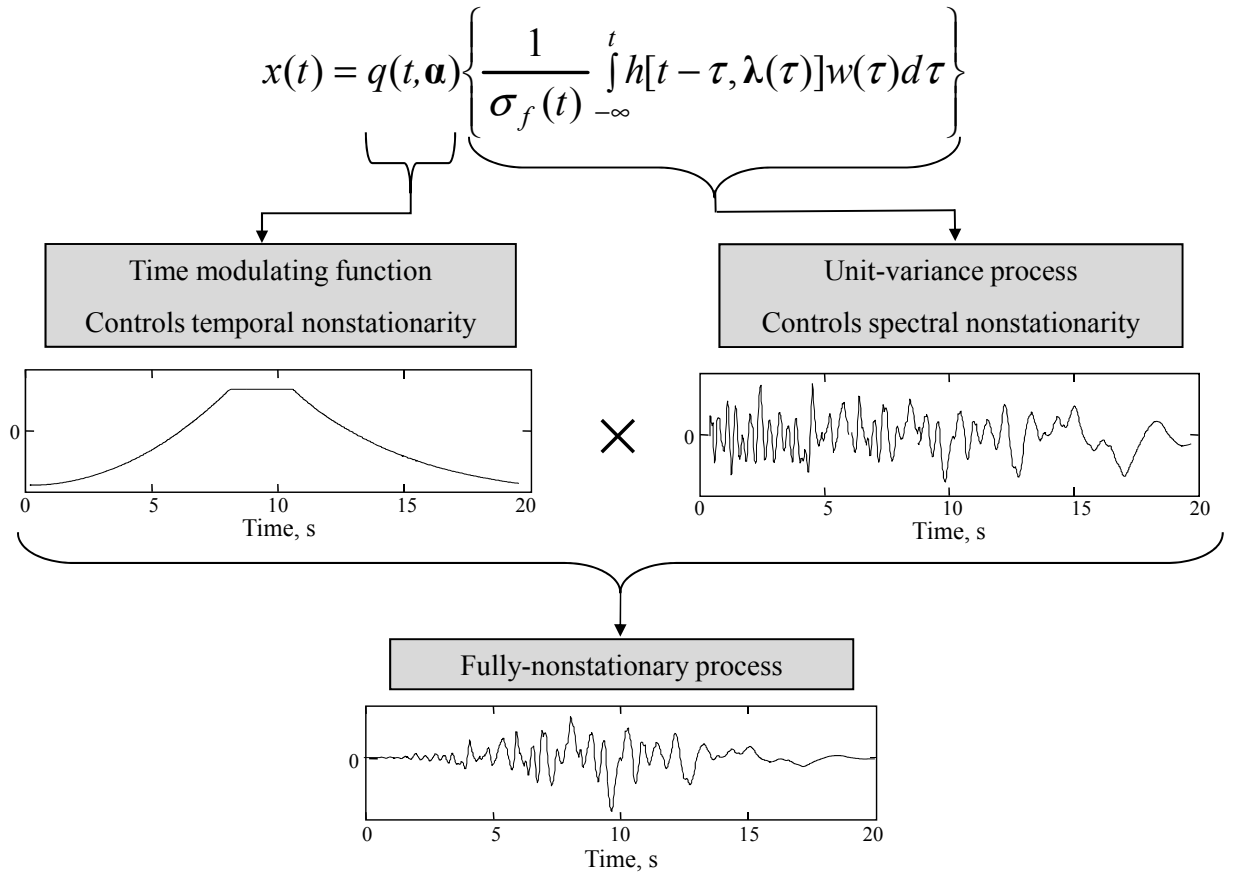
Fig. 2.8   Construction of a fully nonstationary stochastic process according to Eq. (2.5) with separable temporal and spectral nonstationarities.
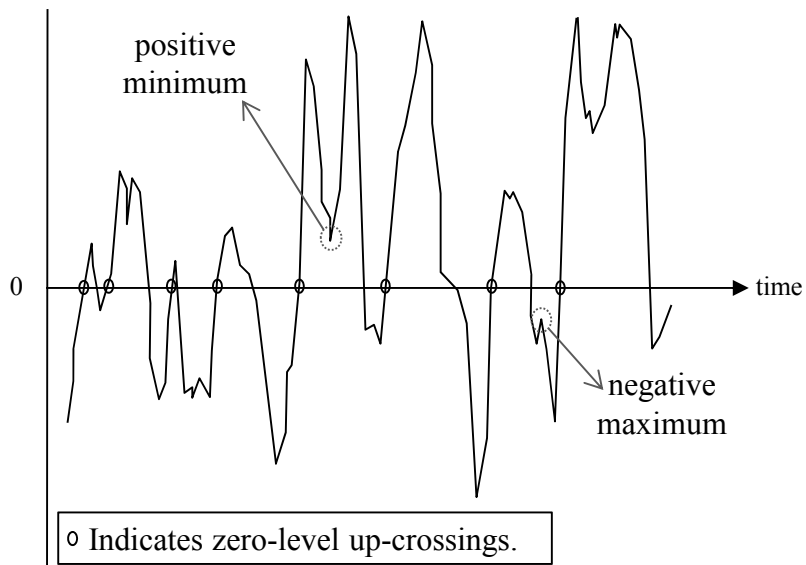
Fig. 2.9 Sample stochastic process, showing zero-level up-crossings, positive minima, and negative maxima.
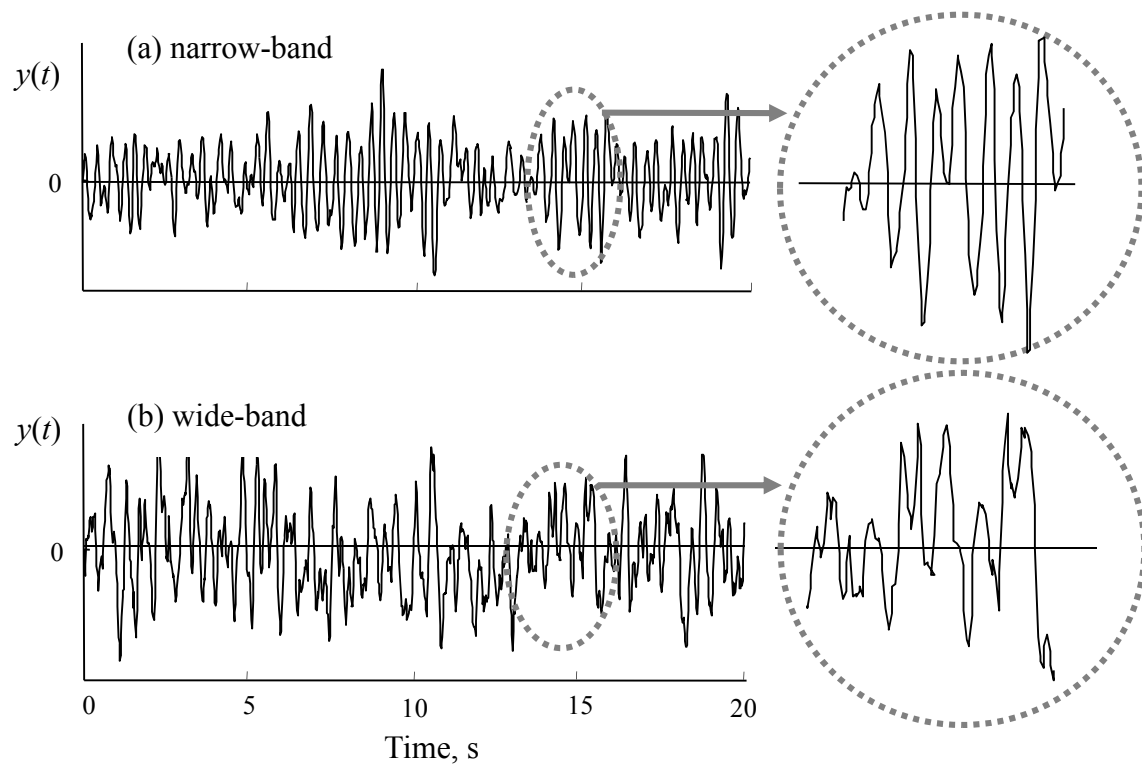
Fig. 2.10 **Segments of (a) a narrow-band process and (b) a wide-band process. Observe the larger number of negative maxima and positive minima in the wide-band process.**

41
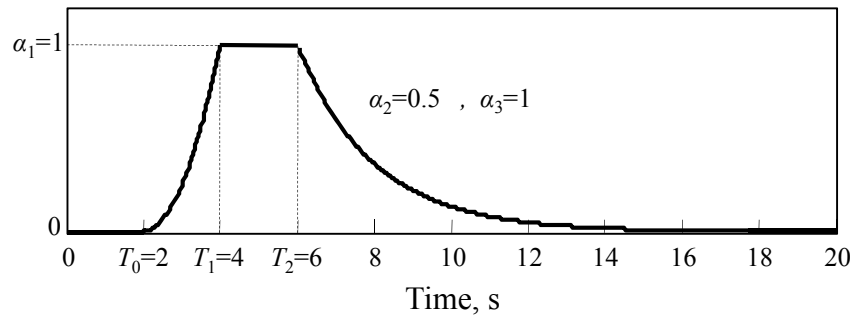
Fig. 2.11 Piece-wise modulating function for selected parameter values.
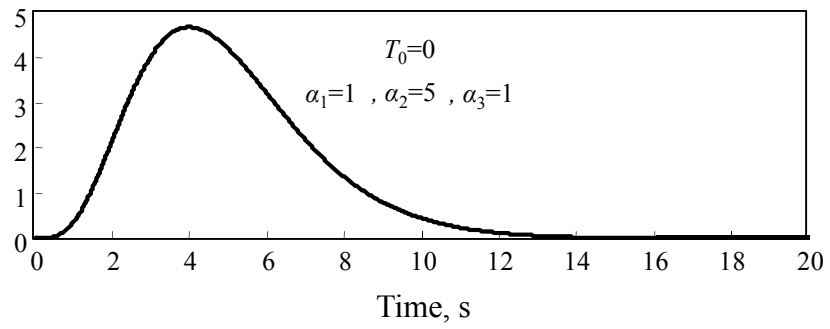
Fig. 2.12 Gamma modulating function for selected parameter values.
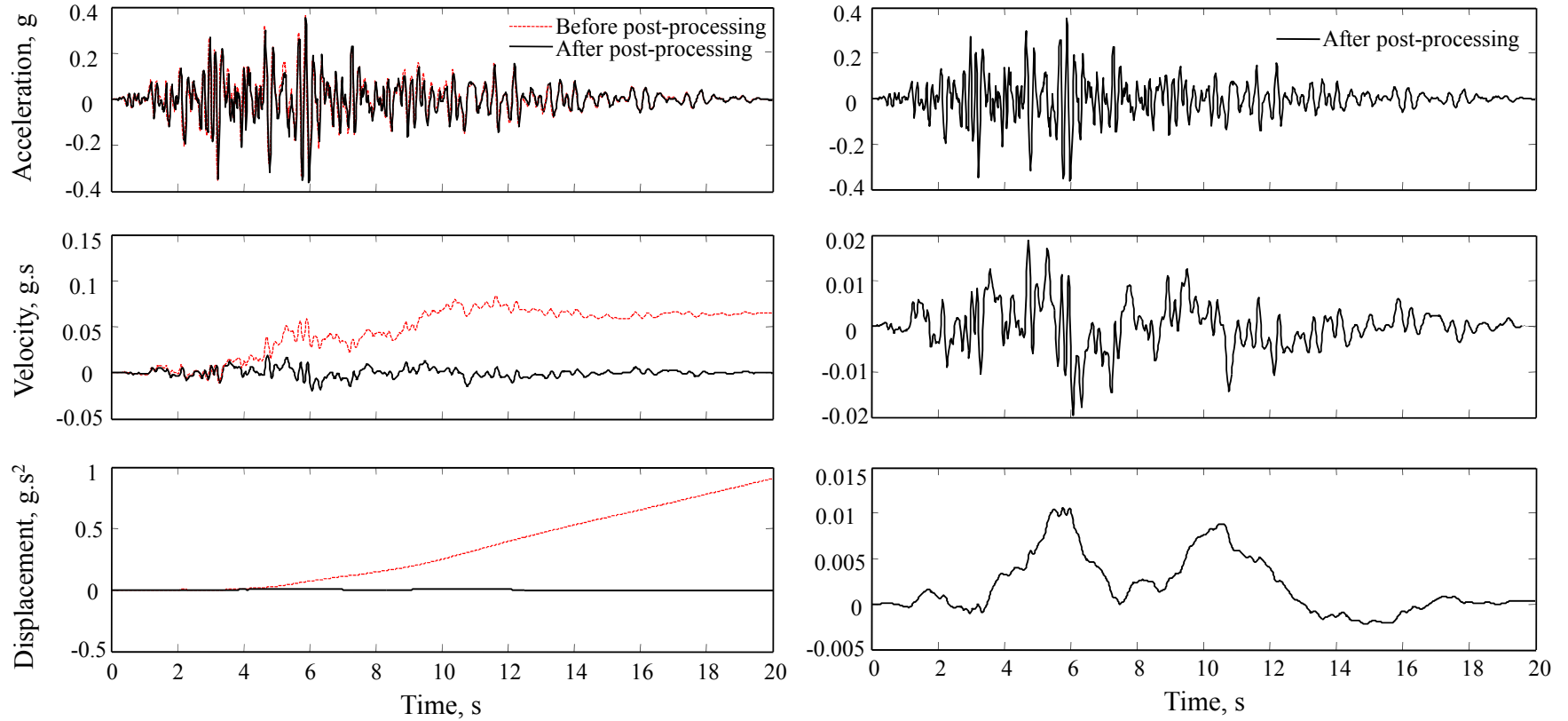
Fig. 2.13 **Realization of a fully nonstationary acceleration process and its integrals before and after high-pass filtering. "Gamma" modulating function with $\alpha_1 = 0.05$, $\alpha_2 = 2.66$, and $\alpha_3 = 0.34$ is used. Linearly decreasing filter frequency from $\frac{\omega_f}{2\pi} = 6$ Hz at $t = 0$ s to $\frac{\omega_f}{2\pi} = 2$ Hz at $t = 20$ s and a damping ratio of $\zeta_f = 0.2$ are selected. Corner frequency of the high-pass filter is 0.2 Hz. Observe the improved velocity and displacement residuals after post-processing.**
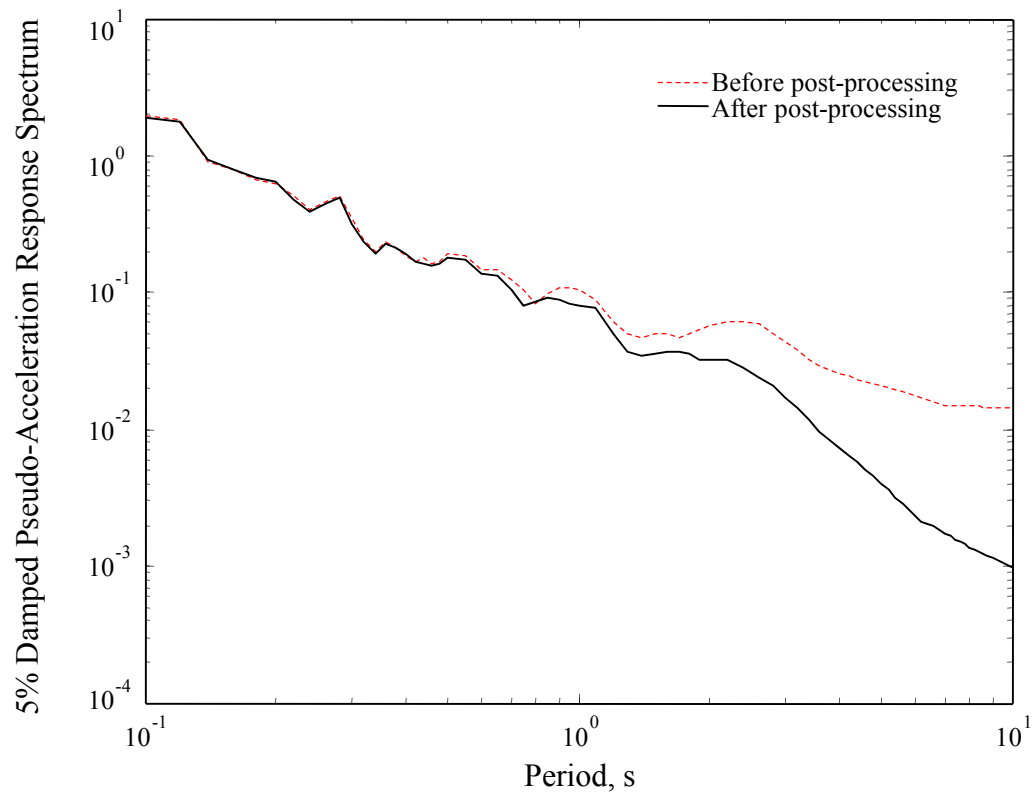
Fig. 2.14 **Response spectra of the realizations in Fig. 2.13. Observe the high spectral content at long periods before post-processing.**
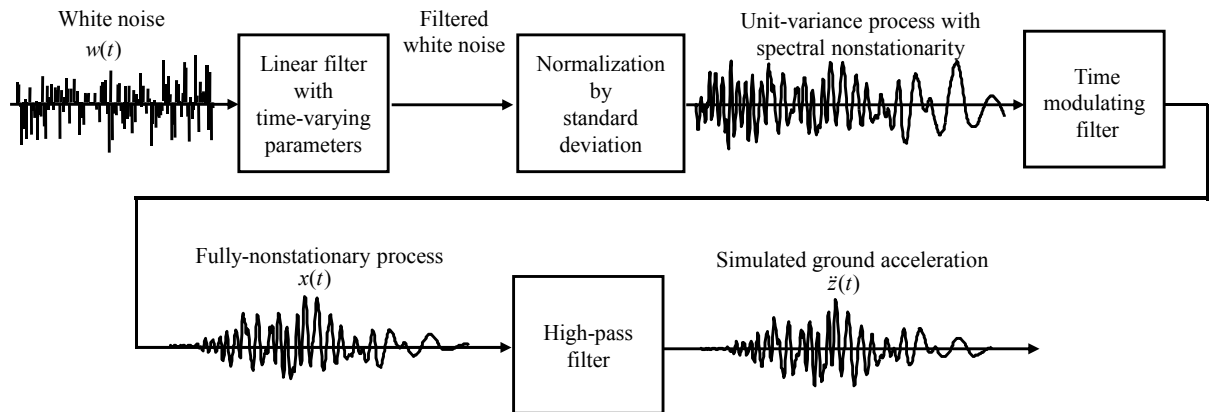
Fig. 2.15 Procedure for generating a single realization of the ground acceleration process according to the proposed model.

3 Fitting to and Simulating a Target Ground Motion

3.1 INTRODUCTION

Given a target accelerogram (e.g., a recorded ground motion), the parameters of the stochastic ground motion model proposed in Chapter 2 may be identified by fitting the statistical characteristics of the stochastic model to those of the target accelerogram. As described in Section 2.3, these statistical characteristics include the time-varying standard deviation of the ground motion process, which controls the evolving intensity of the process, and the mean zero-level up-crossing rate and the rate of negative maxima and positive minima, which together control the frequency content of the process. Once a set of model parameters has been identified, the model formulation is used to simulate realizations of the ground motion. These realizations are all different due to the stochasticity of the model, but they all have the same model parameters and expected statistical characteristics similar to those of the target accelerogram. The target accelerogram may be regarded as a single realization of the ground motion process for a specified set of model parameters, while the simulated motions may be regarded as other random samples of the process for the same set of model parameters.

One of the advantages of simulating a target accelerogram is that this motion will be represented in a form appropriate for nonlinear random vibration analysis. Such analysis requires the input excitation to be stochastic, and recorded time-histories cannot be used directly. The discretized form in (2.12) is ideal for this type of analysis. The statistical characteristics of the stochastic model represent the key features of ground motions (i.e., ground motion intensity, duration, and frequency content) that are important for determination of structural response and estimation of damage induced from earthquakes. Therefore, fitting the model to target accelerograms and identifying their statistical characteristics is useful to study the properties of

earthquake ground motions. Furthermore, generating artificial samples of ground motions with specified statistical characteristics could be useful for various applications, such as parametric studies or determining the statistics of structural response.

This chapter first explains how the stochastic model parameters are identified for a given target accelerogram. From Chapter 2 we know that the model parameters are categorized into two groups: modulating function parameters and linear filter parameters. Parameters of the modulating function are identified first and separate from parameters of the linear filter, which are identified next. A recorded motion is used to demonstrate the procedure. Then, a method to generate synthetic ground motions with the identified model parameters is described. Finally, several examples of recorded ground motions, their identified parameters, and simulations of the resulting stochastic model are presented. All recorded motions used in this chapter are taken from the Pacific Earthquake Engineering Research (PEER) Center strong motion database (see http://peer.berkeley.edu/nga/index.html).

3.2   PARAMETER IDENTIFICATION

As shown in the previous chapter, one of the main advantages of the proposed ground motion model is that the temporal and spectral characteristics are completely separable. Specifically, the modulating function $q(t, \boldsymbol{\alpha})$ completely controls the evolving intensity of the process in time, while the filter IRF $h[t - \tau, \boldsymbol{\lambda}(\tau)]$ completely controls the evolving frequency content of the process. This means that the parameters of the modulating function and of the filter can be independently identified for a target accelerogram, providing ease in the numerical calculations.

3.2.1   Identification of the Modulating Function Parameters

For a target recorded accelerogram, $a(t)$, we determine the modulating function parameters, $\boldsymbol{\alpha}$, by matching the expected cumulative energy of the stochastic process, $E_x(t)$, with the cumulative energy of the target accelerogram, $E_a(t) = \int_0^t a^2(\tau)\mathrm{d}\tau$, over the duration of the ground motion, $0 \leq t \leq t_n$. Consistent with the definition of $E_a(t)$, $E_x(t)$ is defined by

$$E_x(t) = E\left[\int_0^t x^2(\tau)\mathrm{d}\tau\right] \tag{3.1}$$

$$= E \left\{ \left[\int_0^t [q(\tau, \boldsymbol{\alpha}) \mathbf{s}(\tau)^{\mathrm{T}} \mathbf{u}]^2 \mathrm{d}\tau \right] \right\}$$

$$= \int_0^t q^2(\tau, \boldsymbol{\alpha}) \mathrm{d}\tau$$

where $E[.]$ denotes the expectation. The second equality in (3.1) is obtained by substituting the discretized form of $x(t)$ according to (2.14). Switching the orders of expectation and integration and noting that $\mathbf{s}(\tau)^{\mathrm{T}} \mathbf{u}$ is a zero-mean unit-variance process results in the last equality, which is of a convenient form as it depends only on the modulating function. Therefore, the modulating function parameters are obtained by matching the two cumulative energy terms: $E_a(t)$ and $E_x(t)$. This is done by minimizing the integrated squared difference between the two terms:

$$\widehat{\boldsymbol{\alpha}} = \underset{\boldsymbol{\alpha}}{\mathrm{argmin}} \int_0^{t_n} \left[\int_0^t q^2(\tau, \boldsymbol{\alpha}) B(\tau) \mathrm{d}\tau - \int_0^t a^2(\tau) B(\tau) \mathrm{d}\tau \right]^2 \mathrm{d}t \qquad (3.2)$$

where $\widehat{\boldsymbol{\alpha}}$ represents the vector of identified parameters and $B(t)$ is a weight function introduced to avoid dominance by the strong-motion phase of the record. (Otherwise, the tail of the record is not well fitted.) We have found the function:

$$B(t) = \min \left\{ \frac{[\max_t q_0^2(t, \boldsymbol{\alpha}_0)]}{q_0^2(t, \boldsymbol{\alpha}_0)}, 5 \right\} \qquad (3.3)$$

where $q_0(t, \boldsymbol{\alpha}_0)$ is the modulating function obtained in a prior optimization without the weight function, to work well. The objective function in (3.2), which was earlier used by Yeh and Wen (1990) without the weight function, has the advantage that the integral $\int_0^t a^2(\tau) B(\tau) \mathrm{d}\tau$ is a relatively smooth function so that no artificial smoothing is necessary.

As an example, Figure 3.1a shows component 090 of the accelerogram recorded at the LA - 116th Street School station during the 1994 Northridge earthquake. This motion is taken as the target accelerogram, $a(t)$. The squared acceleration, $a^2(t)$, and the cumulative energy, $\int_0^t a^2(\tau) \mathrm{d}\tau$, for this record are shown in Figure 3.1b and 3.1c, respectively. Observe that $\int_0^t a^2(\tau) \mathrm{d}\tau$ is much smoother than either of $a(t)$ or $a^2(t)$, and hence it is easier and more accurate to fit a smooth function to the cumulative energy as is done in (3.2).

The weight function for the target accelerogram is based on a piece-wise modulating function (2.22) (with $T_1 = T_2$) and is presented in Figure 3.1d. Figures 3.1e and 3.1f show the weighted squared acceleration, $a^2(t)B(t)$, and the weighted cumulative energy $\int_0^t a^2(\tau) B(\tau) \mathrm{d}\tau$,

respectively. Comparing Figure 3.1f to 3.1c (also 3.1e to 3.1b) demonstrates the necessity of a weight function. Observe that the plot in Figure 3.1c is rather sharp and quickly flattens reaching the total energy, while the plot in Figure 3.1f rises gradually and there is no sudden flattening. At any given time, the fitted modulating function is proportional to the slope of this plot. Therefore, "sudden flattening" implies that the fitted modulating function reaches nearly zero intensity too quickly, underestimating the tail of the record. This is undesirable because, even though the tail of the record has low intensity, it often has different frequency content from the strong shaking phase of the motion and can influence the response of a nonlinear structure.

Figure 3.2a compares the two energy terms $E_x(t)$ and $E_a(t)$ when fitting to the target accelerogram. Using a piece-wise modulating function with parameters $= (\alpha_1, \alpha_2, \alpha_3, T_0, T_1, T_2)$, identified values of the fitted parameters are $\alpha_1 = 0.0744$ g, $\alpha_2 = 0.413$ s^{-1}, $\alpha_3 = 0.552$, $T_0 = 0.0004$ s, $T_1 = T_2 = 12.2$ s. It can be seen that the fit is excellent at all time points. Figure 3.2b shows the corresponding modulating function superimposed on the target recorded accelerogram.

As a measure of the error in fitting to the cumulative energy of the target accelerogram, we use the ratio:

$$\epsilon_q = \frac{\int_0^{t_n} |E_x(t) - E_a(t)| \mathrm{d}t}{\int_0^{t_n} E_a(t) \mathrm{d}t} \tag{3.4}$$

The numerator is the absolute area between the two cumulative energy curves (see Fig. 3.2a) and the denominator is the area underneath the energy curve of the target accelerogram. For the example shown in Figure 3.2, $\epsilon_q = 0.0248$.

3.2.2   Identification of the Filter Parameters

The parameters ω_0 and ω_n defining the time-varying frequency of the filter [see (2.25)] and the parameters defining the damping ratio of the filter, $\zeta_f(t)$, control the predominant frequency and bandwidth of the process, respectively. Since these parameters have interacting influences, they cannot be identified independently for a target accelerogram. Therefore, we follow a procedure that first optimizes the frequency parameters for a series of constant damping ratios (by matching the cumulative count of zero-level up-crossings of the simulated and target motions), then selects the optimum set of frequency parameters and constant damping ratio by matching the cumulative

count of positive minima and negative maxima of the simulated and target motions. This procedure is for a constant damping ratio [see (2.26)] and is described in detail in this section. If the damping ratio is allowed to vary over time [see (2.27)], further steps are required for optimization, which are described in the next section.

We first determine ω_0 and ω_n, while keeping the filter damping a constant ratio, ζ_f. For a given ζ_f, the parameters ω_0 and ω_n are identified by minimizing the difference between the cumulative expected number of zero-level up-crossings of the process, i.e., $\int_0^t v(0^+, \tau)\mathrm{d}\tau$, and the cumulative count $N(0^+, t)$ of zero-level up-crossings in the target accelerogram for all t, $0 \le t \le t_n$. This is accomplished by minimizing the mean-square error:

$$\left[\widehat{\omega}_0(\zeta_f), \widehat{\omega}_n(\zeta_f)\right] = \underset{\omega_0, \omega_n}{\mathrm{argmin}} \int_0^{t_n} \left[\int_0^t v(0^+, \tau) r(\tau)\mathrm{d}\tau - N(0^+, t)\right]^2 \mathrm{d}t \qquad (3.5)$$

where $\widehat{\omega}_0(\zeta_f)$ and $\widehat{\omega}_n(\zeta_f)$ represent the identified values of frequency parameters dependent on the selected damping ratio, and $r(\tau)$ is an adjustment factor as described below. As can be noted in the equations leading to (2.16), $v(0^+, \tau)$ is an implicit function of the filter characteristics $\omega_f(\tau)$ and $\zeta_f(\tau)$, and therefore, ω_0 and ω_n and ζ_f. The same is true for $r(\tau)$, as explained below.

When a continuous function of time is represented as a sequence of discrete time points of equal intervals Δt, the function effectively loses its content beyond a frequency approximately equal to $\pi/(2\Delta t)$ rad/s (see Fig. 2.7). This truncation of high-frequency components results in undercounting of level crossings. Since digitally recorded accelerograms are available only in discretized form, the count $N(0^+, t)$ underestimates the true number of crossings of the target accelerogram by a factor per unit time, which we denote by $r(\tau)$. Hence, to account for this effect when matching $\int_0^t v(0^+, \tau)\mathrm{d}\tau$ to $N(0^+, t)$, we must multiply the rate of counted up-crossings by the factor $1/r(\tau)$. However, $r(\tau)$ depends on the predominant frequency and bandwidth of the accelerogram. For this reason, it is more convenient to adjust the theoretical mean up-crossing rate [the first term inside the square brackets in (3.5)] by multiplying it by the factor $r(\tau)$. The undercounting factor, $r(\tau)$, may be approximated and incorporated in (3.5) as described in the following.

For a stationary process with power spectral density $\Phi(\omega)$, the mean zero-level up-crossing rate with the frequencies beyond ω_{max} truncated is given by

$$v(0^+, \omega_{\max}) = \frac{1}{2\pi} \sqrt{\frac{\int_0^{\omega_{max}} \omega^2 \Phi(\omega) d\omega}{\int_0^{\omega_{max}} \Phi(\omega) d\omega}} \tag{3.6}$$

The power spectral density for a stationary filtered white-noise process consistent with the IRF in (2.24) with time-invariant parameters is $\Phi(\omega) = 1/[(\omega_f^2 - \omega^2)^2 + 4\zeta_f^2 \omega_f^2 \omega^2]$. Using (3.6), the undercount per unit time, denoted r, can be calculated as the ratio:

$$r = \frac{v(0^+, \pi/2\Delta t)}{v(0^+, \infty)} \tag{3.7}$$

Observe that r is a function of Δt as well as the frequency characteristics of the process, i.e., ω_f and ζ_f. In the present case, since ω_f is a function of τ, r is also a function of τ. The solid lines in Figure 3.3 show the ratio $r(\tau)$ plotted as a function of the filter frequency for the damping values $\zeta_f = 0.3, 0.4, 0.5,$ and 0.6 and for $\Delta t = 0.01$ and 0.02 s. These plots are nearly linear and hence for a specified discretization step, straight-line approximations (dotted lines in Fig. 3.3) are employed in place of (3.7). For $\Delta t = 0.01$ and 0.02 s, these approximations are

$$r(\tau, \Delta t = 0.01) = 1 - 0.00005\big(\omega_f(\tau) + \zeta_f(\tau)\big) - 0.000425\omega_f(\tau)\zeta_f(\tau) \tag{3.8}$$

$$r(\tau, \Delta t = 0.02) = 1 - 0.01\zeta_f(\tau) - 0.009\omega_f(\tau)\zeta_f(\tau) \tag{3.9}$$

It can be seen in Figure 3.3 that representation of a process at discrete-time points can result in undercounting of the zero-level up-crossings by as much as 2-25%, depending on the filter parameters and the time step used.

Figure 3.4 compares the cumulative number of zero-level up-crossings of the target accelerogram (the Northridge record in the previous section) and the adjusted (by the factor $r(\tau)$) mean cumulative number of zero-level up-crossings of the fitted model process for $\zeta_f = 0.3$. The corresponding optimal values of ω_0 and ω_n are obtained for the specified damping ratio by solving (3.5), which is equivalent to minimizing the difference between the two plots shown in Figure 3.4. The optimized parameters $\hat{\omega}_0$ and $\hat{\omega}_n$ are listed in Table 3.1 for different values of the damping ratio, namely $\zeta_f = 0.2, 0.3, 0.4, 0.5, 0.6,$ and 0.7. As a measure of the error in fitting to the cumulative number of zero-level up-crossings, we use

$$\epsilon_\omega = \frac{\int_0^{t_n} \left| \int_0^t v\big(0^+, \tau, \hat{\omega}_0, \hat{\omega}_n, \zeta_f\big) r(\tau) d\tau - N(0^+, t) \right| dt}{\int_0^{t_n} N(0^+, t) dt} \tag{3.10}$$

52

Values of this measure are also provided in Table 3.1. Each set of $\hat{\omega}_0$, $\hat{\omega}_n$, and ζ_f listed in Table 3.1 results in a plot almost identical to Figure 3.4. In this figure, it is evident that the rate of up-crossings (the slope of the curve) decays with time, indicating that the predominant frequency of the ground acceleration decreases with time.

We need to select the optimum value of the filter damping ratio, ζ_f, which controls the bandwidth of the process. We employ a simulation approach to estimate the average cumulative number of negative maxima and positive minima, which characterizes the bandwidth of the model process. The reason for using simulation rather than an analytical expression was explained in Section 2.3. Shown in Figure 3.5 is the cumulative number of negative maxima plus positive minima as a function of time for the target accelerogram (i.e., the Northridge record), as well as the estimated averages of the same quantity for sets of 10 simulations of the theoretical model with damping values $\zeta_f = 0.2, 0.3, 0.4, 0.5, 0.6$, and 0.7. The slopes of these lines should be regarded as instantaneous measures of the bandwidth parameter. By comparing the slopes of the target curve with those of the simulated curves, ζ_f is identified. The parameters $\hat{\omega}_0$ and $\hat{\omega}_n$ for each value of ζ_f are determined as described above and listed in Table 3.1. Note that the modulating function has no effect on this calculation.

Several observations in Figure 3.5 are noteworthy. First note that the curves based on the theoretical model for the various values of ζ_f are nearly straight lines. This implies that a constant value of the filter damping ratio corresponds to a constant bandwidth of the process, even though the predominant frequency varies with time. This also implies that the bandwidth of the model process is solely controlled by the damping ratio of the filter. Secondly, observe that the curve based on the target accelerogram shows relatively small curvatures. This implies that the bandwidth of this particular accelerogram, as measured in terms of the rate of negative maxima and positive minima, remains more or less constant during the excitation. It can be seen that the theoretical curve with $\zeta_f = 0.3$ best matches the bandwidth of the target accelerogram. A measure of error, similar to (3.10), is defined for fitting the bandwidth as the cumulative absolute difference between the cumulative numbers of negative maxima and positive minima of the target accelerogram and of the model process (i.e., the absolute area between the two curves in Fig. 3.5), normalized by the cumulative number for the target accelerogram (i.e., the area underneath the target curve in Fig. 3.5). This measure denoted by ϵ_ζ, is also listed in Table 3.1.

53

Note that this error measure is smallest when $\zeta_f = 0.3$. Also note that the error measure ϵ_ω is nearly the same for all damping values.

In summary, if we select $\zeta_f = 0.3$, the corresponding values of the frequency parameters are $\hat{\omega}_0 = 39.7$ rad/s and $\hat{\omega}_n = 4.68$ rad/s (Table 3.1). These parameter values, together with the parameters identified for the modulating function, completely define the theoretical model fitted to the target accelerogram.

3.2.3 Time-Varying Bandwidth

Closer examination of the target curve in Figure 3.5 shows that the rate of occurrence of negative maxima and positive minima (the slope of the target curve at a given time) is higher during the initial 8 s and final 10 s of the motion relative to the 22 s middle segment. This phenomenon was observed to varying degrees in other accelerograms that were investigated. It appears that ground motions typically have broader bandwidths during their initial and final phases, as compared to their middle segments. This phenomenon may be attributed to mixing of wave forms: In the initial segment, P and S waves are mixed providing a broad bandwidth; the middle segment is dominated by S waves and, therefore, has a narrower bandwidth; while the final segment is a mixture of S waves and surface waves, again providing a broader bandwidth.

To more accurately model the time-varying bandwidth of the accelerogram, the filter damping ratio can be made a function of time. To capture the three-segment behavior described above, we select three values of the damping ratio for the initial, middle, and final segments of the ground motion [see (2.27)]. The dashed line in Figure 3.6 shows the average cumulative number of negative maxima and positive minima for 10 simulations of the fitted model with the filter damping ratio $\zeta_f(\tau) = 0.4$ for $0 < \tau \le 8$ s, $\zeta_f(\tau) = 0.2$ for $8 < \tau \le 30$ s, and $\zeta_f(\tau) = 0.9$ for $30 < \tau \le 40$ s. These values were selected by comparing the slopes of the target curve with those of the simulated curves for different constant damping ratios. The corresponding optimal values of the filter parameters [obtained by using the variable damping values in (3.5)] are $\hat{\omega}_0 = 39.4$ rad/s and $\hat{\omega}_n = 4.86$ rad/s.

It can be seen in Figure 3.6 that the refined model achieves a close fit to the time-varying bandwidth of the target accelerogram and is an improvement to the constant damping ratio

selected previously. The error measures for the variable damping ratio are $\epsilon_\omega = 0.0127$ and $\epsilon_\zeta = 0.0461$.

3.3   GROUND MOTION SIMULATION

For specified parameters of the modulating function and the filter IRF, a sample realization of the proposed stochastic ground motion model is generated by use of (2.12). This requires generation of the standard normal random variables u_i, $i = 1, ..., n$, and their multiplication by the functions $s_i(t)$, which are computed according to (2.13). After multiplication by the modulating function, the resulting motion is then post-processed, as described in Section 2.5, to represent an earthquake ground motion.

It was previously mentioned that without the post-processing, the simulated motions may overestimate the response spectral values at long-period ranges. As an example, Figure 3.7a shows the response spectrum of the target accelerogram used in Section 3.2 (thick line), together with response spectra of 10 simulated motions with the variable-damping model described in Section 3.2.3 (thin lines). It can be seen that, while the simulated spectra match the target spectrum fairly closely for periods shorter than about 2.5 s, at longer periods they all exceed the target spectrum. Figure 3.7b compares the response spectrum of the target accelerogram with the response spectra of the 10 simulated motions, which are post-processed with the filter in (2.28) with $\omega_c = 0.5\pi$ rad/s. It can be seen that the post-processing significantly improves the estimation of spectral values at long periods without affecting the short-period range.

The observed discrepancies between the target and simulated spectra in the short-period range of Figure 3.7b, though not significant, are partly due to the use of a single degree of freedom filter. Such a filter can characterize only a single dominant period in the ground motion. The selected recorded motion clearly shows multiple dominant periods. If a closer match is desired, one can select a two-degrees-of-freedom filter, in which case additional parameters will need to be introduced and identified. This is possible with the proposed model, but is not pursued in this study.

Figure 3.8 shows the target accelerogram (the Northridge record in Section 3.2) together with two sample realizations simulated using the fitted stochastic model. Examples of other target accelerograms and their simulations are provided in Figures 3.9 to 3.12. Figures 3.9 to

3.11 show three different target accelerograms and two simulations for each accelerogram using a piece-wise modulating function, linear filter frequency, and (three-piece) variable damping ratio. The frequency for the high-pass filter is selected so that the response spectra of simulations are well fitted to the response spectra of the recorded motion for spectral periods up to 10 s. Functions that are suggested for the filter frequency and damping ratio in this study are for a typical ground motion. These functions may be refined or altered as desired by the user. For example, in Figure 3.12, instead of a linear function for the filter frequency, an exponential function with three parameters has been used.

The simulated ground motions in Figures 3.8 to 3.12 have evolutionary statistical characteristics, i.e., time-varying intensity, predominant frequency, and bandwidth, which are similar to those of the target accelerogram. Hence, together with the target accelerogram, they can be considered as an ensemble of ground motions appropriate for design or assessment of a structure for those particular statistical characteristics.

3.3.1   Variability of Ground Motion

In the broader context of performance-based earthquake engineering (PBEE), an ensemble of ground motions that represents all possible ground shakings at a site is of interest (not only ground motions with statistical characteristics similar to those of a previously observed motion). The variability among such an ensemble comes from two different sources: (1) the randomness of ground motions for a specified set of model parameters (see the spread of response spectra for simulated motions at a given period in Figure 3.7 and the variability among the time-histories in Fig. 3.8) and (2) the randomness of the model parameters for the site of interest. The former is accounted for when fitting and simulating a target accelerogram (due to the *stochastic* nature of the model), but the latter is not.

It is important to note that model parameters are actually random variables and an identified set of model parameters corresponding to a previously recorded motion is only one realization of these random variables for the earthquake and site characteristics that produced the recorded motion. To produce ground motions with appropriate variability for use in PBEE (i.e., for specified earthquake and site characteristics) the model parameters must be randomized to represent other ground motions that can result from such an earthquake.

Assigning probability distributions to the model parameters and constructing predictive relations between the model parameters and the earthquake and site characteristics are subjects of Chapter 4. The results of Chapter 4 allow one to predict the model parameters for a given set of earthquake and site characteristics (e.g., faulting mechanism, earthquake magnitude, distance to the rupture, and local soil conditions) without the need for a previously recorded motion. Chapter 5 focuses on randomly generating samples of model parameters for specified earthquake and site characteristics, and generating an ensemble of synthetic motions that have the natural variability of real ground motions and are appropriate for use in PBEE.

Table 3.1 Parameter values and error measures.

Damping Ratio	Frequency Parameters (rad/s)		Error Measures	
ζ_f	$\widehat{\omega}_0$	$\widehat{\omega}_n$	ϵ_ω	ϵ_ζ
0.2	40.8	4.16	0.0169	0.3212
0.3	**39.7**	**4.68**	**0.0167**	**0.0858**
0.4	38.6	4.49	0.0166	0.1925
0.5	38.0	4.55	0.0165	0.2949
0.6	37.4	4.56	0.0166	0.3649
0.7	36.9	4.53	0.0168	0.4004
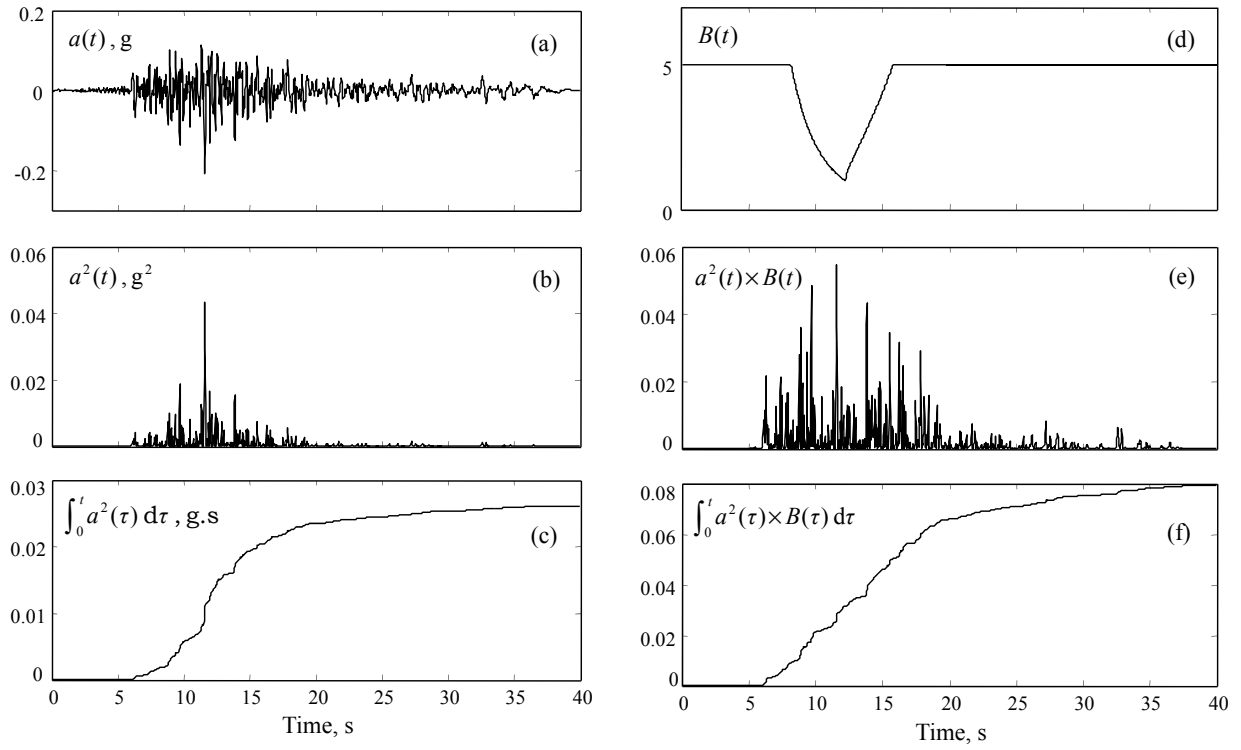
Fig. 3.1 Left: Target accelerogram, its corresponding squared acceleration, and cumulative energy. Right: Selected weight function, weighted squared acceleration, and weighted cumulative energy. (Respectively from top to bottom).
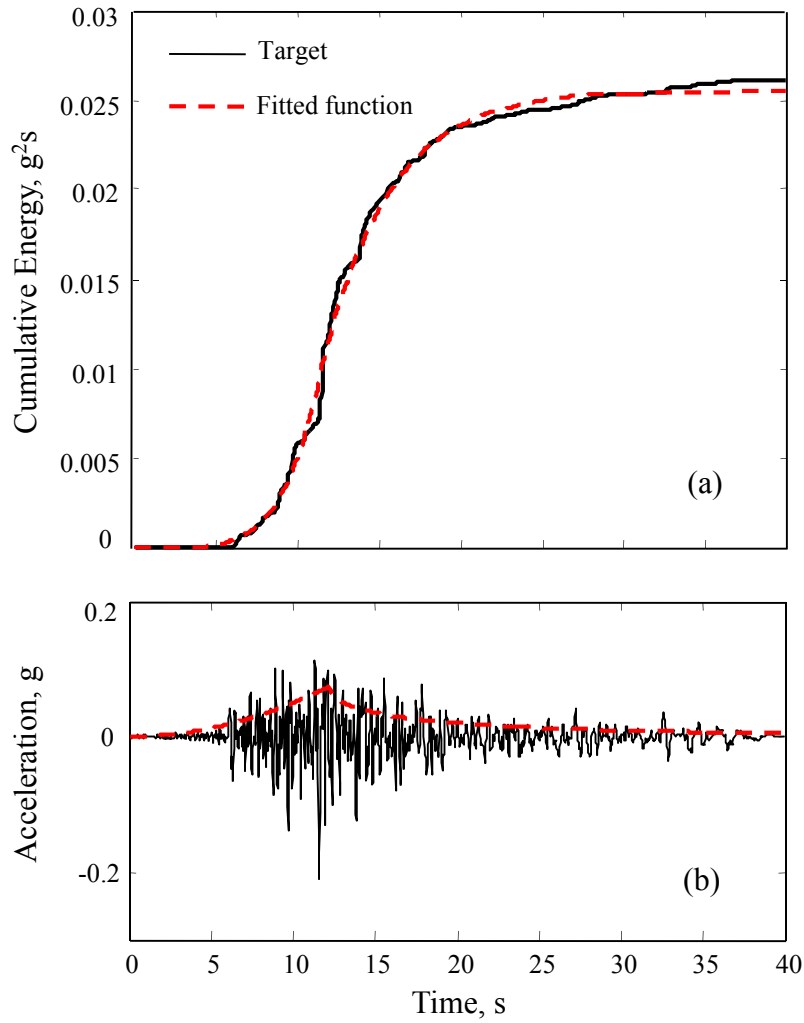
Fig. 3.2 (a) Cumulative energies in the target accelerogram and the fitted modulating function. (b) Corresponding modulating function superimposed on the target accelerogram.
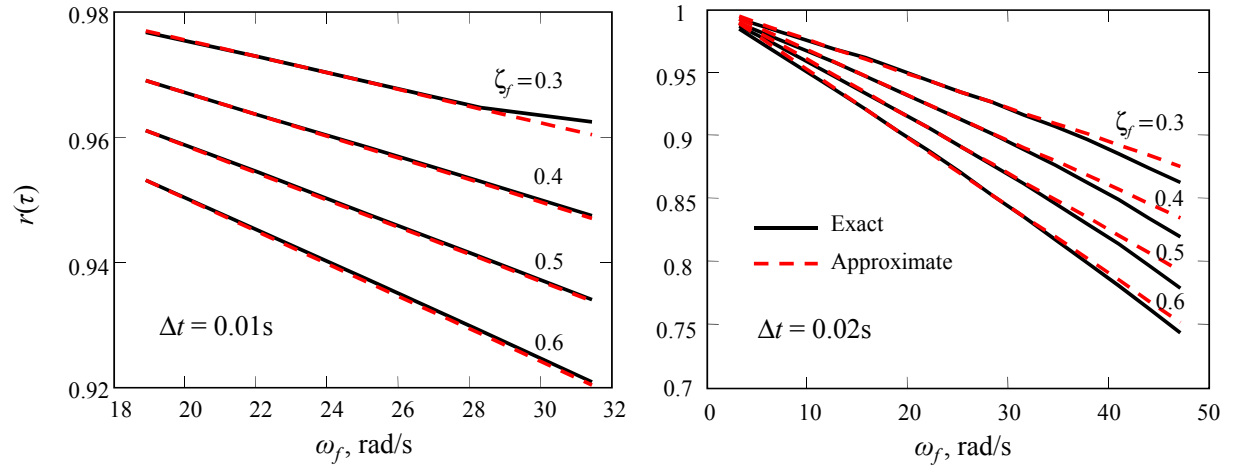
Fig. 3.3 **Adjustment factor for undercounting of zero-level up-crossings of a discretized process.**
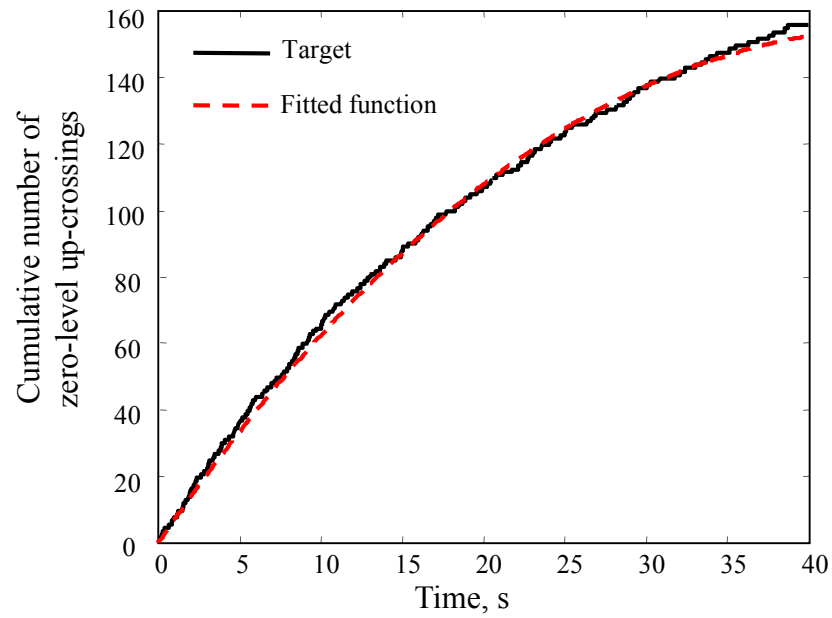
Fig. 3.4 **Cumulative number of zero-level up-crossings in the target accelerogram and fitted model.**
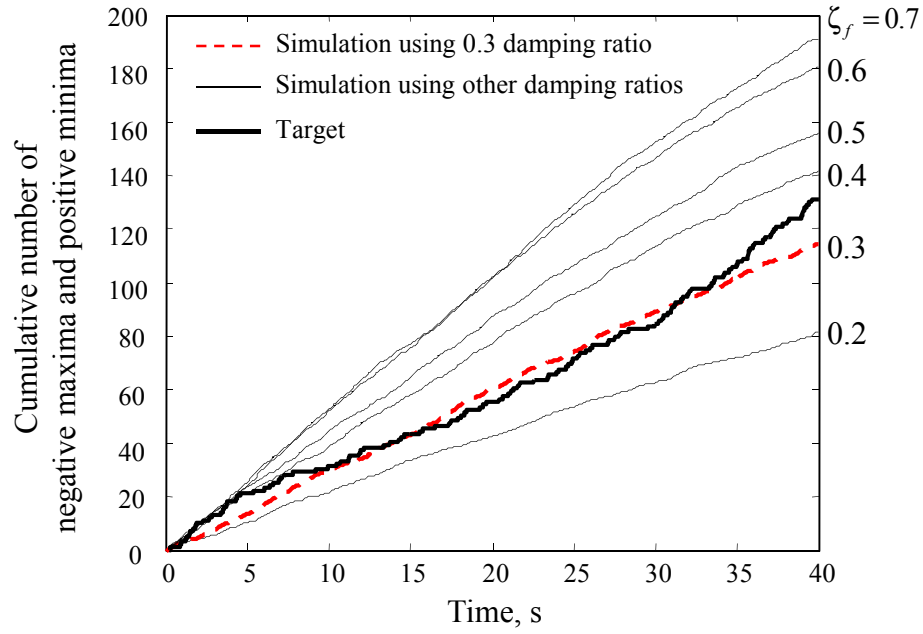
Fig. 3.5 **Fitting to cumulative count of negative maxima and positive minima with constant filter damping ratio.**
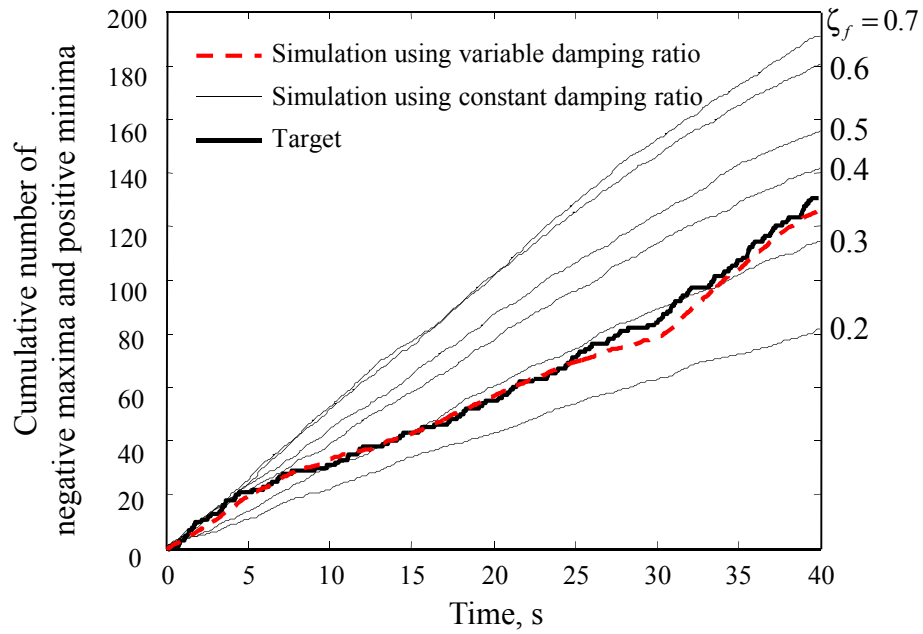
Fig. 3.6 **Fitting to cumulative count of negative maxima and positive minima with variable filter damping ratio.**
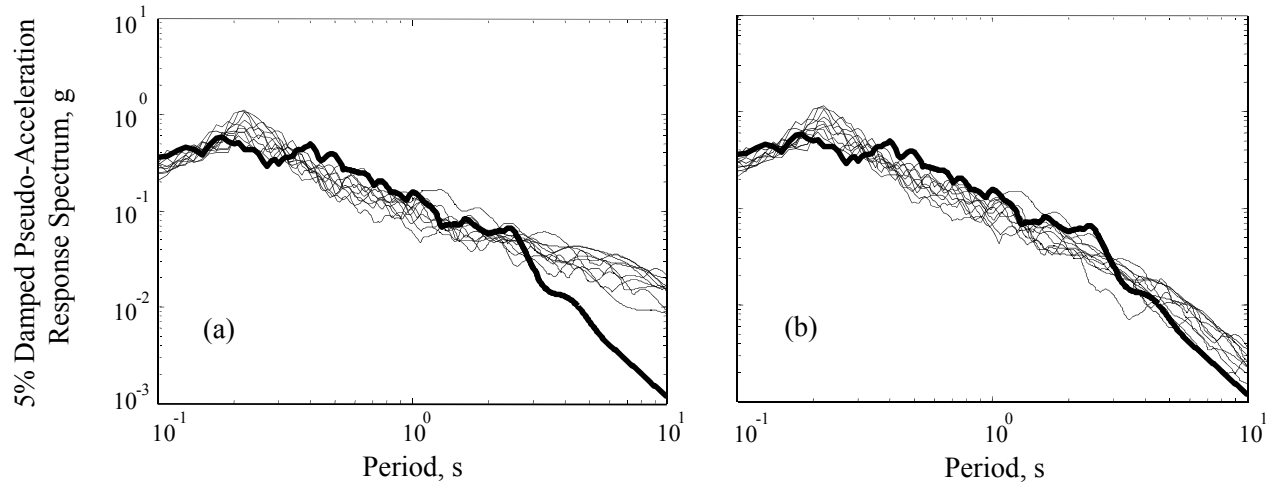
Fig. 3.7 Pseudo-acceleration response spectra of the target accelerogram (thick line) and 10 realizations of the fitted model (thin lines): (a) Before high-pass filtering. (b) After high-pass filtering.
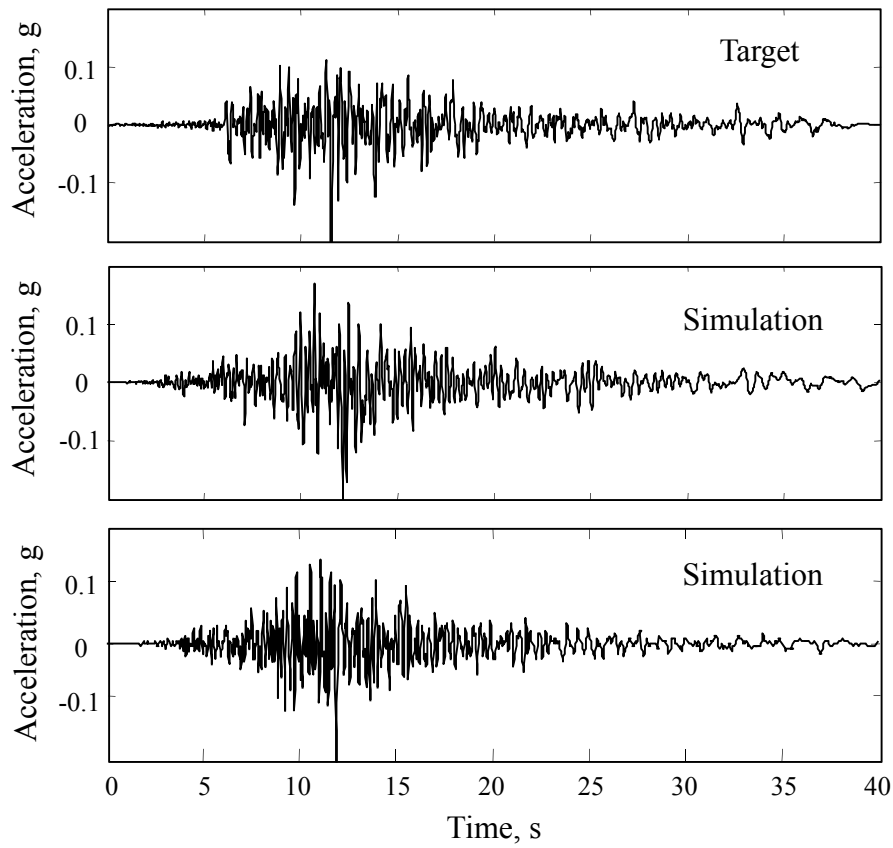
Fig. 3.8 Target accelerogram and two simulations using the fitted model.
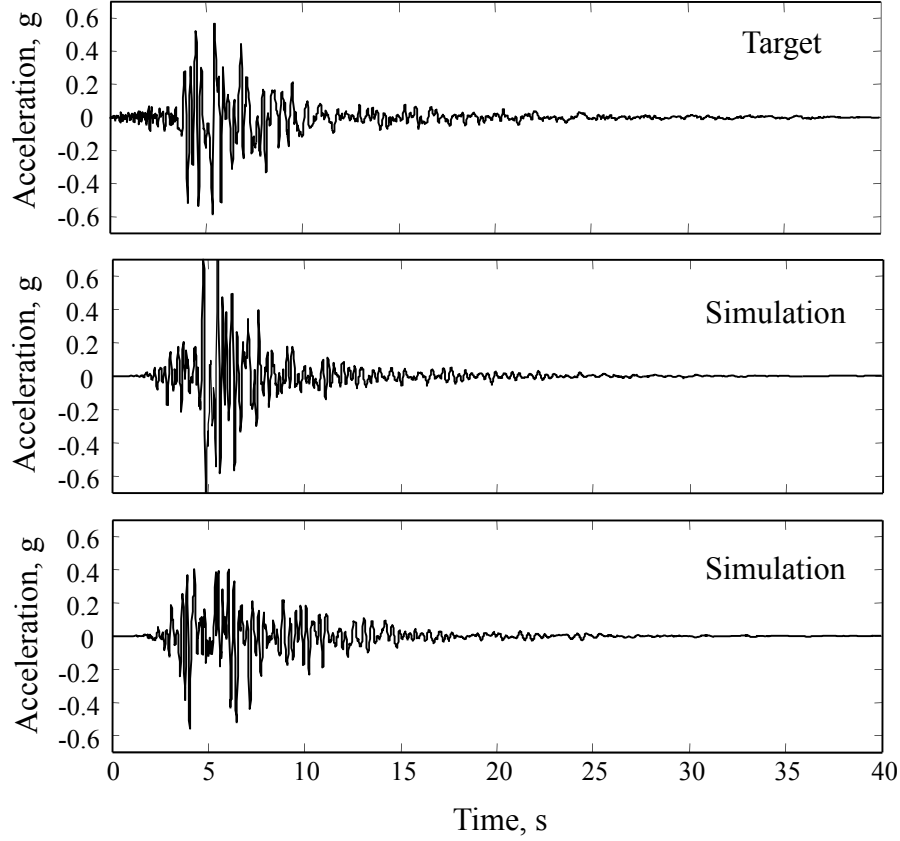
Fig. 3.9 **Target accelerogram and two simulations using the fitted model. Target accelerogram is component 090 of the 1994 Northridge earthquake at the Newhall Fire Station. Corresponding model parameters are $\alpha_1 = 0.362$ g, $\alpha_2 = 0.527$ s^{-1}, $\alpha_3 = 0.682$, $T_0 = 0.9$ s, $T_1 = 5.3$ s, and $T_2 = 5.4$ s for a piece-wise modulating function and $\omega_0 = 24.0$ rad/s and $\omega_n = 5.99$ rad/s for a linear filter frequency function. Variable filter damping ratio is used where $\zeta_f(t) = 0.25$ for $0 < t \leq 13$ s, $\zeta_f(t) = 0.18$ for $13 < t \leq 25$ s, and $\zeta_f(t) = 0.8$ for $25 < t \leq 40$ s. Corresponding error measures are $\epsilon_q = 0.0258$, $\epsilon_\omega = 0.0259$, and $\epsilon_\zeta = 0.0375$. Frequency of 0.12 Hz is selected for the high-pass filter.**
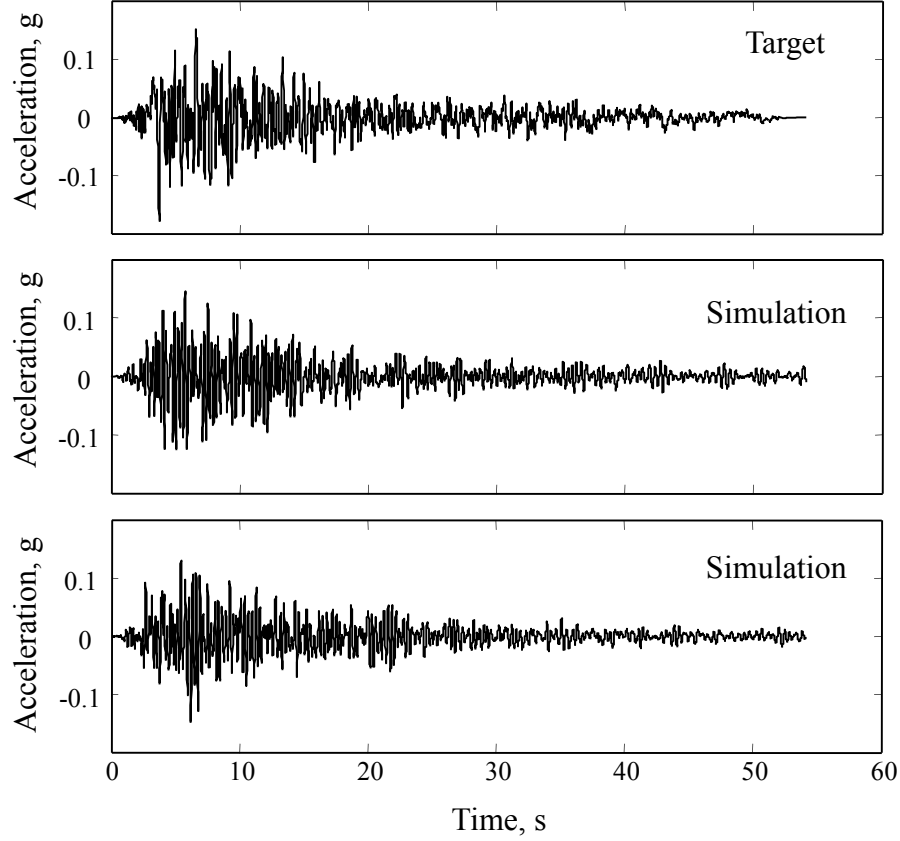
Fig. 3.10 **Target accelerogram and two simulations using the fitted model. Target accelerogram is component 111 of the 1952 Kern County earthquake at the Taft Lincoln School station. Corresponding model parameters are $\alpha_1 = 0.0585$ g, $\alpha_2 = 0.235$ s^{-1}, $\alpha_3 = 0.591$, $T_0 = 0.0001$ s, $T_1 = 3.8$ s, and $T_2 = 8.6$ s for a piece-wise modulating function and $\omega_0 = 24.8$ rad/s and $\omega_n = 13.5$ rad/s for a linear filter frequency function. Variable filter damping ratio is used where $\zeta_f(t) = 0.2$ for $0 < t \leq 3$ s, $\zeta_f(t) = 0.1$ for $3 < t \leq 14$ s, and $\zeta_f(t) = 0.13$ for $14 < t \leq 54.2$ s. Corresponding error measures are $\epsilon_q = 0.0301$, $\epsilon_\omega = 0.0111$, and $\epsilon_\zeta = 0.0381$. Frequency of 0.05 Hz is selected for the high-pass filter.**
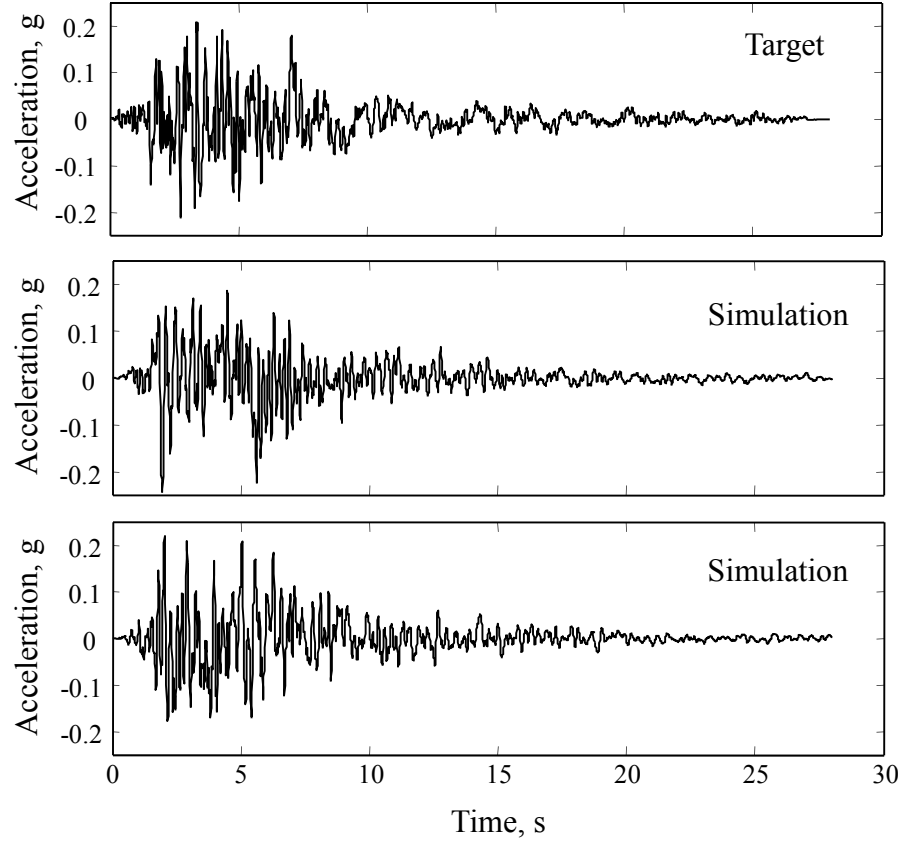
Fig. 3.11 **Target accelerogram and two simulations using the fitted model. Target accelerogram is component 090 of the 1971 San Fernando earthquake at the LA Hollywood Stor Lot station. Corresponding model parameters are $\alpha_1 = 0.0821$ g, $\alpha_2 = 0.369$ s^{-1}, $\alpha_3 = 0.680$, $T_0 = 0.002$ s, $T_1 = 2.0$ s, and $T_2 = 5.7$ s for a piece-wise modulating function and $\omega_0 = 30.2$ rad/s and $\omega_n = 16.5$ rad/s for a linear filter frequency function. Variable filter damping ratio is used where $\zeta_f(t) = 0.4$ for $0 < t \leq 14$ s and $\zeta_f(t) = 0.45$ for $14 < t \leq 28$ s. Corresponding error measures are $\epsilon_q = 0.0155$, $\epsilon_\omega = 0.0494$, and $\epsilon_\zeta = 0.0309$. Frequency of 0.2 Hz is selected for the high-pass filter.**
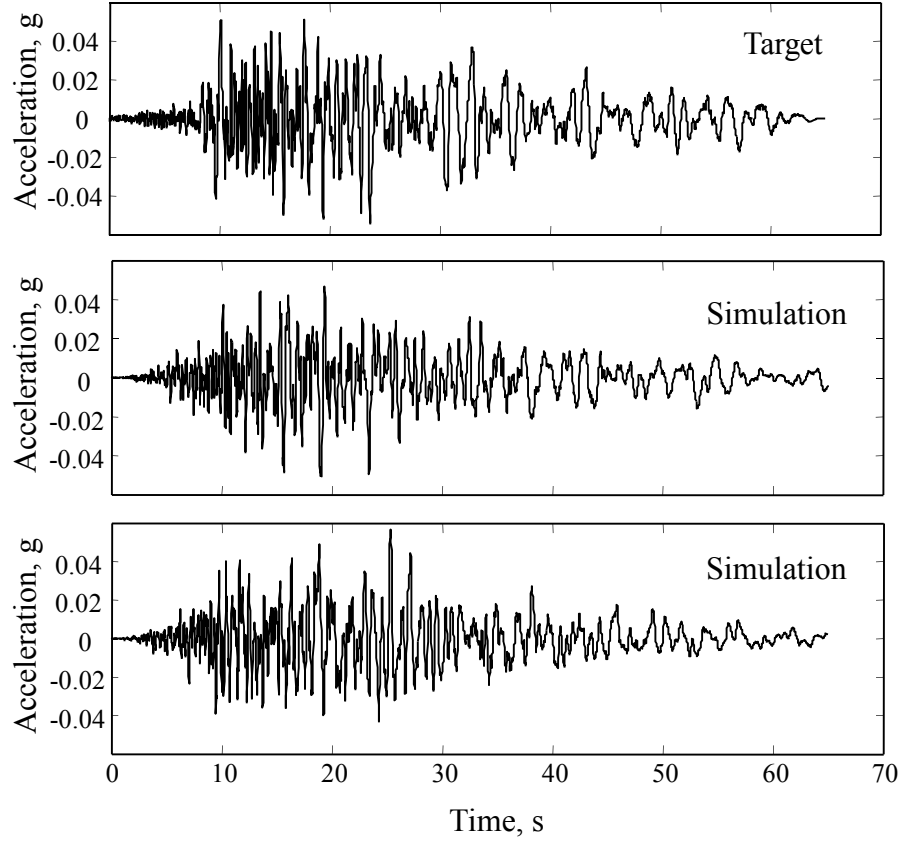
Fig. 3.12 **Target accelerogram and two simulations using the fitted model. Target accelerogram is component 090 of the 1994 Northridge earthquake at the Ventura Harbor & California station. Corresponding model parameters are $\alpha_1 = 0.0201\,\text{g}$, $\alpha_2 = 0.0046\,\text{s}^{-1}$, $\alpha_3 = 1.53$, $T_0 = 0$ s, $T_1 = 11.3$ s, and $T_2 = 17.3$ s for a piece-wise modulating function. Instead of a linear function, an exponentially decreasing function is selected for the filter frequency $\omega_f(t) = 55.1\exp\left(-0.288 t^{0.554}\right)$. Variable filter damping ratio is used where $\zeta_f(t) = 0.5$ for $0 < t \le 12$ s, $\zeta_f(t) = 0.4$ for $12 < t \le 32$ s, and $\zeta_f(t) = 0.99$ for $32 < t \le 65$ s. Corresponding error measures are $\epsilon_q = 0.0389$, $\epsilon_\omega = 0.0102$, and $\epsilon_\zeta = 0.147$. Frequency of 0.2 Hz is selected for the high-pass filter.**

4 Estimation of Model Parameters for Specified Earthquake and Site Characteristics

4.1 INTRODUCTION

In the previous chapter, parameters of the proposed stochastic ground motion model were identified for a target accelerogram by matching the evolutionary statistical characteristics of the model to those of the target accelerogram. Once the model parameters are identified, it is easy to produce an ensemble of ground motion realizations as described in Section 3.3. It is important to recall that this ensemble of ground motion realizations is created from one specific set of model parameters that corresponds to the target accelerogram. A previously recorded ground motion that is considered as the target accelerogram is only one sample observation of all the possible ground motions that can occur at a site of interest from an earthquake of specified characteristics. Therefore, it is more realistic to treat the model parameters that define the target accelerogram as random variables when simulating ground motions for specified earthquake and site characteristics.

To illustrate the above concept, Figure 4.1 shows a real recorded motion and eight simulated motions. The simulated motions on the left are generated using model parameters identical to those of the recorded motion (according to the methods described in Chapter 3). Observe that even though they are different, they all have nearly identical overall characteristics, e.g., intensity, duration, frequency content. The simulated motions on the right are generated using different model parameters that may result from the earthquake and site characteristics that produced the recorded motion. The simulation details are presented in Chapter 5. The variability observed in the intensity, duration and frequency content of these motions is significantly more than that of the set on the left and is representative of the natural variability observed in recorded ground motions for a specified set of earthquake and site characteristics. Such suite of simulated motions (i.e., on the right side of Fig. 4.1) is of interest in performance-based earthquake

engineering (PBEE). The question is: *how do we predict possible realizations of the model parameters for specified earthquake and site characteristics?* This chapter focuses on answering this question.

As reported in Chapter 1, many ground motion models have been developed in the past. The vast majority of these models limit their scope to generating synthetics similar to a target recorded motion. As a result, all the generated synthetic motions with these models correspond to identical model parameters and do not provide a realistic representation of ground motion variability for a specified set of earthquake and site characteristics. In this study, we go one step further by relating the parameters of our model to the earthquake and site characteristics. Furthermore, by accounting for the uncertainty in the model parameters, i.e., assuming that the model parameters for given earthquake and site characteristics are random, we are able to reproduce in the synthetics the variability present in real ground motions, which has been lacking in previous models. There have been a few exceptions in the literature including the paper by Pousse et al. (2006), in which the parameters of an improved version of the model by Sabetta and Pugliese (1996) are fitted to the K-Net Japanese database, and the work by Alamilla et al. (2001), in which the parameters of a model similar to that proposed by Yeh and Wen (1989) were fitted to a database of ground motions corresponding to the subduction zone lying along the southern coast of Mexico. In both cases, the model parameters are randomized to achieve the variability present in real ground motions. Stafford et al. (2009) also relate the parameters of their model to the earthquake and site characteristics, but their model does not account for spectral nonstationarity of ground motion. It is noted that some recent seismological models do properly account for the variability in ground motions. Typically, this is done by varying the values of source parameters, as in Liu et al. (2006), Hutchings et al. (2007), Causse et al. (2008), and Ameri et al. (2009). However, these models are difficult to use in engineering practice due to the unavailability of the model source parameters during the structural design process.

This chapter focuses on developing empirical predictive equations for the stochastic model parameters in terms of earthquake and site characteristics. The stochastic ground motion model is fitted to a large number of accelerograms with known earthquake and recording site characteristics, resulting in a database of the model parameters for the given characteristics. By regressing the former against the latter, predictive relations for the model parameters in terms of the earthquake and site characteristics are developed. For a specified set of earthquake and site

characteristics, an "average" ground motion may then be generated by using the mean model parameter values, while an entire suite of motions can be generated by using other possible values of model parameters obtained from randomizing the regression error. This process can be repeated for different sets of earthquake and site characteristics, thus generating an entire suite of artificial ground motions that are appropriate for design or analysis in PBEE without any need for previously recorded motions.

The methodology for constructing predictive relations for the model parameters is quite general and is proposed at the beginning of this chapter. This methodology is then demonstrated by using a database of strong ground motions on stiff soil, which is a subset of the Next Generation Attenuation (NGA) database. Predictive equations are constructed for each model parameter in terms of the fault mechanism, earthquake magnitude, source-to-site distance, and local soil type. Marginal and conditional distributions are assigned to each model parameter. Finally correlations between the model parameters are determined empirically. The results of this chapter are used in Chapter 5 for random generation of model parameters and simulation of a suite of synthetic ground motions for specified earthquake and site characteristics, which is ultimately of interest in PBEE.

4.2   METHODOLOGY FOR DEVELOPING PREDICTIVE EQUATIONS

For PBEE our interest is in simulating ground motions for a given set of earthquake and site characteristics, i.e., fault mechanism, earthquake magnitude, source-to-site distance, local soil type. In this context, the parameters identified for a specific recorded ground motion are regarded as a single realization of the parameter values that could arise from earthquakes of similar characteristics on similar sites. To develop a predictive model of the ground motion, it is necessary to relate the model parameters to the earthquake and site characteristics. For this purpose, we identify the model parameters for a dataset of recorded ground motions with known earthquake and site characteristics. Using this data, regression models are then developed to relate the stochastic model parameters to the earthquake and site characteristics.

It is a common practice in developing predictive equations of ground motion intensities to work with the logarithm of the data to satisfy the normality requirement of the regression error. This transformation implies the lognormal distribution for the predicted intensity. In our

case, the data for several of the model parameters show distinctly non-lognormal behavior, including negative values and bounds, which cannot be addressed by a logarithmic transformation. To account for this behavior, each model parameter is assigned a marginal probability distribution based on its observed histogram. This distribution is then used to transform the data to the normal space, where empirical predictive equations are constructed. In effect, this is a generalization of the logarithmic transformation.

Let θ_i denote the ith parameter of the stochastic ground motion model, $i = 1, \ldots, n_p$, where n_p is the total number of parameters, and let $F_{\theta_i}(\theta_i)$ denote the marginal cumulative distribution function fitted to the data for θ_i. The marginal transformations:

$$v_i = \Phi^{-1}\left[F_{\theta_i}(\theta_i)\right] \quad i = 1, \ldots, n_p \tag{4.1}$$

where $\Phi^{-1}[.]$ denotes the inverse of the standard normal cumulative distribution function, then define a set of standard normal random variables v_i. Relations of the form in (4.1) transform the data on θ_i to data on v_i, which are then regressed against variables defining the earthquake and site characteristics. This leads to predictive equations of the form:

$$v_i = \mu_i(\text{Earthquake}, \text{Site}, \boldsymbol{\beta}_i) + e_i \quad i = 1, \ldots, n_p \tag{4.2}$$

where μ_i is a selected functional form for the conditional mean of v_i given the earthquake and site characteristics, $\boldsymbol{\beta}_i$ is the vector of regression coefficients, and e_i represents the regression error that has zero mean and is normally distributed. Another important piece of information for predicting model parameters is the correlation between v_i and v_j for $i \neq j$, which is the same as the correlation between the corresponding e_i and e_j. These correlations are determined empirically. Additionally, it is assumed that the error terms e_i are jointly normally distributed. Under this assumption, knowledge of the predictive equations of the form in (4.2) and the correlation coefficients is sufficient to simulate random samples of variables v_i, $i = 1, \ldots, n_p$, for specified earthquake and site characteristics (see Chapter 5 for simulation details). Equations (4.1) are then used in reverse to determine the corresponding simulations of the model parameters in the physical space.

The following sections present the specifics of the stochastic ground motion model used in this chapter; propose a simplified method of parameter identification that is appropriate for analyzing a large database of recorded motions; and elaborate on the selected ground motion database, the fitted distributions $F_{\theta_i}(\theta_i)$, the functional forms of the predictive Equations (4.2),

the method of analysis used to estimate the regression coefficients and the error variance in (4.2), and the correlation analysis between the transformed model parameters v_i.

4.3   STOCHASTIC GROUND MOTION MODEL

The stochastic ground motion model proposed in Chapter 2 is employed. The stochastic process $x(t)$ is obtained by time-modulating a normalized filtered white-noise process with the filter having time-varying parameters. It is formulated according to (2.5) in the continuous form and according to (2.12) in the discrete form. The simulated process is eventually high-pass filtered according to (2.28) to obtain $\ddot{z}(t)$, which represents the acceleration time-history of the earthquake ground motion. This high-pass filtering does not have a significant influence on the statistical characteristics of the process. Therefore, when fitting to a recorded motion, as done in Chapter 3, the process $x(t)$ rather than $\ddot{z}(t)$ is used. $x(t)$ is constructed by multiplication of the deterministic time-modulating function $q(t, \boldsymbol{\alpha})$, and a unit-variance process that is obtained as the response of a linear filter defined by the IRF $h[t - \tau, \boldsymbol{\lambda}(\tau)]$ to a white noise excitation. The functional forms and parameters of $q(t, \boldsymbol{\alpha})$ and $h[t - \tau, \boldsymbol{\lambda}(\tau)]$ separately control the temporal and spectral characteristics of the ground motion process.

For the present study, the gamma modulating function according to (2.23) is used. The set of parameters for this model is $\boldsymbol{\alpha} = (\alpha_1, \alpha_2, \alpha_3, T_0)$. The filter IRF corresponding to (2.24), which represents the pseudo-acceleration response of a single-degree-of-freedom linear oscillator, is employed. The set of time-varying parameters for the filter is $\boldsymbol{\lambda}(\tau) = [\omega_f(\tau), \zeta_f(\tau)]$. The subsequent sections provide more details on selection and identification of these model parameters.

4.3.1   Model Parameters

Since we wish to relate the parameters of the modulating function to the earthquake and site characteristics of recorded motions, it is desirable that these parameters be defined in terms of ground motion properties that have physical meaning. For this reason, $(\alpha_1, \alpha_2, \alpha_3)$ are related to three physically based variables $(\bar{I}_a, D_{5-95}, t_{mid})$. The first variable, $\bar{I}_a$, represents the expected

Arias intensity (Arias, 1970) of the acceleration process $x(t)$ — a measure of the total energy contained in the motion — and is defined as

$$\bar{I}_a = \mathrm{E}\left[\frac{\pi}{2\mathrm{g}}\int_0^{t_n} x^2(t)\mathrm{d}t\right] = \frac{\pi}{2\mathrm{g}}\int_0^{t_n} q^2(t,\boldsymbol{\alpha})\mathrm{d}t \tag{4.3}$$

where g is the gravitational acceleration and t_n denotes the total duration of the motion. The second equality above is obtained by changing the orders of the expectation and integration operations and noting that $q^2(t,\boldsymbol{\alpha})$ is the variance of the process $x(t)$ [see (2.4)]. D_{5-95} represents the effective duration of the motion. Here, motivated by the work of Trifunac and Brady (1975), we define D_{5-95} as the time interval between the instants at which the 5% and 95% of the expected Arias intensity are reached. This definition is selected, since it relates to the strong shaking phase of the time-history, which is critical to nonlinear response of structures. t_{mid} is the time at the middle of the strong shaking phase. Based on investigation of many ground motions in our database, we have selected t_{mid} as the time at which 45% level of the expected Arias intensity is reached. Figure 4.2 illustrates identification of the above three parameters for an acceleration time-history.

The gamma probability density function (PDF) (Ang and Tang 2006) is written as

$$f_T(t,a,b) = \frac{a^b}{\Gamma(b)}t^{b-1}e^{-at} \quad \text{if} \quad t \geq 0$$
$$= 0 \quad \text{otherwise} \tag{4.4}$$

where a and b are the parameters of the distribution and $\Gamma(b) = \int_0^\infty t^{b-1}e^{-t}\mathrm{d}t$ is the gamma function with $b > 0$. For the selected modulating function, $q^2(t,\boldsymbol{\alpha})$ is proportional to a shifted gamma PDF having parameter values $a = 2\alpha_3$ and $b = 2\alpha_2 - 1$. One can write

$$q^2(t,\boldsymbol{\alpha}) = \alpha_1^2(t - T_0)^{(2\alpha_2-1)-1}e^{-2\alpha_3(t-T_0)} \quad \text{if} \quad t \geq T_0$$
$$= 0 \quad \text{otherwise} \tag{4.5}$$

Let t_p represent the p-percentile variate of the gamma cumulative distribution function. Then t_p is given in terms of the inverse of the gamma cumulative distribution function at probability value $p\%$. Since these percentages are not affected by scaling of the gamma probability density function, it follows that t_p is uniquely given in terms of the parameters α_2 and α_3 and the probability $p\%$. We can write

$$D_{5-95} = t_{95} - t_5 \tag{4.6}$$

$$t_{mid} = t_{45} \tag{4.7}$$

For given values of D_{5-95} and t_{mid}, parameters α_2 and α_3 can be numerically computed from the above two equations. In this study, a nonlinear optimization approach is employed to solve (4.6) and (4.7) for α_2 and α_3, which requires initial guesses for optimized values of the two parameters. We have found that a good initial guess is obtained by setting the mode of the gamma distribution, $(b-1)/a$, equal to t_{mid}, which results in solving (4.6) for one variable only. This approach is computationally efficient and is made possible due to the selected functional form of the modulating function. The remaining parameter, α_1, is directly related to the expected Arias intensity. Substituting (4.5) into (4.3) gives

$$
\begin{aligned}
\bar{I}_a &= \frac{\pi}{2g} \int_0^{t_n} \alpha_1^2 (t - T_0)^{(2\alpha_2 - 1) - 1} e^{-2\alpha_3 (t - T_0)} dt \\
&= \frac{\pi}{2g} \alpha_1^2 \int_0^{t_n} (t - T_0)^{2\alpha_2 - 2} e^{-2\alpha_3 (t - T_0)} dt \\
&= \frac{\pi}{2g} \alpha_1^2 \frac{\Gamma(2\alpha_2 - 1)}{(2\alpha_3)^{2\alpha_2 - 1}}
\end{aligned}
\tag{4.8}
$$

For simulation purposes, T_0 is assumed to be 0. Note that the expression inside the integral of the second equality above is proportional to the gamma PDF. Assuming that t_n, the total duration of motion, is sufficiently long for the integral of the PDF from 0 to t_n to be effectively equal to unity, the last equality is obtained, which results in an analytical expression for α_1:

$$\alpha_1 = \sqrt{\frac{2g}{\pi} \bar{I}_a \frac{(2\alpha_3)^{2\alpha_2 - 1}}{\Gamma(2\alpha_2 - 1)}} \tag{4.9}$$

After estimating α_2 and α_3, (4.9) is used to compute α_1 for a given value of $\bar{I}_a$. In the remainder of this study, we work only with $(\bar{I}_a, D_{5-95}, t_{mid})$ as the modulating function parameters. Any simulated values of these parameters are used in (4.6), (4.7), and (4.9) to back-calculate the corresponding values of $(\alpha_1, \alpha_2, \alpha_3)$, which are then used to compute the modulating function.

For the filter frequency a linear function is adopted. However, instead of representing this function with the two parameters ω_0 and ω_n as was done in (2.25), we represent it as

$$\omega_f(t) = \omega_{mid} + \omega'(t - t_{mid}) \tag{4.10}$$

Here, ω_{mid} represents the filter frequency at t_{mid}, and ω' represents the rate of change of the filter frequency with time. Later, in Chapter 5, limits will be assigned to (4.10) to avoid simulating unreasonably high or low frequencies. For the filter damping ratio a constant value,

ζ_f, as in (2.26) is employed. This is done for simplicity and convenience considering that the stochastic model must be fitted to a large number of recorded motions. Observed invariance of the bandwidth parameter for most recorded motions motivates this simplifying approximation.

In summary, the physically based parameters $(\bar{I}_a, D_{5-95}, t_{mid})$ and $(\omega_{mid}, \omega', \zeta_f)$ completely define the time modulation and the evolutionary frequency content of the nonstationary ground motion model. Our simulation procedure is based on generating samples of these parameters for given earthquake and site characteristics.

4.3.2   Identification of Model Parameters for a Target Accelerogram

As described in Chapter 3, given a target accelerogram, the model parameters are identified by matching the properties of the recorded motion with the corresponding statistical measures of the process. The physically based modulating function parameters $(\bar{I}_a, D_{5-95}, t_{mid})$ are naturally matched with the Arias intensity, the effective duration (the time between 5% and 95% levels of Arias intensity), and the time to the middle of the strong shaking phase (time to the 45% level of Arias intensity) of the recorded motion, respectively. In determining t_{mid} for a recorded accelerogram, sometimes it is necessary to make a time shift. This is because the zero point along the time axis of a record is rather arbitrary. (There is no standard as to where to set the initial point of an acceleration signal.) In fact, some records in the NGA database have long stretches of zero motion in their beginning. Four such examples are provided in Figure 4.3. In such cases, a better fit is achieved by identifying an additional parameter, $T_0 \geq 0$. This is done by replacing (4.7) with

$$D_{5-45} = t_{45} - t_5 \tag{4.11}$$

where D_{5-45} is the time interval between 5% and 45% levels of Arias intensity of the record. Similar to the case for $T_0 = 0$, solutions to α_2 and α_3 are obtained by nonlinear optimization on (4.6) and (4.11). A good initial guess is obtained by assuming equality between the mode of the gamma distribution, $(b - 1)/a$, and $D_{0.05-45}$, which results in solving (4.6) for one variable only. $D_{0.05-45}$ represents the time between 0.05% to 45% levels of Arias intensity of the record. 0.05%, which is a small percentile effectively denoting the beginning of the motion, is chosen to avoid the long stretches of zero intensity observed at the beginning of records, which are not of interest in simulation. After identification of $(\alpha_1, \alpha_2, \alpha_3)$, the 45-percentile variate of the

74

corresponding gamma distribution, t_{45}, is calculated. Finally, t_{mid} is determined by (4.7) and T_0, if desired, is computed by

$$T_0 = D_{0-45} - t_{45} \qquad (4.12)$$

As mentioned earlier, the model parameters $(\omega_{mid}, \omega', \zeta_f)$ control the evolving predominant frequency and bandwidth of the process. As a measure of the evolving predominant frequency of the recorded motion, as in Chapter 3, we consider the rate of zero-level up-crossings, and as a measure of its bandwidth, we consider the rate of negative maxima (peaks) and positive minima (valleys). In Chapter 3, the evolution of the predominant frequency was determined by minimizing the difference between the cumulative mean number of zero-level up-crossings of the process in time and the cumulative count of zero-level up-crossings of the recorded accelerogram. The bandwidth parameter, ζ_f, was determined by minimizing the difference between the mean rate of negative maxima and positive minima and the observed rate of the same in the recorded accelerogram. The process required an iterative scheme, since the predominant frequency and bandwidth of the process are interrelated. That method is ideal if the purpose is to closely match the statistical characteristics of a single target accelerogram. For the purpose of identifying the model parameters for a large number of recorded ground motions, such high level of accuracy is not necessary. Instead, the following simpler method is adopted to reduce computational effort, while providing sufficient accuracy.

It is well known that the mean zero-level up-crossing rate of the stationary response of a second-order filter (i.e., the filter used in this study with time-invariant parameters) to a white-noise excitation is equal to the filter frequency (Lutes and Sarkani 2004). This motivates the idea of directly approximating the filter frequency $\omega_f(t)$ by the rate of change of the cumulative count of zero-level up-crossings of the target accelerogram (see Fig. 4.4a). In order to identify the two parameters ω_{mid} and ω' for a given record, a second-order polynomial is fitted to the cumulative count of zero-level up-crossings of the accelerogram. This is done in a least-squares sense at equally spaced time points starting from the time at 1% level of Arias intensity to the time at 99% level of Arias intensity (a total of 9 points are selected). The fitted polynomial is then differentiated to obtain a linear estimate of the filter frequency as a function of time. The value of this line at t_{mid} represents the estimate of ω_{mid}, and its slope represents the estimate of ω'. Figure 4.4a demonstrates this fitting process for the component 090 of the accelerogram recorded at the Silent Valley – Poppet Flat station during the 1992 Landers earthquake.

Comparisons of the estimated filter frequency with those computed by the more exact method described in Chapter 3 for several accelerograms revealed that the method is sufficiently accurate for the intended purpose.

To estimate the filter damping ratio, the cumulative number of negative maxima plus positive minima for the target accelerogram is determined. This value is compared with the estimated averages of the same quantity for sets of 20 simulations of the theoretical model with the already approximated filter frequency and the set of damping values $\zeta_f = 0.1, 0.2, ..., 0.9$ (see Fig. 4.4b). Interpolation between the curves is used to determine the optimal value of ζ_f that best matches the curve for the target accelerogram. This is done by calculating the cumulative difference between the target and simulated curves, $\int_0^{t_n}(\text{target} - \text{average of 20 simulations for } \zeta_f)\mathrm{d}t$ for each value of ζ_f, and interpolating to find the ζ_f value that gives a zero cumulative difference. When ζ_f is less than 0.1, interpolation is performed by assuming a zero damping ratio for a curve that falls on the horizontal axis (i.e., representing a motion with zero numbers of negative maxima and positive minima). For this analysis, only the time interval between 5% to 95% levels of Arias intensity is considered, where it is more likely for ζ_f to remain constant. This procedure is a simplification of the more refined fitting method used in Chapter 3, as it neglects the influence of the filter damping on the predominant frequency. Figure 4.4b shows application of this method to the Landers earthquake record mentioned above.

It is important to note that the modulating function has no influence on the zero-level up-crossings, or the number of negative maxima and positive minima of the process. This facilitates estimation of the filter parameters after determining the modulating function parameters.

4.4   STRONG MOTION DATABASE

The strong motion database used in this study is a subset of the PEER NGA (Pacific Earthquake Engineering Research Center: Next Generation Attenuation of Ground Motions Project; see http://peer.berkeley.edu/smcat/.) database, and a subset of the data used in the development of the Campbell-Bozorgnia NGA ground motion model (Campbell and Bozorgnia 2008). These data were collected for the Western United States (WUS), but some well-recorded, large-

magnitude earthquakes from other regions, which were deemed to be applicable to the WUS, are also included (Abrahamson et al. 2008). As in Campbell and Bozorgnia (2008), the database employed in this study excludes aftershocks. Furthermore, the accelerograms in the database are representatives of "free-field" ground motions generated from shallow crustal earthquakes in active tectonic regions.

Earthquake and site characteristics:

The NGA database lists many characteristics of each earthquake and recording site. Considering the type of information that is commonly available to a design engineer, four parameters are selected for the present study: (F, M, R_{rup}, V_{S30}). F corresponds to the type of faulting with $F = 0$ denoting a strike-slip fault and $F = 1$ denoting a reverse fault (normal faults are not considered, since few records are available); M represents the moment magnitude of the earthquake; R_{rup} represents the closest distance from the recording site to the ruptured area, and V_{S30} represents the shear-wave velocity of the top 30 m of the site soil. Among these parameters, F and M characterize the earthquake source, R_{rup} characterizes the location of the site relative to the earthquake source, and V_{S30} characterizes the local soil conditions. These parameters are believed to have the most significant influences on the ground motion at a site and traditionally have been considered in predicting ground motion intensities. Additional parameters can be included to refine the predictive equations in future studies.

Enforced boundaries:

During the design process, two levels of ground motion are commonly considered: the service-level ground motion and the Maximum Considered Earthquake (MCE) ground motion (see, for example, the 2008 NEHRP provisions by the Building Seismic Safety Council (BSSC), or the report by Holmes et al. (2008) on seismic performance objectives for tall buildings). While response-spectrum analysis is sufficient to evaluate a structure for the service-level motion during which the structure is expected to remain elastic, response-history dynamic analysis is usually recommended or required to capture the likely nonlinear behavior of a structure subjected to the MCE motion. Many predictive models are available that provide the spectral ordinates of ground motion required for the response-spectrum analysis, including the recently

developed and commonly used NGA ground motion prediction equations by Abrahamson and Silva (2008), Boore and Atkinson (2008), Campbell and Bozorgnia (2008), Chiou and Youngs (2008), and Idriss (2008). Aiming at a predictive model of ground motion time-histories for the MCE event, we consider only earthquakes having $6.0 \leq M$. By limiting the database to large earthquakes, the predictive equations presented in this study are customized for earthquakes that are capable of damage and can cause nonlinear behavior in structures.

In the interest of separating the effects of near-fault ground motions, such as the directivity and fling effects, which could dominate the spectral content of the ground motion, only earthquakes with $10 \, \text{km} \leq R_{rup}$ are considered. A separate study for simulation of near-fault ground motions is under way. Furthermore, an upper limit $R_{rup} \leq 100 \, \text{km}$ is selected to exclude ground motions of small intensity.

In the interest of separating the effect of soil nonlinearity, which can also strongly influence the spectral content of the ground motion, the lower limit $600 \, \text{m/s} \leq V_{S30}$ is selected. For smaller V_{S30} values, one can generate appropriate motions at the firm soil layer and propagate through the softer soil deposits using standard methods of soil dynamics that account for the nonlinearity in the shear modulus and damping of the soil.

Database:

Figure 4.5 shows a summary of the selected earthquakes from the Campbell-Bozorgnia NGA database within the above-stated limits. These constraints reduced the data set used in the analysis to 31 pairs of horizontal recordings from 12 earthquakes for strike-slip type of faulting, and 72 pairs of horizontal recordings from 7 earthquakes for reverse type of faulting. The two horizontal components for each recording are orthogonal and along the "as-recorded" directions (as reported in the NGA database). Inclusion of both components not only doubles the sample size in the following statistical analysis ($31 \times 2 + 72 \times 2 = 206$ data points), but it also allows consideration of the correlations between the two components when simulating orthogonal horizontal components of ground motions (see Chapter 7). The selected earthquakes and the number of recordings for each earthquake are listed in Table 4.1. Observe that the number of recordings for each earthquake varies; this is accounted for in the regression analysis. Table 4.2 provides a list of the recording sites.

Even though the imposed constraints on the earthquake and site characteristics have reduced the number of recordings in our database, the resulting predictive equations are simpler (additional terms that reflect influences of low magnitude earthquakes, near-fault ground motions, distant earthquakes, and nonlinearity of soft soil are not required) and more reliable for the intended application of nonlinear response-history analysis for the MCE event. Note that the selection of the database in no way limits the methodology presented in this study.

4.5   IDENTIFIED MODEL PARAMETERS FOR THE SELECTED DATABASE

For each record in the ground motion database, the model parameters $(\bar{I}_a, D_{5-95}, t_{mid}, \omega_{mid}, \omega', \zeta_f)$ are identified according to the simplified methods described in Section 4.3.2. This results in observational data for the model parameters which allow us to investigate the statistical behavior of these parameters for the selected database. Numerical summaries of data are provided in Table 4.3 including the observed minimum and maximum values, sample mean, standard deviation, and coefficient of variation. These data are also graphically represented by their normalized frequency diagrams and empirical cumulative distribution functions, provided, respectively, in Figure 4.6 and Figure 4.7.

Arias intensity, I_a, has the largest coefficient of variation and ranges between 0.000275 to 2.07 s.g. with a mean of 0.0468 s.g. It is observed that the duration parameter D_{5-95} varies between 5.37 to 41.29 s, with a mean of 17.25 s. The parameter t_{mid} assumes values between a fraction of a second to 35.15 s with a mean of 12.38 s. For some records, t_{mid} is found to be greater than D_{5-95} due to a long stretch of low intensity motion in the beginning of the record. Owing to the choice of the modulating function and its flexible shape, this long stretch may be replicated in the simulated motions, if desired.

It is interesting to note that the observed predominant frequency at the middle of strong shaking, $\omega_{mid}/2\pi$, ranges from 1.31 to 21.6 Hz for the records in the data set, with a mean value of 5.87 Hz. The fact that only rock and stiff soils are considered is the reason for this relatively high mean value. It is also interesting to note that $\omega'/2\pi$ is more likely to be negative than positive (see the middle bottom graph in Fig. 4.6), i.e., the predominant frequency of the ground motion during the strong shaking phase is more likely to decrease than increase with time. This is consistent with our expectation. However, a small fraction of the recorded motions

in the database shows positive but small $\omega'/2\pi$ values (i.e., the target plot similar to the one in Figure 4.4a shows a slightly positive or, in rare cases, irregular curvature). Finally, the observed filter damping ratio ζ_f, which is a measure of the bandwidth of the ground motion process, is found to range from 0.027 to 0.767 with a mean of 0.213.

4.5.1 Distribution Fitting

After identifying the model parameter values by fitting to each recorded ground motion in the database, a probability distribution is assigned to the sample of values for each parameter. The form of this distribution is inferred by visually inspecting the corresponding histogram and examining the fit to the corresponding empirical cumulative distribution function (CDF). The parameters of the chosen probability distribution are then estimated by the method of maximum likelihood. Finally the fit is examined by the Kolmogorov-Smirnov (K-S) goodness-of-fit test to identify the optimal distribution when alternative options are available.

Figure 4.6 shows the fitted probability density functions (PDFs) superimposed on the normalized frequency diagrams of the model parameters. Fitted distributions are listed in Table 4.4. As commonly assumed in the current practice, the data for I_a is found to be well represented by the lognormal distribution ($\ln(I_a)$ is normally distributed). But other model parameters show distinct differentiation from the lognormal distribution. In particular, a Beta distribution with specified boundaries is assigned to the parameters D_{5-95}, t_{mid}, and ζ_f, while the frequency parameter $\omega_{mid}/2\pi$ is well represented by a gamma distribution. For $\omega'/2\pi$, the fitted distribution is a two-sided truncated exponential with the PDF:

$$f_{\omega'/2\pi}(\omega'/2\pi) = \begin{cases} 4.85\exp(6.77\,\omega'/2\pi) & -2 < \omega'/2\pi < 0 \\ 4.85\exp(-17.10\,\omega'/2\pi) & 0 < \omega'/2\pi < 0.5 \\ 0 & \text{otherwise} \end{cases} \qquad (4.13)$$

Rounded bounds for the corresponding distributions are provided in Table 4.4. These bounds are assigned to reflect the physical limitations of a model parameter (e.g., frequency cannot be negative or damping ratio cannot be greater than 1) as well as the limits of the observed data.

The K-S test, a widely used goodness-of-fit test that compares the empirical CDF with the CDF of an assumed theoretical distribution, is performed for each model parameter and its assigned distribution. At the significance level of 0.05, the null hypothesis that the observed data

for a model parameter follow the assigned distribution was rejected for $\bar{I}_a$, D_{5-95}, and ω'. At the significance level of 0.01, the null hypothesis was only rejected for $\bar{I}_a$, and ω'. Figure 4.7 shows the fit of the CDFs for the assigned distributions to the empirical CDFs of the computed samples of model parameters. It is observed that the fit is good for all the model parameters, which suggests the appropriateness of the assigned distributions for our purposes regardless of the results from the K-S test.

4.5.2   Transformation to the Standard Normal Space

Using the assigned marginal distributions, the identified model parameters for the database are transformed to the standard normal space according to (4.1). Figure 4.8 shows quantile plots of the data for each parameter, after transformation according to (4.1), versus the corresponding normal quantiles. It is observed that in most cases the data within the first and third quartiles (marked by hollow circles) closely follow a straight line, thus confirming that the transformed data follow the normal distribution reasonably well. The worst fit belongs to the Arias intensity, for which the commonly assumed lognormal distribution was adopted. We conclude that the selected distributions provide an effective means for transforming the data to the normal space. This process helps us satisfy the normality assumption underlying the regression analysis that is used to develop empirical predictive equations for the model parameters, as described in the next section.

4.6   EMPIRICAL PREDICTIVE EQUATIONS FOR THE MODEL PARAMETERS

In this section we construct empirical predictive equations for each of the model parameters in terms of the earthquake and site characteristic variables F, M, R_{rup}, and V_{S30} through regression analysis of the computed data set of fitted parameter values. The correlations between the predicted model parameters are also estimated. For simplicity of the notation, hereafter R_{rup} and V_{S30} are denoted as R and V.

4.6.1 Regression Analysis

As seen in Table 4.1, the database contains different numbers of records from different earthquakes. The records associated with each earthquake correspond to different source-to-site distances, soil types, or orientations (two orthogonal horizontal components are available for each recording station). While there are 48 records from the Chi-Chi earthquake, several earthquakes contribute only 2 records. This uneven clustering of data must be accounted for in the regression analysis, so that the results are not overly influenced by an individual earthquake with many records. Furthermore, each earthquake is expected to have its own particular effect on its resulting ground motions. This effect is random and varies from earthquake to earthquake. Therefore, the data corresponding to ground motions from the same earthquake have a common factor and are correlated, while the data corresponding to different earthquakes are statistically independent observations. To address these issues, a random-effects regression analysis method is employed. This method effectively handles the problem of weighing observations and, unlike ordinary regression analysis, assumes that data within earthquake clusters are statistically dependent. We employ the random-effects regression model in the form:

$$v_{i,jk} = \mu_i\left(F_j, M_j, R_{jk}, V_k, \boldsymbol{\beta}_i\right) + \hat{\eta}_{i,j} + \hat{\epsilon}_{i,jk} \tag{4.14}$$

where $i = 1, \dots, 6$ indexes the model parameters, $j = 1, \dots, 19$ indexes the earthquakes, and $k = 1, \dots, n_j$ indexes the records associated with the jth earthquake with n_j denoting the number of records from that earthquake. The transformed model parameter, $v_{i,jk}$, is chosen as the response parameter of the regression. μ_i and $\boldsymbol{\beta}_i$ are as defined in (4.2). The former is more precisely denoted as $\mu_{v_i|F,M,R,V}$, the predictive (conditional mean) value of v_i for given F, M, R, and V. Having random effects necessitates a more careful definition of the residuals. Therefore, the total residual, defined as the difference between the observed and predicted values of the response variable, is represented as the sum of $\hat{\eta}_{i,j}$ and $\hat{\epsilon}_{i,jk}$, referred to, respectively, as the inter-event (random effect for the jth earthquake) and intra-event (the random effect for the the kth record of jth earthquake) residuals. The superposed hats indicate that these residuals are observed values of independent, zero-mean, normally distributed error terms η_i and ϵ_i with variances τ_i^2 and σ_i^2, respectively. With this arrangement, the total error for the ith model parameter is a zero-mean normally distributed random variable with variance $\tau_i^2 + \sigma_i^2$.

One may argue that since the two horizontal components of each record are correlated, an additional random effect term needs to be included in (4.14). This is not necessary because the two components are included for all the records of the database. In effect, the dependence between the pairs of components at each site is accounted for through the random effect term for all recordings of the same earthquake. Therefore, the resulting parameter estimates are unbiased. Eventually, the resulting sample correlations between the data corresponding to the two horizontal components of ground motion at each site provide a means for simulating pairs of ground motion components at a site of interest, as described in Chapter 7.

For each model parameter, a predictive equation of the form in (4.14) is constructed by selecting an appropriate functional form for μ_i and estimating the regression coefficients, $\boldsymbol{\beta}_i$, and variance components, τ_i^2 and σ_i^2. The validity of these predictive equations are then examined by standard statistical methods including inspection of residual diagnostic plots, investigation of estimated variance components for alternative functional forms, and performing standard significance tests on the regression as well as on the regression parameters.

4.6.1.1 *Estimation of the Regression Coefficients and Variance Components*

Random-effects modeling is sometimes referred to as variance-components modeling because for a given database, in addition to estimating the regression coefficients $\boldsymbol{\beta}_i$, one needs to individually estimate the error variances τ_i^2 and σ_i^2. In this study we employ the maximum likelihood technique to obtain estimates of all the regression coefficients and variances at one step. Although this method requires the use of a numerical optimization technique, it is not computationally intensive and, unlike other proposed methods (e.g., Abrahamson and Youngs [1992]; Brillinger and Preisler [1985]), does not require a complicated algorithm that calculates the regression coefficients and the variance components in separate, iterative steps. The likelihood function is formulated by noting that the observed values of the total residuals are jointly normal with a zero mean vector and a block-diagonal covariance matrix. Therefore, for the ith model parameter, the likelihood function of the regression coefficients and variance components is equal to the joint normal PDF evaluated for the observed values of the total residuals. Writing the total residuals as $v_{i,jk} - \mu_i\big(F_j, M_j, R_{jk}, V_k, \boldsymbol{\beta}_i\big)$ and collecting the values for all j and k into vectors $\mathbf{v}_i$ and $\boldsymbol{\mu}_i(\boldsymbol{\beta}_i)$, the likelihood function assumes the form:

$$L(\boldsymbol{\beta}_i, \tau_i^2, \sigma_i^2) = \frac{1}{|\boldsymbol{\Sigma}_i|^{1/2}} \exp\left(-\frac{1}{2}[\mathbf{v}_i - \boldsymbol{\mu}_i(\boldsymbol{\beta}_i)]^{\mathrm{T}} \boldsymbol{\Sigma}_i^{-1}[\mathbf{v}_i - \boldsymbol{\mu}_i(\boldsymbol{\beta}_i)]\right) \qquad (4.15)$$

where $\boldsymbol{\Sigma}_i$ is the covariance matrix, which is expressed as a function of the variance components τ_i^2 and σ_i^2 in the form:

$$\boldsymbol{\Sigma}_i(\tau_i^2, \sigma_i^2) = \begin{bmatrix} \sigma_i^2 \mathbf{I}_{n_1} + \tau_i^2 \mathbf{1}_{n_1} & \mathbf{0} & \cdots & \mathbf{0} \\ \mathbf{0} & \sigma_i^2 \mathbf{I}_{n_2} + \tau_i^2 \mathbf{1}_{n_2} & \cdots & \mathbf{0} \\ \vdots & \vdots & \ddots & \vdots \\ \mathbf{0} & \mathbf{0} & \cdots & \sigma_i^2 \mathbf{I}_{n_{19}} + \tau_i^2 \mathbf{1}_{n_{19}} \end{bmatrix}_{N \times N} \qquad (4.16)$$

$$= \sigma_i^2 \mathbf{I}_N + \tau_i^2 \left(\sum_{j=1,\ldots,19}^{+} \mathbf{1}_{n_j}\right)$$

In the above, $\mathbf{I}_n$ is the identity matrix of size n, $\mathbf{1}_n$ is an $n \times n$ matrix of 1's, and N is the total number of observations (206 in the present case). $\mathbf{0}$ denotes a matrix of zero values. The first equality shows the overall appearance of the covariance matrix, while the second equally represents the more commonly used form of this matrix (e.g., Searle 1971). This compact form facilitates computer programming when maximizing the likelihood in (4.15). In this expression, Σ^+ indicates a direct sum[2] operation. The above formulation takes into consideration the fact that data corresponding to records from different earthquakes are uncorrelated (off-diagonal blocks are zero), data corresponding to the records from the same earthquake have correlation $\tau_i^2/(\tau_i^2 + \sigma_i^2)$ (off-diagonal elements of the diagonal blocks), and each data point is fully correlated with itself (diagonal elements equal $\tau_i^2 + \sigma_i^2$). The maximum likelihood estimates of the parameters $\boldsymbol{\beta}_i$, τ_i^2, and σ_i^2 for each transformed stochastic model parameter v_i are obtained by maximizing the function in (4.15) relative to these parameters. In this study, the MATLAB optimization toolbox is used for this purpose.

4.6.1.2 Model Testing: Computing Residuals

To assess the sufficiency of the selected functional forms for each predictive equation, one widely used approach is to inspect the residuals. The residuals are inspected to examine

---

[2] The direct sum of matrices of different sizes $\boldsymbol{A}_i, i = 1, \ldots, n$, is $\Sigma_{i=1,\ldots n}^{+} \boldsymbol{A}_i = \begin{bmatrix} \mathbf{A}_1 & \mathbf{0} & \cdots & \mathbf{0} \\ \mathbf{0} & \mathbf{A}_2 & \cdots & \mathbf{0} \\ \vdots & \vdots & \ddots & \vdots \\ \mathbf{0} & \mathbf{0} & \cdots & \mathbf{A}_n \end{bmatrix}.$

departures from normality. This is done by inspecting their histograms and Q-Q plots (Q stands for quantile). Furthermore, the plots of the residuals versus predictor variables (sometimes referred to as the residual diagnostic plots) are constructed and examined for any systematic patterns. This process, which is commonly known as analysis of residuals, requires calculation of the residuals which involves partitioning of the total residuals into inter-event and intra-event residuals. The inter-event residuals for each group (data corresponding to the records of a single earthquake) are estimated as

$$\hat{\eta}_{i,j} = \left(\frac{\tau_i^2}{\tau_i^2 + \frac{\sigma_i^2}{n_j}} \right) \times \left(\frac{\sum_{k=1}^{n_j} \left(v_{i,jk} - \mu_{v_{i,jk}|F_j,M_j,R_{jk},V_k} \right)}{n_j} \right)$$

(4.17)

$$= \frac{\tau_i^2 \sum_{k=1}^{n_j} (v_{i,jk} - \mu_{v_{i,jk}|F_j,M_j,R_{jk},V_k})}{n_j \tau_i^2 + \sigma_i^2}$$

where a shrinkage factor, reflecting the relative size of the variation in a group to the total variation in the database, is multiplied with the raw residual (i.e., average of the total residuals in a group) for that group. Observe that the shrinkage factor involves n_j, the number of records from earthquake j, and thereby adjusts for the sparseness of information from an earthquake with a small number of records. The second equality is the form that is commonly used in the literature for construction of ground motion predictive equations based on one of the earliest studies on this subject by Abrahamson and Youngs (1992). After calculating the inter-event residuals, the intra-event residuals are computed from

$$\hat{\epsilon}_{i,jk} = \left(v_{i,jk} - \mu_{v_{i,jk}|F_j,M_j,R_{jk},V_k} \right) - \hat{\eta}_{i,j}$$

(4.18)

where the expression in the parenthesis is the total residual.

4.6.1.3 Regression Results

For the sake of simplicity, and considering the relatively narrow range of earthquake magnitudes, a linear form of the regression equation for each transformed model parameter in terms of explanatory functions representing the type of faulting, earthquake magnitude, source-to-site distance and soil effect is employed. Various linear and nonlinear forms of the explanatory

functions were examined. In view of the availability of previous predictive formulas for Arias intensity and duration (e.g., Travasarou et al. [2003]; Abrahamson and Silva [1996]), more possible forms of the explanatory functions for these two parameters were investigated. For the other model parameters, alternative forms were considered only if the linear form revealed inadequate behavior of the residuals. For each model parameter, the relative performances of the resulting functional forms were assessed by inspecting the residuals and estimates of the variance components. Functional forms with smaller variances that demonstrated adequate behavior of the residuals (i.e., lack of systematic patterns in the plots of residuals versus the predictor variables) were selected. The resulting predictive equations are given by

$$v_1 = \beta_{1,0} + \beta_{1,1}(F) + \beta_{1,2}\left(\frac{M}{7.0}\right) + \beta_{1,3}\left(\ln\frac{R}{25\text{ km}}\right) + \beta_{1,4}\left(\ln\frac{V}{750\text{ m/s}}\right) + \eta_1 + \epsilon_1 \qquad (4.19)$$

$$v_i = \beta_{i,0} + \beta_{i,1}(F) + \beta_{i,2}\left(\frac{M}{7.0}\right) + \beta_{i,3}\left(\frac{R}{25\text{ km}}\right) + \beta_{i,4}\left(\frac{V}{750\text{ m/s}}\right) + \eta_i + \epsilon_i \quad i = 2, \dots 6 \qquad (4.20)$$

with the estimated regression parameters and standard deviations listed in Table 4.5. Standard significance tests verified the adequacy of the regression for each model parameter at the 90% and higher confidence levels (P-value for the F-test with the null hypothesis $\beta_{i,1} = \beta_{i,2} = \beta_{i,3} = \beta_{i,4} = 0$ is reported in Table 4.5). Furthermore, the regression coefficients $\beta_{i,1}, \beta_{i,2}, \beta_{i,3}$, and $\beta_{i,4}$ ($i = 1, \dots, 6$) were individually tested ($\beta_{i,0}$ was skipped because inclusion of a constant term in the regression formulation was not questioned); those with statistical significance at the 95% confidence level are shown in bold in Table 4.5. Furthermore, 95% confidence intervals for these regression coefficients are reported in Table 4.6. Inclusion of zero in a confidence interval indicates that the corresponding regression coefficient is not of much significance; this is consistent with the reported results in Table 4.5. Table 4.7 presents the P-values for the t-test with the null hypothesis $\beta_{i,j} = 0$ ($j = 1, \dots, 4$). The smaller this number is, the more significant the estimate of the corresponding coefficient in Table 4.5 is. In the subsequent analysis (Chapter 5), all the coefficients in Table 4.5 are used (regardless of the significance level) to randomly generate the model parameters and simulate ground motions.

The first three terms in (4.19) and (4.20) reflect the effect of the source that generates the seismic waves. For strike-slip type of faulting, $F = 0$, this effect is controlled by $\beta_{i,0}$ and $\beta_{i,2}$; while for reverse type of faulting, $F = 1$, it is controlled by $\beta_{i,0}$, $\beta_{i,1}$, and $\beta_{i,2}$. The fourth term reflects the effect of the travel path on waves (including geometric spreading and other

attenuating factors). The fifth term reflects the effect of the site conditions on the waves. The last two terms, random errors, represent the natural variability of the response parameters for the specified set of earthquake and site characteristics. The moment magnitude, source-to-site distance, and shear-wave velocity terms in the predictive Equations (4.19) and (4.20) have each been normalized by a typical value for engineering purposes. This normalization renders the regression coefficients dimensionless. Therefore, by simply comparing the estimated regression coefficients one can gain insight into the relative contribution of the earthquake and site characteristics to a model parameter.

The estimated parameters in Table 4.5 provide some interesting insight. For example, we observe that, as expected, Arias intensity tends to increase with magnitude and decrease with distance and site stiffness. The effective duration as well as t_{mid} tend to increase with magnitude and distance (more distant sites tend to experience longer motions) and tend to decrease with site stiffness. These findings are consistent with prior observations (Travasarou et al. [2003]); Abrahamson and Silva [1996]; Trifunac and Brady [1975]). The results also suggest that the effective duration and t_{mid} tend to be shorter for reverse faulting compared to strike-slip faulting. Furthermore, the results indicate that the predominant frequency at the middle of strong shaking tends to decrease with increasing magnitude and source-to-site distance, while the rate of change of the predominant frequency (which has a negative mean) tends to increase, i.e., a slower change with increasing magnitude and distance. Finally, the filter damping, which is a measure of the bandwidth of the ground motion, tends to increase with the moment magnitude and site stiffness and decrease with source-to-site distance. These trends are in general consistent with our expectations.

Figure 4.9 shows quantile plots of the residuals for each model parameter versus the corresponding normal quantiles (zero-mean with the estimated variance). It is observed that the data within the first and third quartiles (marked by hollow circles) closely follow a straight line, thus confirming that the residuals follow the normal distribution. Figure 4.10 shows the diagnostic scatter plots of the residuals versus the predictor variables. These plots show that the residuals are evenly scattered above and below the zero level with no obvious systematic trends. This implies lack of bias and a good fit of the regression models to the data.

As a further item of interest, Table 4.8 compares the estimated total variances obtained by the method described above with those obtained from a standard regression analysis according to

(4.2) that disregards the random effects in the data. As can be seen, the estimated variances tend to be larger with the random-effects regression. This is not surprising because by neglecting intra-event correlations, the standard regression assumes more information is available in the data than really is. By correctly accounting for the dependence between groups of observations, the random-effects regression method avoids underestimating the total error variance.

4.6.2 Correlation Analysis

For a given set of earthquake and site characteristics (F, M, R, V), the parameters v_i, $i = 1, ... ,6$, and, therefore, θ_i are correlated. These are estimated as the correlations between the total residuals $\hat{\eta}_i + \hat{\epsilon}_i$. Table 4.9 lists the correlation coefficients between the jointly normal variables v_i. Several of these estimated correlations provide interesting insight. Observe the negative correlation between v_1 and v_2 (corresponding to I_a and D_{5-95}). This is somewhat surprising, since one would expect a higher Arias intensity for a longer duration. However, since Arias intensity is more strongly related to the amplitude of the motion than to the duration (it is related to the square of the amplitude but linear in duration), this result may be due to the tendency of motions with high amplitude to have shorter durations. This negative correlation has also been observed by Trifunac and Brady (1975). Second, a strong positive correlation is observed between v_2 and v_3 (corresponding to D_{5-95} and t_{mid}), which is as expected. Interestingly, v_4 (corresponding to ω_{mid}) has negative correlations (though small) with all three previous parameters. Thus, higher intensity and longer duration motions tend to have lower predominant frequency. The correlation between v_4 and v_5 (corresponding to ω_{mid} and ω') is negative, indicating that motions with higher predominant frequency tend to have a faster decay of the frequency with time. Finally, the positive correlation between v_4 and v_6 (corresponding to ω_{mid} and ζ_f) suggests that high-frequency motions tend to have broader bandwidth.

4.7 SUMMARY

For the proposed stochastic ground motion model to be of practical use in earthquake engineering, empirical predictive equations are constructed for the model parameters in terms of earthquake and site characteristics. A general methodology for construction of empirical

predictive equations is presented which is demonstrated for a selected database of recorded ground motions. The database used in this study is a subset of the NGA database and is limited to strong motions on stiff soil with source-to-site distance greater than 10 km. Model parameters are identified for each accelerogram in the database by fitting the evolutionary statistical characteristics of the stochastic model to those of the recorded motion. For convenience in obtaining observational data, alternative model parameters are proposed and adjustments are made to the methods of parameter identification previously proposed in Chapter 3. By performing statistical analysis on the identified model parameters, marginal distributions are assigned to each parameter. Using these distributions the data are transformed to the standard normal space, where they are regressed on the earthquake and site characteristics resulting in predictive Equations (4.19) and (4.20) and corresponding parameter estimates shown in Table 4.5. The specifics of regression analysis are described in detail and the resulting regression models are tested. Correlation analysis is then performed to find dependencies among the model parameters. The results are presented in Table 4.9. The equations in (4.19) and (4.20), and the information provided in Tables 4.5 and 4.9 facilitate probabilistic prediction of the model parameters $(\bar{I}_a, D_{5-95}, t_{mid}, \omega_{mid}, \omega', \zeta_f)$ if the earthquake and site characteristics (F, M, R, V) are specified without any need for a previously recorded ground motion.

Table 4.1 Selected earthquakes from the Campbell-Bozorgnia NGA database, type of faulting, magnitude, and number of records.

Earthquake Number	Earthquake ID in NGA Database[3]	Earthquake Name	Faulting Mechanism	Moment Magnitude	Number of Records
1	0050	Imperial Valley-06	Strike-Slip	6.53	2
2	0064	Victoria, Mexico	Strike-Slip	6.33	2
3	0090	Morgan Hill	Strike-Slip	6.19	10
4	0125	Landers	Strike-Slip	7.28	4
5	0126	Big Bear-01	Strike-Slip	6.46	10
6	0129	Kobe, Japan	Strike-Slip	6.90	4
7	0136	Kocaeli, Turkey	Strike-Slip	7.51	4
8	0138	Duzce, Turkey	Strike-Slip	7.14	2
9	0140	Sitka, Alaska	Strike-Slip	7.68	2
10	0144	Manjil, Iran	Strike-Slip	7.37	2
11	0158	Hector Mine	Strike-Slip	7.13	16
12	0169	Denali, Alaska	Strike-Slip	7.90	4
13	0030	San Fernando	Reverse	6.61	14
14	0046	Tabas, Iran	Reverse	7.35	2
15	0076	Coalinga-01	Reverse	6.36	2
16	0101	N. Palm Springs	Reverse	6.06	12
17	0118	Loma Prieta	Reverse	6.93	28
18	0127	Northridge-01	Reverse	6.69	38
19	0137	Chi-Chi, Taiwan	Reverse	7.62	48

Table 4.2 Selected ground motion records, source-to-site distances, and shear-wave velocities of recording sites.

Earthquake Number	Record ID in NGA Database[4]	Station Name	Closest Distance to The Ruptured Area (km)	Shear-wave Velocity of Top 30 meters (m/s)
1	164	Cerro Prieto	15.19	659.6
2	265	Cerro Prieto	14.37	659.6
3	454	Gilroy – Gavilan Coll.	14.84	729.6
3	455	Gilroy Array #1	14.91	1428
3	471	San Justo Dam (L Abut)	31.88	622.86
3	472	San Justo Dam (R Abut)	31.88	622.86
3	476	UCSC Lick Observatory	45.47	714
4	891	Silent Valley – Poppet Flat	50.85	684.94
4	897	Twentynine Palms	41.43	684.94

---

[3] A unique number assigned to each earthquake in the NGA database for identification purposes.
[4] A unique number assigned to each record in the NGA database for identification purposes.

Table 4.2—*Continued.*

Earthquake Number	Record ID in NGA Database[5]	Station Name	Closest Distance to The Ruptured Area (km)	Shear-wave Velocity of Top 30 meters (m/s)
5	922	Pear Blossom – Pallet Creek	99.5	684.94
5	925	Rancho Cucamonga – Deer Can	66	821.69
5	928	Sage – Fire Station	61.8	622.86
5	934	Silent Valley – Poppet Flat	31.5	684.94
5	938	Winchester Bergman Ran	58.8	684.94
6	1109	MZH	70.26	609
6	1112	OKA	86.94	609
7	1154	Bursa Sivil	65.53	659.6
7	1169	Maslak	55.3	659.6
8	1619	Mudurnu	34.3	659.6
9	1626	Sitka Observatory	34.61	659.6
10	1633	Abbar	12.56	723.95
11	1763	Anza – Pinyon Flat	89.98	724.89
11	1767	Banning – Twin Pines Road	83.43	684.94
11	1786	Heart Bar State Park	61.21	684.94
11	1787	Hector	11.66	684.94
11	1795	Joshua Tree N.M. – Keys View	50.42	684.94
11	1824	San Bernardino – Del Rosa Wk Sta	96.91	684.94
11	1832	Seven Oaks Dam Project Office	87.2	659.6
11	1836	Twentynine Palms	42.06	684.94
12	2107	Carlo (temp)	50.94	963.94
12	2111	R109 (temp)	43	963.94
13	59	Cedar Springs, Allen Ranch	89.72	813.48
13	63	Fairmont Dam	30.19	684.94
13	71	Lake Hughes #12	19.3	602.1
13	72	Lake Hughes #4	25.07	821.69
13	73	Lake Hughes #9	22.57	670.84
13	87	Santa Anita Dam	30.7	684.94
13	89	Tehachapi Pump	63.79	669.48
14	139	Dayhook	13.94	659.6
15	369	Slack Canyon	27.46	684.94
16	511	Anza – Red Mountain	38.43	684.94
16	512	Anza - Tule Canyon	52.06	684.94
16	528	Murrieta Hot Springs	54.82	684.94
16	536	Santa Rosa Mountain	39.14	684.94
16	537	Silent Valley – Poppet Flat	17.03	684.94
16	541	Winchester Bergman Ran	49.08	684.94
17	769	Gilroy Array #6	18.33	663.31
17	771	Golden Gate Bridge	79.81	641.56

---

[5] A unique number assigned to each record in the NGA database for identification purposes.

Table 4.2—*Continued.*

Earthquake Number	Record ID in NGA Database[6]	Station Name	Closest Distance to The Ruptured Area (km)	Shear-wave Velocity of Top 30 meters (m/s)
17	781	Lower Crystal Springs Dam dwnst	48.39	712.82
17	782	Monterey City Hall	44.35	684.94
17	788	Piedmont Jr High	73	895.36
17	789	Point Bonita	83.45	1315.9
17	791	SAGO South – Surface	34.32	684.94
17	795	SF – Pacific Heights	76.05	1249.9
17	797	SF – Rincon Hill	74.14	873.1
17	801	San Jose – Santa Teresa Hills	14.69	671.77
17	804	So. San Francisco, Sierra Pt.	63.15	1020.6
17	809	UCSC	18.51	714
17	810	UCSC Lick Observatory	18.41	714
17	813	Yerba Buena Island	75.17	659.81
18	943	Anacapa Island	68.93	821.69
18	946	Antelope Buttes	46.91	821.69
18	957	Burbank – Howard Rd.	16.88	821.69
18	989	LA – Chalon Rd	20.45	740.05
18	994	LA – Griffith Park Observatory	23.77	1015.9
18	1011	LA – Wonderland Ave	20.3	1222.5
18	1012	LA 00	19.07	706.22
18	1020	Lake Hughes #12A	21.36	602.1
18	1021	Lake Hughes #4 – Camp Mend	31.66	821.69
18	1023	Lake Hughes #9	25.36	670.84
18	1027	Leona Valley #1	37.19	684.94
18	1029	Leona Valley #3	37.33	684.94
18	1033	Littlerock – Brainard Can	46.58	821.69
18	1041	Mt Wilson – CIT Seis Sta	35.88	821.69
18	1060	Rancho Cucamonga – Deer Can	79.99	821.69
18	1074	Sandberg – Bald Mtn	41.56	821.69
18	1078	Santa Susana Ground	16.74	715.12
18	1091	Vasquez Rocks Park	23.64	996.43
18	1096	Wrightwood – Jackson Flat	64.66	821.69
19	1206	CHY042	28.17	680
19	1234	CHY086	28.42	679.98
19	1245	CHY102	37.72	679.89
19	1257	HWA003	56.14	1525.9
19	1273	HWA024	43.15	630.08
19	1278	HWA029	54.29	614.05
19	1287	HWA038	42.54	642.73
19	1293	HWA046	51.8	617.52

---

[6] A unique number assigned to each record in the NGA database for identification purposes.

Table 4.2—*Continued.*

Earthquake Number	Record ID in NGA Database[7]	Station Name	Closest Distance to The Ruptured Area (km)	Shear-wave Velocity of Top 30 meters (m/s)
19	1302	HWA057	50.6	678.6
19	1325	ILA031	83.31	649.25
19	1347	ILA063	61.06	996.51
19	1350	ILA067	38.82	680
19	1377	KAU050	40.49	679.97
19	1391	KAU077	82.96	680
19	1485	TCU045	26	704.64
19	1517	TCU084	11.24	680
19	1518	TCU085	58.09	999.66
19	1520	TCU088	18.16	680
19	1548	TCU128	13.15	599.64
19	1576	TTN024	60.01	645.49
19	1577	TTN025	65.79	704.96
19	1585	TTN040	48.33	728.01
19	1587	TTN042	65.25	845.34
19	1594	TTN051	36.7	680

Table 4.3 Summary statistical data of identified model parameters

Parameter	Minimum	Maximum	Sample Mean	Sample Standard Deviation	Coefficient of Variation
I_a (s.g.)	0.000275	2.07	0.0468	0.164	3.49
D_{5-95} (s)	5.37	41.29	17.25	9.31	0.54
t_{mid} (s)	0.93	35.15	12.38	7.44	0.60
$\omega_{mid}/2\pi$ (Hz)	1.31	21.6	5.87	3.11	0.53
$\omega'/2\pi$ (Hz/s)	-1.502	0.406	-0.089	0.185	2.07
ζ_f (Ratio)	0.027	0.767	0.213	0.143	0.67

---

[7] A unique number assigned to each record in the NGA database for identification purposes.

Table 4.4 Distribution models and bounds assigned to the model parameters.

Parameter	Fitted Distribution[8]	Distribution Bounds
$\bar{I}_a$ (s.g.)	Lognormal	$(0, \infty)$
D_{5-95} (s)	Beta	$[5, 45]$
t_{mid} (s)	Beta	$[0.5, 40]$
$\omega_{mid}/2\pi$ (Hz)	Gamma	$(0, \infty)$
$\omega'/2\pi$ (Hz)	Two-sided Truncated Exponential	$[-2, 0.5]$
ζ_f (Ratio)	Beta	$[0.02, 1]$

Table 4.5 Maximum likelihood estimates of regression coefficients and standard error components.

i	$\beta_{i,0}$	$\beta_{i,1}$	$\beta_{i,2}$	$\beta_{i,3}$	$\beta_{i,4}$	τ_i	σ_i	P-value[9]
1	-1.844	-0.071	**2.944**	-1.356	-0.265	0.274	0.594	0.000
2	-6.195	-0.703	**6.792**	**0.219**	-0.523	0.457	0.569	0.000
3	-5.011	-0.345	**4.638**	**0.348**	-0.185	0.511	0.414	0.000
4	2.253	-0.081	-1.810	-0.211	0.012	0.692	0.723	0.001
5	-2.489	0.044	**2.408**	0.065	-0.081	0.129	0.953	0.095
6	-0.258	-0.477	0.905	-0.289	0.316	0.682	0.760	0.002

Table 4.6 95% confidence intervals for the regression coefficients.

i	Confidence Intervals $\beta_{i,1}$	$\beta_{i,2}$	$\beta_{i,3}$	$\beta_{i,4}$
1	$[-0.266, 0.124]$	$[1.715, 4.173]$	$[-1.512, -1.200]$	$[-0.749, 0.218]$
2	$[-0.929, -0.478]$	$[5.383, 8.204]$	$[0.106, 0.331]$	$[-0.980, -0.065]$
3	$[-0.592, -0.098]$	$[3.094, 6.181]$	$[0.225, 0.471]$	$[-0.685, 0.316]$
4	$[-0.377, 0.215]$	$[-3.668, 0.049]$	$[-0.359, -0.063]$	$[-0.589, 0.613]$
5	$[-0.255, 0.343]$	$[0.532, 4.284]$	$[-0.084, 0.215]$	$[-0.688, 0.526]$
6	$[-0.774, -0.180]$	$[-0.959, 2.765]$	$[-0.437, -0.140]$	$[-0.287, 0.919]$

---

[8] Means and standard deviations of these distributions are according to columns 4 and 5 of Table 4.3.
[9] The smallest significance level at which the null hypothesis $\beta_{i,1} = \beta_{i,2} = \beta_{i,3} = \beta_{i,4} = 0$ is rejected. F-test is employed.

Table 4.7 P-values for the t-test with the null hypothesis, $\beta_{i,j} = 0$.

| i	P-value[10]			
	$\beta_{i,1}$	$\beta_{i,2}$	$\beta_{i,3}$	$\beta_{i,4}$
1	0.476	0.000	0.000	0.281
2	0.000	0.000	0.000	0.025
3	0.006	0.000	0.000	0.467
4	0.591	0.056	0.005	0.968
5	0.772	0.012	0.391	0.792
6	0.002	0.339	0.000	0.303

Table 4.8 Total standard deviations obtained by two different regression methods.

| i	Regular Regression	Random-Effects Regression
1	0.647	0.654
2	0.681	0.730
3	0.655	0.658
4	0.908	1.000
5	0.826	0.962
6	0.959	1.021

Table 4.9 Sample correlation coefficients between the transformed model parameters (estimated as the correlation coefficients between the total error terms).

	v_1	v_2	v_3	v_4	v_5	v_6
v_1	1					
v_2	−0.36	1			Sym.	
v_3	0.01	0.67	1			
v_4	−0.15	−0.13	−0.28	1		
v_5	0.13	−0.16	−0.20	−0.20	1	
v_6	−0.01	−0.20	−0.22	0.28	−0.01	1

---

[10] The smaller this number is, the more significant the estimate of the corresponding coefficient in Table 4.5 is.
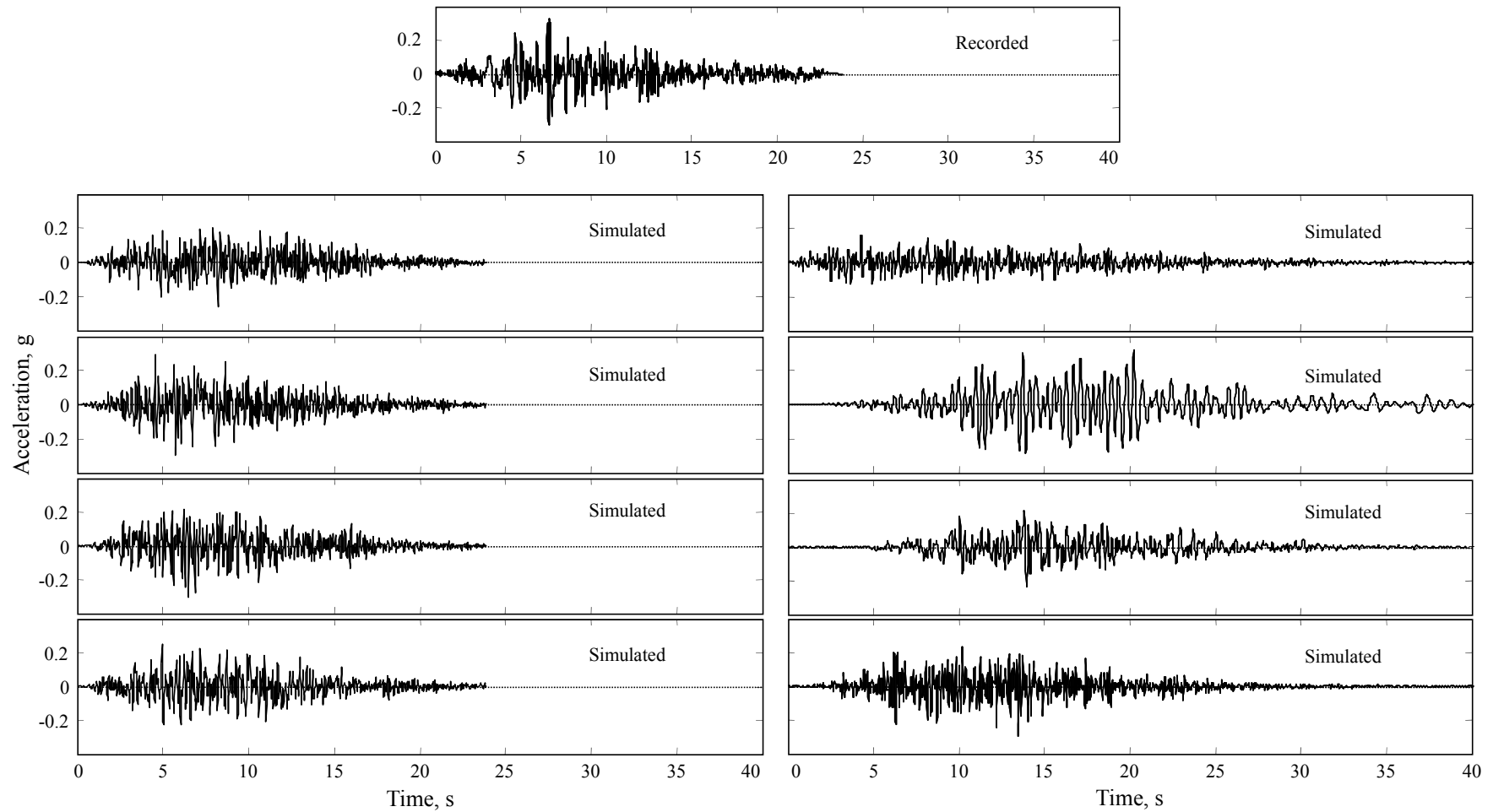
Fig. 4.1 Top: recorded motion. Left: simulated motions with model parameters identical to those of the recorded motion. Right: simulated motions with different sets of model parameters that correspond to the characteristics of the earthquake and site that produced the recorded motion.
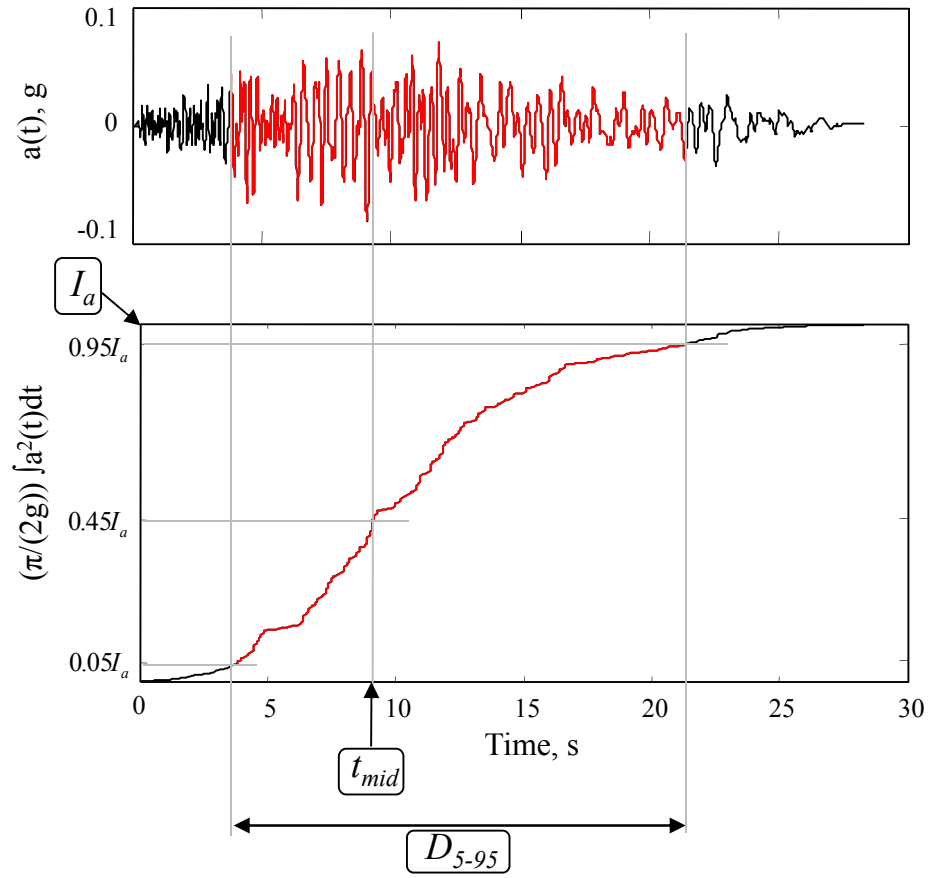
Fig. 4.2 Modulating function parameters identified for an acceleration time-history.
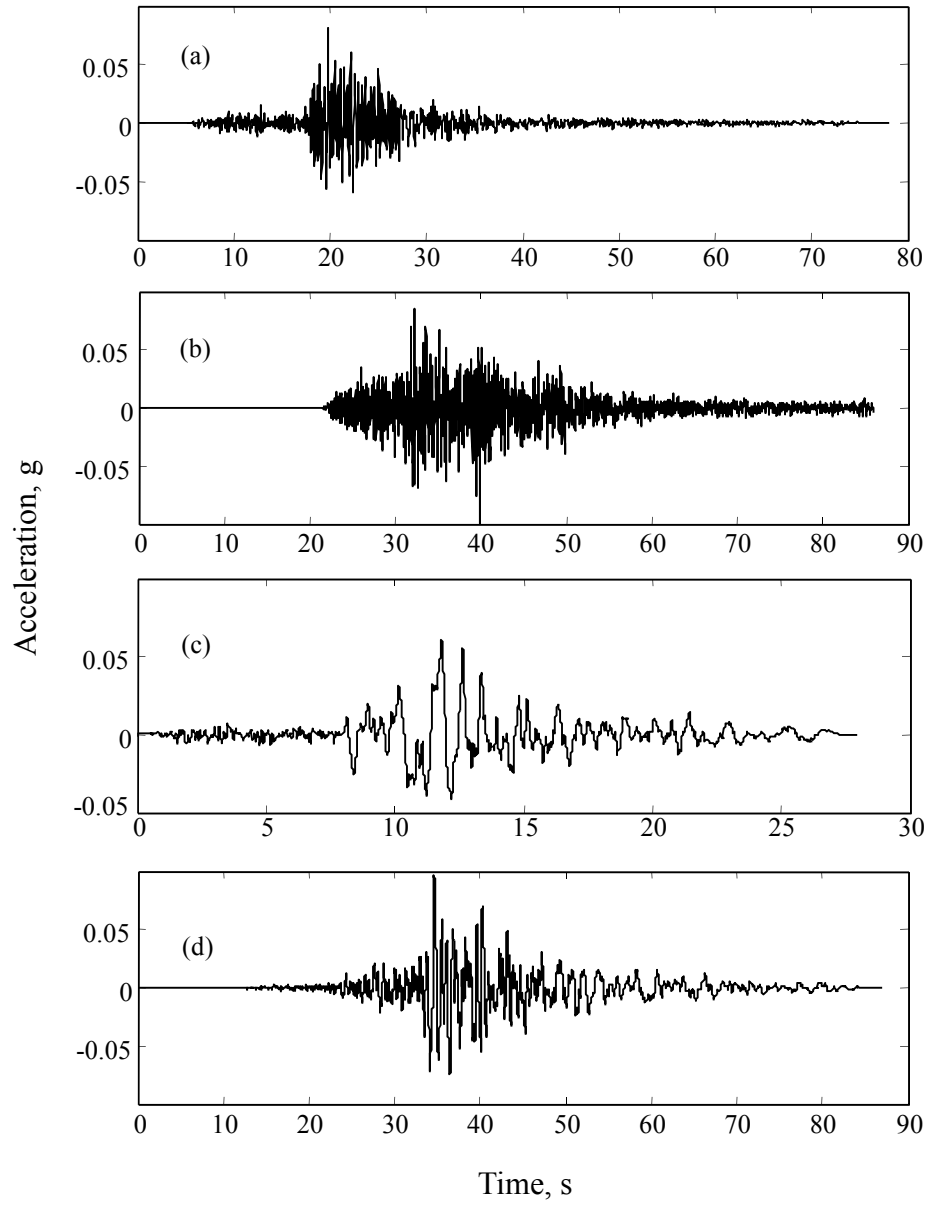
Fig. 4.3 **Examples of recorded acceleration time-histories with long stretches at the beginning ($T_0 \neq 0$). (a) Component 000 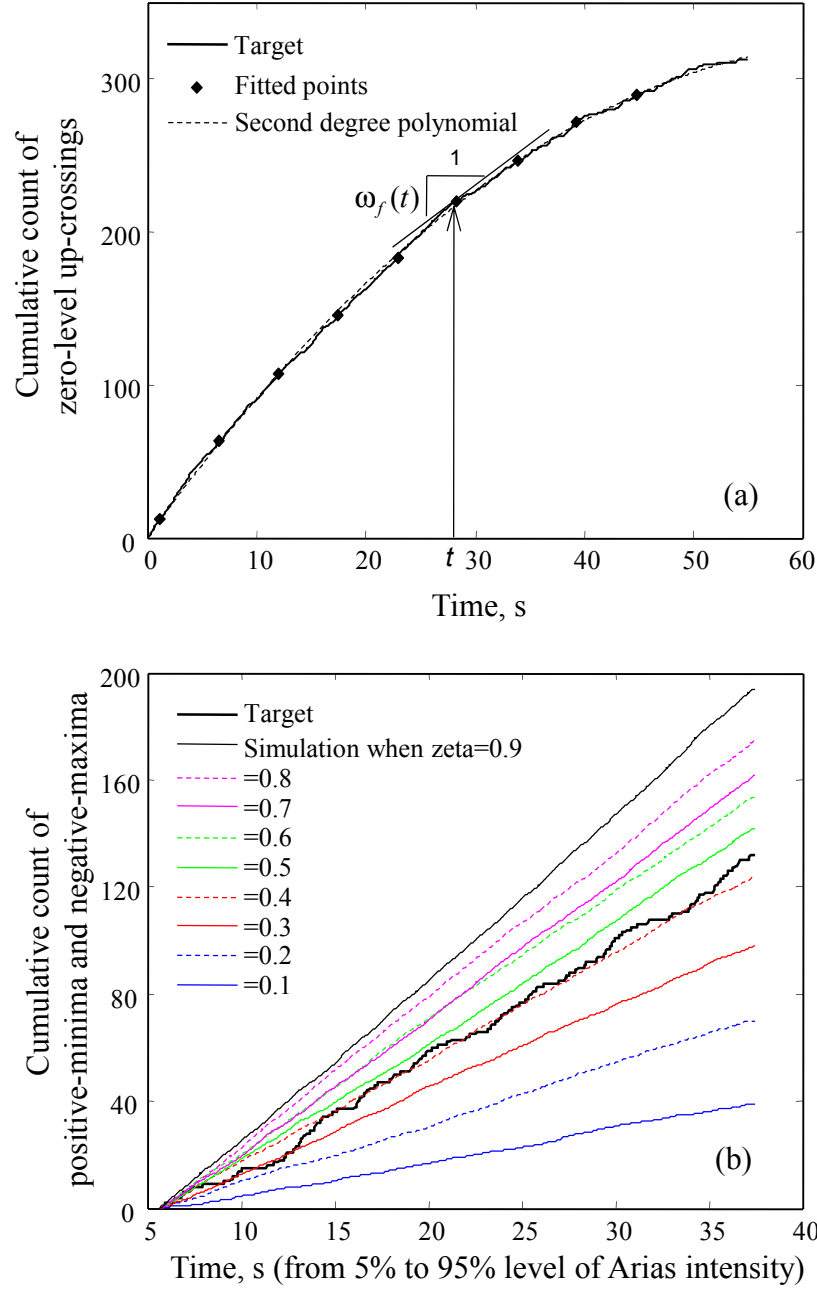of 1995 Kobe, Japan, earthquake recorded at OKA station. (b) Component 090 of 2002 Denali, Alaska, earthquake recorded at Carlo station. (c) Component 270 of 1989 Loma Prieta earthquake recorded at SF–Pacific Heights station. (d) Component E of 1999 Chi-Chi, Taiwan, earthquake recorded at HWA029 station.**

Fig. 4.4 **Identification of filter parameters. (a) Matching the cumulative number of zero-level up-crossings results in $\omega_{mid}/2\pi = 6.92$ Hz and $\omega'/2\pi = -0.14$ Hz/s. (b) Matching the cumulative count of negative maxima and positive minima gives $\zeta_f = 0.40$.**

Fig. 4.5 Distribution of moment magnitude and source-to-site distance in the considered database.
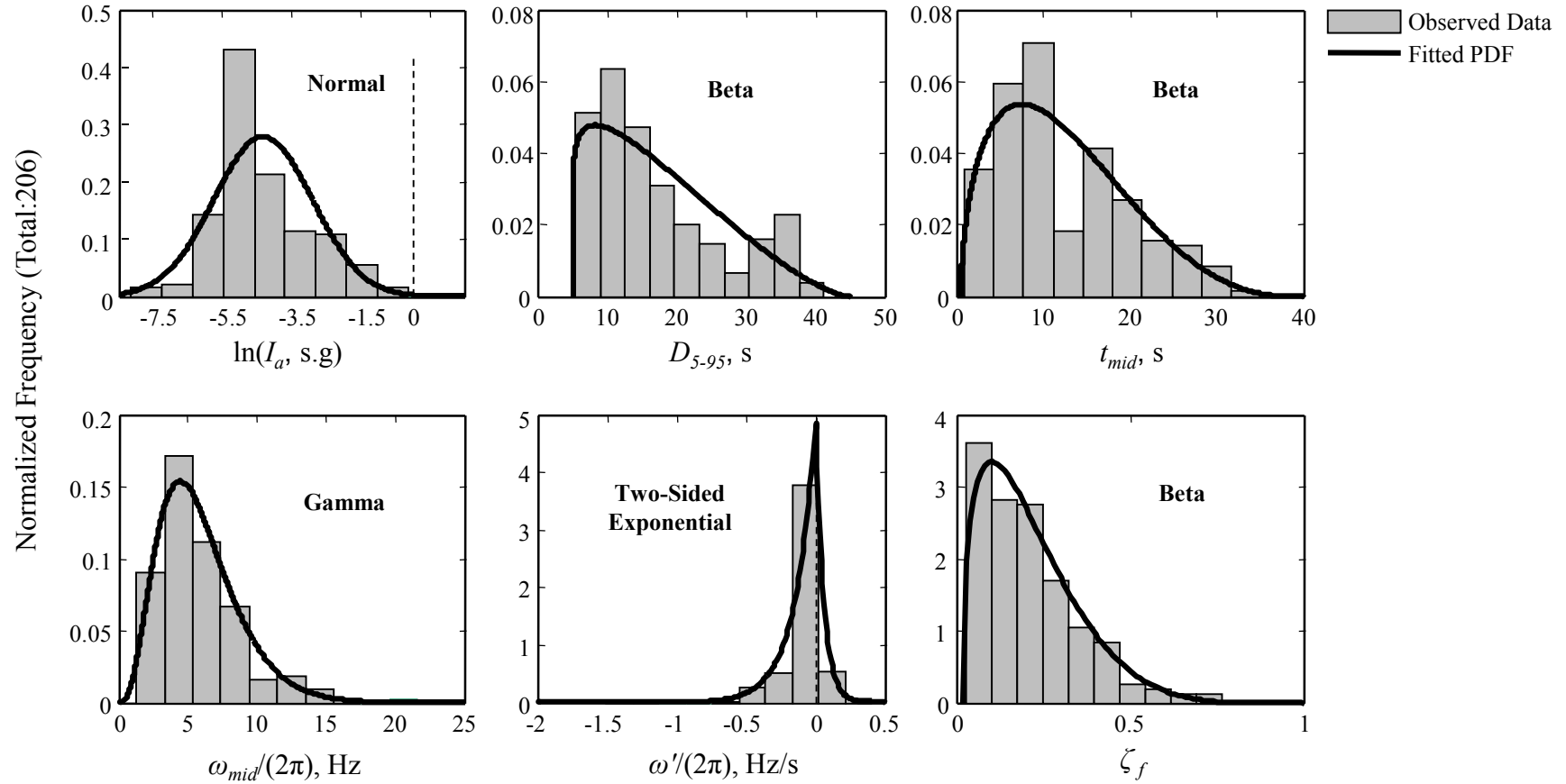
Fig. 4.6 Normalized frequency diagrams of the identified model parameters for the entire data set (combined strike-slip and reverse faulting mechanisms). Fitted probability density functions (PDFs) are superimposed and their parameter values and distribution types are listed in Tables 4.3 and 4.4.
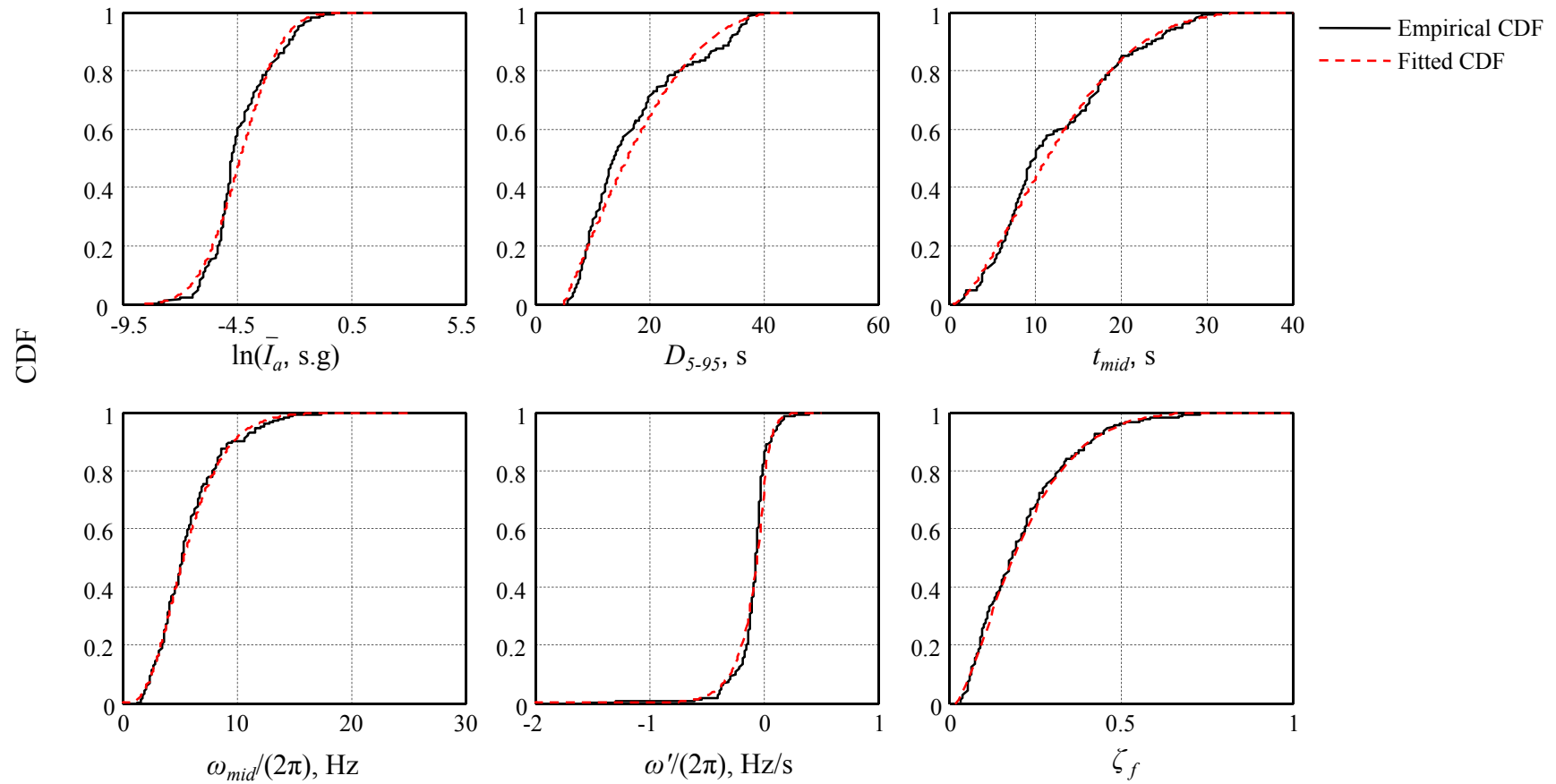
Fig. 4.7 Empirical cumulative distribution functions (CDFs) of the identified model parameters for the entire data set (combined strike-slip and reverse faulting mechanisms). CDFs of the fitted distributions are superimposed.
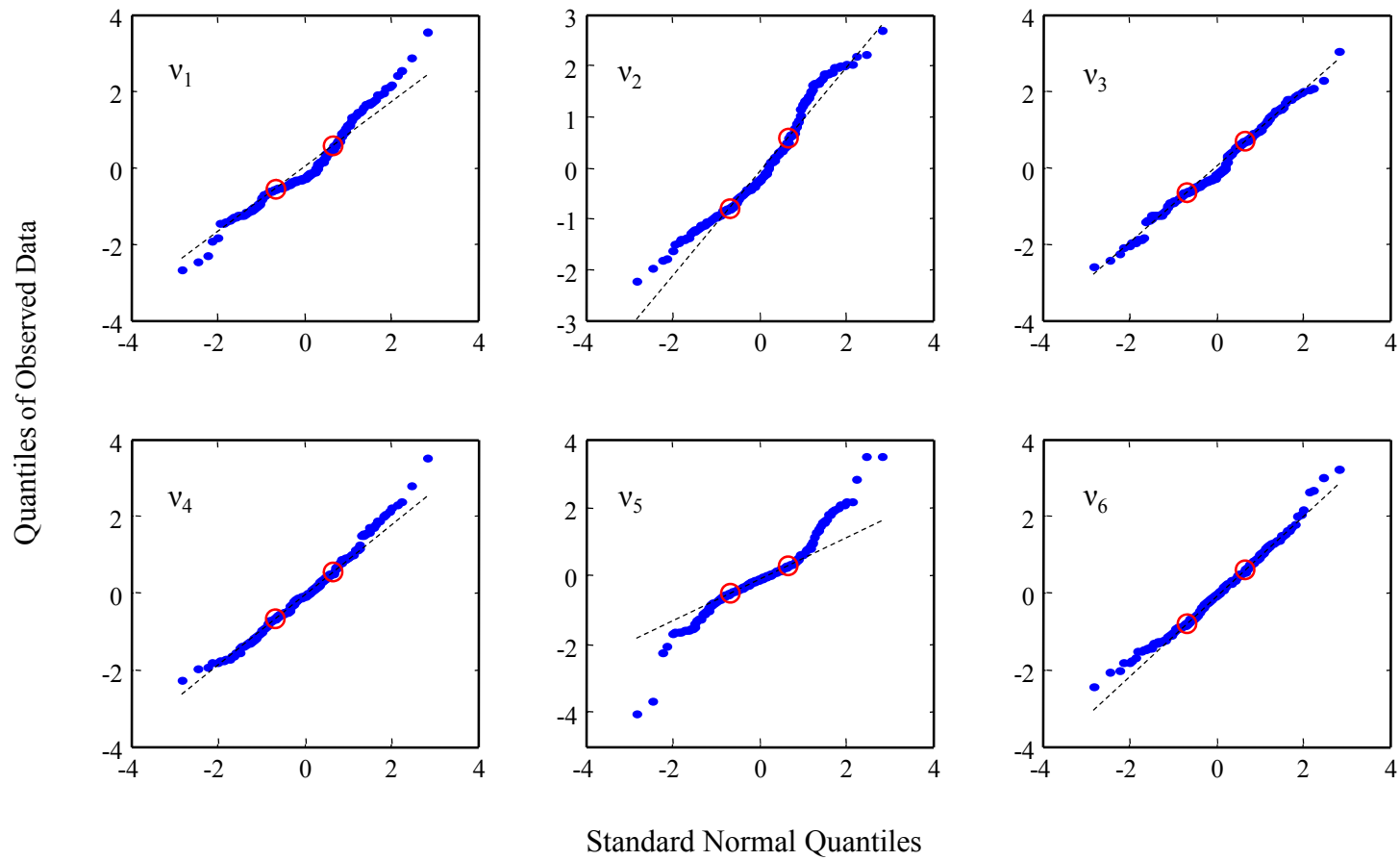
Fig. 4.8 Q-Q plots of transformed data for each model parameter. Hollow circles indicate the first and third quartiles.
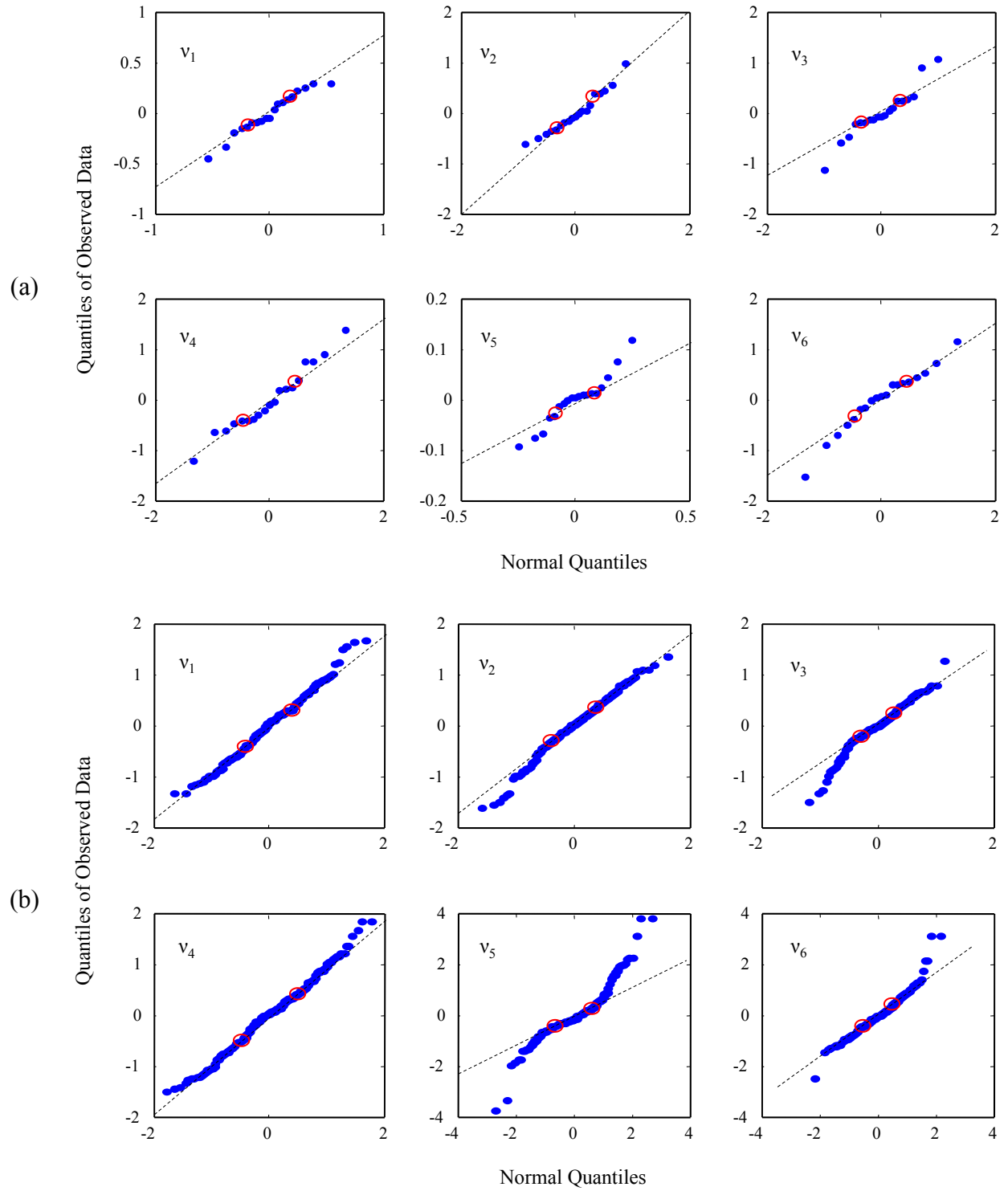
Fig. 4.9 Q-Q plots of the (a) inter-event residuals (b) intra-event residuals. Hollow circles indicate the first and third quartiles.

104
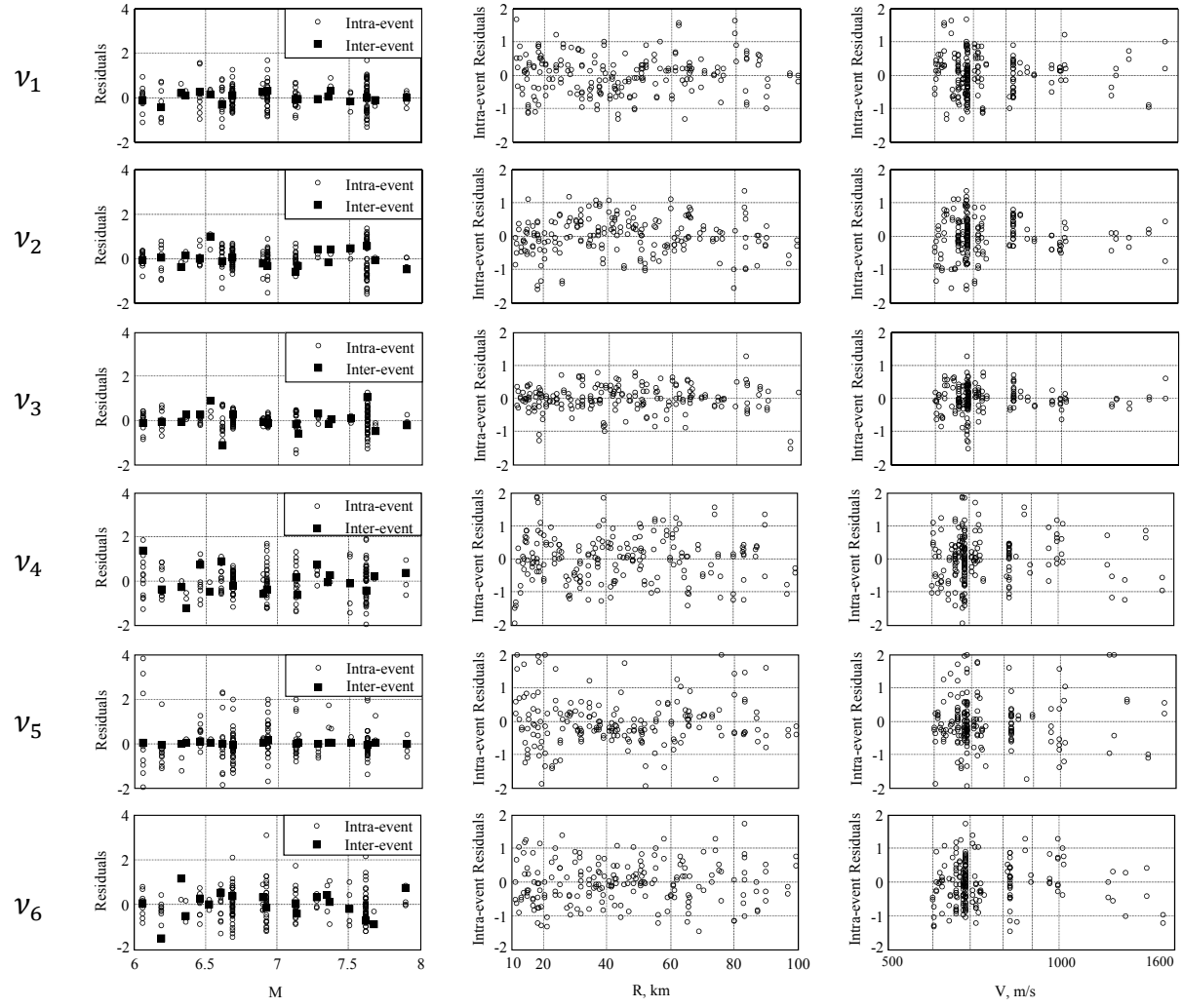
Fig. 4.10   Scatter plots of residuals against earthquake magnitude, source-to-site distance, and shear-wave velocity for each transformed model parameter.

105

5 Simulation of Ground Motions for Specified Earthquake and Site Characteristics and Their Use in PBEE

5.1 INTRODUCTION

In seismic design and analysis of structures, development of ground motions is a crucial step because even with the most sophisticated and accurate methods of structural analysis, the validity of predicted structural responses depends on the validity of the input excitations. Several levels of ground motions are commonly considered for seismic assessment of a structure.

For lower levels of intensity, when the structure is expected to remain elastic, response-spectrum analysis is usually sufficient. This type of analysis requires knowledge only of the ground motion spectral values. One of the most practical approaches to obtain these values is to use empirically based ground motion prediction equations (GMPEs), also known as attenuation relations. Many GMPEs have been developed that predict the median and standard deviation of ground motion spectral values for a range of spectral periods. The most recent of them is the Next Generation Attenuation (NGA) relations (Abrahamson et al. 2008). These GMPEs have been calibrated against observed data and are commonly used in practice.

For higher levels of intensity, when nonlinear structural behavior is likely, response-history dynamic analysis is necessary. This type of analysis requires knowledge of acceleration time-histories. It is common practice to use real recorded ground motions for this purpose. However, difficulties in this approach arise because ground motion properties vary for different earthquake and site characteristics, and recorded motions are not available for all types of earthquakes in all regions. As a result, the engineer is often forced to select motions recorded on sites other than the site of interest and to modify the records (e.g., scale them or modify their frequency contents) in ways that are often questionable and may render motions that are not realistic. Another alternative is to use synthetic motions. A suite of synthetic motions for specified earthquake and site

characteristics can be used in conjunction with or in place of previously recorded ground motions in performance-based earthquake engineering (PBEE). PBEE considers the entire spectrum of structural response, from linear to grossly nonlinear and even collapse, and thereby requires ground motions with various levels of intensity for different earthquake scenarios. Such a collection is scarce among previously recorded motions. Therefore, generation of an appropriate suite of synthetic motions that have characteristics similar to those of real earthquake ground motions is especially valuable in PBEE.

Many models have been developed in the past to synthetically generate ground motions (see the review in Chapter 1). One group of models are physics-based seismological models that produce realistic accelerograms at low frequencies but often need to be combined with stochastic models known to be more appropriate at high frequencies; the resulting combination is usually referred to as a hybrid model. The physics-based seismological models tend to be too complicated for use in engineering practice, as they require a thorough knowledge of the source, wave path, and site characteristics, which are typically not available to a design engineer. As a result, these models are rarely used for engineering purposes. Our aim in this study is to develop a method for generating synthetic ground motions that uses information that is readily available to the practicing engineer. We employ a site-based (as opposed to modeling the seismic source) stochastic ground motion model that focuses on realistically representing those features of the ground motion that are known to be important to the structural response, e.g., intensity, duration, and frequency content of the ground shaking at the site of interest. If the model parameters are known, synthetic acceleration time-histories can be generated. In the previous chapter, the proposed stochastic ground motion model was calibrated against recorded ground motions, and predictive equations for the model parameters were developed in terms of earthquake and site characteristics that are typically required as input arguments to GMPEs, i.e., the faulting mechanism, earthquake magnitude, source-to-site distance, and shear-wave velocity of the local soil. Considering the success of GMPEs in practice, in this chapter, we develop a method for generating synthetic ground motions that requires as input arguments only the earthquake and site characteristics mentioned above.

This chapter starts by describing a method for simulating jointly normal random variables. Then the discussion leads to random simulation of the stochastic model parameters for specified earthquake and site characteristics. The marginal distributions, predictive equations and correlation coefficients developed in Chapter 4 are incorporated for this purpose. Each set of randomly

simulated model parameters is then used in turn in the stochastic ground motion model, resulting in an ensemble of synthetic motions that account for the natural variability of real ground motions for the specified earthquake and site characteristics. Examples of simulated and recorded ground motions are provided. Finally, the importance of this study in PBEE is discussed.

5.2   SIMULATION OF JOINTLY NORMAL RANDOM VARIABLES

Realizations of a set of statistically independent random variables with known marginal distributions (e.g., normal) may be obtained by using standard *random number generators*. These generators are available in most statistical toolboxes. In this study, we employ the random number generator in the statistics toolbox of MATLAB, which starts by generating realizations of uniformly distributed random variables and then produces realizations of random variables for other distributions either directly (i.e., from the definition of the distribution) or by using inversion (i.e., by applying the inverse function for the distribution to a uniformly distributed random number[11]) or rejection (an iterative scheme used when the functional form of a distribution makes it difficult or time consuming to use direct or inversion methods) methods. In this study, for generating normally distributed random variables, the Ziggurat algorithm by Marsaglia and Tsang (2000) is employed as the default in MATLAB.

To generate realizations of jointly normal random variables, the correlation coefficients between the variables must be accounted for. Therefore, simple use of random number generators that result in uncorrelated realizations is not sufficient. Some statistical toolboxes, including the statistics toolbox in MATLAB, have the capability to generate correlated normal random variables. The approach used in this study to generate realizations of jointly normal random variables given realizations of uncorrelated standard normal random variables is presented below.

Let $\mathbf{X} = [X_1, X_2, \dots, X_n]^T$, where the superposed T indicates the matrix transpose, be a vector of n jointly normal random variables with the mean vector, $\mathbf{M_X}$, and covariance matrix, $\mathbf{\Sigma_{XX}}$, such that

---

[11] If F is a continuous distribution with inverse F^{-1}, and U is a uniformly distributed random variable on the unit interval [0,1], then $F^{-1}(U)$ has distribution F.

$$\mathbf{M_X} = \begin{bmatrix} \mu_1 \\ \mu_2 \\ \vdots \\ \mu_n \end{bmatrix} \qquad \boldsymbol{\Sigma_{XX}} = \begin{bmatrix} Var[X_1] & & & sym. \\ Cov[X_2, X_1] & Var[X_2] & & \\ \vdots & \vdots & \ddots & \\ Cov[X_n, X_1] & Cov[X_n, X2\,] & \cdots & Var[X_n] \end{bmatrix} \qquad (5.1)$$

where μ_i and $Var[X_i]$, $i = 1, \dots, n$, denote the mean and the variance of X_i respectively, and $Cov[X_i, X_j]$ denotes the covariance of X_i and X_j. The realizations of **X** may be obtained by use of the linear transformation:

$$\mathbf{x} = \mathbf{M_X} + \mathbf{L_{XX}^T y} \qquad (5.2)$$

In the above expression, the lower case, **x**, is used to denote a realization of the vector of random variables **X**; **y** is a realization of the vector of uncorrelated standard normal random variables $\mathbf{Y} = [Y_1, Y_2, \dots, Y_n]^T$; and $\mathbf{L_{XX}^T}$ is a lower triangular matrix obtained from the Cholesky decomposition of the covariance matrix $\boldsymbol{\Sigma_{XX}}$ such that $\boldsymbol{\Sigma_{XX}} = \mathbf{L_{XX}^T L_{XX}}$. The Cholesky decomposition is made possible because the covariance matrix $\boldsymbol{\Sigma_{XX}}$ is positive definite (provided there is no linear relation between the random variables). This means that for any non-zero column-vector **a** of size n, $\mathbf{a^T \Sigma_{XX} a} > 0$.

The expression in (5.2) transforms uncorrelated standard normal random variables into jointly normal random variables (i.e., transforms **y** to **x**). By definition, **y** has a zero mean vector and an identity covariance matrix. It follows that the mean vector and the covariance matrix of $\mathbf{M_X} + \mathbf{L_{XX}^T y}$ are $\mathbf{M_X}$ and $\boldsymbol{\Sigma_{XX}}$ respectively. Hence, (5.2) is a realization of vector **X**. To obtain a realization of **X**, we first obtain a realization of **y** by individually simulating its components, and then use (5.2) to compute the corresponding realization, **x**.

5.2.1   Conditional Simulation of a Subset of Jointly Normal Random Variables

It may be of interest to generate realizations of a subset of jointly normal random variables $\mathbf{X_a} = [X_1, X_2, \dots, X_k]^T$, $k < n$, given observed values for the remainder of variables $\mathbf{X_b} = [X_{k+1}, \dots, X_n]^T$. When simulating, it is important to account for the correlations between the variables of $\mathbf{X_a}$ and $\mathbf{X_b}$,; hence, conditional simulation is necessary. If the set of random variables $\mathbf{X} = [X_1, X_2, \dots, X_n]^T$ is jointly normal, then the conditional distribution of the subset $\mathbf{X_a}$ given $\mathbf{X_b} = \mathbf{x_b}$ is also jointly normal. Once the corresponding conditional mean vector $\mathbf{M_{a|b}}$ and

covariance matrix $\Sigma_{aa|bb}$ are determined, the linear transformation in (5.2) can be used to generate realizations of the subset X_a.

Obtaining the conditional mean vector and covariance matrix requires partitioning of the mean vector and covariance matrix of X in the form:

$$M_X = \begin{bmatrix} M_a \\ -- \\ M_b \end{bmatrix} \qquad \Sigma_{XX} = \begin{bmatrix} \Sigma_{aa} & | & \Sigma_{ab} \\ -- & -- & -- \\ \Sigma_{ba} & | & \Sigma_{bb} \end{bmatrix} \qquad (5.3)$$

Then the conditional mean vector and covariance matrix are given by

$$M_{a|b} = M_a + \Sigma_{ab}\Sigma_{bb}^{-1}(x_b - M_b) \qquad (5.4)$$

$$\Sigma_{aa|bb} = \Sigma_{aa} - \Sigma_{ab}\Sigma_{bb}^{-1}\Sigma_{ba} \qquad (5.5)$$

which are used in (5.2) to generate realizations of the subset X_a given $X_b = x_b$.

For more details on properties of multinormal probability distribution and conditional simulation of random variables, refer to standard probability and statistics books such as Kotz et al. (2000) or Anderson (1958). Specifically for conditional simulation and partitioning of the mean vector and the covariance matrix refer to Theorem 2.5.1 of Anderson (1958).

5.3   RANDOM SIMULATION OF MODEL PARAMETERS

When generating synthetic ground motions, it is desired to maintain the natural variability that exists among real earthquake ground motions for a given set of earthquake and site characteristics. This requires accounting for the variability in the model parameters, i.e., $(\bar{I}_a, D_{5-95}, t_{mid}, \omega_{mid}, \omega', \zeta_f)$, which are regarded as random variables. To achieve this goal, it is necessary to randomly simulate realizations of the model parameters using their joint distribution conditioned on the earthquake and site characteristics. This joint distribution is unknown, but marginal distributions for each model parameter were proposed in Chapter 4. The proposed marginal distributions allow transformation of the model parameters to the standard normal space by (4.1), resulting in the vector of random variables $\mathbf{v} = [v_1, v_2, \dots, v_6]^T$. Each transformed model parameter, v_i, $i = 1, \dots, 6$, follows a normal distribution with mean $\mu_i(F, M, R, V, \boldsymbol{\beta}_i)$, which is a function of the earthquake and site characteristics and can be computed using the predictive equations provided by (4.19) and (4.20). It has a standard deviation equal to the standard deviation of the total error in the predictive equations (i.e., $\sqrt{\tau_i^2 + \sigma_i^2}$). Furthermore,

estimated correlation coefficients between the transformed model parameters are provided in Table 4.9. For $\mathbf{v}$, we assume a jointly normal distribution which is consistent with the set of marginals and correlations mentioned above. This is equivalent to assuming that the original parameters have the Nataf joint distribution (Liu and Der Kiureghian 1986). Due to the dependence of the mean on F, M, R, and V, the joint distribution is conditioned on the earthquake and site characteristics. Therefore, given a set of earthquake and site characteristics, transformed model parameters are simulated as jointly normal random variables, which are then transformed back to their physical space by using the inverse of (4.1).

To randomly simulate realizations of the vector of jointly normal random variables $\mathbf{v} = [v_1, v_2, \ldots, v_6]^\mathrm{T}$, we construct the mean vector, $\mathbf{M_v}$, and the covariance matrix, $\mathbf{\Sigma_{vv}}$, according to (5.1). The linear transformation in (5.2) is then employed to generate sample realizations of $\mathbf{v}$. Alternatively, the total error terms in the predictive equations of Chapter 4 may be regarded as jointly normal random variables with zero mean vector and covariance matrix $\mathbf{\Sigma_{vv}}$. They can be simulated according to (5.2) and added to the predicted mean values of each v_i to generate sample realizations of $\mathbf{v}$. If the values for a subset of the model parameters are given (e.g., v_1 is fixed), the conditional mean vector (e.g., $\mathbf{M}_{[v_2,\ldots,v_6]|v_1}$) and the conditional covariance matrix (e.g., $\mathbf{\Sigma}_{[v_2,\ldots,v_6],[v_2,\ldots,v_6]|v_1 v_1}$) are computed for the remainder of these random variables as described in Section 5.2.1 and are employed in (5.2) to generate sample realizations. As previously mentioned, the simulated realizations of $\mathbf{v}$ are transformed to the original space of the corresponding model parameter by using the inverse of (4.1) and the assigned marginal distributions in Table 4.4. This results in realizations of $\bar{I}_a$, D_{5-95}, t_{mid}, ω_{mid}, ω', and ζ_f for the specified earthquake and site characteristics used to construct $\mathbf{M_v}$.

As an example, four sets of model parameters are simulated for the earthquake and site characteristics: $F = 1$, $M = 7.35$, $R = 14$ km, and $V = 660$ m/s. These characteristics correspond to the earthquake and site that produced a real ground motion recorded at Dayhook station during the 1978, Tabas, Iran, earthquake. The model parameters for the recorded motion are identified and reported along with the simulated model parameters in Table 5.1. These values belong to the records of Figure 4.1, previously discussed in Chapter 4, which demonstrates the effect of using different model parameters on the variability in a suite of ground motions. The model parameters for the records on the left of the figure are identical to the model parameters of

112

the recorded motion, while the model parameters for the records on the right of the figure are all different but correspond to the same earthquake and site characteristics. The set of motions with variable model parameters demonstrates a larger variability, representative of the natural variability among real ground motions (examples in the upcoming sections will support this statement), and are better suited for use in assessment or design of structures for a given design scenario, i.e., given earthquake and site characteristics.

Now that we are able to simulate sets of model parameters for specified earthquake and site characteristics, each set may be used in the stochastic ground motion model to generate a single synthetic ground motion. The next section provides more details and examples on simulation of ground motions for specified earthquake and site characteristics.

5.4   RANDOM SIMULATION OF GROUND MOTIONS

Given a design scenario expressed in terms of F, M, R, and V, any number of synthetic ground motions can be generated based on the information provided in the preceding sections and without the need for any previously recorded motion. The details are described below. Here, we employ the stochastic ground motion model of Chapter 4 (i.e., stochastic model proposed in Chapter 2 with the modulating function, the linear filter, and the model parameters that were specified in Chapter 4).

Given F, M, R, and V, sample realizations of random variables v_i, $i = 1, ..., 6$, are generated and transformed to sample realizations of model parameters ($\bar{I}_a, D_{5-95}, t_{mid}$, $\omega_{mid}, \omega', \zeta_f$) according to Section 5.3. The first three parameters are then converted to the gamma modulating function parameters $\boldsymbol{\alpha} = (\alpha_1, \alpha_2, \alpha_3)$ according to (4.6), (4.7), and (4.9), yielding the set $(\alpha_1, \alpha_2, \alpha_3, \omega_{mid}, \omega', \zeta_f)$. $T_0 = 0$ is assumed for simulation purposes. These parameter values together with a set of n statistically independent standard normal random variables u_i, $i = 1, ..., n$, are used in the stochastic model in (2.12) and the high-pass filter in (2.28) to generate a synthetic accelerogram, $\ddot{z}(t)$. Any number of accelerograms for the given earthquake and site characteristics can be synthesized by generating new realizations of v_i and u_i. This procedure is summarized in Figure 5.1. The following presents examples of simulations for Scenario I: when all the model parameters are unknown, and for Scenario II: when a subset of the model parameters is specified.

113

5.4.1 Scenario I: All Model Parameters Are Unknown

The simulation method described above maintains the natural variability of ground motions for a given set of earthquake and site characteristics. To demonstrate this, in Figures 5.2, 5.3, and 5.4 we show three sets of ground motions for given values of $F, M, R,$ and V. (To better observe traces of the time-histories provided in these and subsequent figures, different scaling is used for the vertical axes.) Each set includes one recorded motion and four simulated motions. For each motion the acceleration, velocity, and displacement time-histories are given. Also listed in the figures are the model parameters for each motion (identified for the recorded motions and randomly simulated for the synthetic motions). For the synthetic motions, a discretization step of $\Delta t = 0.02$ s and the high-pass filter frequency $\omega_c/2\pi = 0.15$ Hz are used. Observe that although the three events have almost[12] identical earthquake and site characteristics (all are reverse faulting; $M =$ 6.61, 6.93, and 6.69; $R =$ 19.3, 18.3, and 19.1 km; and $V =$ 602, 663, and 706 m/s), the three recorded motions are vastly different in their characteristics. Specifically, their Arias intensities range from 0.040 to 0.109 s.g., effective durations range from 5.95 to 12.62 s, predominant frequencies range from 3.97 to 14.58 Hz, and bandwidth parameters range from 0.03 to 0.24. Furthermore, the acceleration, velocity, and displacement traces and their peak values are vastly different. Similar variability can be observed among the simulated motions (compare the parameter values and the traces). Also, observe that the general features of the simulated motions are similar in character to those of the recorded motions. In a blind test, it would be difficult, or impossible, for anyone to ascertain as to which of the presented ground motions in these figures is the recorded one and which are synthetic.

Another three sets of ground motions are provided in Figures 5.5–5.7. Similar results are observed. The three events have almost identical earthquake and site characteristics (all are strike-slip faulting; $M =$ 6.53, 6.33, and 6.19; $R =$ 15.2, 14.4, and 14.8 km; and $V =$ 660, 660, and 730 m/s), but vastly different in their characteristics. Similar variability is observed among the simulated motions. And the general features of the simulated motions, i.e., the traces of

---

[12] Due to scarcity of recorded motions, it is difficult to find records that have resulted from different earthquake events but belong to identical earthquake and site characteristics. In fact, many researchers create large magnitude-distance bins (often larger than what has been selected in this study) to select recorded motions and declare them as records with similar earthquake and site characteristics.

acceleration, velocity, and displacement time-histories, are similar in character to those of the recorded motions.

5.4.2   Scenario II: Some Model Parameters Are Specified

It might be of interest to simulate ground motions with given values for a subset of the model parameters, e.g., Arias intensity, effective duration, or predominant frequency. In such cases, the corresponding v_i variables are fixed, while the remaining v_j, $j \neq i$, variables are generated using the conditional mean vector and covariance matrix for the given values of the fixed variables. These conditional matrices are computed based on formulas provided in Section 5.2.1. Conditional simulation is necessary in such cases to account for the correlations among the fixed and varying parameters.

As an example, Figure 5.8 shows the recorded motion in Figure 5.4 together with four synthetic accelerograms, which are conditioned to have the Arias intensity of the recorded motion. The synthetics are obtained by generating sets of the five variables v_2 to v_6 for the given value $v_1 = \ln(0.109)$ of the first variable. Observe that the variability among the simulated motions is somewhat smaller compared to the case in Figure 5.4, where the Arias intensity was not specified.

Since Arias intensity and duration of the ground motion are of particular interest in the fields of geotechnical and structural engineering, empirical relations for these parameters have been developed by other researchers (e.g., Travasarou et al. [2003], Abrahamson and Silva [1996]). If desired, it is possible to use other empirical formulas to estimate one or more of the model parameters, such as $\bar{I}_a$ and D_{5-95}. However, ground motion databases used in other studies are generally different from the one used in this study. On the other hand, the estimates of correlations between the model parameters depend on the selected database. Therefore, the correlation coefficients provided in this study (corresponding to a database of strong ground motions on firm soil with source-to-site distance of at least 10 km) would only be rough estimates if used. Finally, it should be emphasized that if more than one parameter is approximated by alternative empirical relations, the correlations between these parameters must also be taken into consideration in constructing the conditional mean vector and covariance matrix according to (5.4) and (5.5).

5.4.3 Total Duration of Motion and Filter Frequency

When simulating ground motions, the total duration of motion, t_n, is rather arbitrary. However, some care must be exercised to ensure that the resulting synthetic motion is simulated sufficiently long for the residuals to reach zero. At the same time, if t_n is large, the filter frequency, which is in the form of a linear function in time, may assume zero, negative, or unreasonably high values. To avoid these situations, we need certain limitations on t_n and $\omega_f(t)$.

We have found that a total duration equal to two or three times the effective duration D_{5-95} is usually sufficient to achieve zero residuals. Two examples are presented in Figures 5.9 and 5.10, respectively for linearly decreasing and linearly increasing filter frequencies, where $t_n = 3D_{5-95}$ is used. The linear filter frequency functions used to generate these motions, based on (4.10), are also plotted for each figure. To avoid unreasonably low or high values of filter frequency (e.g., beyond 25 s in Fig. 5.9, or 40 s in Fig. 5.10), limits must be assigned to (4.10). Recalling that the database for the two parameters ω_{mid} and ω' was created by analyzing recorded motions within 1% to 99% levels of their Arias intensities, we modify $\omega_f(t)$ such that it is a linear function within 1% to 99% of the expected Arias intensity $\bar{I}_a$ [see (4.3)], and constant outside that time bracket with a minimum value of 0.3 Hz.

$$\omega_f(t) = \begin{cases} \max[\omega_{mid} + \omega'(t_s - t_{mid}), 0.3(2\pi)] & \text{if} \quad 0 \le t < t_s \\ \max[\omega_{mid} + \omega'(t - t_{mid}), 0.3(2\pi)] & \text{if} \quad t_s \le t \le t_e \\ \max[\omega_{mid} + \omega'(t_e - t_{mid}), 0.3(2\pi)] & \text{if} \quad t_e < t \le t_n \end{cases} \tag{5.6}$$

In the above expression, t_s and t_e refer to the times of 1% and 99% $\bar{I}_a$. Plots of simulated motions with filter frequency according to (5.6) are also shown in Figures 5.9 and 5.10. Inside the time bracket $[t_s, t_e]$, the two simulated motions with filter frequencies according to (4.10) and (5.6) are identical. Outside this time bracket, differences between time-histories are insignificant, but unlike (4.10), the filter frequency according to (5.6) is physically reasonable.

5.5 USE IN PBEE

The growing interest in performance-based earthquake engineering (PBEE) in recent years , e.g., see Bozorgnia and Bertero (2004), and the scarcity of recorded ground motions for many regions of the world necessitate the use of synthetic ground motions with specified earthquake and site characteristics. In PBEE, an ensemble of ground motions that represents all possible realizations

for an earthquake of given characteristics at a given site is of interest. As described in this chapter, such an ensemble may be obtained by generating ground motion realizations that correspond to various realizations of the stochastic model parameters, randomly generated from probability distributions that are conditioned on the given earthquake and site characteristics.

The main attraction of PBEE is going above and beyond the code specifications (i.e., life-safety performance objective for rare earthquake ground motions) to meet the specific needs of the owners and other stakeholders. As a result, various performance objectives (e.g., life-safety, cost, and post-earthquake functionality) for specified hazard levels are to be considered, resulting in multiple design scenarios and increasing the number of required ground motion time-histories. Synthetic ground motions can be generated for specified design scenarios for which recorded motions are lacking.

Furthermore, the simulation approach proposed in this study can be used to investigate structural responses to various ground motion intensities. This is useful because PBEE analysis typically considers the entire spectrum of structural response, from linear to grossly nonlinear and even collapse. Therefore, there is need for ground motions with different levels of intensity. Since the number of available recordings is limited, the current practice requires modification of recorded motions to achieve various intensity levels. However, to adequately capture nonlinear structural responses, realistic characterization of the ground motion is essential and unless extreme care is taken, scaled (in time or frequency) ground motions with unrealistic properties are difficult to avoid. It has been the focus of the present study to realistically represent the evolutionary characteristics of ground motions such as the time-varying frequency content that can greatly influence the nonlinear responses of degrading structures. Furthermore, the parameters of the stochastic model are fitted to a database of real earthquake records so that the model captures the natural characteristics and variability of recorded motions. Therefore, realistic synthetic motions may be generated based on this study to complement the existing recorded motions for a specified set of earthquake and site characteristics.

Finally, in PBEE, fragility models for structural damage measures (Vamvatsikos and Cornell 2002) are often utilized to determine failure and damage probabilities. The method of ground motion simulation presented in this study can facilitate evaluation of fragility models for a given design scenario that is specified by its earthquake and site characteristics.

Table 5.1 Four sets of simulated and one set of identified model parameters for a single set of earthquake and site characteristics. Observe the variability among the model parameters.

	I_a (s.g.)	D_{5-95} (s)	t_{mid} (s)	$\omega_{mid}/2\pi$ (Hz)	$\omega'/2\pi$ (Hz/s)	ζ_f (Ratio)
	0.075	20.1	7.0	4.84	-0.012	0.25
Simulated model parameters	0.288	21.3	16.5	2.48	-0.054	0.12
(corresponding to the motions on the right side of Figure 4.1, respectively from top to bottom)	0.124	15.3	14.9	3.72	0.0039	0.40
	0.147	15.5	10.0	6.22	0.00046	0.18
Identified model parameters (corresponding to the recorded motion and simulated motions on the left side of Fig. 4.1)	0.145	12.3	6.8	5.90	0.12	0.26

Fig. 5.1 Simulating ground motions for specified earthquake and site characteristics.

Specify earthquake and site characteristics.

F, M, R, V

Empirical predictive equations
$\left(\begin{array}{c}\text{use (4.19), (4.20), and} \\ \text{Tables 4.5 and 4.9}\end{array}\right)$

$\mu_{v_i|F,M,R,V}$, $\tau_i^2+\sigma_i^2$, $\rho_{vi,vj}$
$i=1,...,6$, $j=1,...,6$

Set up $\mathbf{M_v}$ and Σ_{vv}.
$\left(\text{use (5.1)}\right)$

Repeat N times to obtain a suite of N simulated motions.

Generate one sample realization of the model parameters in standard normal space.
$\left(\text{use (5.2)}\right)$

$\mathbf{v}=[v_1,\ldots,v_6]^T$

Transform to the original space of each model parameter.
$\left(\begin{array}{c}\text{use inverse of (4.1) and marginal} \\ \text{distributions reported in Table 4.4}\end{array}\right)$

$\bar{I}_a$, D_{5-95} , t_{mid} , ω_{mid} , ω' , ζ_f

Select a modulating function and transform $\bar{I}_a$, D_{5-95} , and t_{mid} , to the modulating function parameters
$\left(\text{use (4.6), (4.7), (4.9) for gamma modulating function}\right)$

α_1 , α_2 , α_3 , ω_{mid} , ω' , ζ_f

Fully-nonstationary stochastic process
use (2.12) and statistically independent standard normal random variables u_i , $i=1,\ldots,n$

$x(t)$

Post-process
$\left(\text{use (2.28)}\right)$

$\ddot{z}(t)$
(simulated ground acceleration)

Realizations of model parameters:					
I_a	$D_{5\text{-}95}$	t_{mid}	$\omega_{mid}/2\pi$	$\omega'/2\pi$	ζ_f
s.g.	s	s	Hz	Hz/s	
0.040	5.95	0.93	14.58	−0.53	0.18
0.028	15.03	11.33	4.35	−0.18	0.07
0.067	8.92	3.42	10.05	−0.53	0.49
0.021	10.02	3.34	7.84	−0.16	0.33
0.123	9.73	5.12	3.12	−0.004	0.58
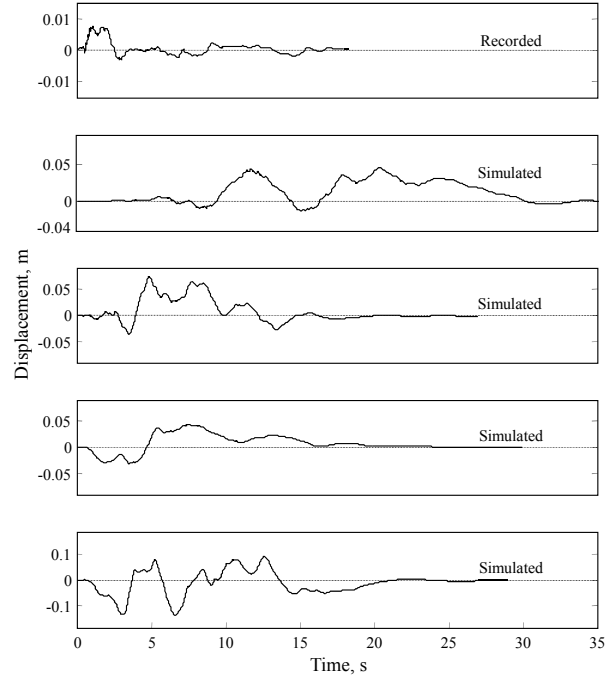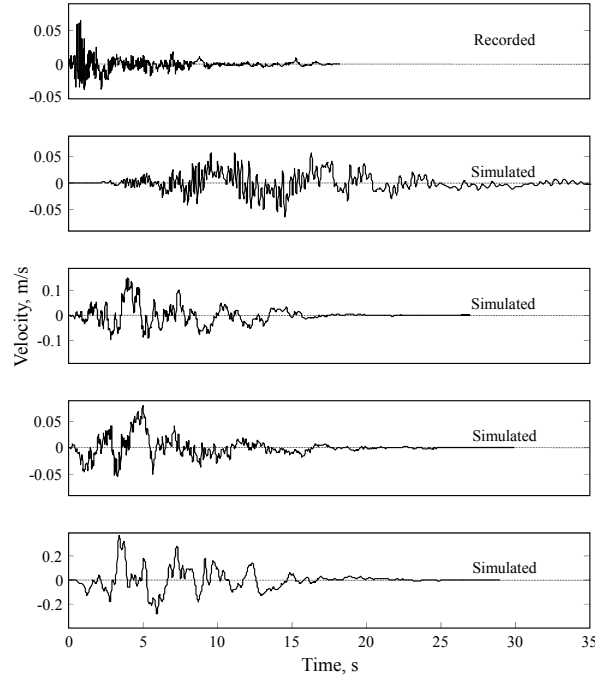
Fig. 5.2 **Recorded and synthetic motions corresponding to $F = 1$ (reverse faulting), $M = 6.61$, $R = 19.3$ km, $V = 602$ m/s. Recorded motion is component 291 of the 1971 San Fernando earthquake at the Lake Hughes #12 station.**

120
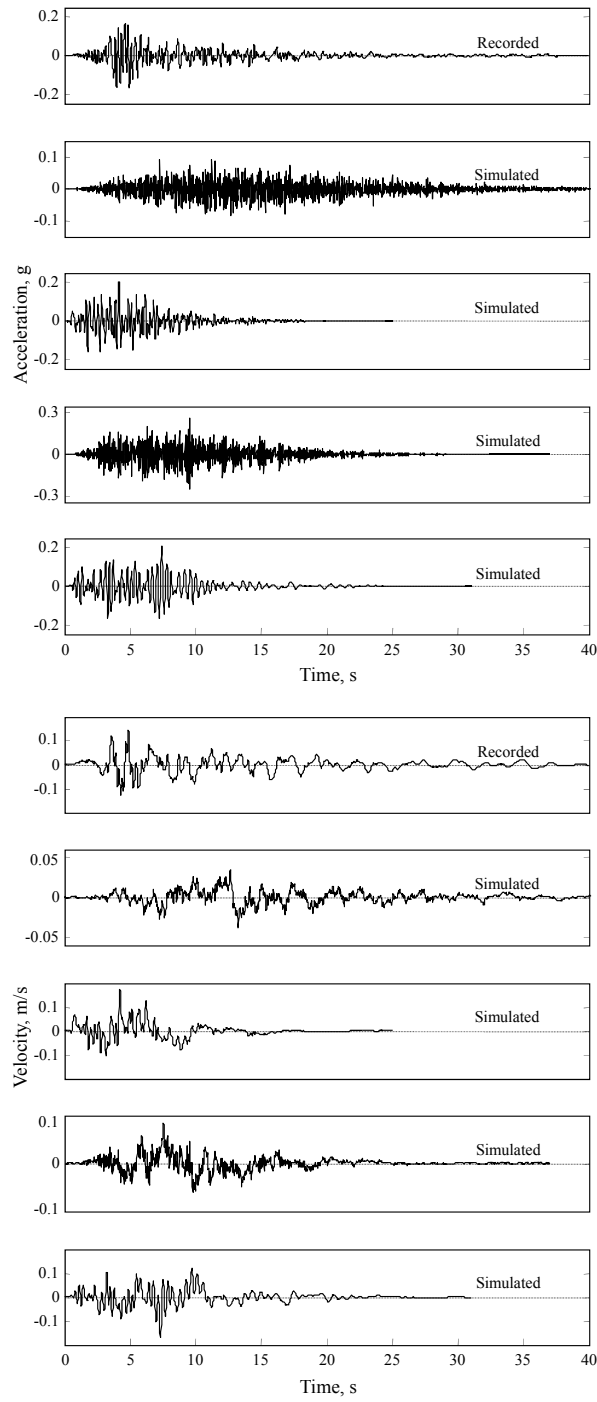
Realizations of model parameters:					
I_a	$D_{5\text{-}95}$	t_{mid}	$\omega_{mid}/2\pi$	$\omega'/2\pi$	ζ_f
s.g.	s	s	Hz	Hz/s	
0.045	12.62	4.73	3.97	−0.08	0.03
0.023	20.02	11.23	15.67	−0.08	0.34
0.043	8.50	3.35	4.04	0.09	0.25
0.126	12.22	7.48	11.05	0.01	0.10
0.070	10.33	4.74	3.10	−0.15	0.09
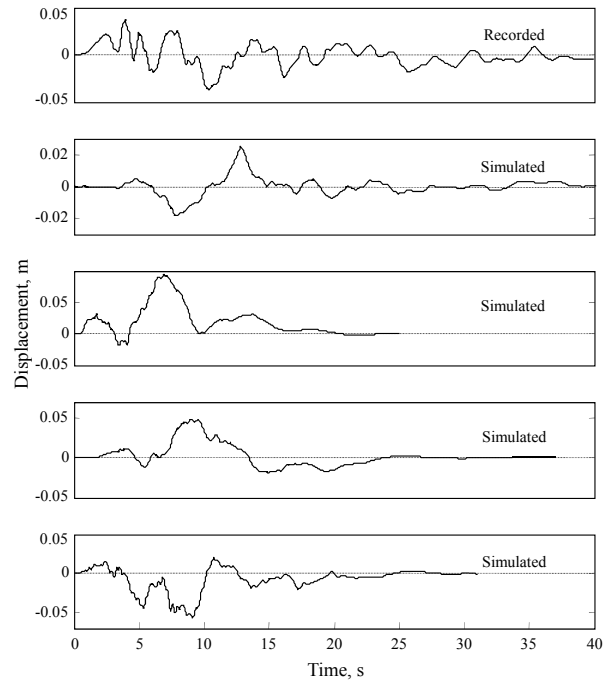
Fig. 5.3 **Recorded and synthetic motions corresponding to $F = 1$ (reverse faulting), $M = 6.93$, $R = 18.3$ km, , $V = 663$ m/s. Recorded motion is component 090 of the 1989 Loma Prieta earthquake at the Gilroy Array #6 station.**

121

Realizations of model parameters:					
I_a	$D_{5\text{-}95}$	t_{mid}	$\omega_{mid}/2\pi$	$\omega'/2\pi$	ζ_f
s.g.	s	s	Hz	Hz/s	
0.109	7.96	7.78	4.66	−0.09	0.24
0.140	13.06	13.24	3.73	−0.18	0.03
0.150	11.27	6.41	6.07	−0.07	0.29
0.010	12.05	4.09	11.45	−0.45	0.11
0.244	16.63	10.23	5.71	−0.04	0.14
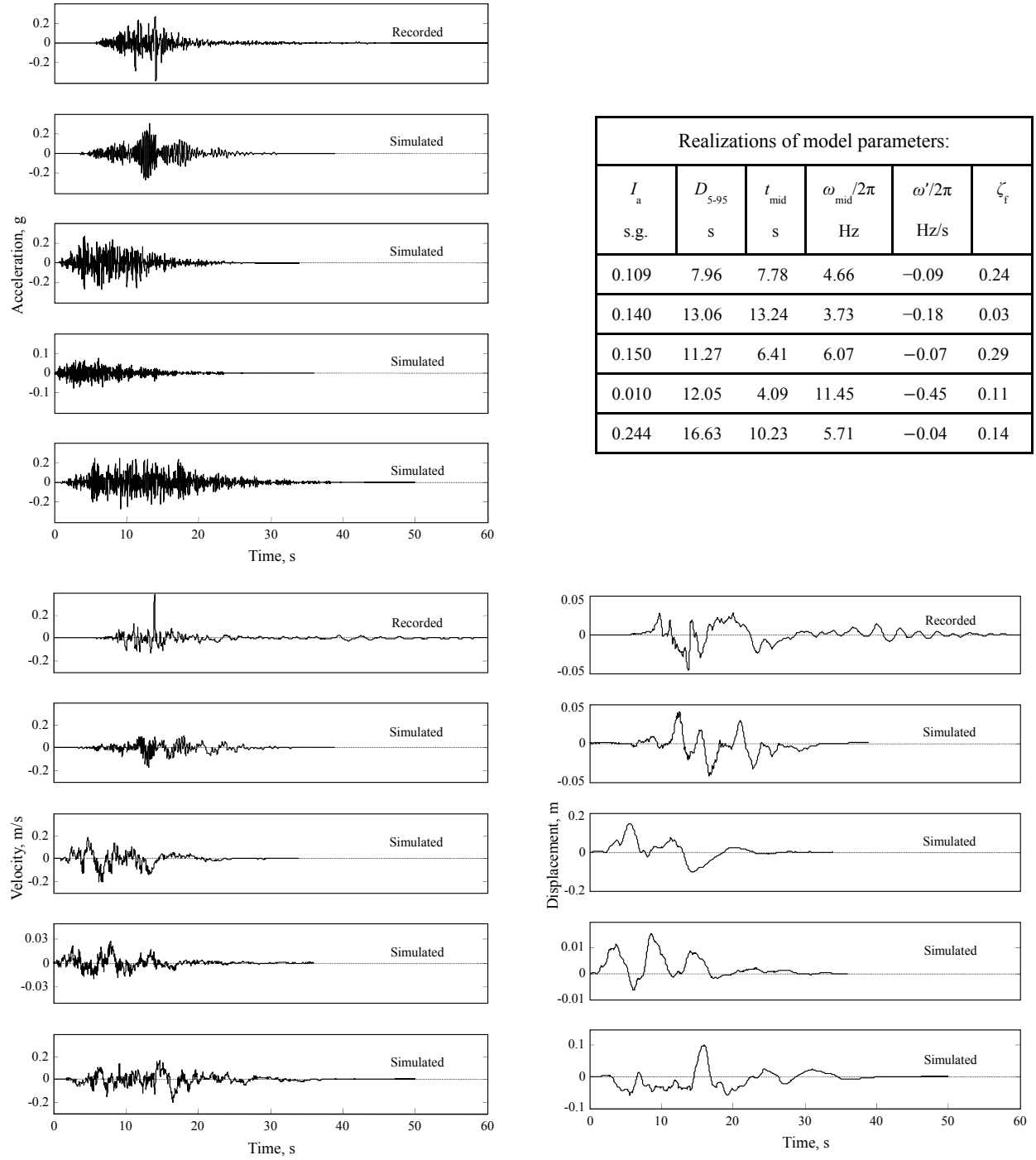
Fig. 5.4   Recorded and synthetic motions corresponding to $F = 1$ (reverse faulting), $M = 6.69$, $R = 19.1$ km, $V = 706$ m/s. Recorded motion is component 090 of the 1994 Northridge earthquake at the LA 00 station.

122

Realizations of model parameters:					
I_a s.g.	$D_{5\text{-}95}$ s	t_{mid} s	$\omega_{mid}/2\pi$ Hz	$\omega'/2\pi$ Hz/s	ζ_f
0.137	36.23	17.60	4.16	−0.06	0.34
0.088	11.14	5.63	2.72	−0.11	0.19
0.038	24.66	8.07	3.43	−0.06	0.08
0.146	16.60	10.89	2.28	−0.03	0.21
0.301	10.24	11.12	5.55	−0.01	0.27
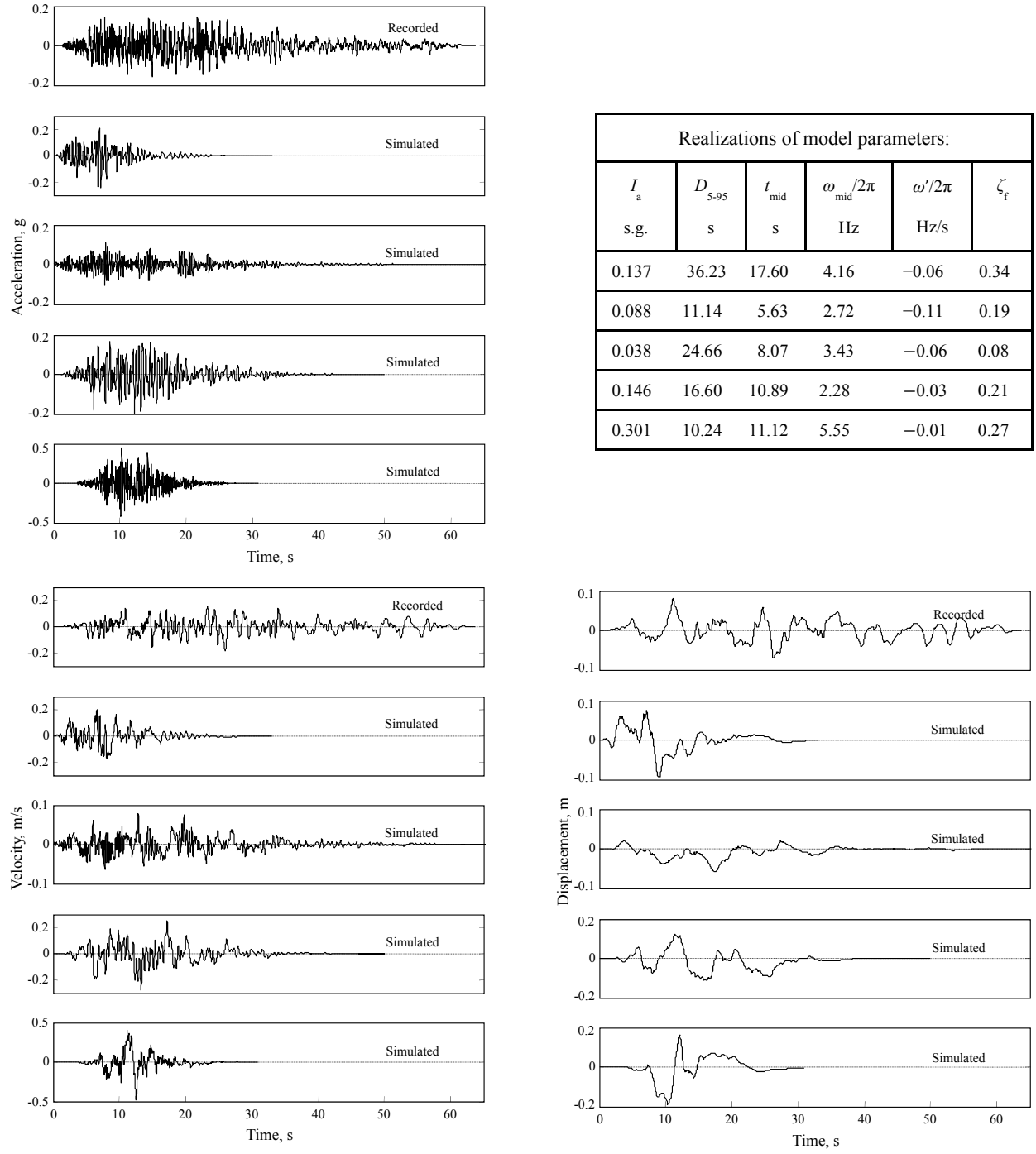
Fig. 5.5 Recorded and synthetic motions corresponding to $F = 0$ (strike-slip faulting), $M = 6.53$, $R = 15.2$ km, $V = 660$ m/s. Recorded motion is component 237 of the 1979 Imperial Valley-06 earthquake at the Cerro Prieto station.

Realizations of model parameters:					
I_a s.g.	$D_{5\text{-}95}$ s	t_{mid} s	$\omega_{mid}/2\pi$ Hz	$\omega'/2\pi$ Hz/s	ζ_f
0.102	7.56	5.68	5.99	−0.23	0.73
0.095	19.61	14.98	13.01	−0.43	0.43
0.003	21.66	4.00	11.67	−0.16	0.23
0.016	13.86	5.15	8.43	−0.43	0.55
0.233	8.67	3.40	4.23	0.03	0.41
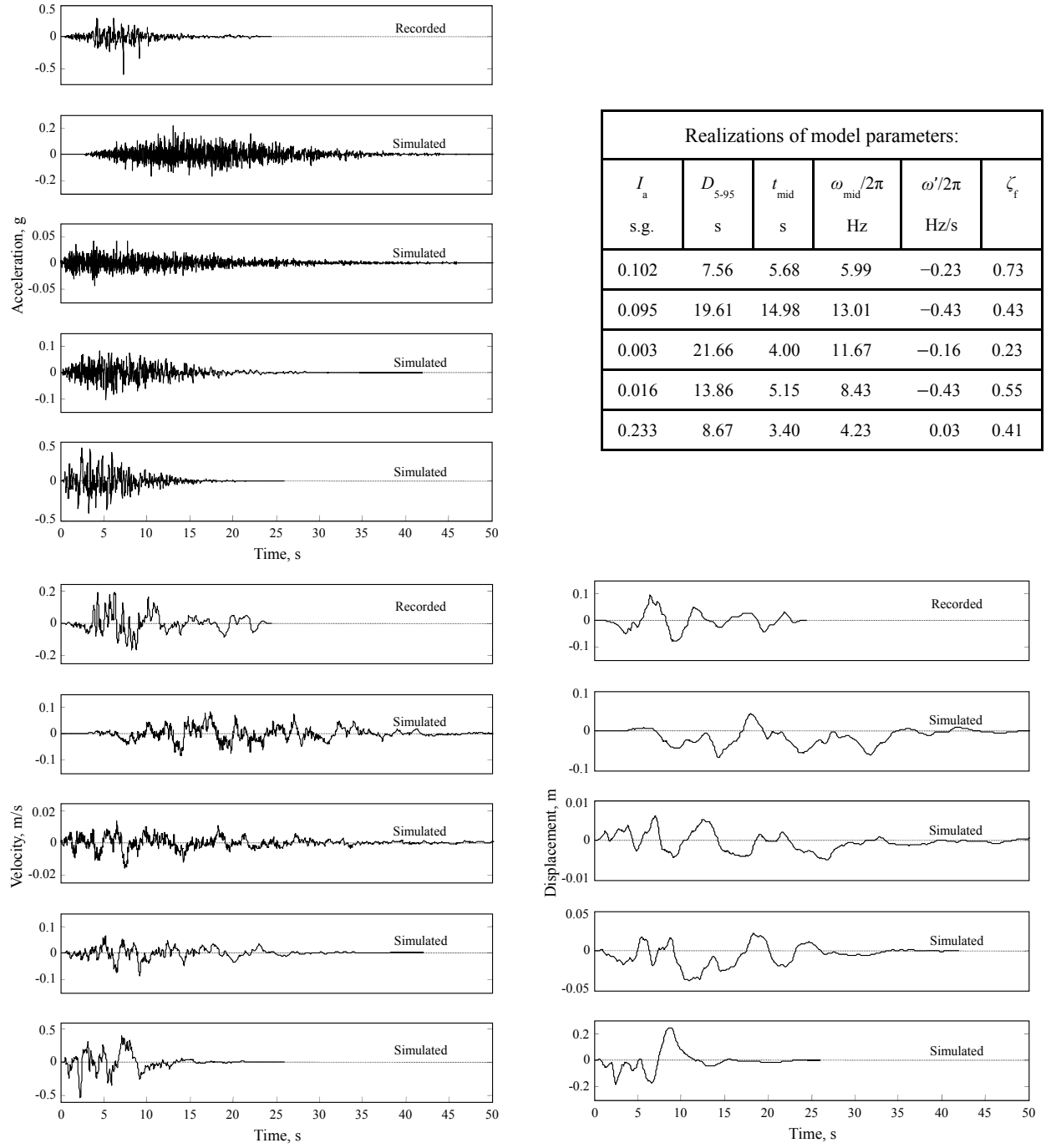
Fig. 5.6 Recorded and synthetic motions corresponding to $F = 0$ (strike-slip faulting), $M = 6.33$, $R = 14.4$ km, $V = 660$ m/s. Recorded motion is component 315 of the 1980 Victoria, Mexico, earthquake at the Cerro Prieto station.
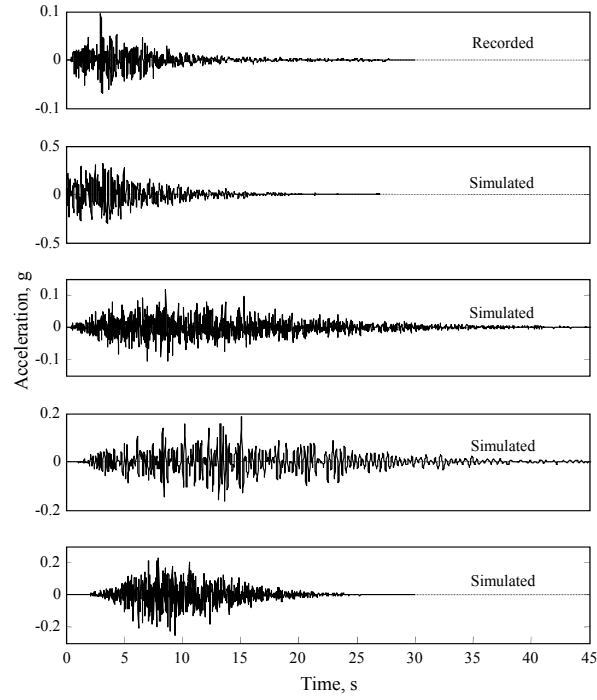
Realizations of model parameters:					
I_a s.g.	$D_{5\text{-}95}$ S	t_{mid} s	$\omega_{mid}/2\pi$ Hz	$\omega'/2\pi$ Hz/s	ζ_f
0.005	8.18	3.78	7.43	−0.16	0.07
0.219	8.89	1.54	5.61	−0.09	0.24
0.027	18.94	8.20	9.86	−0.10	0.35
0.079	22.00	12.12	3.95	−0.09	0.11
0.088	10.07	8.90	9.67	−0.02	0.34
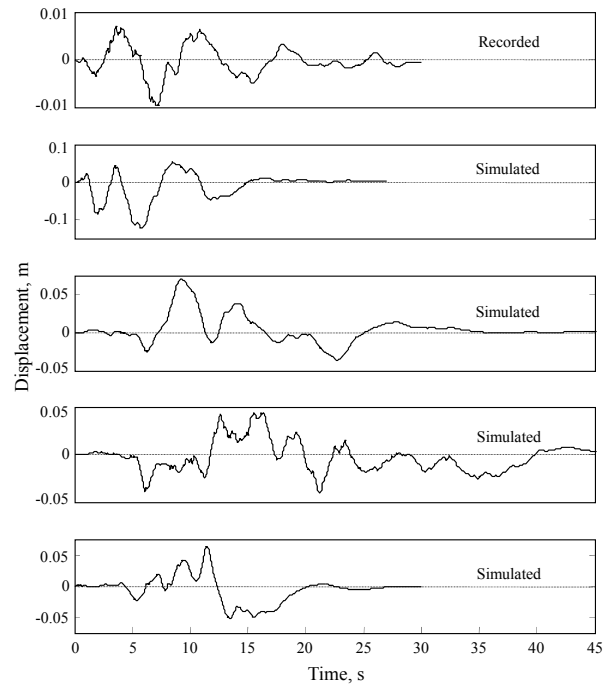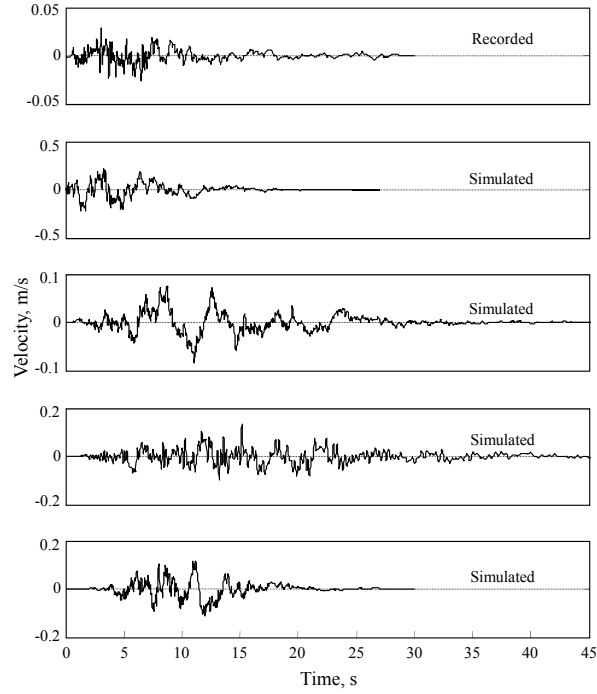
Fig. 5.7   Recorded and synthetic motions corresponding to $F = 0$ (strike-slip faulting), $M = 6.19$, $R = 14.8$ km, $V = 730$ m/s. Recorded motion is component 337 of the 1984 Morgan Hill earthquake at the Gilroy − Gavilan Coll. station.

125

Realizations of model parameters:					
I_a s.g.	D_{5-95} s	t_{mid} s	$\omega_{mid}/2\pi$ Hz	$\omega'/2\pi$ Hz/s	ζ_f
0.109	7.96	7.78	4.66	−0.09	0.24
0.109	5.42	1.67	5.95	−0.50	0.44
0.109	11.72	5.61	5.30	0.003	0.22
0.109	5.86	3.13	9.57	−0.10	0.34
0.109	8.76	6.16	11.85	−0.20	0.21
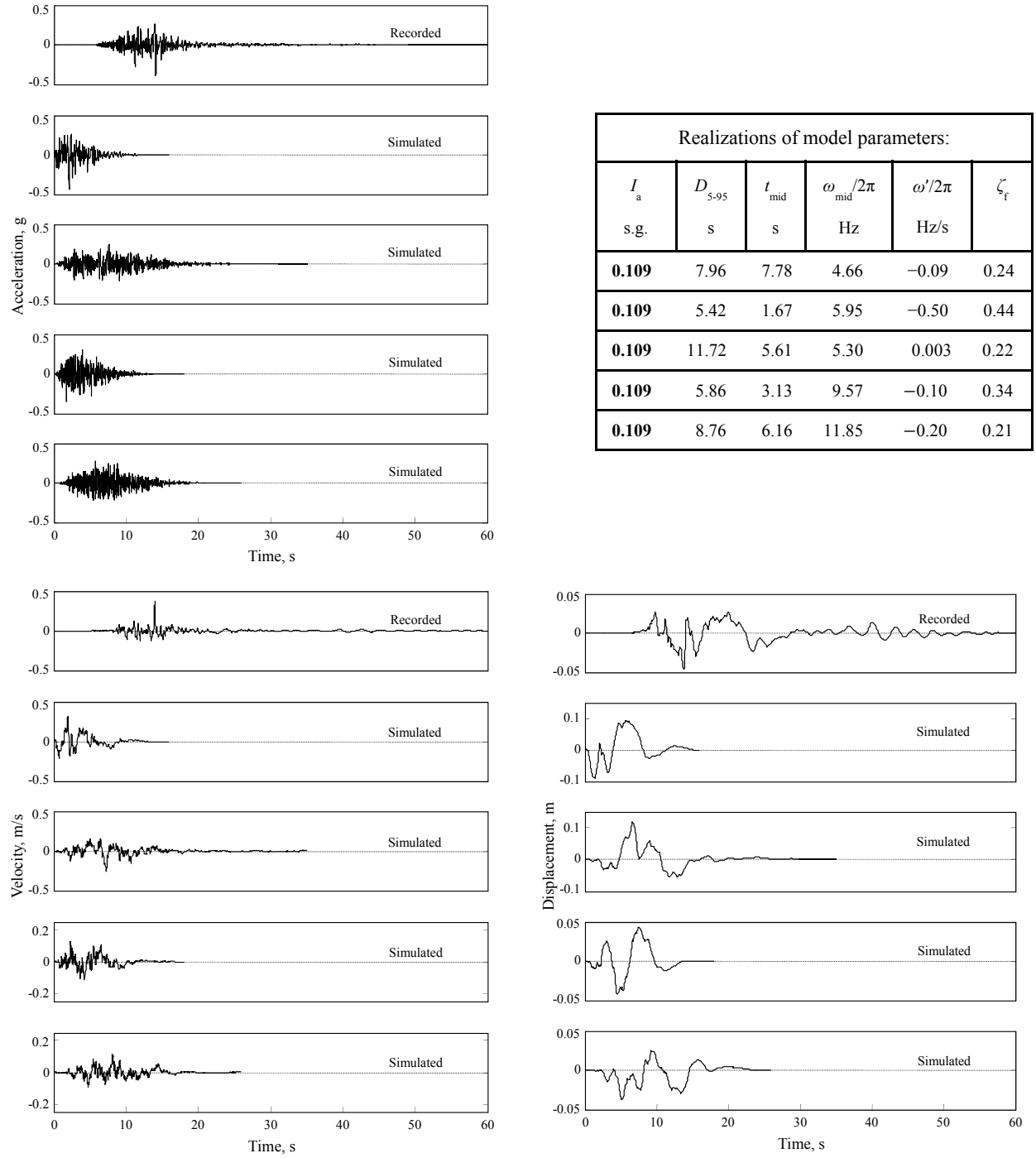
Fig. 5.8   Recorded and synthetic motions with specified Arias intensity. Recorded motion and earthquake and site characteristics are the same as in Fig. 5.4.
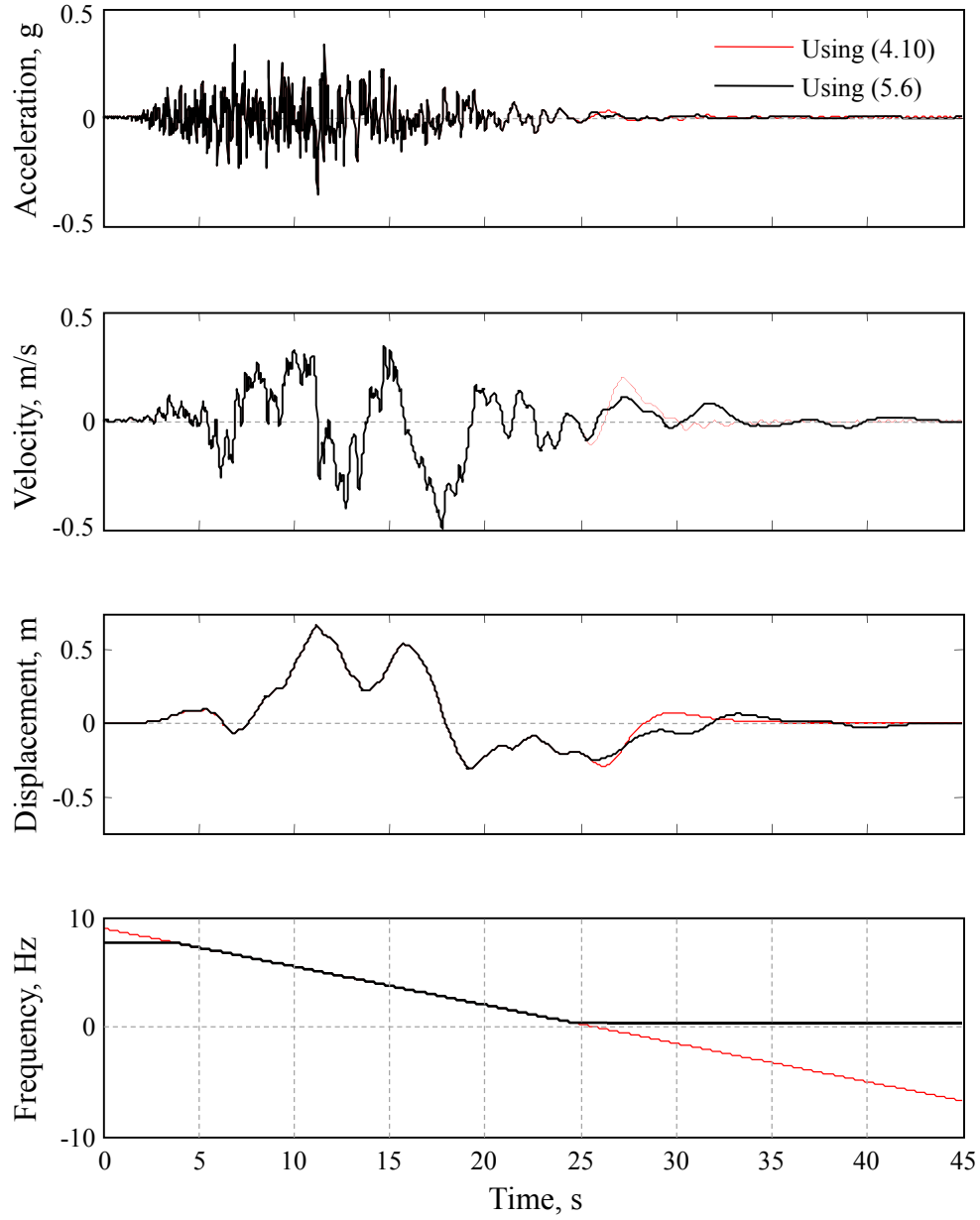
Fig. 5.9 Two simulated motions: one has a linearly decreasing filter frequency according to Eq. (4.10); the other has a filter frequency with imposed limits according to Eq. (5.6). Both motions have a total duration of $t_n = 3D_{5-95}$. Model parameters are $\bar{I}_a = 0.3$ s.g., $D_{5-95} = 15$ s, $t_{mid} = 10$ s, $\omega_{mid}/2\pi = 5.5$ Hz, $\omega'/2\pi = -0.35$ Hz/s, $\zeta_f = 0.55$.
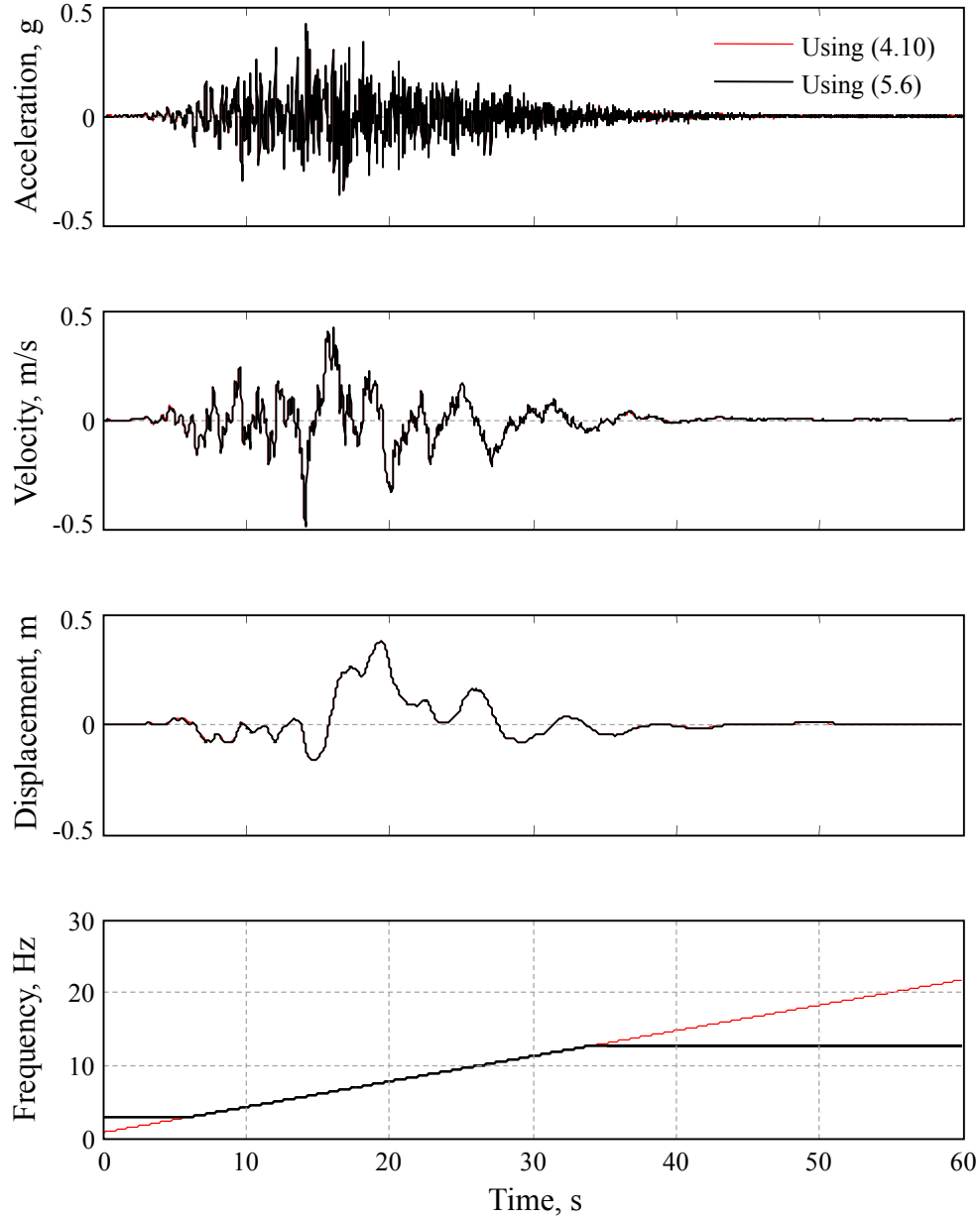
Fig. 5.10 Two simulated motions: one has a linearly increasing filter frequency according to Eq. (4.10); the other has a filter frequency with imposed limits according to Eq. (5.6). Both motions have a total duration of $t_n = 3D_{5-95}$. Model parameters are $\bar{I}_a = 0.3$ s.g., $D_{5-95} = 20$ s, $t_{mid} = 15$ s, $\omega_{mid}/2\pi = 6$ Hz, $\omega'/2\pi = +0.35$ Hz/s, $\zeta_f = 0.55$.

6   Model Validation

6.1   INTRODUCTION

The proposed method of generating a suite of synthetic ground motions for specified earthquake and site characteristics provides an appropriate representation of real ground motions that could result from an earthquake and a site with the given characteristics. This claim was partially validated in the previous chapters through modeling and examination of simulated time-histories, showing that synthetics are representative of real ground motions. For example, the stochastic process that models acceleration time-histories possesses both temporal and spectral nonstationary characteristics observed in real ground motions. Adjustments have been made to the model to ensure that residual velocity and displacement are zero (equivalent of base-line correction with recorded motions). Furthermore, we know that these synthetic acceleration time-histories have evolutionary statistical characteristics similar to real accelerograms. This was achieved by scrutinizing the statistical characteristics of many recorded ground motions and modeling the stochastic process accordingly. Among these evolutionary statistical characteristics were the evolving cumulative energy (controlling intensity and duration of the motion), which was measured by graphs similar to the one in Figure 3.2a, and the evolving frequency content, which was measured by graphs similar to the ones in Figures 3.4 and 3.5. In addition to acceleration, velocity and displacement time-histories were studied and qualitatively (considering their general features such as frequency contents and time-history traces) compared with real ground motions recorded during previous earthquakes (see Chapter 5). These comparisons indicated that not only acceleration, but also velocity and displacement time-histories of synthetic motions have characteristics and variability similar to those of real earthquake ground motions. In this chapter, the proposed method of generating a suite of synthetic ground motions for specified earthquake and site characteristics is validated through examination of elastic response spectra. Working with the elastic response spectrum allows the

variability among synthetic and real ground motions to be measured and compared quantitatively (as opposed to the qualitative comparison between time-histories presented in Chapter 5).

The response spectrum of an acceleration time-history is the plot of the absolute peak responses of single-degree-of-freedom oscillators with a specified damping subjected to that acceleration time-history at its base against their natural frequencies (or periods). Response spectra are useful tools in earthquake engineering because structural design is usually based on the peak values of earthquake-induced forces and deformations. A response spectrum corresponding to a design scenario (identified by its earthquake and site characteristics) is usually referred to as the design response spectrum. Code provisions and empirical ground motion prediction equations (GMPEs) are available that aid in constructing design response spectra for given earthquake and site characteristics. While a response spectrum may be used directly to calculate an exact solution for the response of a single-degree-of-freedom linear system, it may be utilized to obtain an approximate solution for the response of a multi-degree-of-freedom linear system (e.g., by modal combination). This type of structural analysis is referred to as response-spectrum analysis, which due to its simplicity is frequently used in practice, though it is applicable only to linear systems. If a structure is expected to behave nonlinearly, more complex approaches such as response-history analysis are necessary, which requires knowledge of acceleration time-histories. The subject of this study has been to generate time-histories for response-history analysis. Considering the frequent use of response spectrum in practice, a reasonable validation approach for the simulated time-histories in this study is to investigate the validity of their elastic response spectra by comparisons against the response spectra of real ground motions and by comparisons against existing GMPEs that are used and trusted in practice for prediction of design response spectra.

In this chapter, first the elastic response spectra of synthetic motions are compared to those of recorded motions. For selected earthquake and site characteristics, specific examples are provided to illustrate that the response spectrum of a recorded motion (regarded as just one realization of possible ground motions for the specified design scenario) is within the range predicted by synthetic motions at any given spectral period. Then, the statistics of the elastic response spectra of a large number of simulated motions are compared to values predicted by the existing GMPEs for various design scenarios. It is concluded that, in general, the median and variability of the response spectra of simulated ground motions closely agree with the median

and variability predicted by the Next Generation Attenuation (NGA) GMPEs. Also, limitations on the applicability of synthetic motions (e.g., in terms of spectral periods and earthquake and site characteristics) are discussed.

6.2   VALIDATION AGAINST RECORDED GROUND MOTIONS

To validate the simulated ground motions against real ground motions, for specified earthquake and site characteristics 5% damped elastic response spectra of a large number of synthetic motions are calculated and compared to those of a recorded motion having the specified earthquake and site characteristics. The objective of this comparison is to examine each spectral period and see whether the corresponding recorded spectral value falls within the range predicted by the synthetic spectral values. This result is expected if the suite of synthetic motions adequately represents the natural variability of real ground motions for the given earthquake and site characteristics. To compute the response spectrum of an acceleration time-history, single-degree-of-freedom oscillators with a range of natural frequencies and damping ratio of 0.05 are subjected to the acceleration time-history. Numerical time-stepping methods are then used to estimate the response of the oscillator over time. For each oscillator with natural frequency, ω_n, the peak displacement response over time, D_n, is selected. The plot of peak displacement responses, D_n, versus spectral periods, $T_n = 2\pi/\omega_n$, is referred to as the *displacement response spectrum*, while the plot of $A_n = \omega_n^2 D_n$ versus T_n is referred to as the *pseudo-acceleration response spectrum*. In particular, the response spectra shown in the figures of this report have been computed using the central difference method (see Chopra [2001], Chapter 5), which is stable when $\Delta t/T_n < 1/\pi$.

Six sets of comparisons are provided in Figures 6.1–6.6. Each figure shows 5% damped elastic response spectra of two horizontal components of a recorded ground motion against 5% damped elastic response spectra of 50 synthetic ground motions generated for the same fault type, moment magnitude, source-to-site distance, and V (abbreviated notation for V_{S30}, the shear-wave velocity of top 30 m) values as the recorded motion. The synthetic motions are simulated for a total duration of $t_n = 2D_{5-95}$, a time discretization step equal to 0.01 s, and a filter frequency of 0.1 Hz for the high-pass filtering according to (2.28). Figures 6.1 and 6.2 show accelerograms recorded during the 1994 Northridge earthquake (reverse faulting, $M = 6.69$), but

at different locations. Figure 6.1 corresponds to a distance of $R = 20.3$ km with $V = 1223$ m/s, while Figure 6.2 corresponds to a distance of $R = 41.6$ km with $V = 822$ m/s. It is seen that the spectra of the recorded motions, which should be regarded as resulting from just one pair of realizations of possible ground motions produced by an earthquake of similar characteristics, are within the range of variability of the spectra of the simulated motions throughout the period range considered. This supports our claim that the variability observed in the spectra of the synthetic motions is representative of the variability inherent in real ground motions for given earthquake and site characteristics. Similar results are observed in Figures 6.3–6.6, which have been selected to represent ground motions induced from earthquakes of different magnitudes. Moment magnitudes of the events that produced the records presented in these figures are $M = 6.36$, 6.93, 7.35, and 7.62, respectively, each belonging to a different magnitude bin: 6.0 to 6.5, 6.5 to 7.0, 7.0 to 7.5, and 7.5 to 8.0.

The recorded ground motions of the response spectra shown in Figures 6.1–6.6 have been processed and high-passed filtered by various reporting agencies. The corner frequency of the applied high-pass filter for each record is reported in the PEER-NGA database. These corner frequencies are 0.13 and 0.1 Hz for the records of Figure 6.1; 0.12, 0.2, 0.05, and 0.1 Hz for both components of the records in Figures 6.2, 6.3, 6.4, and 6.5, respectively; and 0.04 and 0.03 Hz for the records of Figure 6.6. Even though the corner frequencies of recorded motions vary significantly, the filter frequency of 0.1 Hz used for high-pass filtering of the synthetic motions according to (2.28) appears to give satisfactory results even for long periods. For example, in Figure 6.3, where the recorded motion has been processed with the rather large corner frequency of 0.2 Hz, deviations between the synthetic and recorded response spectra are not too large. As for the other cases, the spectra of the recorded motions are well within the range of variability of the spectra of the 50 synthetic motions.

In Figures 6.1–6.6, the spectral values are shown up to a period of 10 s. Such long spectral periods (e.g., longer than 5 s) are typically unnecessary for structural design and analysis. Furthermore, the spectra values at such long periods may not be reliable, as they can be sensitive to the procedure selected for processing and high-pass filtering that recorded motions are subjected to. We have considered such long periods merely to examine the limitations of our simulation method, which appears not to be restricted by spectral periods, at least in the range of periods of interest in structural engineering.

6.3 VALIDATION AGAINST NGA MODELS

The Next Generation Attenuation (NGA) models are five sets of ground motion models for shallow crustal earthquakes in the Western United States and similar active tectonic regions. The five teams who worked on these models were the developers of five pre-existing and widely used ground motion attenuation models: (1) Abrahamson and Silva, (2) Boore and Atkinson, (3) Campbell and Bozorgnia, (4) Chiou and Youngs, and (5) Idriss. Power et al. (2008) provide an overview of the NGA project, and Abrahamson et al. (2008) compare the five NGA models and provide explanations for their differences. In addition to many formal publications, reports documenting NGA models and the ground motion database are available electronically from the PEER website (http://peer.berkeley.edu/ngawest/index.html).

The NGA models describe the probability distribution (more precisely, the median and variability of an assumed distribution) of peak ground motion intensities in terms of the properties of the earthquake source (faulting mechanism and magnitude), the wave propagation path (source-to-site distance), and site response (site class or V_{S30}). For more refinement in modeling, additional factors have been introduced in some NGA models. For example, the model by Chiou and Youngs (2008) includes additional factors to account for the effects of rupture-depth, hanging-wall, soil/sediment depth, nonlinear site amplification, etc. Other models either explicitly or implicitly account for or completely neglect the above mentioned effects. The ground motion intensities that have been modeled by NGA project include the peak motion values (i.e., peak ground acceleration, velocity, and displacement) and the 5% damped elastic pseudo-acceleration response spectra at oscillator periods ranging from 0.01 to 10.0 s. These models provide predictions for the geometric average of the two horizontal components. The models for response spectra are used in this section for comparison with the spectra of synthetic motions.

6.3.1 Probabilistic Nature of Response Spectrum

At a given period, the response spectrum ordinate for specified earthquake and site characteristics is a random variable. The distribution of this random variable has implicitly been assumed to be lognormal by attenuation modelers (including NGA modelers), who have

regressed the natural logarithm of the response spectrum ordinate against earthquake and site characteristics. Figure 6.7 illustrates the probabilistic nature of the response spectrum. Let $A(T)$ represent elastic pseudo-acceleration response spectrum at period T. Figure 6.7 shows the natural logarithm of $A(T)$ for an ensemble of 30 simulated records for earthquake and site characteristics $F = 0$, $M = 7.0$, $R = 20$ km, and $V = 760$ m/s plotted as a function of T. At any given period T, this ensemble represents sample realizations of $\ln(A)$ at that period. As an example, at 0.5 s period, the mean and mean $\pm$ one standard deviation of the sample realizations of $\ln(A)$ are indicated by black dots in the figure. Assuming that A is lognormally distributed, the corresponding probability density function of $\ln(A)$, which is normal, is plotted in the figure at the period of 0.5 s. The NGA models predict the mean and standard deviation of the natural logarithm of response spectrum at a given period, i.e., the black dots in Figure 6.7. These statistics correspond to the median and logarithmic standard deviation of the response spectrum at the given period. In the following, these statistics are compared with their corresponding values obtained for synthetic motions.

Error is inherent in statistical descriptors when they are estimated using sample realizations of a random variable. The magnitude of this error depends on the sample size. A study was performed to identify the required number of simulations that would provide adequate accuracy in the sample statistics of the synthetic response spectra. In these studies, 10 sets of N synthetic records were simulated. For each set, the logarithmic mean and standard deviation of the response spectra were calculated and the variability was examined among the 10 sets. Figure 6.8 provides plots of the logarithmic means (solid lines) and means $\pm$ one standard deviations (dotted lines) of response spectra for each of the 10 sets for $N = 10$, 30, 100, and 500. It was concluded that the accuracy of the statistics estimated from 500 simulations is adequate for our comparison purposes.

6.3.2 Comparison with NGA Models

The synthetic ground motions are intended for use in engineering practice as predictions of future earthquake ground motions at a given site. Therefore, a reasonable validation approach is to examine how these motions compare with ground motion prediction equations used in practice. For this purpose, we compare the statistics of 5% damped elastic response spectra of a

set of 500 synthetic accelerograms with the corresponding statistics of response spectra using ground motion prediction equations developed by Abrahamson and Silva (2008), Boore and Atkinson (2008), Campbell and Bozorgnia (2008), and Chiou and Youngs (2008), which are all based on various subsets of the NGA strong-motion database. Recall that the database used in this study is a subset of the database used in Campbell and Bozorgnia (2008). Therefore, comparisons with Campbell and Bozorgnia model are more appropriate. However, to have a more comprehensive study, and considering that usually a combination of the four models mentioned above is used in practice, the other three models have also been included.

To compare the statistics of response spectra for simulated motions with their corresponding values predicted by NGA models, 500 realizations of $\log_{10}(A)$ are generated. At any given period, sample median and standard deviations, denoted by $\text{med}(\log_{10}(A))$ and $\text{std}(\log_{10}(A))$, are computed. Then $10^{\text{med}(\log_{10}(A))}$ and $10^{\text{med}(\log_{10}(A))\pm\text{std}(\log_{10}(A))}$ are plotted in the logarithmic scale. In the following, these plots are referred to as the median and median $\pm$ one logarithmic standard deviation of response spectra. Equivalent plots are generated for NGA models. Since NGA models predict $\text{med}(A)$ and $\text{std}(\ln(A))$, at a given period, we first calculate

$$\text{med}(\log_{10}(A)) = \log_{10}(\text{med}(A)) \tag{6.1}$$

$$\text{std}(\log_{10}(A)) = \frac{\text{std}(\ln(A))}{\ln(10)} \tag{6.2}$$

and then plot $10^{\text{med}(\log_{10}(A))}$ and $10^{\text{med}(\log_{10}(A))\pm\text{std}(\log_{10}(A))}$ in the logarithmic scale.

Figures 6.9 through 6.15 compare the median and median $\pm$ one logarithmic standard deviation values of the two sets of response spectra (i.e., simulated and predicted) for periods up to 5 s for selected moment magnitude ($M = 6.0, 6.5, 7.0, 7.5,$ and 8.0) and source-to-site distance values ($R = 10, 20,$ and 40 km for $M = 7.0$; $R = 20$ km for other magnitudes). Strike-slip faulting and $V = 760$ m/s are selected in all cases. Also shown, as dashed lines, are the averages of the four selected NGA prediction equations. Interpolation is used for periods where NGA models are not available. Typical values are chosen for the earthquake and site parameters used in NGA models, which are not included in the simulation model. These values are reported in the captions of Figures 6.9–6.15.

Note that the plots are presented in the logarithmic scale. As a result, the spectral values and their deviations for long periods appear larger than they really are. It can be seen that except for the case of $M = 6.0$, both the median curves and dispersions of the synthetic response spectra

135

are in close agreement with the corresponding statistics of the four NGA-based prediction equations. The case of $M = 6.0$ coincides with the lower boundary of our database, where few records are available and the model fit is not as good. In any case, this magnitude level is not of interest for design against "strong" ground motions, where nonlinear response-history analysis may be of interest. For all other magnitudes and for all distances (even magnitudes as high as 8.0, or distances as short as 10 km), the observed deviations are much smaller than the variabilities present in the prediction equations. Thus, we conclude that the method presented in this study for generating synthetic ground motions for given earthquake and site characteristics is viable and consistent with existing prediction equations for source-to-site distances $R \geq 10$ km and moment magnitudes greater than about $M = 6.5$.
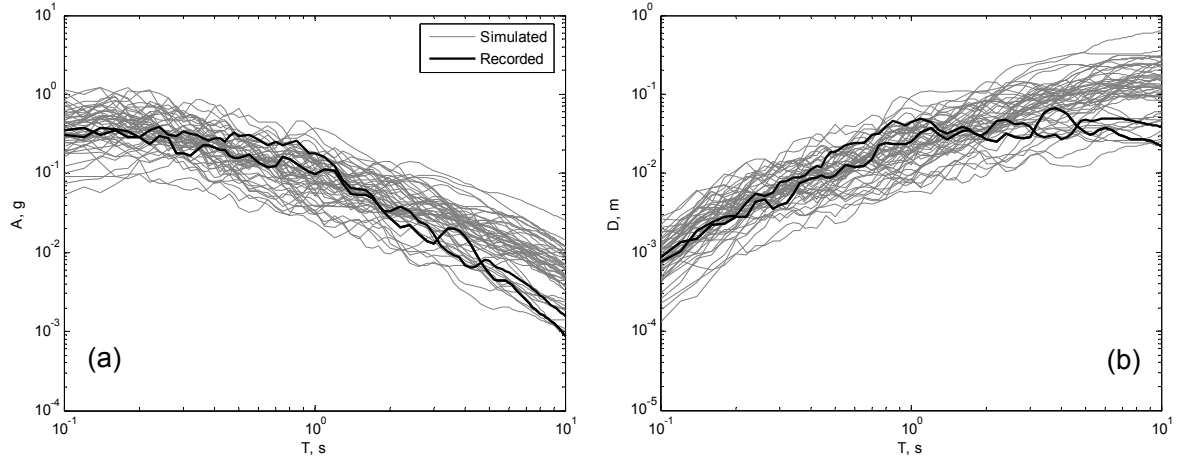
Fig. 6.1 **Elastic 5% damped response of two horizontal components of the 1994 Northridge earthquake recorded at the LA Wonderland Ave station and of 50 synthetic motions: (a) pseudo-acceleration spectra, (b) displacement spectra. Motions correspond to $F = 1$ (reverse faulting), $M = 6.69$, $R = 20.3$ km, and $V = 1223$ m/s.**
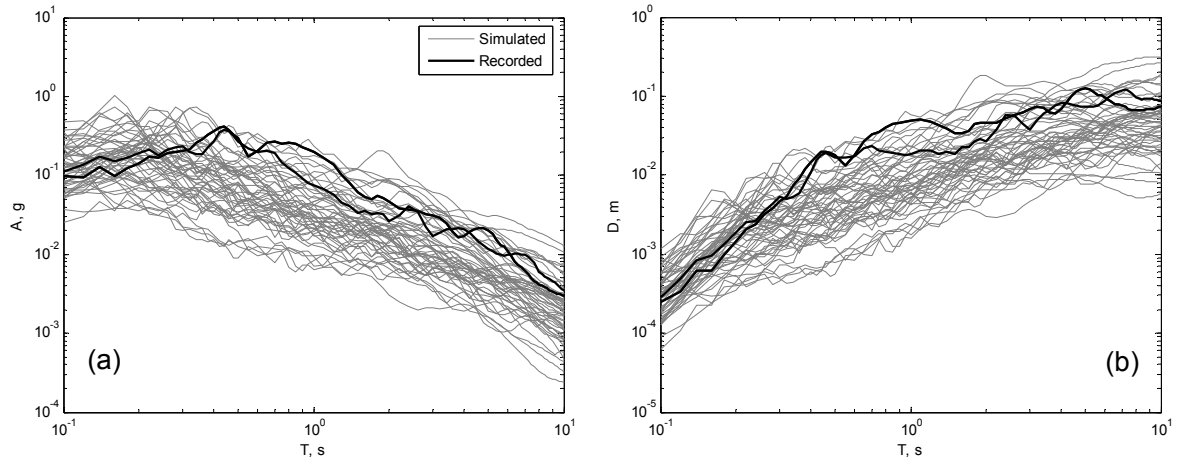
Fig. 6.2 **Elastic 5% damped response of two horizontal components of the 1994 Northridge earthquake recorded at the Sandberg – Bald Mtn station and of 50 synthetic motions: (a) pseudo-acceleration spectra, (b) displacement spectra. Motions correspond to $F = 1$ (reverse faulting), $M = 6.69$, $R = 41.6$ km, and $V = 822$ m/s.**
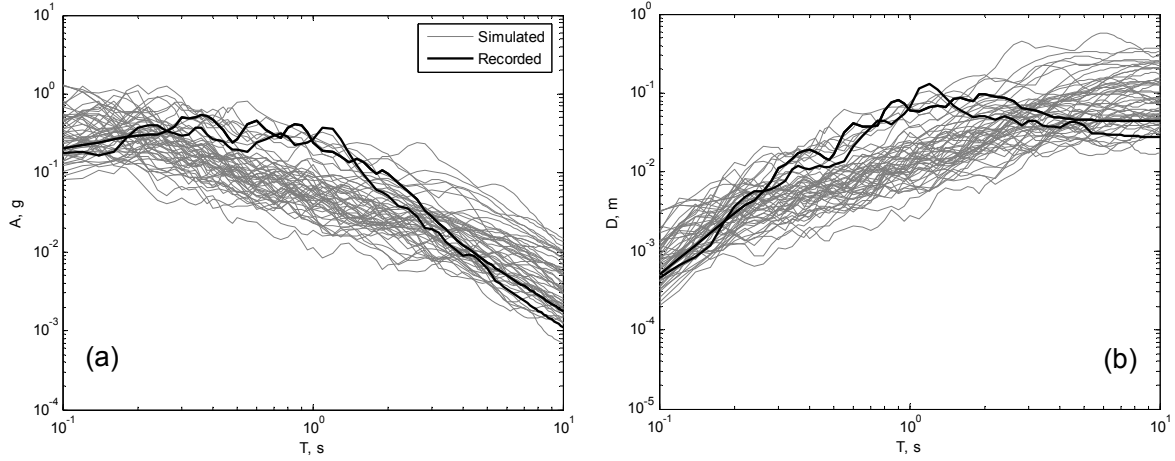
Fig. 6.3　**Elastic 5% damped response of two horizontal components of the 1983 Coalinga-01 earthquake recorded at the Slack Canyon station and of 50 synthetic motions: (a) pseudo-acceleration spectra, (b) displacement spectra. Motions correspond to $F = 1$ (reverse faulting), $M = 6.36$, $R = 27.5$ km, and $V = 685$ m/s.**
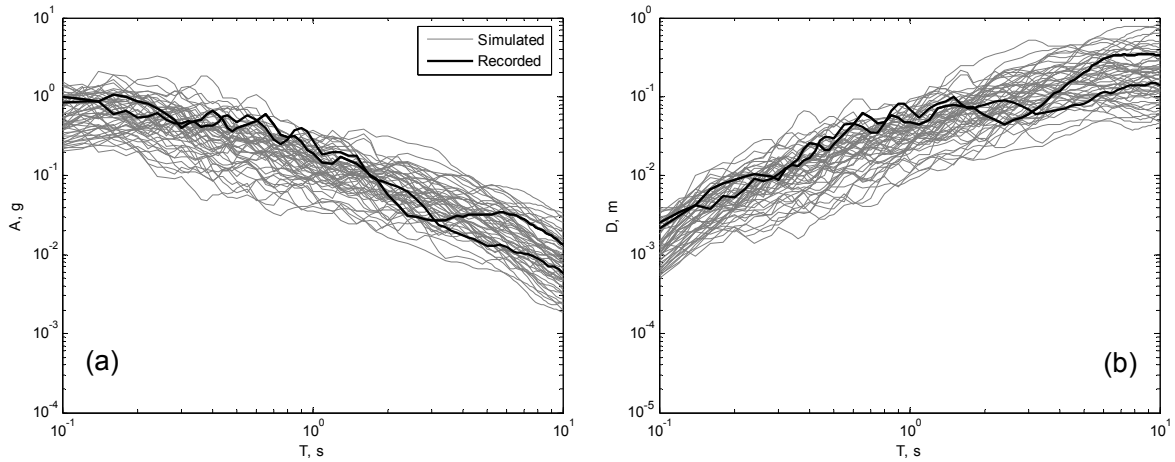
Fig. 6.4　**Elastic 5% damped response of two horizontal components of the 1989 Loma Prieta earthquake recorded at the San Jose – Santa Teresa Hills station and of 50 synthetic motions: (a) pseudo-acceleration spectra, (b) displacement spectra. Motions correspond to $F = 1$ (reverse faulting), $M = 6.93$, $R = 14.7$ km, and $V = 672$ m/s.**
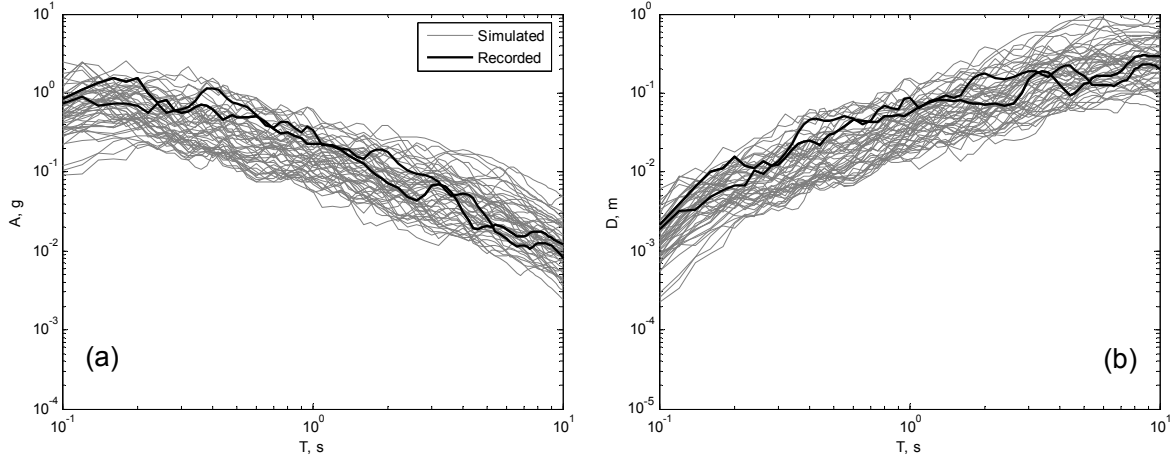
Fig. 6.5 **Elastic 5% damped response of two horizontal components of the 1978 Tabas, Iran, earthquake recorded at the Dayhook station and of 50 synthetic motions: (a) pseudo-acceleration spectra, (b) displacement spectra. Motions correspond to $F = 1$ (reverse faulting), $M = 7.35$, $R = 13.9$ km, and $V = 660$ m/s.**
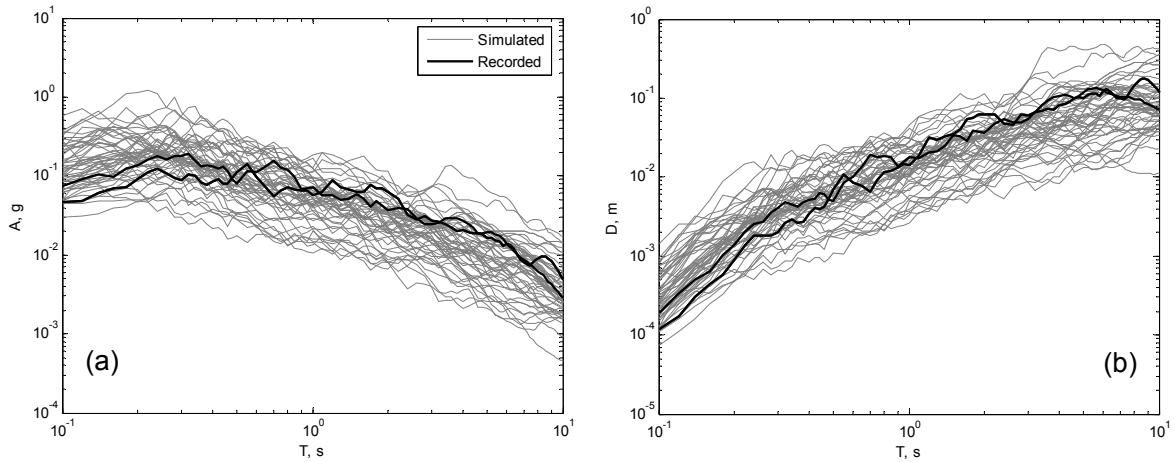
Fig. 6.6 **Elastic 5% damped response of two horizontal components of the 1999 Chi-Chi, Taiwan, earthquake recorded at the HWA038 station and of 50 synthetic motions: (a) pseudo-acceleration spectra, (b) displacement spectra. Motions correspond to $F = 1$ (reverse faulting), $M = 7.62$, $R = 42.5$ km, and $V = 643$ m/s.**
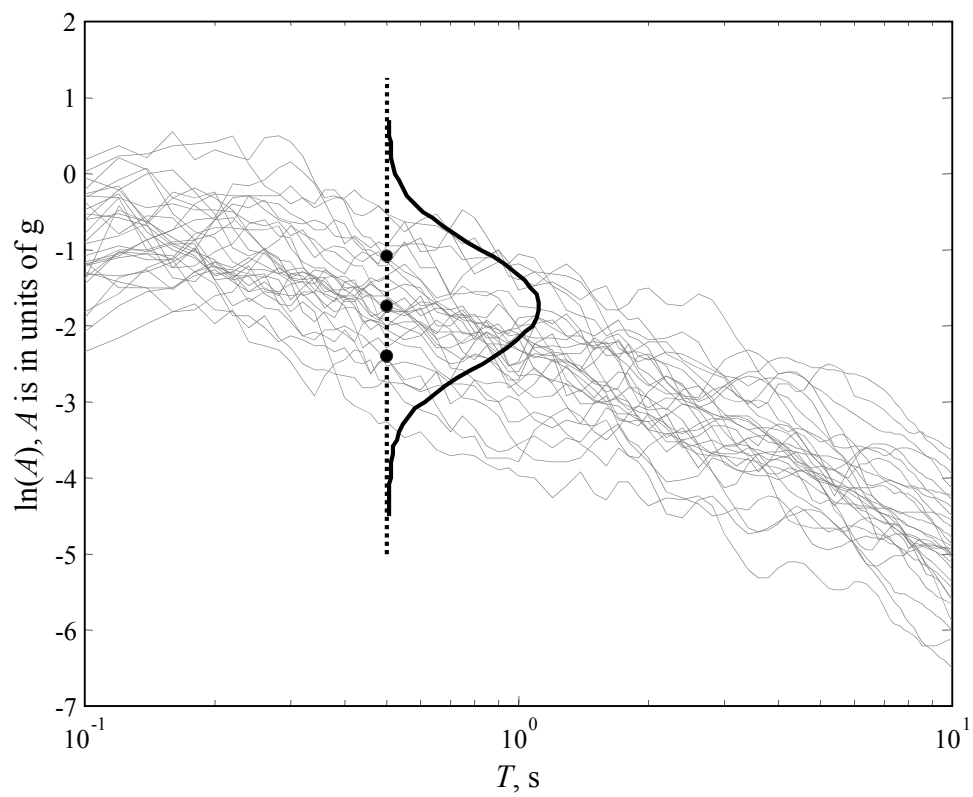
Fig. 6.7 Probabilistic nature of response spectrum.
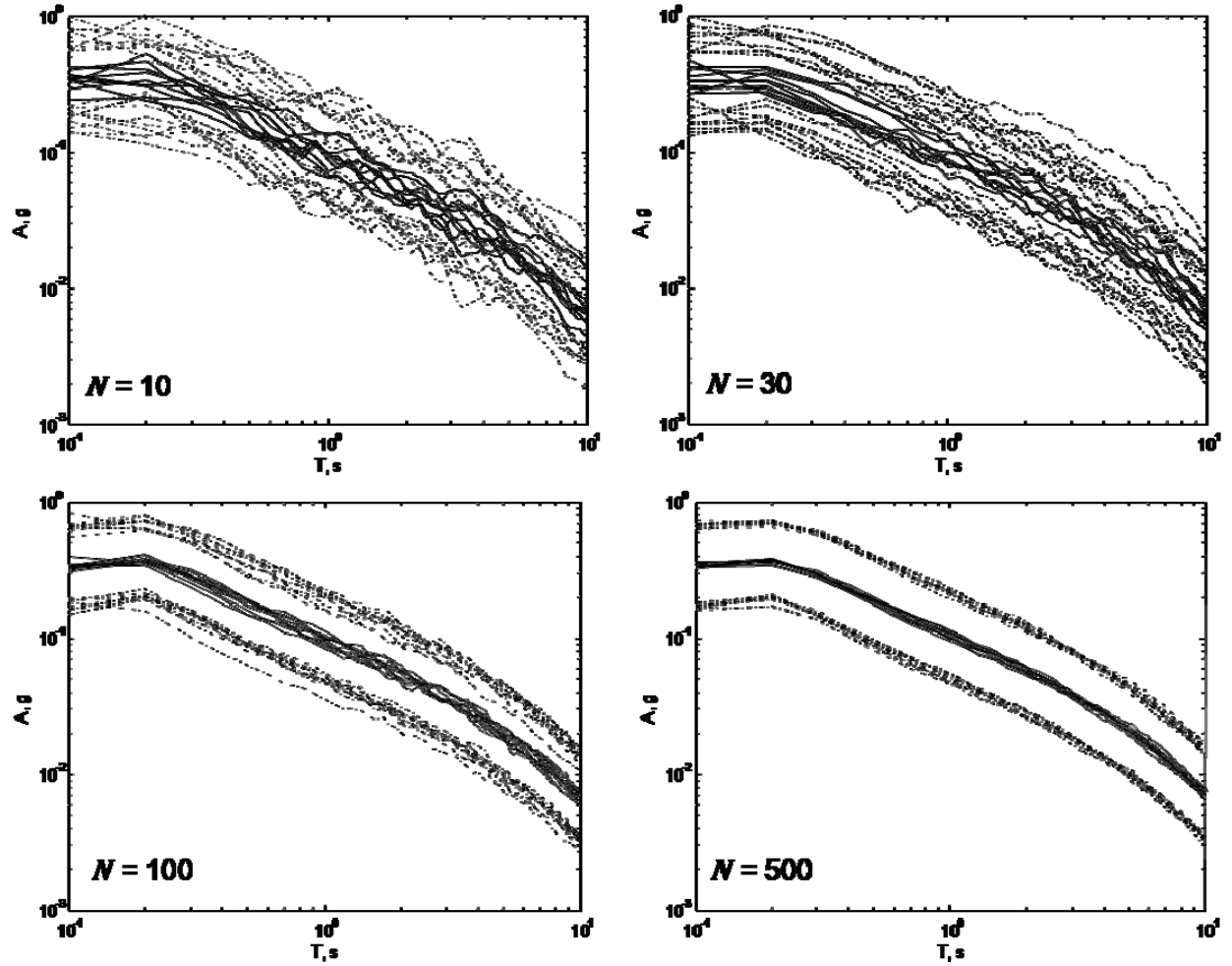
Fig. 6.8 **Examining the stability of statistical measures for 10, 30, 100, and 500 simulations. Each solid line represents the sample mean of logarithm of response spectra for *N* synthetic motions; dotted lines are their corresponding mean $\pm$ one logarithmic standard deviations.**
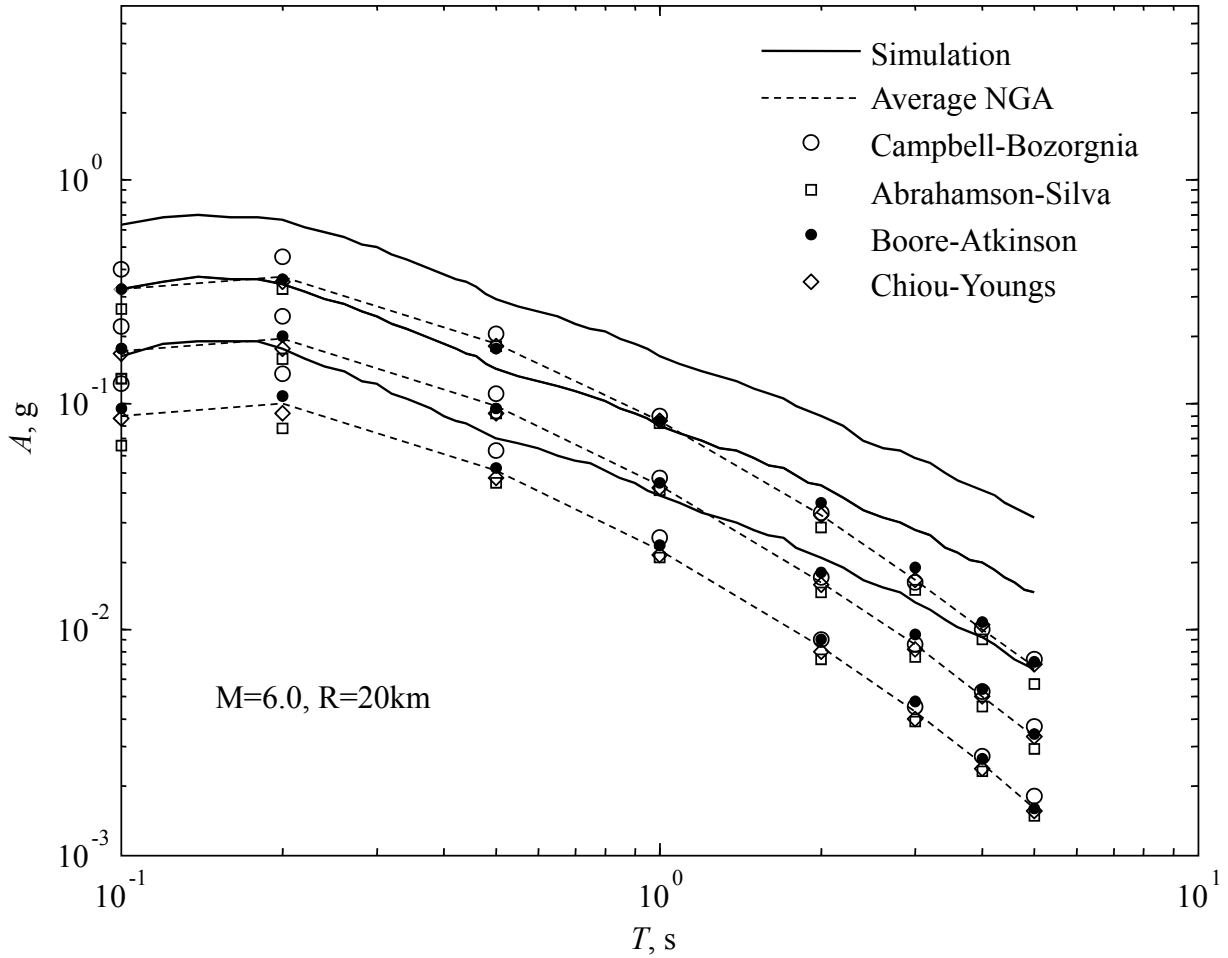
Fig. 6.9 Median and median $\pm$ one logarithmic standard deviation of 5% damped pseudo acceleration response spectra for 500 synthetic motions and corresponding values predicted by the average of four NGA-based prediction models for $F = 0$ (strike-slip faulting), $M = 6.0$, $R = 20$ km, $V = 760$ m/s. Estimated NGA values are based on a rupture width of 20 km, depth to top of rupture of 1 km, $Z_{2.5} = 1$ km for Campbell-Bozorgnia, $Z_{1.0} = 0.034$ km for Abrahamson-Silva, and $Z_{1.0} = 0.024$ km for Chiou-Youngs.
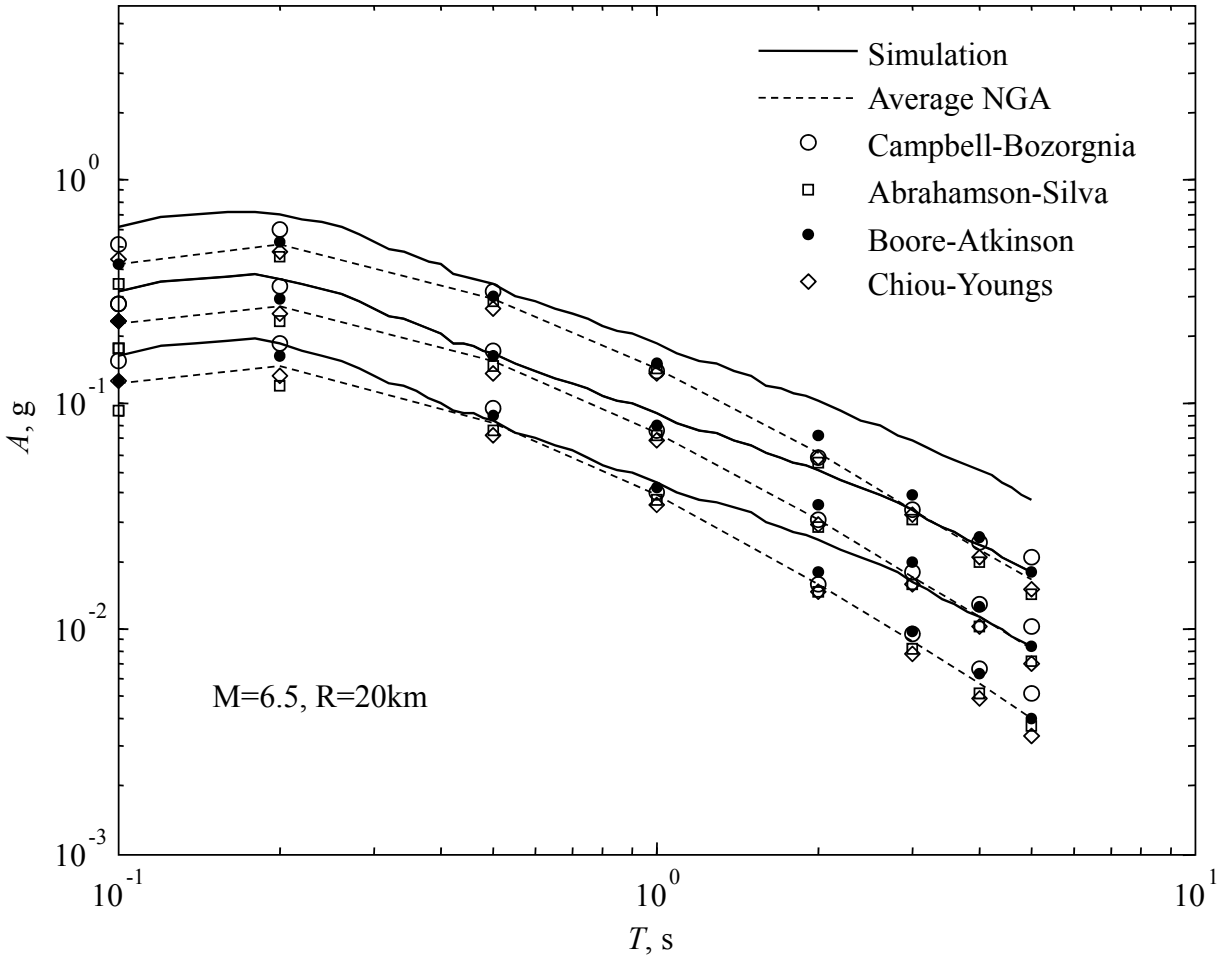
Fig. 6.10 **Median and median $\pm$ one logarithmic standard deviation of 5% damped pseudo acceleration response spectra for 500 synthetic motions and corresponding values predicted by the average of four NGA-based prediction models for $F = 0$ (strike-slip faulting), $M = 6.5$, $R = 20$ km, $V = 760$ m/s. Estimated NGA values are based on a rupture width of 20 km, depth to top of rupture of 1 km, $Z_{2.5} = 1$ km for Campbell-Bozorgnia, $Z_{1.0} = 0.034$ km for Abrahamson-Silva, and $Z_{1.0} = 0.024$ km for Chiou-Youngs.**
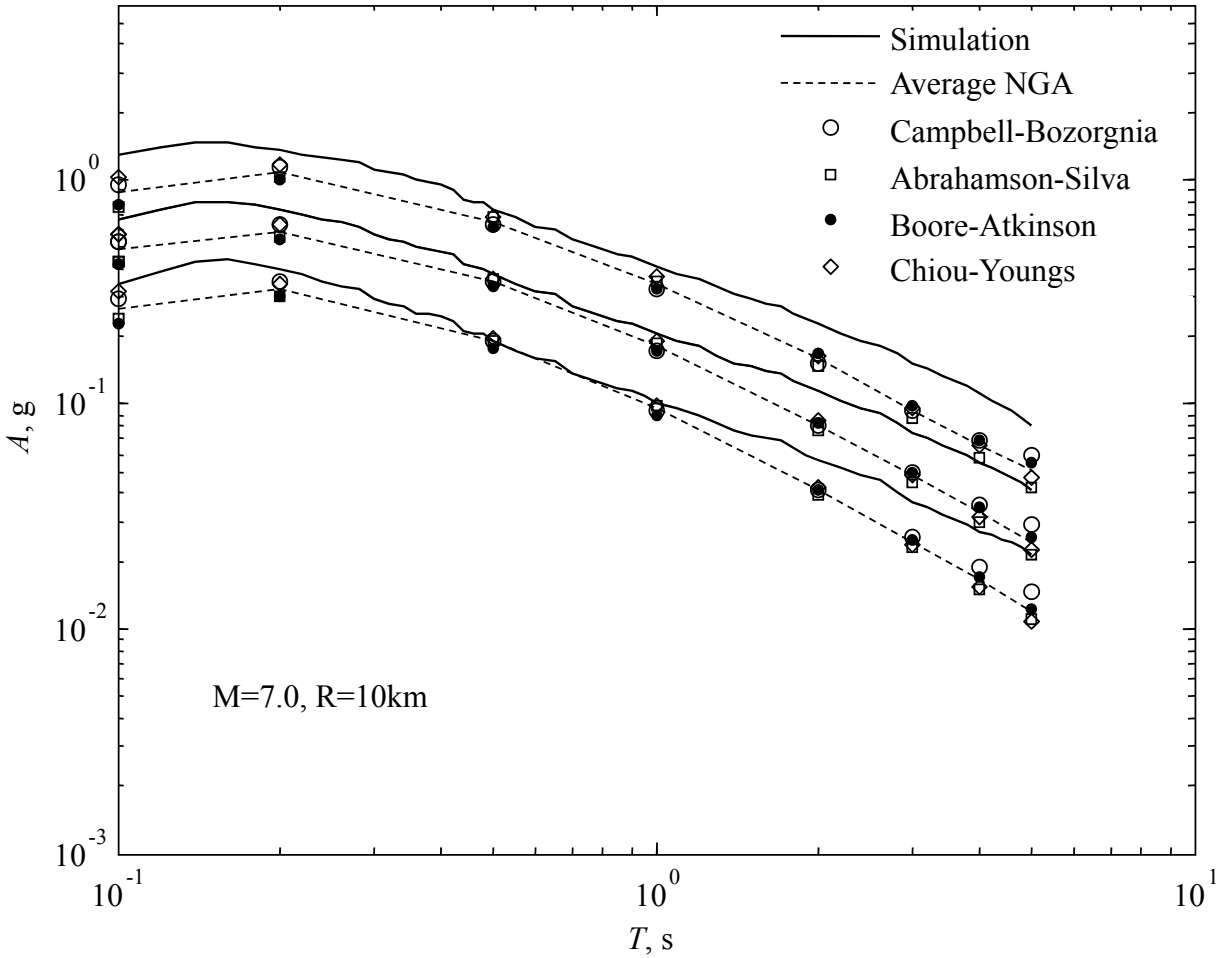
Fig. 6.11 **Median and median $\pm$ one logarithmic standard deviation of 5% damped pseudo acceleration response spectra for 500 synthetic motions and corresponding values predicted by the average of four NGA-based prediction models for $F = 0$ (strike-slip faulting), $M = 7.0$, $R = 10$ km, $V = 760$ m/s. Estimated NGA values are based on a rupture width of 20 km, depth to top of rupture of 1 km, $Z_{2.5} = 1$ km for Campbell-Bozorgnia, $Z_{1.0} = 0.034$ km for Abrahamson-Silva, and $Z_{1.0} = 0.024$ km for Chiou-Youngs.**
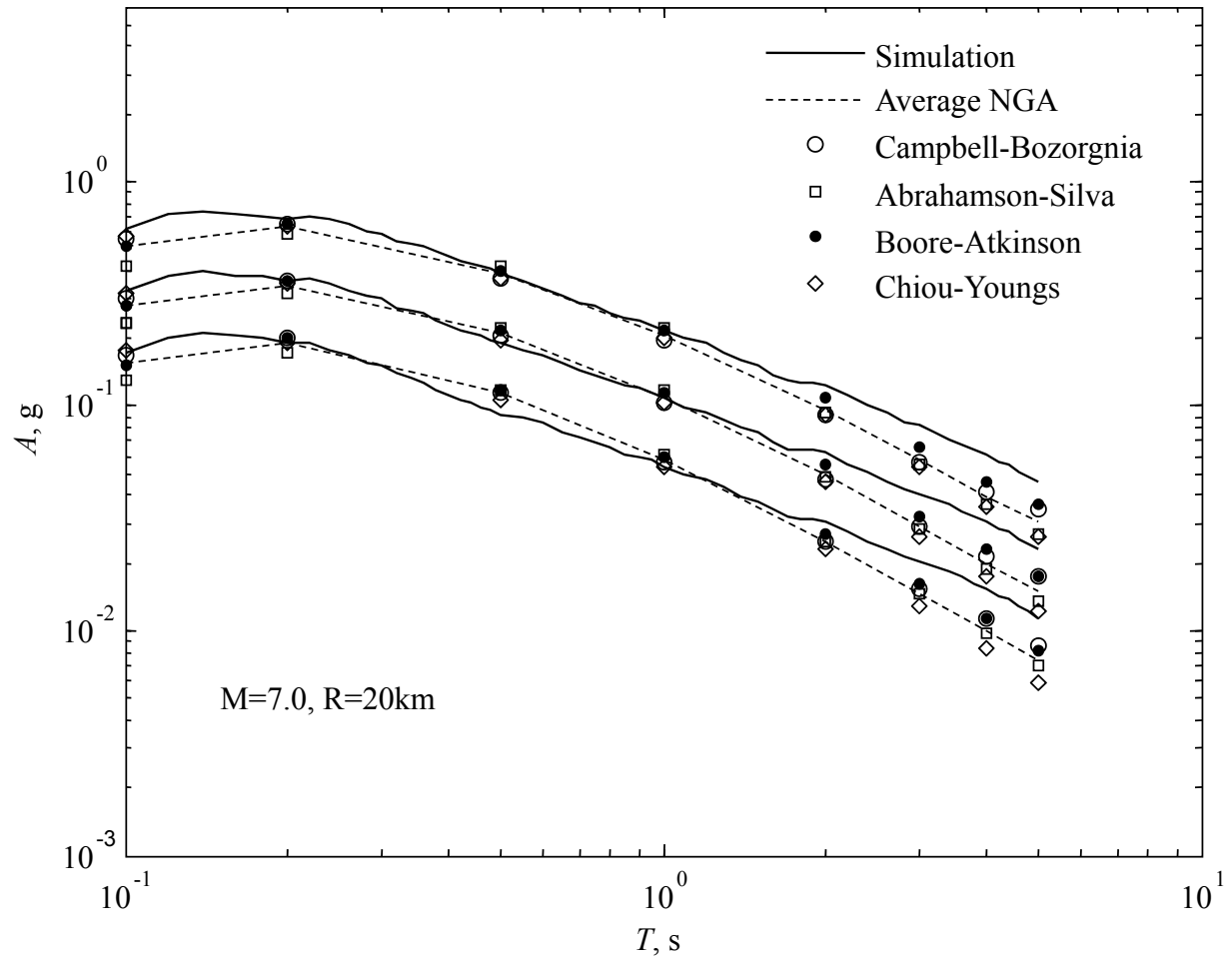
Fig. 6.12 Median and median $\pm$ one logarithmic standard deviation of 5% damped pseudo acceleration response spectra for 500 synthetic motions and corresponding values predicted by the average of four NGA-based prediction models for $F = 0$ (strike-slip faulting), $M = 7.0$, $R = 20$ km, $V = 760$ m/s. Estimated NGA values are based on a rupture width of 20 km, depth to top of rupture of 1 km, $Z_{2.5} = 1$ km for Campbell-Bozorgnia, $Z_{1.0} = 0.034$ km for Abrahamson-Silva, and $Z_{1.0} = 0.024$ km for Chiou-Youngs.
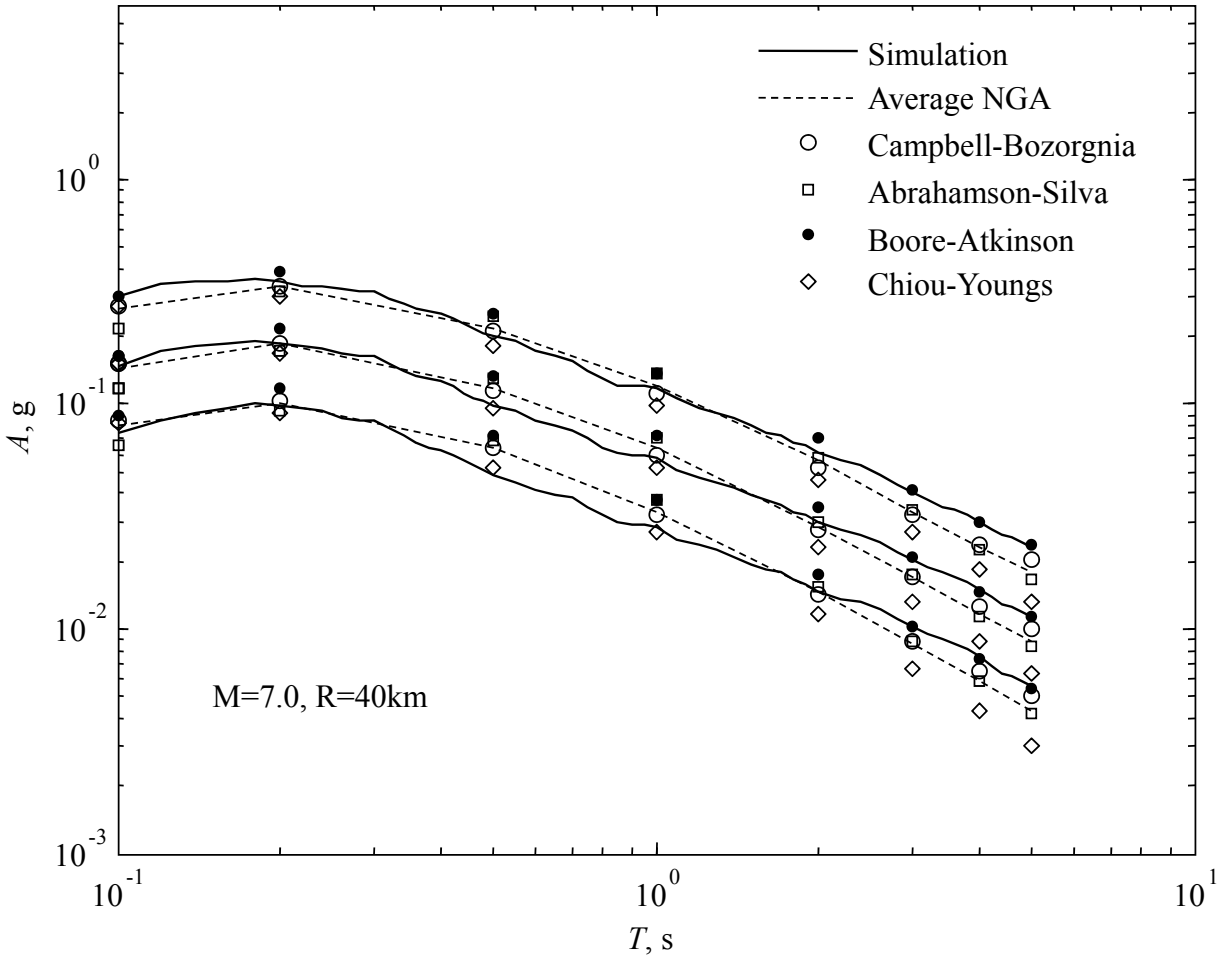
Fig. 6.13 **Median and median $\pm$ one logarithmic standard deviation of 5% damped pseudo acceleration response spectra for 500 synthetic motions and corresponding values predicted by the average of four NGA-based prediction models for $F = 0$ (strike-slip faulting), $M = 7.0$, $R = 40$ km, $V = 760$ m/s. Estimated NGA values are based on a rupture width of 20 km, depth to top of rupture of 1 km, $Z_{2.5} = 1$ km for Campbell-Bozorgnia, $Z_{1.0} = 0.034$ km for Abrahamson-Silva, and $Z_{1.0} = 0.024$ km for Chiou-Youngs.**
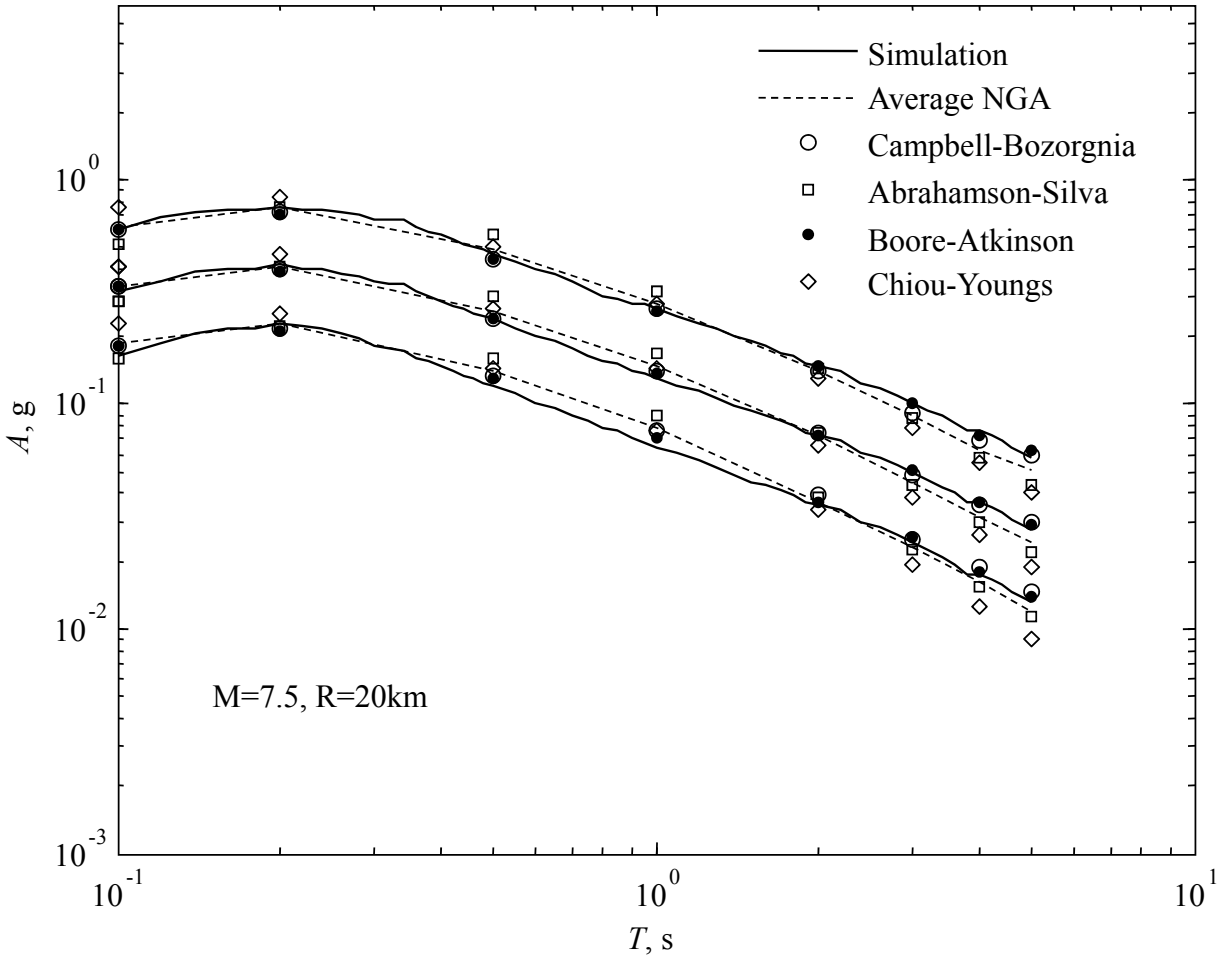
Fig. 6.14 **Median and median ± one logarithmic standard deviation of 5% damped pseudo acceleration response spectra for 500 synthetic motions and corresponding values predicted by the average of four NGA-based prediction models for $F = 0$ (strike-slip faulting), $M = 7.5$, $R = 20$ km, $V = 760$ m/s. Estimated NGA values are based on a rupture width of 20 km, depth to top of rupture of 1 km, $Z_{2.5} = 1$ km for Campbell-Bozorgnia, $Z_{1.0} = 0.034$ km for Abrahamson-Silva, and $Z_{1.0} = 0.024$ km for Chiou-Youngs.**
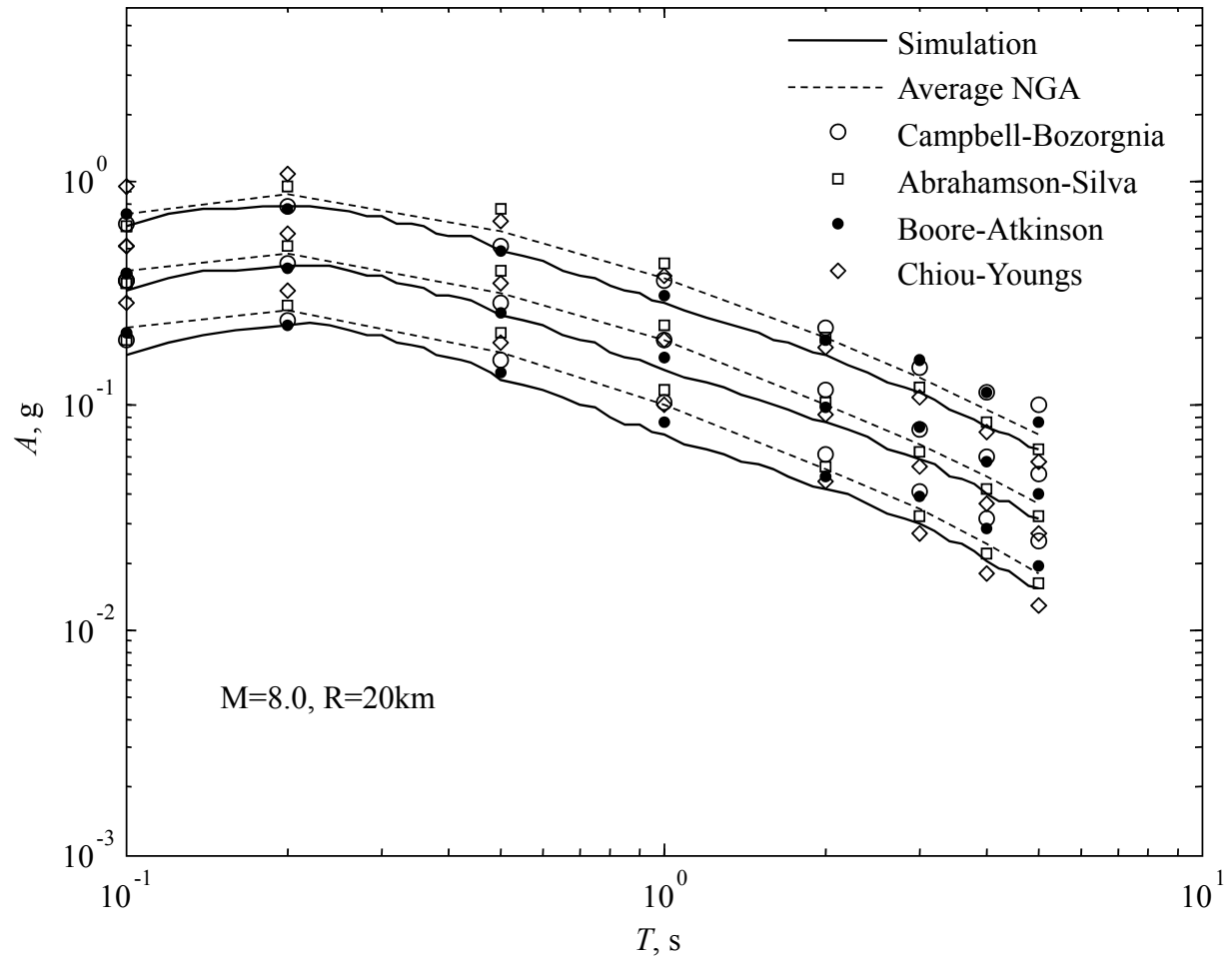
Fig. 6.15 **Median and median $\pm$ one logarithmic standard deviation of 5% damped pseudo acceleration response spectra for 500 synthetic motions and corresponding values predicted by the average of four NGA-based prediction models for $F = 0$ (strike-slip faulting), $M = 8.0$, $R = 20$ km, $V = 760$ m/s. Estimated NGA values are based on a rupture width of 20 km, depth to top of rupture of 1 km, $Z_{2.5} = 1$ km for Campbell-Bozorgnia, $Z_{1.0} = 0.034$ km for Abrahamson-Silva, and $Z_{1.0} = 0.024$ km for Chiou-Youngs.**

7 Simulation of Two Orthogonal Horizontal Components

7.1 INTRODUCTION

In this chapter, the proposed method of ground motion simulation for specified earthquake and site characteristics is extended to simulate two orthogonal horizontal components of the ground motion. The most novel aspect of this extension is proper accounting of the correlations between parameters of the two components in the simulation model. Accounting for these correlations is essential in order to obtain synthetic ground motion components that are realistic. Representation of realistic ground motion components is especially important when analyzing asymmetric structures that are vulnerable to torsion.

As shown in this chapter, the correlations mentioned above can be very high. This is expected, since the ground motion components are generated from the same earthquake source and seismic waves that travel through the same medium. Some previous studies assume that the parameters of the two components are identical. For example, Yeh and Wen (1989) assume identical frequency content for the component of ground motion along any horizontal direction. In the context of the method developed in this study, this assumption implies identical filter parameters for all directions of the ground motion. The same study uses distinct deterministic intensity envelopes, equivalent of our time modulating functions, for the different components, the parameters of which are identified from recorded accelerograms. Other studies that simulate ground motion components, such as Kubo and Penzien (1979) or Heredia-Zavoni and Machicao-Barrionuevo (2004), also use real recorded accelerograms to identify the parameters of their ground motion model, and thereby indirectly account for the correlations between parameters of the ground motion components in the simulation. The present study allows simulation of bi-directional ground motion time-histories for a future seismic event without any need for previously recorded motions. This is possible because predictive equations are developed for the

model parameters in terms of earthquake and site characteristics, and the correlations between the parameters of the ground motion components are empirically determined.

It should be noted that most seismological source-based models are capable of simulating multi-directional ground motions at a specific location without any need for previously recorded accelerograms. However, as discussed in previous chapters, these models are computationally intensive and require a thorough knowledge of seismic sources in the area, information that is usually not available to the practicing engineer.

This chapter starts by presenting an extension of the stochastic ground motion model for two components. Two stochastic processes are considered, each representing one ground motion component. Differences between the two stochastic processes originate from different underlying white-noise processes that excite the filter and different model parameters, i.e., Arias intensity, effective duration, filter frequency, etc. Ground motion components with a source-to-site distance of at least 10 km are simulated along the principal axes where the white-noise processes are statistically independent. A new database of recorded ground motion components is developed by rotating the as-recorded components into their principal axes. Based on this database, empirical predictive equations for the model parameters are constructed and correlations between parameters of the two components are empirically determined. The outcomes allow one to randomly generate correlated model parameters for two orthogonal horizontal ground motion components along the principal axes. The simulated components can then be rotated back into any desired direction, e.g., principal directions of the structure, through a simple transformation. Example simulations are provided at the end of the chapter.

7.2   STOCHASTIC GROUND MOTION MODEL

Following Chapter 2, orthogonal horizontal ground motion components are modeled by the fully nonstationary stochastic processes:

$$x_1(t) = q(t, \boldsymbol{\alpha_1}) \left\{ \frac{1}{\sigma_{f_1}(t)} \int_{-\infty}^{t} h[t - \tau, \boldsymbol{\lambda_1}(\tau)] w_1(\tau) \mathrm{d}\tau \right\} \tag{7.1}$$

$$x_2(t) = q(t, \boldsymbol{\alpha_2}) \left\{ \frac{1}{\sigma_{f_2}(t)} \int_{-\infty}^{t} h[t - \tau, \boldsymbol{\lambda_2}(\tau)] w_2(\tau) \mathrm{d}\tau \right\} \tag{7.2}$$

where $x_1(t)$ and $x_2(t)$, respectively, denote acceleration time-histories, prior to high-pass filtering, of components 1 and 2 of the ground motion. The time-modulating function and the linear filter employed in this chapter are identical to those used in the ground motion model of Chapter 4. Similarly, the model parameters are based on definitions given in Chapter 4, i.e., $\boldsymbol{\alpha_1} = (\bar{I}_{a1}, D_{5-95_1}, t_{mid_1})$ and $\boldsymbol{\lambda_1} = (\omega_{mid_1}, \omega_1', \zeta_{f_1})$ represent the modulating function parameters and filter parameters of component 1, and $\boldsymbol{\alpha_2} = (\bar{I}_{a2}, D_{5-95_2}, t_{mid_2})$ and $\boldsymbol{\lambda_2} = (\omega_{mid_2}, \omega_2', \zeta_{f_2})$ represent the corresponding parameters of component 2. The differences between the acceleration time-histories in (7.1) and (7.2) originate from two sources: (1) different model parameters, $(\boldsymbol{\alpha_1}, \boldsymbol{\lambda_1})$ and $(\boldsymbol{\alpha_2}, \boldsymbol{\lambda_2})$, (2) different input excitations, i.e., white-noise processes, $w_1(\tau)$ and $w_2(\tau)$. Whereas the model parameters $(\boldsymbol{\alpha_1}, \boldsymbol{\lambda_1})$ and $(\boldsymbol{\alpha_2}, \boldsymbol{\lambda_2})$ characterize the evolutionary intensity and frequency contents of the two components, the white-noise processes $w_1(\tau)$ and $w_2(\tau)$ describe the stochastic nature of the ground motion components.

When simulating bi-directional ground motions, in addition to differences, similarities and dependencies between the two components must be accounted for. Since the ground motion components are generated from the same earthquake source and seismic waves that travel through the same medium, high correlations between model parameters of the two components are expected. The correlation matrix, $\boldsymbol{\rho}_{(\boldsymbol{\alpha_1}, \boldsymbol{\lambda_1}), (\boldsymbol{\alpha_2}, \boldsymbol{\lambda_2})}$, may be estimated empirically by analyzing a large number of recorded ground motion pairs. Furthermore, dependence between $w_1(\tau)$ and $w_2(\tau)$ must be incorporated in the simulation. In general, ground motion components are correlated processes. However, as shown by Penzien and Watabe (1975), along a unique set of orthogonal axes, referred to as *principal axes*, the translational components of ground motion may be considered uncorrelated. Therefore, we assume that $w_1(\tau)$ and $w_2(\tau)$ are statistically independent, provided that $x_1(t)$ and $x_2(t)$ are in the directions of principal axes.

In the subsequent sections, a new database of ground motion components is developed by rotating the ground motion pairs of the database used in Chapter 4 into their principal axes. The empirical predictive equations developed in Chapter 4 are no longer appropriate, as they do not correspond to the directions of principal axes. Therefore, model parameters are identified for the new database, empirical predictive equations are developed, and correlation coefficients between model parameters of the ground motion components are estimated.

151

7.3 DATABASE OF PRINCIPAL GROUND MOTION COMPONENTS

The strong motion database introduced in Chapter 4 contains ground motion recordings with orthogonal horizontal pairs, directions of which depend on the orientation of the recording instruments. We refer to this database as the *as-recorded* database. Recall that the as-recorded database contains 103 pairs of horizontal recordings. Each pair is rotated into directions along which the components are statistically uncorrelated, i.e., the principal axes directions. The result is a new strong motion database, which is employed in the subsequent statistical analysis. More details on the principal axes and rotation of ground motion components are presented below.

7.3.1 Principal Axes of Ground Motion

Earthquake ground motions are multi-dimensional. Neglecting the rotational components, a set of principal axes are defined by Penzien and Watabe (1975) for the three translational components of ground motion. These include the major, intermediate, and minor principal axes along which the components of ground motion are uncorrelated and have intensities in decreasing order. Furthermore, based on examination of real accelerograms, it is shown in the same study that the major principal axis usually points in the general direction of the epicenter, the intermediate principal axis is horizontal and perpendicular to the major principal axis, and the minor principal axis is almost vertical. Figure 7.1a demonstrates this configuration where $a_{major}(t)$, $a_{intermediate}(t)$, and $a_{vertical}(t)$ are acceleration time-histories along the major, intermediate, and minor principal axes. Subsequent studies on stochastic modeling and generation of synthetic ground motion components have based their studies on the definition of principal axes by Penzien and Watabe (1975). Examples include Kubo and Penzien (1979), Smeby and Der Kiureghian (1985), Yeh and Wen (1989), and Heredia-Zavoni and Machicao-Barrionuevo (2004). We also take advantage of the above definition to simulate the major and intermediate ground motion components.

Let $a_1(t)$ and $a_2(t)$ represent a set of orthogonal horizontal components of ground acceleration. The correlation coefficient between these two components over the time interval $\tau_1 \leq t \leq \tau_2$ is calculated by

$$\rho_{a_1(t),\,a_2(t)} = \frac{\int_{\tau_1}^{\tau_2} a_1(t)a_2(t)\mathrm{d}t}{\sqrt{\int_{\tau_1}^{\tau_2} a_1(t)^2\mathrm{d}t \int_{\tau_1}^{\tau_2} a_2(t)^2\mathrm{d}t}} \tag{7.3}$$

In general, the correlation coefficient is time dependent and fluctuates over successive time intervals. However, Penzien and Watabe (1975) found that $\rho_{a_1(t),\,a_2(t)}$ remains reasonably stable for different time intervals of recorded ground motions. Therefore, we define $\rho_{a_1(t),\,a_2(t)}$ for the entire duration of the ground motion, i.e., we use $\tau_1 = 0$ and $\tau_2 = t_n$. (Recall that t_n represents the total duration of the motion). This correlation coefficient varies if the ground motion components are rotated by an angle θ to an alternative set of orthogonal axes (see Fig. 7.1b). Therefore, it is a function of the rotation angle, $\rho_{a_1(t),\,a_2(t)}(\theta)$. The *principal axes* of the ground motion are the directions along which $\rho_{a_1(t),\,a_2(t)}(\theta) = 0$, and the *principal components* are components of ground motion along these axes.

In addition to the rotation angle, $\rho_{a_1(t),\,a_2(t)}(\theta)$ is a function of the difference between the intensities of the principal components. This dependence, which was pointed out by Smeby and Der Kiureghian (1985), is also verified in this study. Specifically, the larger the difference between the intensities of the principal components, the higher the correlation coefficient for a given θ. In the extreme case, where the principal components have equal intensities, the correlation coefficient is zero for all rotation angles.

In this study, Arias intensity, defined by (4.3), is used to distinguish the major component from the intermediate component. The major component is defined as the principal horizontal component with the larger Arias intensity. Consequently, the intermediate component is defined as the principal horizontal component with the smaller Arias intensity. This definition is used to sort the data when estimating the correlation coefficients between model parameters of the major and intermediate components, as well as in the simulation algorithm.

7.3.2 Rotation of Ground Motion Components

Let $a_1(t)$ and $a_2(t)$ represent a pair of orthogonal horizontal acceleration time-histories in the as-recorded directions, and $a_{1,\theta}(t)$ and $a_{2,\theta}(t)$ represent their counterclockwise rotation by angle θ. This orthogonal transformation is illustrated in Figure 7.1b and is obtained by

153

$$\begin{bmatrix} a_{1,\theta}(t) \\ a_{2,\theta}(t) \end{bmatrix} = \begin{bmatrix} \cos(\theta) & -\sin(\theta) \\ \sin(\theta) & \cos(\theta) \end{bmatrix} \begin{bmatrix} a_1(t) \\ a_2(t) \end{bmatrix} \tag{7.4}$$

Every pair of as-recorded ground motion components in the database are rotated according to (7.4) for rotation angles ranging from 0° to 90° with a discretization of 1°. The correlation coefficient is calculated according to (7.3) and the rotation angle, $\hat{\theta}$, is selected such that $\rho_{a_{1,\hat{\theta}}(t),a_{2,\hat{\theta}}(t)}(\hat{\theta}) = 0$. The corresponding rotated components, $a_{1,\hat{\theta}}(t)$ and $a_{2,\hat{\theta}}(t)$, are then used to develop the database of principal ground motion components. Table 7.1 provides the correlation coefficient between as-recorded components, $\rho_{a_1(t),a_2(t)}$, and the selected rotation angle, $\hat{\theta}$, for all the records in the database.

The components of two as-recorded ground motions, (a) the Northridge earthquake recorded at Mt Wilson – CIT Station and (b) the Chi-Chi, Taiwan, earthquake recorded at HW A046 Station, are plotted in Figure 7.2. Each pair is rotated according to (7.4) and correlations between their two components are plotted against the rotation angle in Figure 7.3. Figure 7.4 plots the corresponding principal components of these two pairs of ground motions. Observe in Figure 7.3 that the correlation coefficient as a function of the rotation angle is a smooth curve and represents half of a complete cycle between 0° to 90°. Furthermore, the dependence of the correlation coefficient on the difference between the intensities of the principal components is apparent in this figure. The ratio between the Arias intensities of the principal components for the Northridge record is 0.38, while the same measure for the Chi-Chi earthquake is 0.82. As expected, a higher ratio, which implies a smaller difference between the intensities of principal components, has resulted in lower overall correlations.

7.4   EMPIRICAL PREDICTIVE EQUATIONS FOR THE MODEL PARAMETERS

Sample observations of the model parameters are obtained by fitting the stochastic ground motion model in (7.1) and (7.2) to the database of principal ground motion components. This is done according to the methods described in Chapter 4 by fitting to the time-varying intensity and evolutionary frequency content of each component. Recall that the physically based modulating function parameters, Arias intensity, $\bar{I}_a$, effective duration, D_{5-95}, and time at the middle of strong shaking, t_{mid}, are identified directly from the recorded accelerogram based on their definitions. The identified modulating function parameters for all the rotated records in the

154

database are presented in Table 7.2. Figure 7.5 demonstrates the adequacy of this parameter identification method. In this figure three example pairs of components are shown that are typical of the entire database. Given the identified model parameters from Table 7.2, the modulating function parameters $(\alpha_1, \alpha_2, \alpha_3)$ are calculated and the resulting modulating functions are superimposed on the recorded acceleration time-histories. Observe that for a typical motion, as exemplified in the top and middle plots in Figure 7.5, whether $T_0 = 0$ or $T_0 > 0$, the fitted modulating function is in general a good representation of the evolving energy in the record. Also observe that for the few cases in which the target accelerogram behaves irregularly, as in the bottom plots, the fitted modulating function provides a reasonable representation of the evolving energy.

Recall that the filter parameters, which include the filter frequency at the middle of strong shaking, ω_{mid}, the rate of change of frequency with time, ω', and the filter damping ratio, ζ_f, are identified by fitting to the mean zero-level up-crossing rate and the rate of change of the cumulative number of negative maxima and positive minima of the target accelerogram. Simplified procedures that were presented in Chapter 4 are employed. The identified filter parameters for all the principal components in the database are presented in Table 7.3. The error measures, ϵ_ω and ϵ_ζ, which are calculated based on definitions in Chapter 3, are listed in Table 7.4. These error measures are calculated only for the time intervals, over which fitting is performed, i.e., the time between 1% to 99% levels of Arias intensity for the frequency parameters, and the time between 5% to 95% levels of Arias intensity for the damping ratio (see Chapter 4 for details on the method of fitting). Observe that, in general, error measurements are remarkably small, verifying the adequacy of the simplified methods for identification of filter parameters. For damping ratios smaller than 0.1, a few cases exhibit rather large values for ϵ_ζ. This is due to the definition we have chosen for the error measure. Referring to Figure 4.4, ϵ_ζ is defined as the ratio of the area between the target and simulated curves divided by the area underneath the target curve. As a result, when the damping ratio is small, the area underneath the target curve is small, thereby producing a large value of ϵ_ζ for a constant difference between the target and simulated curves.

Summary statistics of the identified model parameters for the new database are presented in Table 7.5. The data for the Arias intensity are divided into two groups: Arias intensity for the

155

major principal component, $I_{a,major}$, and Arias intensity for the intermediate principal component, $I_{a,inter}$. This division reduces the number of data points for statistical analysis from 206 to 103 for each parameter, but this is necessary for simulation of pairs of ground motion components. The statistical analysis for the remainder of model parameters is performed for the entire data set, i.e., data corresponding to both components are combined resulting in 206 data points for each model parameter. Comparing the statistics provided in Table 7.5 to those of Table 4.3 reveals similar behavior of model parameters corresponding to principal motions and model parameters corresponding to as-recorded motions.

Probability distributions are assigned to the model parameters in the manner described in Chapter 4. Distribution types and their assigned boundaries are presented in Table 7.6. Compared to the as-recorded database, the lower boundary of the beta distribution assigned to D_{5-95} has dropped from 5 s to 4 s, and the upper boundary of beta distribution assigned to t_{mid} has decreased from 40 s to 35 s. These are insignificant differences. Figures 7.6 and 7.7 show the assigned marginal probability density functions (PDFs) superimposed on the normalized frequency diagrams of the model parameters. In these figures, the fitted PDFs corresponding to the as-recorded database are also plotted for comparison. Again, differences are not significant. Figures 7.8 and 7.9 show the fit of the cumulative distribution functions (CDFs) for the assigned distributions to the empirical CDFs of the identified model parameters. It is observed that the fit is good for all the model parameters, confirming the appropriateness of the assigned distributions.

7.4.1 Regression

Regression analysis is performed according to the methods described in Chapter 4 to develop predictive equations for the model parameters in terms of earthquake and site characteristics, F, M, R, and V. The resulting predictive equations for $v_{1,major} = \ln(\bar{I}_{a,major})$ and $v_{1,inter} = \ln(\bar{I}_{a,inter})$ are similar to (4.19). The resulting predictive equations for the remainder of model parameters after transformation to the standard normal space are similar to (4.20). The maximum likelihood estimates of regression coefficients and variance components are presented in Table 7.7. For each predictive equation, a standard significance test on the linear regression formula is performed, i.e., an F-test with null hypothesis that $\beta_{i,1} = \beta_{i,2} = \beta_{i,3} = \beta_{i,4} = 0$, for $i =$

$1_{major}, 1_{inter}, 2, ... ,6$. The P-values are reported in Table 7.7. The regression coefficients $\beta_{i,1}, \beta_{i,2}, \beta_{i,3}$, and $\beta_{i,4}$ ($i = 1, ... ,6$) were individually tested ($\beta_{i,0}$ was skipped because inclusion of a constant term in the regression formulation was not questioned), i.e., the t-test with null hypothesis that $\beta_{i,j} = 0$, $i = 1, ... ,6$, $j = 1, ... ,4$. Those coefficients with statistical significance at the 95% confidence level are shown in bold in Table 7.7. Furthermore, 95% confidence intervals are presented in Table 7.8. If a confidence interval contains zero, then the corresponding regression coefficient is not significant at the given confidence level. The results are consistent with Table 7.7. Table 7.9 presents the P-values for each t-test. Regardless of the significance level, as done in Chapter 5, all the coefficients in Table 7.7 are used in the simulation.

Comparisons of Tables 7.7, 7.8, and 7.9 respectively with Tables 4.5, 4.6, and 4.7 reveal insignificant differences. Therefore, we conclude that the model validations against recorded motions and against NGA relations in Chapter 6 still hold.

7.4.2   Correlation Analysis

Perhaps the most important result of this chapter is obtaining the correlation matrix between the model parameters of the major and intermediate principal components. This correlation matrix is presented in Table 7.10. Similar to Chapter 4, correlation coefficients between two model parameters are estimated as the sample correlation coefficients between their corresponding total residuals. Observe that the off-diagonal block, which represents correlations between the transformed model parameters of the major and intermediate components, contains high numbers. Namely, correlation coefficients between pairs of similar model parameters of the two components are 0.92 for v_1 (corresponding to Arias intensities), 0.89 for v_2 (corresponding to the effective durations), 0.96 for v_3 (corresponding to t_{mid} values), 0.94 for v_4 (corresponding to ω_{mid} values), 0.52 for v_5 (corresponding to ω' values), and 0.75 for v_6 (corresponding to ζ_f values). High correlations are also observed between different model parameters of the two components. For example, a correlation of 0.68 is observed between v_3 (corresponding to t_{mid}) of the intermediate component and v_2 (corresponding to the effective duration) of the major component. These high correlations should not be neglected in simulation of ground motion components.

The diagonal blocks in Table 7.10 represent correlation coefficients between model parameters of the individual components. Observe that the two diagonal blocks are not significantly different from each other and from the correlation coefficients for one component simulation listed in Table 4.9.

7.5   SIMULATION AND EXAMPLES

For specified earthquake and site characteristics, F, M, R, and V, 12 model parameters (6 for each component) are randomly simulated according to the methods described in Chapter 5, which accounts for the correlations between the parameters. Since by definition the Arias intensity of the major component must be greater than the Arias intensity of the intermediate component, the simulation of the parameters must satisfy this condition. Because predictive equations have been developed for sorted Arias intensities of the two principal components, the probability that $\bar{I}_{a,major} > \bar{I}_{a,inter}$ is high. A simple way to observe the required relationship is to simply discard the small subset of simulations with $\bar{I}_{a,major} < \bar{I}_{a,inter}$. This essentially conditions the joint probability distribution of the model parameters on the event $\bar{I}_{a,major} > \bar{I}_{a,inter}$. The simulated model parameters are then used in (7.1) and (7.2) with statistically uncorrelated white-noise processes, $w_1(\tau)$ and $w_2(\tau)$, to generate a synthetic pair of ground accelerations in the directions of principal axes. High-pass filtering according to (2.28) is then performed on the simulated motions.

As an example, Figure 7.10 shows pairs of acceleration time-histories of the major and intermediate components for one recorded and three simulated ground motions. Figures 7.11 and 7.12 show the corresponding velocity and displacement time-histories. The simulated motions are generated for the earthquake and site characteristics of the recorded motion. Observe that, for each pair, simulated components are different but have similar overall characteristics in the same manner as the recorded pair of motions. These similarities are more apparent by looking at the model parameters, which are provided in the figure for each component of the recorded and simulated ground motion.

The method of ground motion simulation presented in this chapter allows generation of synthetic horizontal ground motion components in the principal directions without any need for previously recorded motions. It requires information only on the earthquake and site

158

characteristic values $F, M, R,$ and V. The two synthetic components may then be rotated to any desired direction according to the orthogonal transformation in (7.4). As mentioned earlier, according to Penzien and Watabe (1975), the principal axes are usually directed towards the general direction of the earthquake source and the corresponding perpendicular direction. This allows placement of the synthetic principal components when the location of the potential earthquake source is known. The two synthetic principal components may then be rotated into the input directions of the structure, e.g., the longitudinal and transverse directions of the structure. If the earthquake source is unknown, one may wish to consider a variety of directions to obtain the maximum structural response. If the analysis is linear, the critical directions for each response quantity can be obtained in closed form (see Smeby and Der Kiureghian [1985]). However, for nonlinear analysis, this angle must be determined by trial. In fact, in the current practice, ground motion components are often rotated to alternative axes in order to obtain the maximum structural response.

Table 7.1 Database of principal ground motion components. For each pair of records, the correlation between the two as-recorded horizontal components and the rotation angle for principal axes are listed. Order of records is similar to Table 4.2.

Record ID in NGA Database		Correlation Between As-Recorded Components (ρ when $\theta = 0°$)	Rotation Angle for Principal Axes (degrees): $\hat{\theta}$
	164	−0.147	54
	265	−0.034	3
	454	0.042	61
	455	−0.023	79
	471	0.187	74
	472	−0.145	46
	476	0.032	1
	891	0.104	55
	897	0.023	77
	922	0.038	8
	925	−0.226	12
	928	0.022	13
Strike-Slip	934	0.240	27
	938	−0.203	50
	1109	0.078	59
	1112	−0.087	11
	1154	−0.122	54
	1169	0.110	41
	1619	0.307	72
	1626	0.072	16
	1633	−0.182	72
	1763	0.002	90
	1767	0.131	36
	1786	0.171	41
	1787	−0.262	74

Table 7.1—*Continued.*

Record ID in NGA Database		Correlation Between As-Recorded Components (ρ when $\theta = 0°$)	Rotation Angle for Principal Axes (degrees): $\hat{\theta}$
Strike-Slip	1795	−0.084	71
	1824	−0.178	53
	1832	−0.005	1
	1836	0.038	74
	2107	−0.052	73
	2111	−0.044	83
Reverse	59	0.066	83
	63	0.466	36
	71	−0.116	27
	72	0.350	52
	73	−0.136	19
	87	−0.374	48
	89	0.018	89
	139	0.060	56
	369	−0.005	1
	511	−0.104	28
	512	0.084	49
	528	−0.194	47
	536	−0.161	23
	537	0.455	59
	541	−0.143	70
	769	0.306	21
	771	0.057	84
	781	−0.029	88
	782	0.160	68
	788	−0.403	47
	789	0.068	11
	791	0.145	34

Table 7.1—*Continued.*

Record ID in NGA Database		Correlation Between As-Recorded Components (ρ when $\theta = 0°$)	Rotation Angle for Principal Axes (degrees): $\hat{\theta}$
Reverse	795	−0.454	36
	797	0.188	31
	801	0.053	79
	804	−0.071	82
	809	0.213	17
	810	−0.377	35
	813	0.303	15
	943	−0.133	6
	946	0.162	49
	957	0.051	7
	989	0.019	19
	994	0.118	85
	1011	0.165	22
	1012	0.229	40
	1020	−0.210	65
	1021	−0.030	64
	1023	−0.556	50
	1027	0.417	54
	1029	0.087	74
	1033	0.357	50
	1041	−0.422	35
	1060	−0.127	9
	1074	0.313	60
	1078	0.382	47
	1091	0.003	89
	1096	−0.184	19
	1206	−0.042	3

Table 7.1—*Continued.*

Record ID in NGA Database		Correlation Between As-Recorded Components (ρ when $\theta = 0°$)	Rotation Angle for Principal Axes (degrees): $\hat{\theta}$
Reverse	1234	0.363	18
	1245	0.014	72
	1257	0.286	77
	1273	0.000	90
	1278	−0.149	27
	1287	0.039	7
	1293	−0.091	34
	1302	0.413	27
	1325	0.122	25
	1347	−0.171	32
	1350	0.088	22
	1377	−0.116	62
	1391	0.105	48
	1485	−0.355	38
	1517	0.095	87
	1518	−0.117	15
	1520	−0.168	53
	1548	−0.132	68
	1576	0.011	87
	1577	0.062	79
	1585	−0.015	77
	1587	−0.090	11
	1594	−0.224	58

Table 7.2 Identified modulating function parameters for the principal ground motion components. For records with $T_0 > 0$, t_{mid} is the time starting from T_0.

Record ID in NGA Database		I_a (s.g.)		D_{5-95} (s)		t_{mid} (s)	
		Major Component	Intermediate Component	Major Component	Intermediate Component	Major Component	Intermediate Component
	164	0.1506	0.1105	34.41	32.60	17.17	14.60
	265	0.2007	0.1022	8.57	7.57	5.47	5.72
	454	0.0059	0.0054	8.44	8.72	3.61	3.66
	455	0.0061	0.0054	8.89	9.56	4.13	4.35
	471	0.0195	0.0095	17.68	20.79	9.05	9.20
	472	0.0119	0.0089	22.14	19.38	10.41	11.45
	476	0.0082	0.0025	7.59	7.81	3.85	3.79
	891	0.0081	0.0065	29.18	32.10	15.90	18.44
	897	0.0120	0.0107	30.84	30.82	17.18	16.64
	922	0.0023	0.0018	27.89	25.18	20.12	19.72
	925	0.0066	0.0023	22.57	26.58	14.60	15.91
	928	0.0565	0.0509	18.51	16.89	14.91	14.13
	934	0.0084	0.0046	13.28	14.32	8.30	8.72
	938	0.0098	0.0064	13.56	15.48	12.02	11.60
	1109	0.0073	0.0061	20.04	25.50	14.23	15.18
Strike-Slip	1112	0.0096	0.0060	13.04	22.78	14.13	17.04
	1154	0.0084	0.0065	33.70	34.49	17.52	18.19
	1169	0.0032	0.0025	33.50	39.06	17.13	19.04
	1619	0.0221	0.0079	15.34	16.45	5.06	7.12
	1626	0.0165	0.0126	24.52	28.51	9.14	9.95
	1633	0.8090	0.4345	30.50	28.52	10.96	10.84
	1763	0.0022	0.0016	19.57	23.44	18.54	15.98
	1767	0.0010	0.0008	27.46	25.50	20.07	19.15
	1786	0.0165	0.0116	15.88	16.97	17.70	16.13
	1787	0.1998	0.0751	9.71	12.55	8.28	7.15
	1795	0.0109	0.0083	15.43	17.15	15.94	15.29
	1824	0.0027	0.0019	14.87	14.18	7.37	4.99
	1832	0.0066	0.0052	20.54	18.91	18.97	19.43
	1836	0.0072	0.0062	17.38	18.22	8.30	9.44
	2107	0.0185	0.0154	19.44	24.82	14.09	14.65
	2111	0.0115	0.0079	18.99	23.38	17.06	13.45
	59	0.0005	0.0003	10.41	10.13	3.18	3.44
Reverse	63	0.0079	0.0027	12.07	15.06	1.43	2.31
	71	0.0498	0.0374	5.12	6.22	1.05	0.93

Table 7.2—*Continued.*

Record ID in NGA Database		I_a (s.g.)		D_{5-95} (s)		t_{mid} (s)	
		Major Component	Intermediate Component	Major Component	Intermediate Component	Major Component	Intermediate Component
Reverse	72	0.0316	0.0148	11.85	13.67	3.82	3.92
	73	0.0160	0.0103	9.47	11.58	1.70	1.85
	87	0.0410	0.0186	10.77	13.04	3.95	4.35
	89	0.0017	0.0004	8.79	9.50	1.25	1.96
	139	0.1509	0.1326	12.36	11.76	6.29	6.98
	369	0.0291	0.0233	9.15	11.61	6.74	7.47
	511	0.0091	0.0071	6.41	6.50	2.16	1.62
	512	0.0065	0.0055	5.00	10.28	6.82	7.57
	528	0.0025	0.0017	7.31	9.77	6.44	7.30
	536	0.0068	0.0043	7.97	8.36	6.64	6.06
	537	0.0117	0.0039	6.25	8.50	3.36	3.91
	541	0.0048	0.0031	8.66	9.43	3.72	4.27
	769	0.0488	0.0190	12.09	13.59	4.70	5.30
	771	0.0495	0.0277	5.90	7.37	10.01	9.98
	781	0.0107	0.0048	12.86	13.10	8.77	9.67
	782	0.0087	0.0054	12.79	13.84	9.52	8.92
	788	0.0070	0.0030	10.52	12.11	8.52	9.74
	789	0.0091	0.0063	8.15	9.73	8.38	9.90
	791	0.0106	0.0077	16.30	17.53	7.23	7.59
	795	0.0068	0.0024	8.43	11.52	9.67	10.57
	797	0.0074	0.0049	10.69	15.37	10.08	11.48
	801	0.1345	0.1008	10.18	9.58	7.81	7.78
	804	0.0080	0.0048	9.52	11.93	8.69	9.13
	809	0.1691	0.0794	8.41	9.26	6.50	7.44
	810	0.3344	0.1446	9.68	9.14	6.70	7.15
	813	0.0044	0.0014	7.98	18.40	9.42	11.24
	943	0.0076	0.0021	12.20	13.98	12.16	12.11
	946	0.0035	0.0025	13.78	15.18	9.14	9.10
	957	0.0337	0.0219	7.96	11.71	5.13	5.43
	989	0.0664	0.0623	6.79	9.21	8.12	7.19
	994	0.1555	0.0409	8.89	11.95	7.16	7.71
	1011	0.0216	0.0134	6.68	8.86	4.85	5.88
	1012	0.1287	0.0802	7.64	8.44	7.05	7.63
	1020	0.0517	0.0299	8.97	11.14	7.05	7.63
	1021	0.0082	0.0076	13.14	13.64	8.42	7.98
	1023	0.0341	0.0096	6.52	12.36	5.61	6.98

Table 7.2—*Continued.*

Record ID in NGA Database		I_a (s.g.)		D_{5-95} (s)		t_{mid} (s)	
		Major Component	Intermediate Component	Major Component	Intermediate Component	Major Component	Intermediate Component
Reverse	1027	0.0106	0.0042	11.68	13.12	8.30	8.88
	1029	0.0106	0.0077	12.84	13.36	8.52	8.50
	1033	0.0086	0.0040	11.88	19.79	8.79	12.24
	1041	0.0388	0.0149	8.70	11.82	9.95	9.82
	1060	0.0104	0.0048	15.32	16.12	17.54	18.12
	1074	0.0174	0.0083	13.54	17.41	10.58	10.55
	1078	0.1223	0.0545	6.57	9.78	4.77	6.50
	1091	0.0381	0.0325	8.28	7.34	6.94	6.16
	1096	0.0059	0.0032	11.66	18.42	16.77	15.71
	1206	0.0323	0.0148	30.63	37.29	18.18	20.28
	1234	0.1107	0.0318	26.30	31.24	14.62	18.42
	1245	0.0081	0.0078	35.93	36.11	24.18	24.09
	1257	0.0264	0.0073	14.13	27.05	21.83	28.72
	1273	0.0026	0.0021	35.12	34.19	25.63	27.31
	1278	0.0236	0.0163	19.52	23.81	15.16	19.23
	1287	0.0080	0.0058	32.07	32.23	24.21	27.75
	1293	0.0165	0.0135	16.70	17.01	18.26	17.82
	1302	0.0185	0.0064	19.70	18.86	22.74	20.96
	1325	0.0107	0.0078	19.64	21.19	22.99	24.04
	1347	0.0094	0.0064	21.28	25.58	23.31	21.73
	1350	0.0757	0.0586	16.90	18.05	13.57	12.78
	1377	0.0070	0.0053	37.67	33.88	26.09	22.68
	1391	0.0022	0.0018	41.53	35.92	31.13	33.59
	1485	0.1788	0.0834	9.45	12.53	21.17	21.80
	1517	2.0744	0.3897	14.69	23.19	16.03	21.66
	1518	0.0084	0.0053	19.78	22.36	16.43	21.20
	1520	0.3125	0.2198	8.81	10.52	8.77	8.74
	1548	0.0881	0.0601	20.98	19.02	18.34	19.98
	1576	0.0032	0.0027	37.12	38.86	29.01	29.04
	1577	0.0072	0.0051	36.18	34.48	27.95	26.00
	1585	0.0026	0.0025	35.04	34.14	28.01	29.25
	1587	0.0099	0.0061	34.33	34.24	24.93	26.25
	1594	0.0061	0.0037	36.87	36.19	26.70	26.54

Table 7.3 Identified filter parameters for the principal ground motion components.

Record ID in NGA Database		$\omega_{mid}/2\pi$ (Hz)		$\omega'/2\pi$ (Hz/s)		ζ_f (ratio)	
		Major Component	Intermediate Component	Major Component	Intermediate Component	Major Component	Intermediate Component
Strike-Slip	164	4.00	5.61	−0.063	−0.070	0.37	0.31
	265	5.09	6.18	−0.383	−0.211	0.61	0.71
	454	8.40	7.60	−0.232	−0.212	0.06	0.11
	455	8.00	8.67	−0.409	−0.351	0.12	0.10
	471	3.44	4.07	−0.146	−0.163	0.05	0.09
	472	3.59	3.56	−0.222	−0.188	0.06	0.08
	476	3.91	5.30	0.069	−0.176	0.07	0.05
	891	7.97	7.72	−0.082	−0.154	0.39	0.44
	897	8.81	9.55	−0.084	−0.133	0.30	0.40
	922	5.87	5.16	−0.089	−0.082	0.24	0.31
	925	4.37	5.19	0.003	−0.037	0.18	0.28
	928	11.58	13.61	0.071	−0.055	0.26	0.22
	934	8.58	8.80	−0.010	−0.090	0.32	0.44
	938	11.40	11.29	−0.050	−0.036	0.21	0.17
	1109	2.39	3.14	−0.002	−0.058	0.24	0.22
	1112	3.64	3.91	−0.021	−0.039	0.15	0.21
	1154	1.85	2.38	−0.008	−0.016	0.10	0.12
	1169	8.20	8.74	−0.037	−0.042	0.37	0.32
	1619	3.23	3.32	−0.003	0.001	0.22	0.36
	1626	6.56	6.88	0.045	−0.014	0.11	0.09
	1633	7.82	6.87	−0.034	−0.010	0.20	0.46
	1763	8.17	9.36	−0.158	−0.091	0.14	0.12
	1767	5.51	4.78	−0.073	−0.013	0.33	0.58
	1786	6.08	6.14	−0.153	−0.110	0.18	0.17
	1787	3.12	3.72	0.123	0.053	0.48	0.23
	1795	5.61	5.78	−0.164	−0.103	0.32	0.20
	1824	2.43	3.83	−0.127	−0.116	0.14	0.09
	1832	6.08	5.94	−0.118	−0.064	0.12	0.12
	1836	8.96	8.13	−0.122	−0.044	0.36	0.42
	2107	7.04	9.15	−0.054	−0.097	0.47	0.42
	2111	4.35	5.41	0.004	−0.025	0.47	0.46
Reverse	59	6.00	6.02	−0.025	0.146	0.21	0.24
	63	8.09	9.02	−0.164	−0.099	0.50	0.28
	71	12.28	14.00	−0.004	−0.369	0.14	0.19

Table 7.3—*Continued.*

Record ID in NGA Database		$\omega_{mid}/2\pi$ (Hz)		$\omega'/2\pi$ (Hz/s)		ζ_f (ratio)	
		Major Component	Intermediate Component	Major Component	Intermediate Component	Major Component	Intermediate Component
Reverse	72	10.61	9.64	−0.056	−0.068	0.30	0.21
	73	13.04	10.60	−0.337	−0.235	0.44	0.44
	87	7.72	8.83	−0.149	−0.207	0.14	0.21
	89	8.73	8.97	−0.127	0.071	0.25	0.30
	139	6.42	6.42	0.114	−0.030	0.24	0.27
	369	2.39	1.95	−0.062	−0.087	0.08	0.15
	511	7.20	7.30	0.187	0.382	0.14	0.18
	512	6.99	9.03	−0.619	−0.319	0.24	0.11
	528	12.23	15.46	−0.172	−0.196	0.22	0.22
	536	18.71	21.98	−1.219	−1.437	0.24	0.26
	537	12.13	12.59	−0.131	−0.122	0.15	0.30
	541	14.88	13.56	0.029	0.100	0.15	0.16
	769	3.88	4.85	−0.052	−0.116	0.05	0.13
	771	1.81	1.79	0.050	0.028	0.06	0.05
	781	4.05	4.43	−0.055	−0.038	0.20	0.23
	782	4.76	5.54	0.051	−0.054	0.09	0.06
	788	2.47	4.21	0.042	−0.069	0.17	0.16
	789	2.40	2.14	−0.074	0.050	0.09	0.06
	791	2.53	2.94	−0.046	−0.031	0.21	0.21
	795	1.79	2.74	0.067	−0.054	0.10	0.12
	797	6.58	8.22	−0.242	−0.200	0.28	0.29
	801	6.78	7.47	0.044	−0.092	0.38	0.39
	804	4.07	6.94	0.038	−0.141	0.20	0.24
	809	7.76	11.02	0.130	−0.291	0.14	0.14
	810	5.64	6.16	−0.054	0.068	0.07	0.13
	813	3.29	4.93	0.132	−0.101	0.16	0.15
	943	5.63	5.24	−0.070	−0.093	0.05	0.16
	946	5.11	5.68	−0.078	−0.126	0.32	0.17
	957	4.81	4.46	−0.092	−0.115	0.23	0.35
	989	4.09	3.38	−0.367	−0.082	0.54	0.29
	994	5.83	7.89	−0.016	−0.372	0.23	0.48
	1011	5.25	7.53	0.056	−0.261	0.38	0.20
	1012	4.65	6.01	−0.148	−0.244	0.21	0.62
	1020	7.48	6.83	−0.208	−0.069	0.07	0.16

168

Table 7.3—*Continued*

Record ID in NGA Database		$\omega_{mid}/2\pi$ (Hz)		$\omega'/2\pi$ (Hz/s)		ζ_f (ratio)	
		Major Component	Intermediate Component	Major Component	Intermediate Component	Major Component	Intermediate Component
Reverse	1021	6.85	5.47	−0.109	−0.113	0.31	0.43
	1023	6.69	6.53	−0.258	−0.152	0.15	0.32
	1027	5.00	4.80	−0.103	−0.067	0.20	0.53
	1029	5.17	4.75	−0.139	0.009	0.36	0.28
	1033	5.62	5.89	−0.185	−0.213	0.22	0.21
	1041	6.01	6.87	−0.168	−0.180	0.13	0.29
	1060	4.76	4.42	−0.123	−0.089	0.05	0.16
	1074	2.68	3.29	−0.030	−0.135	0.16	0.19
	1078	5.03	6.00	−0.020	−0.049	0.20	0.28
	1091	5.30	5.58	0.062	−0.066	0.40	0.27
	1096	3.80	3.51	−0.080	−0.031	0.22	0.17
	1206	2.17	2.93	−0.014	−0.026	0.09	0.08
	1234	2.08	2.07	−0.010	−0.007	0.05	0.09
	1245	6.64	5.88	−0.050	−0.058	0.11	0.15
	1257	2.03	2.91	−0.010	−0.032	0.05	0.05
	1273	3.23	3.25	−0.093	−0.069	0.17	0.23
	1278	2.32	1.99	−0.051	−0.039	0.09	0.10
	1287	2.77	2.51	−0.056	−0.078	0.06	0.12
	1293	3.87	4.12	−0.077	−0.020	0.12	0.11
	1302	5.77	6.60	−0.090	−0.093	0.10	0.10
	1325	3.54	3.96	−0.038	−0.052	0.09	0.15
	1347	5.11	5.45	−0.097	−0.126	0.09	0.13
	1350	5.61	4.33	−0.080	−0.092	0.05	0.09
	1377	5.32	4.66	−0.088	−0.045	0.11	0.11
	1391	4.33	3.45	−0.079	−0.058	0.03	0.04
	1485	4.45	4.85	−0.029	−0.054	0.49	0.47
	1517	1.33	1.85	0.009	−0.023	0.09	0.15
	1518	4.90	6.85	−0.148	−0.273	0.28	0.18
	1520	10.14	11.44	0.128	0.205	0.13	0.15
	1548	2.21	2.47	−0.063	−0.065	0.14	0.13
	1576	3.68	3.71	−0.034	−0.038	0.07	0.07
	1577	3.68	3.49	−0.041	−0.043	0.05	0.07
	1585	3.87	3.86	−0.073	−0.073	0.10	0.09
	1587	3.62	3.59	−0.025	−0.029	0.04	0.04
	1594	4.75	4.86	−0.077	−0.071	0.09	0.13

Table 7.4 Error measures for optimized values of filter parameters given in Table 7.3.

| Record ID in NGA Database | | ϵ_ω (Calculated for 1% to 99% levels of I_a) | | ϵ_ζ (Calculated for 5% to 95% levels of I_a) | |
		Major Component	Intermediate Component	Major Component	Intermediate Component
Strike-Slip	164	0.02	0.02	0.09	0.09
	265	0.01	0.02	0.06	0.03
	454	0.01	0.02	0.15	0.16
	455	0.03	0.02	0.09	0.12
	471	0.02	0.02	0.24	0.21
	472	0.01	0.02	0.21	0.18
	476	0.02	0.01	0.34	0.12
	891	0.01	0.01	0.06	0.03
	897	0.01	0.01	0.08	0.05
	922	0.02	0.03	0.06	0.07
	925	0.02	0.02	0.07	0.04
	928	0.01	0.01	0.05	0.06
	934	0.01	0.02	0.07	0.10
	938	0.01	0.01	0.10	0.10
	1109	0.01	0.01	0.16	0.09
	1112	0.01	0.01	0.12	0.08
	1154	0.00	0.00	0.08	0.07
	1169	0.01	0.01	0.05	0.04
	1619	0.01	0.03	0.15	0.17
	1626	0.01	0.01	0.04	0.10
	1633	0.01	0.01	0.05	0.09
	1763	0.01	0.02	0.08	0.08
	1767	0.02	0.05	0.06	0.11
	1786	0.02	0.04	0.15	0.12
	1787	0.02	0.01	0.06	0.06
	1795	0.02	0.02	0.13	0.12
	1824	0.06	0.04	0.11	0.12
	1832	0.02	0.02	0.11	0.11
	1836	0.01	0.01	0.08	0.06
	2107	0.01	0.01	0.05	0.05
	2111	0.00	0.00	0.02	0.06
Reverse	59	0.02	0.02	0.06	0.09
	63	0.02	0.01	0.05	0.06
	71	0.02	0.01	0.17	0.14

Table 7.4—*Continued.*

Record ID in NGA Database		ϵ_ω (Calculated for 1% to 99% levels of I_a)		ϵ_ζ (Calculated for 5% to 95% levels of I_a)	
		Major Component	Intermediate Component	Major Component	Intermediate Component
	72	0.02	0.02	0.07	0.10
	73	0.02	0.01	0.05	0.09
	87	0.01	0.02	0.07	0.05
	89	0.02	0.02	0.07	0.07
	139	0.02	0.02	0.08	0.07
	369	0.02	0.02	0.15	0.11
	511	0.02	0.02	0.09	0.14
	512	0.06	0.03	0.13	0.04
	528	0.02	0.02	0.03	0.09
	536	0.02	0.03	0.11	0.08
	537	0.02	0.02	0.12	0.04
	541	0.01	0.01	0.12	0.12
	769	0.01	0.02	0.35	0.08
	771	0.01	0.01	0.33	0.71
	781	0.01	0.02	0.18	0.06
	782	0.01	0.01	0.15	0.23
	788	0.02	0.02	0.11	0.13
	789	0.02	0.01	0.23	0.49
	791	0.02	0.02	0.19	0.14
	795	0.02	0.02	0.19	0.18
	797	0.03	0.05	0.06	0.04
	801	0.02	0.01	0.11	0.13
	804	0.02	0.03	0.09	0.07
	809	0.01	0.02	0.05	0.12
	810	0.02	0.01	0.31	0.10
	813	0.02	0.02	0.06	0.09
	943	0.02	0.01	0.21	0.12
	946	0.02	0.02	0.07	0.19
	957	0.01	0.01	0.08	0.06
	989	0.03	0.03	0.03	0.04
	994	0.03	0.04	0.05	0.06
	1011	0.01	0.01	0.08	0.11
	1012	0.01	0.01	0.10	0.11
	1020	0.01	0.01	0.14	0.07

Table 7.4—*Continued.*

Record ID in NGA Database		ϵ_ω (Calculated for 1% to 99% levels of I_a)		ϵ_ζ (Calculated for 5% to 95% levels of I_a)	
		Major Component	Intermediate Component	Major Component	Intermediate Component
Reverse	1021	0.02	0.02	0.10	0.04
	1023	0.01	0.02	0.30	0.08
	1027	0.03	0.03	0.09	0.04
	1029	0.01	0.02	0.08	0.04
	1033	0.02	0.02	0.12	0.11
	1041	0.01	0.02	0.22	0.11
	1060	0.01	0.01	0.09	0.16
	1074	0.01	0.01	0.19	0.10
	1078	0.01	0.02	0.07	0.05
	1091	0.01	0.01	0.14	0.13
	1096	0.02	0.01	0.12	0.12
	1206	0.00	0.00	0.16	0.05
	1234	0.00	0.00	0.53	0.09
	1245	0.00	0.00	0.05	0.05
	1257	0.02	0.02	0.37	0.20
	1273	0.00	0.00	0.06	0.05
	1278	0.00	0.01	0.12	0.09
	1287	0.00	0.00	0.13	0.12
	1293	0.01	0.01	0.05	0.04
	1302	0.00	0.00	0.06	0.09
	1325	0.00	0.01	0.05	0.06
	1347	0.01	0.01	0.11	0.07
	1350	0.00	0.00	0.13	0.04
	1377	0.00	0.00	0.05	0.03
	1391	0.01	0.00	0.30	0.30
	1485	0.00	0.00	0.07	0.10
	1517	0.00	0.00	0.12	0.06
	1518	0.00	0.01	0.05	0.07
	1520	0.00	0.00	0.08	0.05
	1548	0.00	0.01	0.04	0.13
	1576	0.01	0.00	0.21	0.20
	1577	0.00	0.00	0.18	0.30
	1585	0.01	0.01	0.02	0.05
	1587	0.01	0.01	0.30	0.41
	1594	0.00	0.00	0.06	0.03

Table 7.5 Summary statistical data of the identified model parameters of principal ground motion components.

Parameter	Minimum	Maximum	Sample Mean	Sample Standard Deviation	Coefficient of Variation
$I_{a,major}$ (s.g.)	0.0005	2.0744	0.0646	0.2227	3.45
$I_{a,inter}$ (s.g.)	0.0003	0.4345	0.0290	0.0648	2.24
D_{5-95} (s)	5.00	41.53	17.42	9.31	0.53
t_{mid} (s)	0.93	33.59	12.41	7.42	0.60
$\omega_{mid}/2\pi$ (Hz)	1.33	21.98	5.93	3.18	0.54
$\omega'/2\pi$ (Hz/s)	-1.437	0.382	-0.090	0.168	1.87
ζ_f (Ratio)	0.03	0.71	0.21	0.14	0.64

Table 7.6 Distribution models assigned to the model parameters.

Parameter	Fitted Distribution[13]	Distribution Bounds
$\bar{I}_{a,major}$ (s.g.)	Lognormal	$(0, \infty)$
$\bar{I}_{a,inter}$ (s.g.)	Lognormal	$(0, \infty)$
D_{5-95} (s)	Beta	$[4,45]$
t_{mid} (s)	Beta	$[0.5,35]$
$\omega_{mid}/2\pi$ (Hz)	Gamma	$(0, \infty)$
$\omega'/2\pi$ (Hz)	Two-sided Truncated Exponential	$[-2,0.5]$
ζ_f (Ratio)	Beta	$[0.02,1]$

Table 7.7 Maximum likelihood estimates of regression coefficients and standard error components.

i	$\beta_{i,0}$	$\beta_{i,1}$	$\beta_{i,2}$	$\beta_{i,3}$	$\beta_{i,4}$	τ_i	σ_i	P-value[14]
1_{major}	-1.841	0.008	**3.065**	-1.351	-0.168	0.176	0.614	0.000
1_{inter}	-2.408	-0.073	**3.307**	-1.295	-0.246	0.474	0.583	0.000
2	-5.859	-0.707	**6.472**	**0.231**	-0.565	0.475	0.577	0.000
3	-5.038	-0.296	**4.614**	**0.350**	-0.175	0.495	0.431	0.000
4	2.086	-0.041	-1.660	-0.217	0.037	0.696	0.714	0.001
5	-3.224	0.067	**3.262**	0.029	-0.144	0.168	0.921	0.019
6	0.692	-0.676	0.296	-0.341	0.181	0.704	0.709	0.000

---

[13] Means and standard deviations of these distributions are according to columns 4 and 5 of Table 7.5.
[14] The smallest significance level at which the null hypothesis $\beta_{i,1} = \beta_{i,2} = \beta_{i,3} = \beta_{i,4} = 0$ is rejected. F-test is employed.

Table 7.8 95% confidence intervals for the regression coefficients.

i	Confidence Intervals			
	$\beta_{i,1}$	$\beta_{i,2}$	$\beta_{i,3}$	$\beta_{i,4}$
1_{major}	$[-0.273\,,0.289]$	$[1.293\,,4.838]$	$[-1.576\,,-1.126]$	$[-0.865\,,0.530]$
1_{inter}	$[-0.342\,,0.196]$	$[1.613\,,5.001]$	$[-1.510\,,-1.080]$	$[-0.912\,,0.421]$
2	$[-0.936\,,-0.478]$	$[5.037\,,7.907]$	$[0.117\,,0.346]$	$[-1.030\,,-0.101]$
3	$[-0.543\,,-0.048]$	$[3.062\,,6.167]$	$[0.226\,,0.474]$	$[-0.678\,,0.327]$
4	$[-0.338\,,0.256]$	$[-3.521\,,0.201]$	$[-0.365\,,-0.068]$	$[-0.566\,,0.639]$
5	$[-0.223\,,0.358]$	$[1.443\,,5.081]$	$[-0.116\,,0.174]$	$[-0.733\,,0.445]$
6	$[-0.963\,,-0.338]$	$[-1.506\,,2.098]$	$[-0.484\,,-0.198]$	$[-0.402\,,0.764]$

Table 7.9 P-values for the t-test with the null hypothesis, $\boldsymbol{\beta_{i,j}} = \mathbf{0}$.

i	P-value[15]			
	$\beta_{i,1}$	$\beta_{i,2}$	$\beta_{i,3}$	$\beta_{i,4}$
1_{major}	0.955	0.001	0.000	0.634
1_{inter}	0.592	0.000	0.000	0.466
2	0.000	0.000	0.000	0.017
3	0.020	0.000	0.000	0.492
4	0.784	0.080	0.004	0.904
5	0.647	0.001	0.697	0.631
6	0.000	0.746	0.000	0.542

---

[15] The smaller this number is, the more significant the estimate of the corresponding coefficient in Table 7.7 is.

Table 7.10 Sample correlation coefficients between the transformed model parameters of two horizontal ground motion components.

		Major Component						Intermediate Component					
		v_1	v_2	v_3	v_4	v_5	v_6	v_1	v_2	v_3	v_4	v_5	v_6
Major Component	v_1	1											
	v_2	−0.38	1										
	v_3	−0.04	+0.68	1									
	v_4	−0.21	−0.07	−0.24	1					Sym.			
	v_5	−0.25	−0.21	−0.22	−0.19	1							
	v_6	−0.06	−0.26	−0.26	+0.28	−0.06	1						
Intermediate Component	v_1	+0.92	−0.31	+0.04	−0.13	+0.19	−0.01	1					
	v_2	−0.30	+0.89	+0.65	−0.15	−0.21	−0.23	−0.31	1				
	v_3	−0.03	+0.68	+0.96	−0.29	−0.22	−0.29	+0.01	+0.69	1			
	v_4	−0.13	−0.17	−0.30	+0.94	−0.10	+0.32	−0.08	−0.20	−0.34	1		
	v_5	+0.09	−0.11	−0.24	−0.10	+0.52	−0.02	+0.07	−0.18	−0.24	−0.19	1	
	v_6	+0.02	−0.17	−0.21	+0.29	−0.13	+0.75	−0.00	−0.17	−0.22	+0.29	−0.05	1
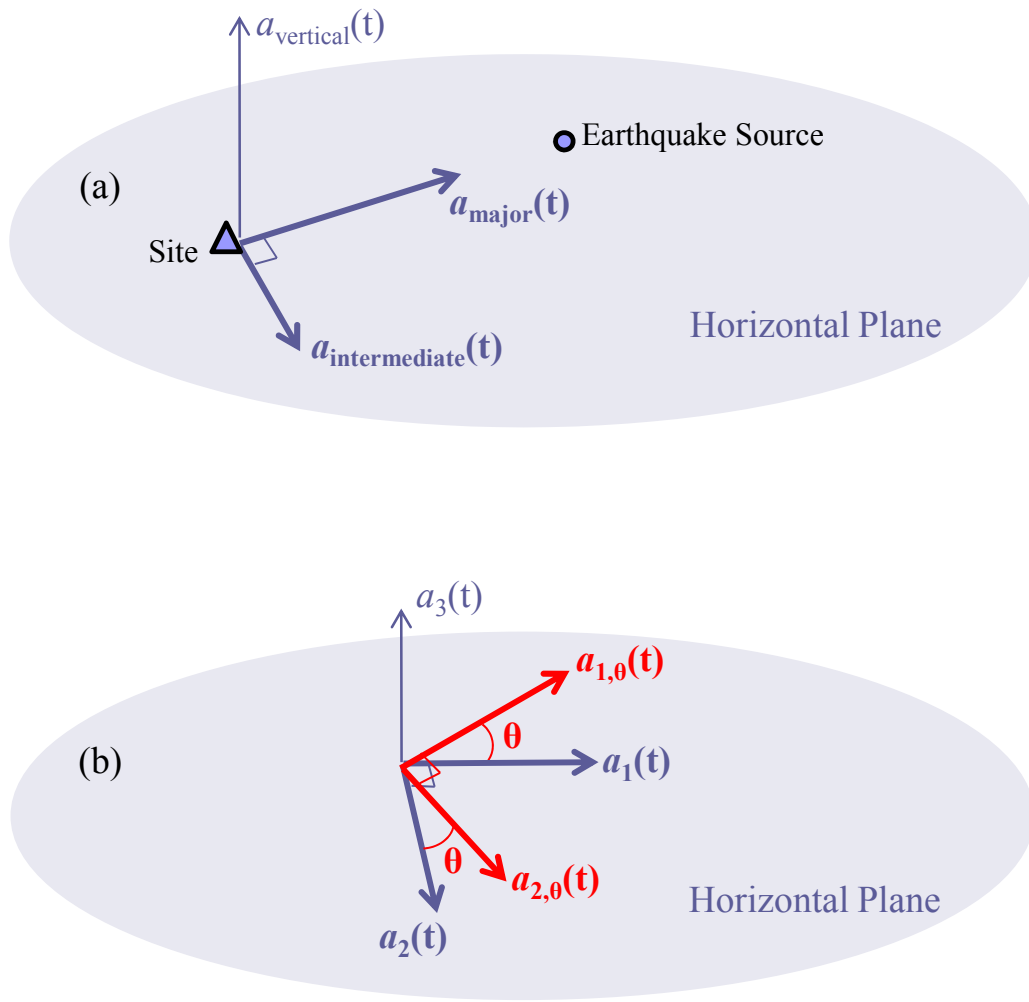
**Fig. 7.1 (a) Directions of principal axes according to Penzien and Watabe (1975).
(b) Rotation of two orthogonal horizontal components by angle θ.**
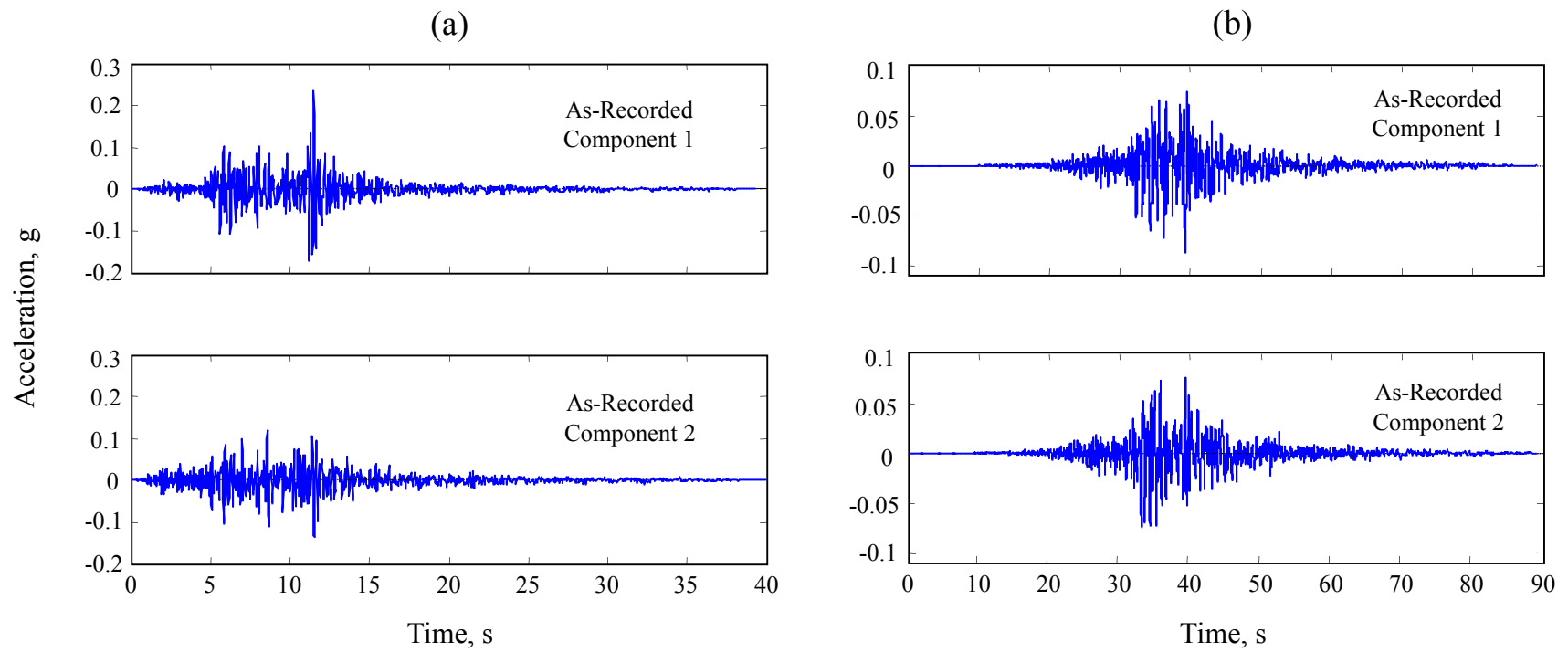
Fig. 7.2   **Horizontal as-recorded components of (a) Northridge earthquake recorded at Mt Wilson – CIT Station, and (b) Chi-Chi, Taiwan, earthquake recorded at HW A046 Station.**
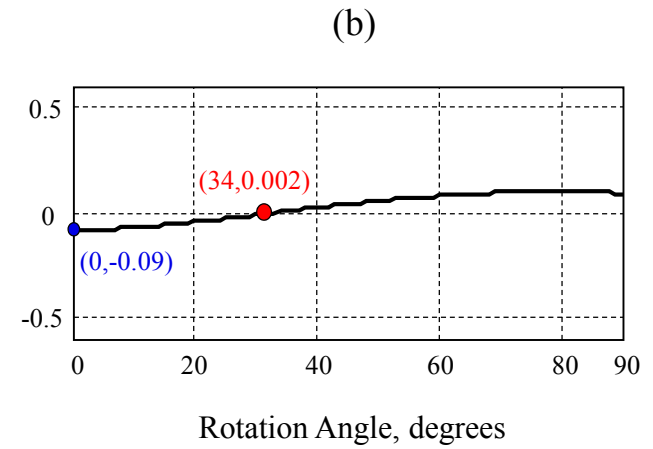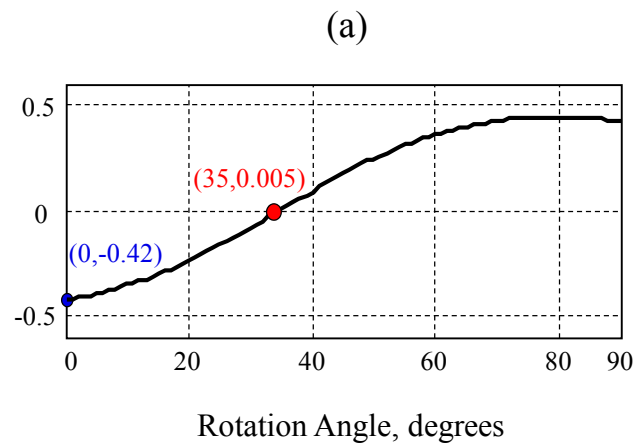
Fig. 7.3 Correlation coefficient between two horizontal components of records in Fig. 7.2 after they have been rotated counterclockwise according to Eq. (7.4).

178
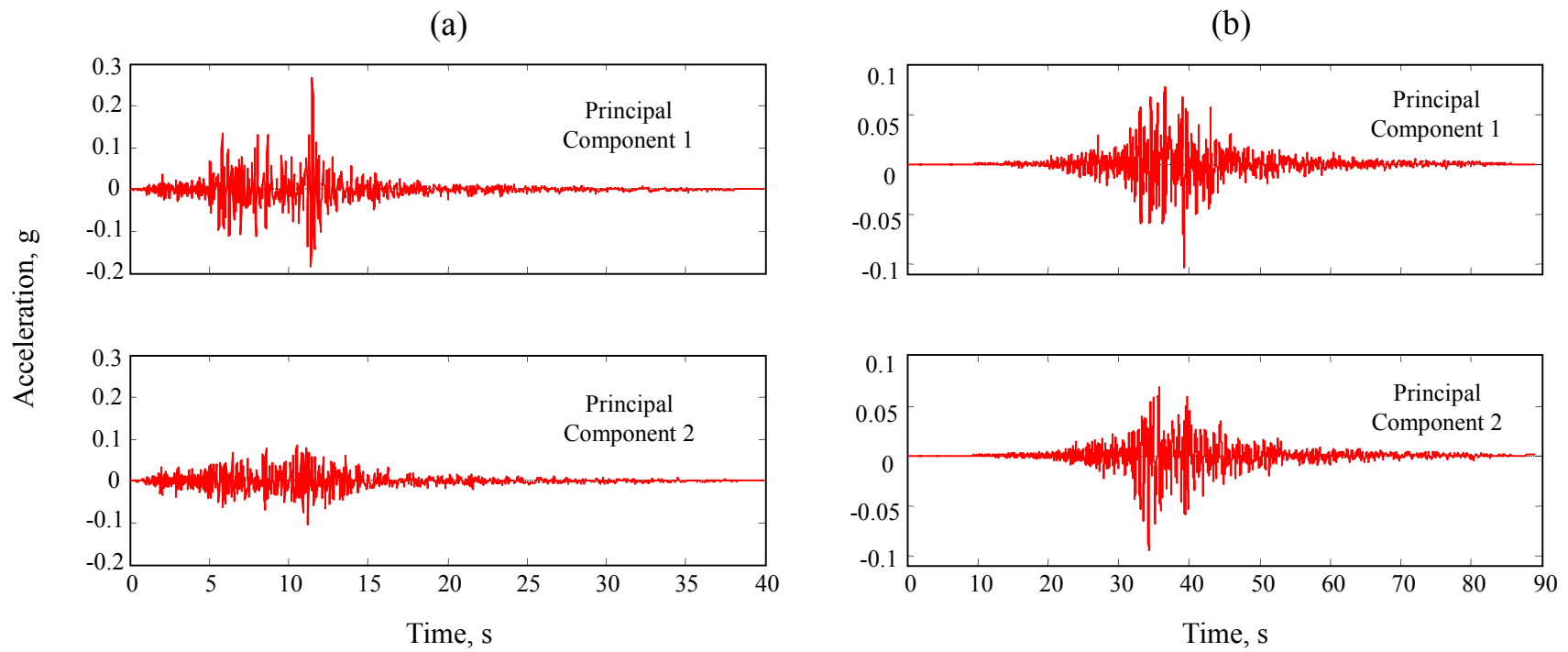
Fig. 7.4 Horizontal components of records in Fig. 7.2, rotated into principal components.

179
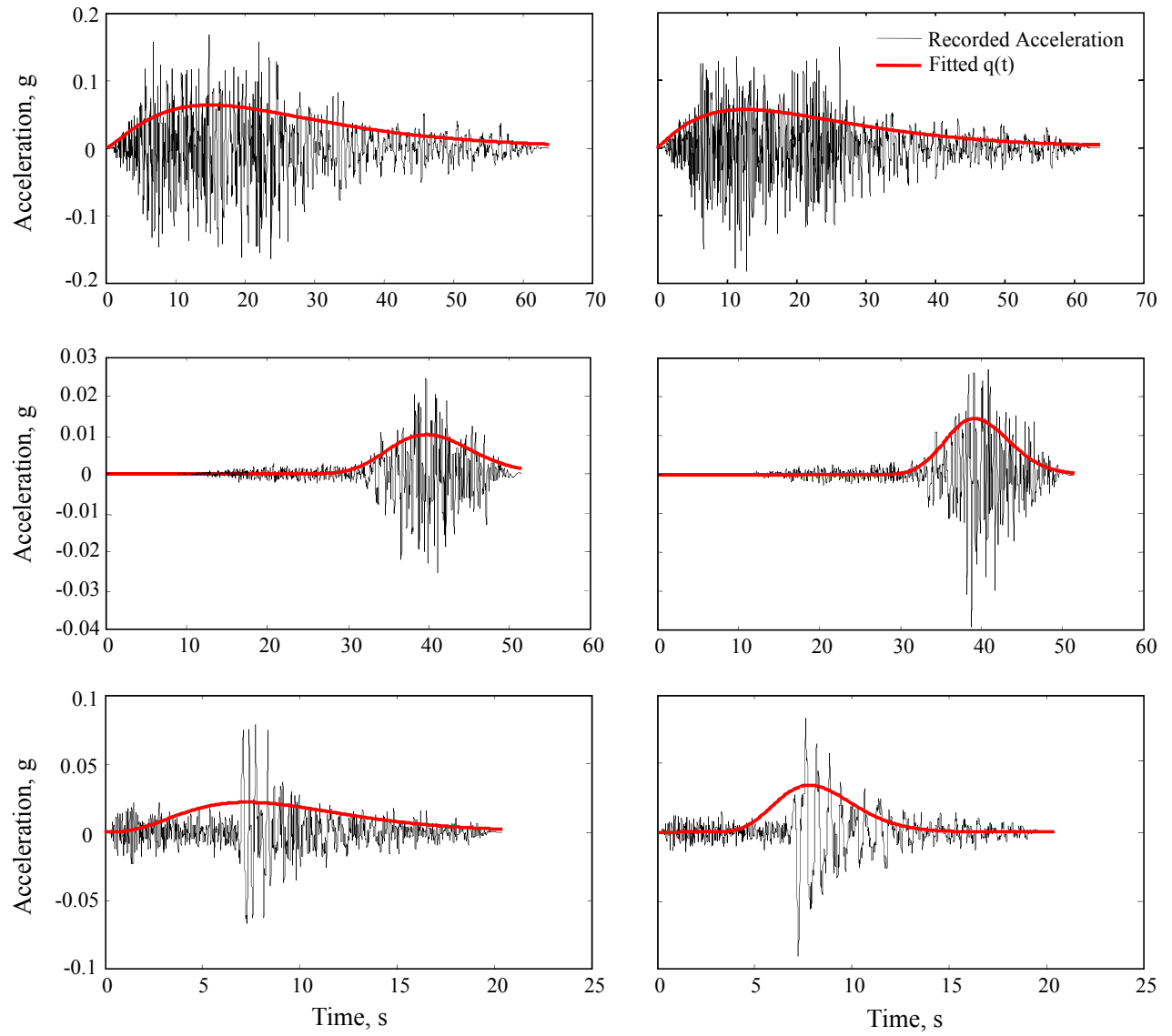
Fig. 7.5 **Rotated ground motion components and fitted modulating functions. Each row shows a pair of horizontal components in principal directions. Figures on the top row show an example with $T_0 = 0$. Figures in the middle row show an example with $T_0 > 0$. Figures in the bottom row provide an example of uncommon irregular behavior of the recorded motion.**
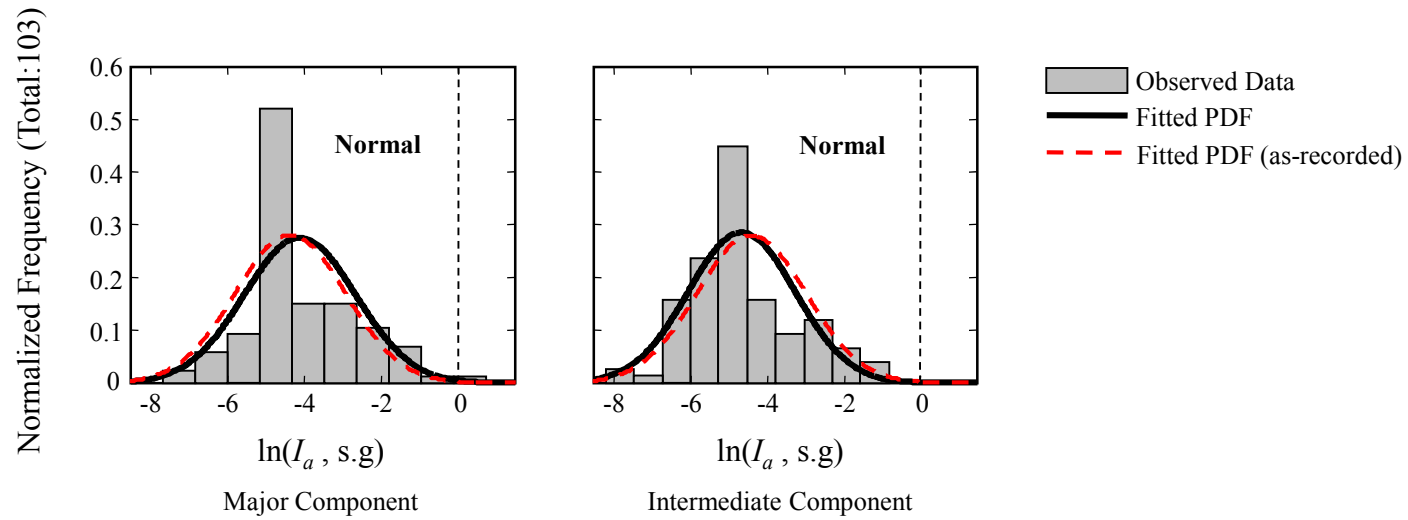
Fig. 7.6 **Normalized frequency diagrams of the identified Arias intensity for the major and intermediate components of records in the principal ground motion components database. Fitted probability density functions are superimposed.**
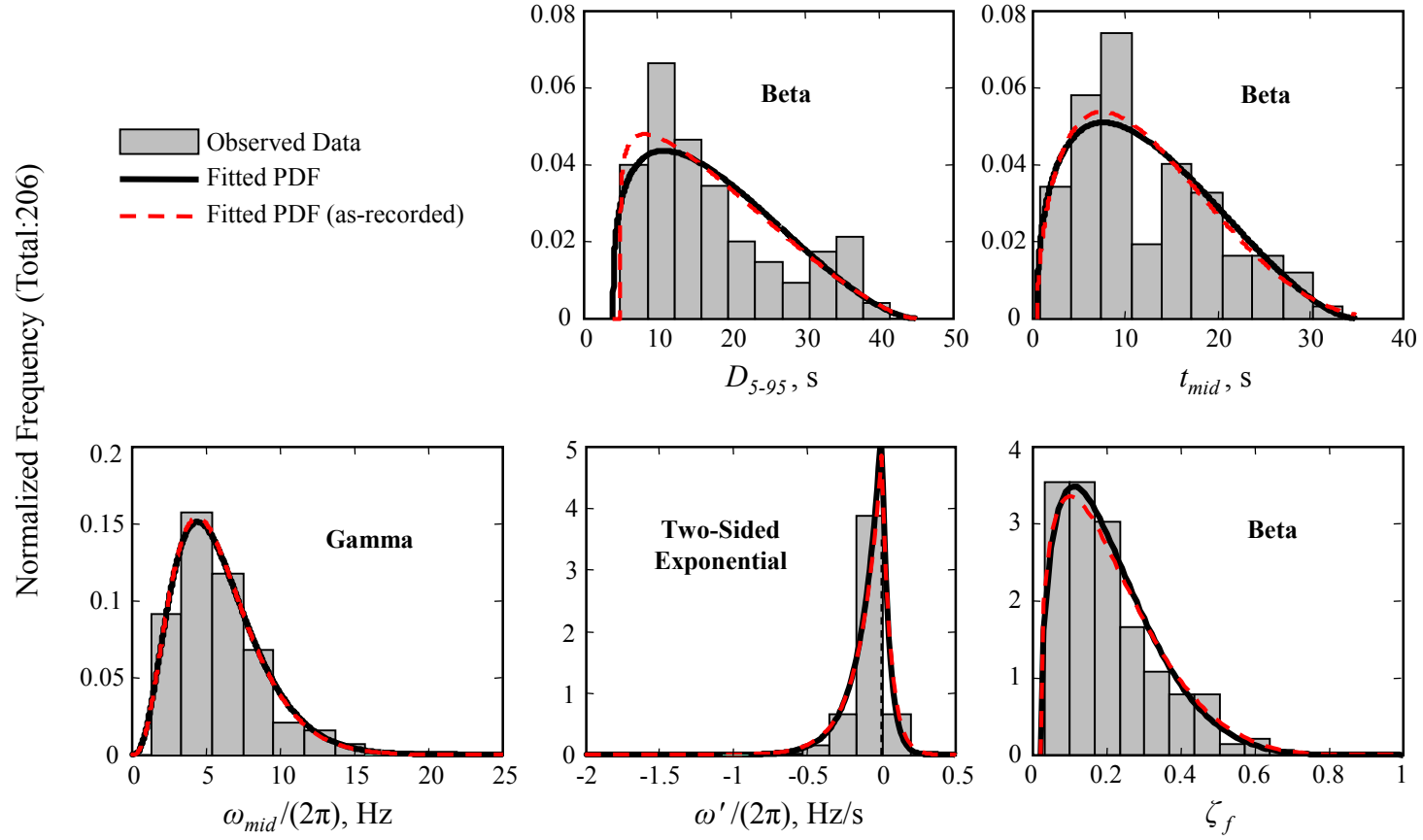
Fig. 7.7 Normalized frequency diagrams of the identified model parameters for the principal ground motion components database. Data corresponding to major and intermediate components are combined. Fitted probability density functions are superimposed.
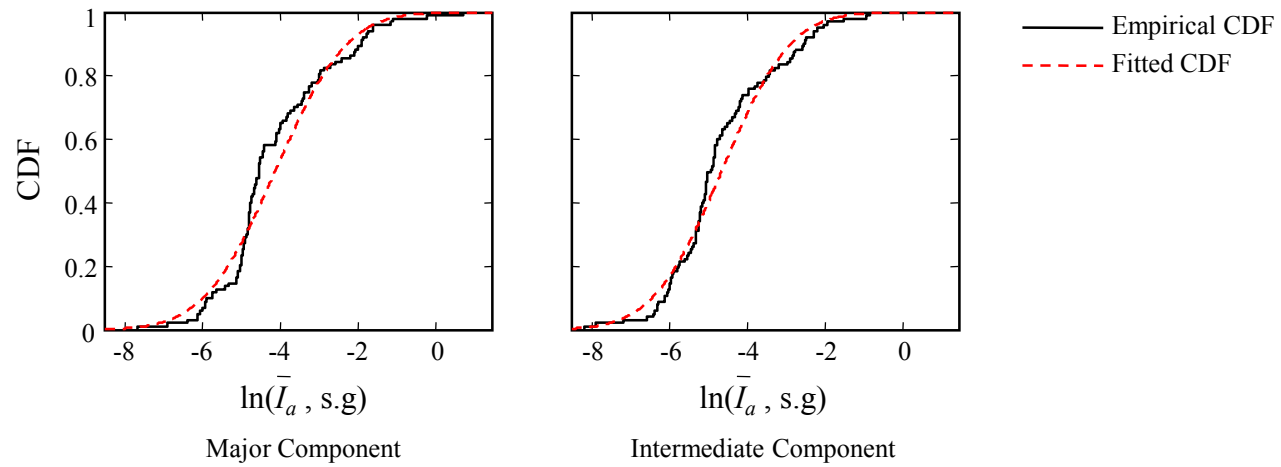
Fig. 7.8 **Empirical cumulative distribution functions (CDFs) of the identified Arias intensity for the major and intermediate components of records in the principal ground motion components database. CDFs of the fitted distributions are superimposed.**
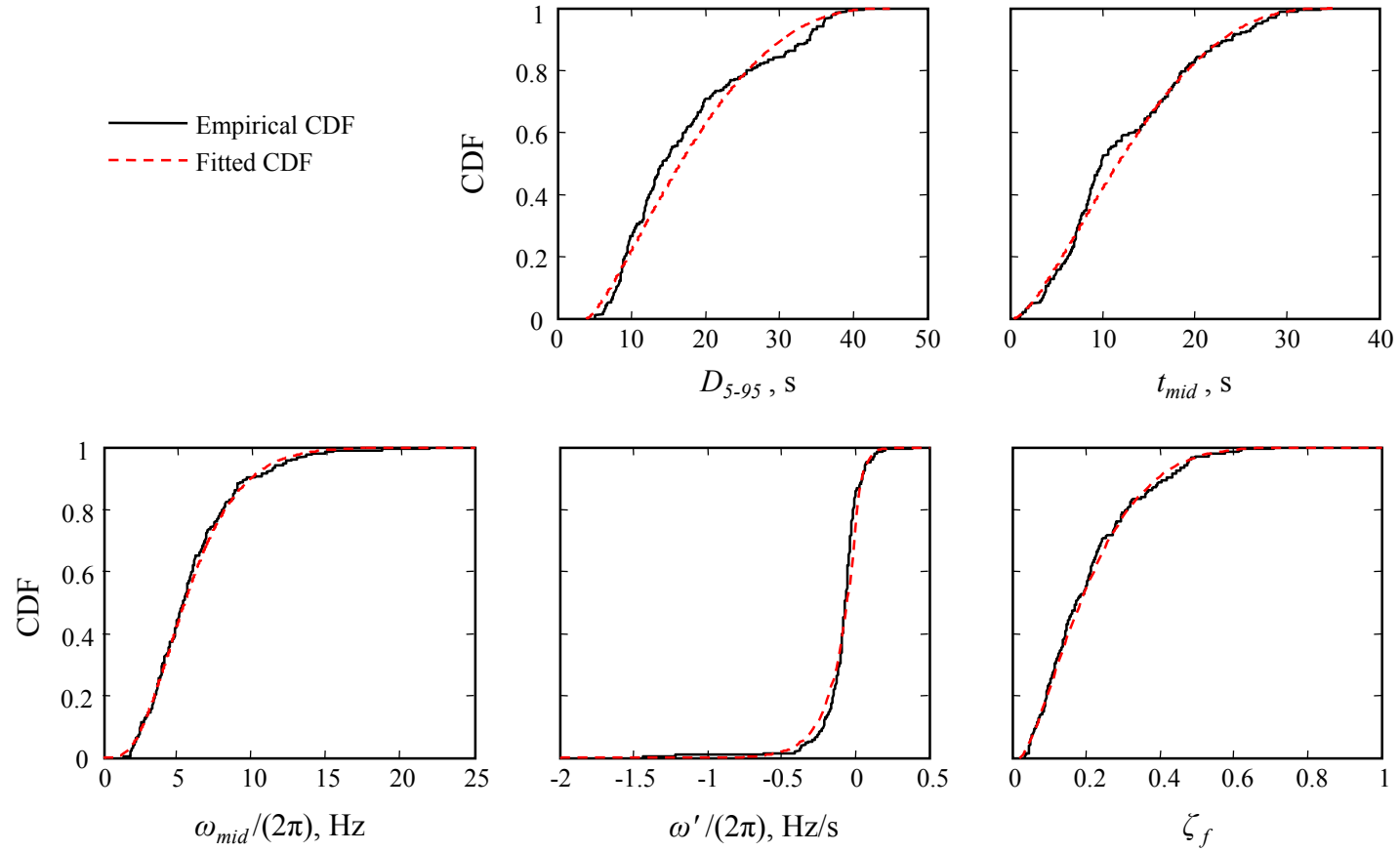
Fig. 7.9 **Empirical cumulative distribution functions (CDFs) of the indentified model parameters for the principal ground motion components database. Data corresponding to major and intermediate components are combined. CDFs of the fitted distributions are superimposed.**

Recorded motion (Major component):
$I_a = 0.0165$g.s , $D_{5-95} = 16.7$s , $t_{mid} = 18.3$s
$\frac{\omega_{mid}}{2\pi} = 3.9$Hz , $\frac{\omega'}{2\pi} = -0.08$Hz/s , $\zeta_f = 0.12$

Recorded motion (Intermediate component):
$I_a = 0.0135$g.s , $D_{5-95} = 17.0$s , $t_{mid} = 17.8$s
$\frac{\omega_{mid}}{2\pi} = 4.1$Hz , $\frac{\omega'}{2\pi} = -0.02$Hz/s , $\zeta_f = 0.11$

Simulated motion (Major component):
$\bar{I}_a = 0.0070$g.s , $D_{5-95} = 22.1$s , $t_{mid} = 14.6$s
$\frac{\omega_{mid}}{2\pi} = 4.5$Hz , $\frac{\omega'}{2\pi} = -0.18$Hz/s , $\zeta_f = 0.15$

Simulated motion (Intermediate component):
$\bar{I}_a = 0.0031$g.s , $D_{5-95} = 25.7$s , $t_{mid} = 16.5$s
$\frac{\omega_{mid}}{2\pi} = 3.5$Hz , $\frac{\omega'}{2\pi} = -0.05$Hz/s , $\zeta_f = 0.08$

Simulated motion (Major component):
$\bar{I}_a = 0.0147$g.s , $D_{5-95} = 17.3$s , $t_{mid} = 10.1$s
$\frac{\omega_{mid}}{2\pi} = 8.1$Hz , $\frac{\omega'}{2\pi} = -0.12$Hz/s , $\zeta_f = 0.42$

Simulated motion (Intermediate component):
$\bar{I}_a = 0.0047$g.s , $D_{5-95} = 21.0$s , $t_{mid} = 10.7$s
$\frac{\omega_{mid}}{2\pi} = 8.6$Hz , $\frac{\omega'}{2\pi} = -0.18$Hz/s , $\zeta_f = 0.50$

Simulated motion (Major component):
$\bar{I}_a = 0.0099$g.s , $D_{5-95} = 27.2$s , $t_{mid} = 17.1$s
$\frac{\omega_{mid}}{2\pi} = 3.2$Hz , $\frac{\omega'}{2\pi} = -0.03$Hz/s , $\zeta_f = 0.20$

Simulated motion (Intermediate component):
$\bar{I}_a = 0.0034$g.s , $D_{5-95} = 24.8$s , $t_{mid} = 16.9$s
$\frac{\omega_{mid}}{2\pi} = 3.7$Hz , $\frac{\omega'}{2\pi} = -0.13$Hz/s , $\zeta_f = 0.35$

Fig. 7.10 Pairs of acceleration time-histories of one recorded (same as in Fig. 7.4b) and three simulated ground motion components along principal directions. Model parameters for each record are provided on the left. All motions correspond to $F = 1$, $M = 7.62$, $R = 51.8$ km, and $V = 618$ m/s.

Major Component

Intermediate Component

Fig. 7.11 Velocity time-histories corresponding to the records in Fig. 7.10.
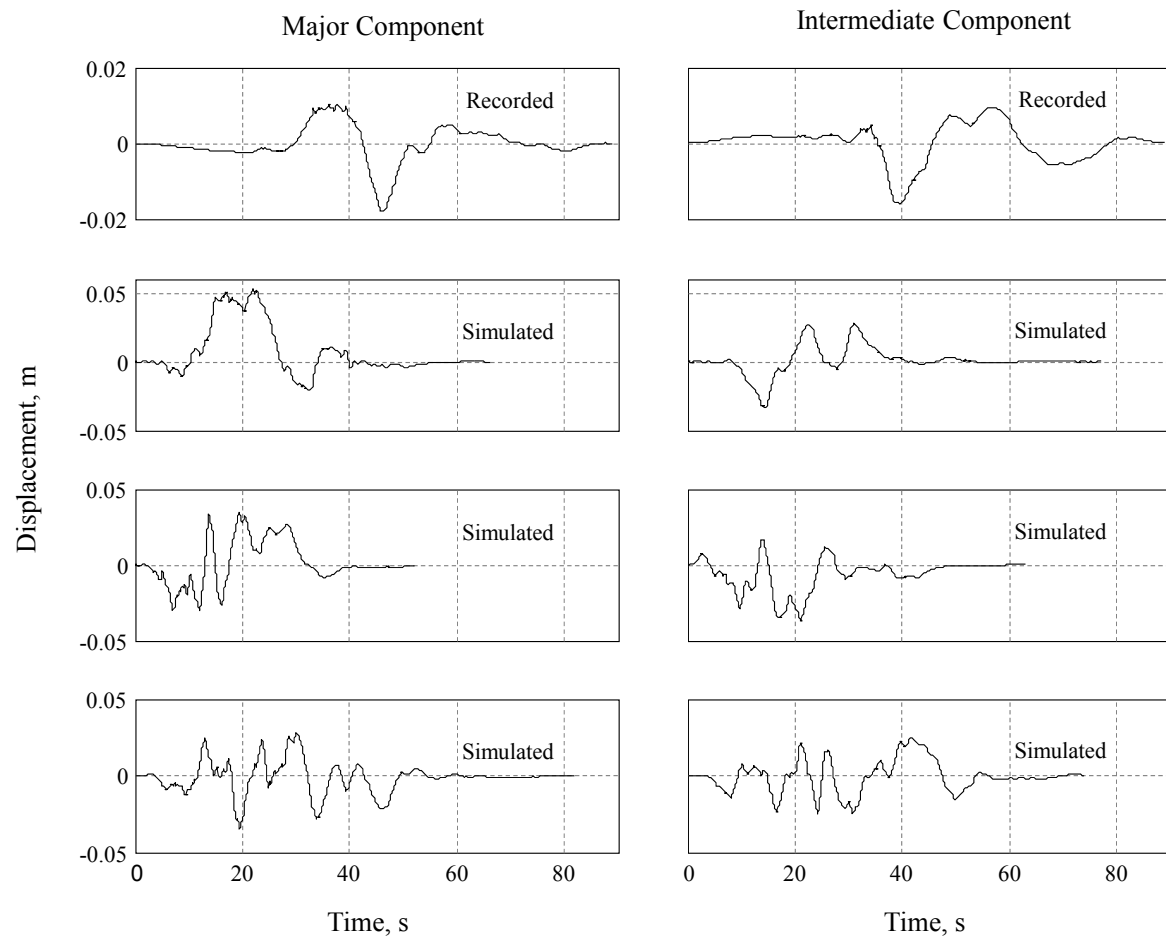
Fig. 7.12 Displacement time-histories corresponding to the records in Fig. 7.10.

187

8 Summary, Conclusions, and Future Studies

8.1 MAJOR DEVELOPMENTS AND FINDINGS

The research described in this report focuses on stochastic modeling and simulation of ground motion time-histories for use in response-history or stochastic dynamic analysis. Ultimately, this research benefits the emerging field of performance-based earthquake engineering (PBEE) by providing a convenient method of generating synthetic ground motions for specified design scenarios that have characteristics similar to those of real earthquake ground motions. The two main objectives proposed in Chapter 1 are fulfilled: (1) a stochastic model for strong ground motion is developed that has important advantages over existing models; an overview of the model is presented in Figure 2.15, (2) a method for generating an ensemble of synthetic ground motions for specified earthquake and site characteristics is developed; an overview of the method is presented in Figure 5.1.

The major developments and findings of this study are summarized as follows:

- A new site-based, fully nonstationary stochastic model to describe earthquake ground motions is developed. The model is based on time modulation of the response of a linear filter with time-varying characteristics to a discretized white-noise excitation. The resulting stochastic process is completely defined by the form of the modulating function, the form of the unit impulse response function of the filter, and the parameters that define these functions.
- Specific functional forms for the filter frequency and filter damping ratio are proposed based on investigation of recorded ground motions. It is concluded that for a typical strong ground motion the filter frequency can be represented by a linear (typically decreasing) function,

whereas the filter damping ratio can be represented by a constant or a piece-wise constant function.

- Acceleration time-histories obtained by simulating the stochastic model are high-pass filtered to achieve zero velocity and displacement residuals. The selected filter is a critically damped oscillator. The oscillator frequency determines the level of high-pass filtering and helps to avoid overestimation of simulated response spectrum ordinates at long periods.

- The proposed stochastic ground motion model has a number of important advantages over existing models:

  (a) The stochastic model represents both the temporal and spectral nonstationary characteristics of real earthquake ground motions. Furthermore, these characteristics are completely decoupled, facilitating identification and interpretation of the model parameters. Separation of the temporal and spectral nonstationarities is achieved through normalization of the stochastic process by its standard deviation prior to time modulation. As a result, the modulating function characterizes the variation of the intensity in time, whereas the time-varying filter describes the evolving frequency content.

  (b) The model has a small number of parameters with physical interpretations. These parameters can be as few as six, with three parameters controlling the evolving intensity of the motion, two parameters controlling the evolving predominant frequency of the motion, and one parameter controlling the bandwidth.

  (c) Modeling is done entirely in the time-domain.

  (d) The discretized form of the model facilitates digital simulation as well as nonlinear stochastic dynamic analysis.

  (e) Simulation of a synthetic ground motion for specified model parameters is simple and requires little more than generation of standard normal random variables, their multiplication with deterministic time-varying functions, and post-processing through a high-pass filter.

- Given a recorded ground motion, the stochastic model parameters are estimated by fitting to selected statistical characteristics of the target accelerogram. There is no need for complicated processing of the recorded motion, such as Fourier analysis or estimation of evolutionary power spectral density. Instead, the model fitting requires computation of the cumulative energy, the cumulative count of zero-level up-crossings, and the cumulative

190

count of negative maxima and positive minima of the accelerogram. This innovative parameter identification method is simple and efficient. Furthermore, the entire analysis is done in the time domain.

- A new framework is proposed for generating an ensemble of synthetic ground motions for specified earthquake and site characteristics. By fitting the stochastic model to a database of recorded ground motions with known earthquake and site characteristics, sample observations of the model parameters are obtained. Statistical data analyses are then performed to develop predictive equations for the model parameters in terms of selected earthquake and site characteristics. Uncertainty in the model parameters are properly accounted for. For a given design scenario with known earthquake and site characteristics, the predictive equations are employed to simulate realizations of the model parameters. Inputting each set of parameter realizations into the stochastic model results in an ensemble of synthetic ground motions that can be used in place of or in conjunction with recorded ground motions.

- The above framework is applied to a database of ground motions taken from the widely used PEER NGA strong-motion database to develop predictive equations for the model parameters in terms of the faulting mechanism, moment magnitude, source-to-site distance, and the shear-wave velocity of the local soil. The database contains ground motions from shallow crustal earthquakes in active tectonic regions. Only strong motions corresponding to earthquakes of magnitude 6.0 and greater, source-to-site distances of at least 10 km, and stiff soil conditions with V_{S30} of at least 600 m/s are considered. Simplified parameter identification methods, suitable for analyzing a large database of recorded motions, are developed to identify the model parameters for every record in the database. The model parameters are assigned probability distributions based on empirical data. Using the assigned probability distributions, model parameters are transformed to the standard normal space to satisfy the normality requirement of subsequent regression analysis. Because the database contains different numbers of recordings from different earthquakes, a random-effects regression analysis method is employed to separately account for the inter- and intra-event uncertainties. The maximum likelihood method is used to estimate the regression coefficients and the error variances, resulting in an empirical predictive equation for each transformed

191

model parameter. Correlation analysis is performed to determine the correlation coefficients among the transformed model parameters.

- The method of generating a suite of synthetic ground motions for specified earthquake and site characteristics is presented in detail. Cases where all the model parameters are unknown and where some model parameters are specified are considered. The simulation method is based on randomly generating realizations of the model parameters from their joint distribution, conditioned on the earthquake and site characteristics. This joint distribution is determined from the empirical predictive equations for the model parameters and their corresponding correlation coefficients.

- The proposed method of generating a suite of synthetic ground motions for specified earthquake and site characteristics accounts for the variability in the model parameters as well as the stochasticity in the ground motion process. Hence, it maintains the natural variability of real ground motions.

- The proposed ground motion simulation method is validated by comparing the resulting synthetics to real recorded motions and to NGA models:

  (a) Synthetic acceleration, velocity, and displacement time-histories are compared with recorded time-histories, indicating similar characteristics and variability between synthetic and real earthquake ground motions.

  (b) The elastic response spectra of synthetic motions are compared to those of recorded motions. It is concluded that the response spectrum of a recorded motion, which is regarded as just one realization of possible ground motions for the specified earthquake and site characteristics, is within the range of the spectral values predicted by synthetic motions.

  (c) The statistics of the elastic response spectra of a large number of synthetic motions for various magnitude and source-to-site distances are compared to their corresponding predicted values by four of the NGA models. In general, the median and variability of elastic response spectra for synthetics are in close agreement with those of the NGA models. This holds true for all spectral periods of interest in structural engineering, moment magnitudes greater than about 6.5, and source-to-site distances greater than 10 km. The results of this study correspond to stiff soil conditions where nonlinear soil behavior is not expected.

- A method for simulating orthogonal horizontal ground motion components for specified earthquake and site characteristics is developed. A new ground motion database is constructed by rotating recorded horizontal ground motion component pairs into their principal axes, i.e., the orthogonal axes along which the components are statistically uncorrelated. Model parameters are identified for each principal component and new predictive equations are constructed. Correlation coefficients between model parameters of the two horizontal principal components are estimated empirically. As expected, these correlation coefficients are high and should not be neglected in the simulation. An extension of the stochastic ground motion model is utilized to simulate two horizontal ground motion components with correlated parameters along the principal axes. The synthetic components can then be rotated into any desired direction, e.g., the input axes of a structure, through a simple orthogonal transformation.

8.2   RECOMMENDATIONS FOR FUTURE STUDIES

In order to improve the accuracy of the stochastic model and the predictive equations and to improve the applicability of the ground motion simulation methods presented in this study following topics are recommended for future research:

- In this study, we selected a single-degree-of-freedom linear filter with time-varying frequency and damping ratio. As mentioned in Chapter 2, such a filter can characterize only a single dominant frequency in the ground motion. To simulate ground motions with multiple dominant frequencies, a multi-degree-of-freedom filter may be selected. Selection of such a filter is possible with the proposed stochastic model. However, additional parameters will need to be introduced and identified, which may reduce the efficiency in modeling and simulation.
- In this study, recommendations on the selection of the corner frequency for high-pass filtering, ω_c, were provided and the sensitivity of simulated motions to this parameter was briefly discussed in Chapter 5. Further studies should be conducted to gain a better understanding of the effect of ω_c on the characteristics of the simulated ground motion.

Preliminary analyses suggest that displacement time-histories are somewhat sensitive with respect to ω_c, but further studies are required.

- The predictive equations and correlation coefficients for the model parameters were developed using a specific database of recorded ground motions. This database was considered adequate for the intended applications of the present study. Limits on earthquake magnitude, source-to-site distance, and local soil stiffness were imposed to obtain simpler (fewer terms in regression formulas) and more reliable (customized for strong earthquakes that are capable of causing nonlinear behavior) predictive equations. The selection of the database in no way limits the methodology presented in this study. As more earthquakes occur and the number of recorded ground motions increases, the ground motion database can be expanded and the predictive equations can be validated or new equations can be developed.

- In this study, only four basic parameters were considered for earthquake and site characteristics: faulting mechanism, moment magnitude, source-to-site distance, and shear-wave velocity of the soil. For more refinement in modeling, future studies may include additional parameters characterizing the earthquake source, travel path, or local site conditions. For example, parameters to account for the effects of soil/sediment depth, nonlinear soil amplification, or factors to account for magnitude saturation may be considered. Additionally, various functional forms for the predictive equations can be investigated. In this study, several functional forms for the explanatory functions were examined, but a linear form was chosen for the overall regression formula for the sake of simplicity and considering the relatively narrow range of earthquake magnitudes. Other forms may be investigated in future studies.

- Currently our method of ground motion simulation is limited to shallow crustal earthquakes in tectonically active regions. The applicability of the methods proposed in this study for other seismic environments such as subduction zones and stable continental regions, where lack of recorded ground motions is a much bigger problem, should be investigated. Subduction zones are capable of creating disastrous earthquakes with very large magnitudes at great depths, and stable continental regions are vulnerable to earthquakes. As a result, if validated, synthetic generation of ground motions would be extremely beneficial in these areas. Since the physical and geological characteristics of subduction zones are different

from shallow and brittle parts of the crust, appropriate changes that reflect these differences must be made to the stochastic ground motion model. Furthermore, suitable databases of ground motions must be selected for each region to construct new relations between the model parameters and the earthquake and site characteristics. In development of predictive equations, due to lack of data in these areas, more emphasis should be placed on the physics of seismic wave propagation than on empirical analysis.

- The simulation methods presented in this study are applicable only to sites that are located at least 10 km from the fault. These methods should be extended to near-fault ground motions. Due to scarcity of recorded near-fault ground motions, this extension would be of particular interest in PBEE. A study is under way that models the distinct characteristics of near-fault ground motions such as rupture directivity effects and the presence of a dominant long-period pulse. The residue motion, i.e., the ground motion after removal of the directivity pulse, is modeled by a stochastic process similar to the one proposed in this study.

- The simulation methods presented in this study are applicable to linear soil conditions with $V_{S30} > 600$ m/s. For softer soil conditions, one can generate synthetic motions at the firm soil layer and propagate them through the softer soil deposits using standard methods of soil dynamics that account for the nonlinearity in the shear modulus and damping of the soil. Alternatively, future studies may be conducted to directly account for the nonlinear soil behavior in the simulation approach. One way is to use additional factors in the predictive equations that account for nonlinear soil amplification effects.

- Modeling of multi-dimensional ground motions is valuable for 3D dynamic analyses of structural systems. The techniques used in this study to model and simulate two horizontal components of ground motion can be easily extended to include the vertical component.

REFERENCES

Abrahamson NA, Atkinson G, Boore D, Bozorgnia Y, Campbell K, Chiou B, Idriss IM, Silva W, Youngs R (2008). Comparisons of the NGA ground-motion relations. *Earthquake Spectra*, **24**:45-66.

Abrahamson NA, Silva WJ (2008). Summary of the Abrahamson & Silva NGA ground-motion relations. *Earthquake Spectra,* **24**:67-97.

Abrahamson NA, Silva WJ (1996). *Empirical ground motion models*, Section 5: *Empirical model for duration of strong ground motion*. Report, Brookhaven National Laboratory.

Abrahamson NA, Somerville PG, Cornell CA (1990). Uncertainty in numerical strong motion predictions. *Proceedings of Fourth U.S. National Conference on Earthquake Engineering.* May 20-24, Palm Springs, California.

Abrahamson N, Youngs R (1992). A stable algorithm for regression analyses using the random effects model. *Bulletin of the Seismological Society of America*, **82**:505-510.

Ahmadi G (1979). Generation of artificial time-histories compatible with given response spectra – a review. *Solid Mechanics Archives*, **4**:207-239.

Alamilla L, Esteva L, Garcia-Perez J, Diaz-Lopez O (2001). Evolutionary properties of stochastic models of earthquake accelerograms: Their dependence on magnitude and distance. *Journal of Seismology*, **5**:1-21.

Ameri G, Gallovic F, Pacor F, Emolo A (2009). Uncertainties in strong ground-motion prediction with finite-fault synthetic seismograms: An application to the 1984 M 5.7 Gubbio, central Italy, earthquake. *Bulletin of the Seismological Society of America*, **99**:647-663.

Amin M, Ang AHS (1968). Nonstationary stochastic model of earthquake motions. *Journal of Engineering Mechanics Division* (ASCE), **94**:559–583.

Anderson TW (1958). *An introduction to multivariate statistical analysis*. Wiley: New York. Theorem 2.5.1.

Ang A, Tang W (2006). *Probability concepts in engineering: Emphasis on applications to civil and environmental engineering, 2nd edition*. Wiley: Hoboken, NJ.

Arias A (1970). A measure of earthquake intensity. In *Seismic design for nuclear power plants*, Hansen RJ (ed.). MIT Press: Cambridge, MA, 438-483.

Au SK, Beck JL (2003). Subset simulation and its applications to seismic risk based on dynamic analysis. *Journal of Engineering Mechanics*, ASCE, **129**:901-917.

Au SK, Beck JL (2001a). Estimation of small failure probability in high dimensions by subset simulation. *Probabilistic Engineering Mechanics*, **16**:263-277.

Bolotin VV (1960). Statistical theory of the aseismic design of structures. *Proceedings of the 2nd World Conference on Earthquake Engineering*, vol. II, Tokyo and Kyoto, Japan, 1365-1374.

Bommer JJ, Acevedo AB (2004). The use of real earthquake accelerograms as input to dynamic analysis. *Journal of Earthquake Engineering*, **8**:43-91.

Boore D, Atkinson G (2008). Ground-motion prediction equations for the average horizontal component of PGA, PGV, and 5%-damped PSA at spectral periods between 0.01 s and 10.0 s. *Earthquake Spectra*, **24**:99-138.

Bozorgnia Y, Bertero VV, Eds. (2004). *Earthquake engineering: From engineering seismology to performance-based engineering*. CRC Press, Boca Raton, FL.

Bozorgnia Y, Hachem MM, Campbell K (2010). Ground motion prediction equation ("Attenuation relationship") for inelastic response spectra. *Earthquake Spectra*, **26**:1-23.

Bozorgnia Y, Hachem MM, Campbell K (2010). Deterministic and probabilistic predictions of yield strength and inelastic displacement spectra. *Earthquake Spectra*, **26**:25-40.

Brillinger DR, Preisler HK (1985). Further analysis of the Joyner-Boore attenuation data. *Bulletin of the Seismological Society of America*, **75**:611-614.

Brune JN (1971). Correction. *Journal of Geophysical Research*, **76**:5002.

Brune JN (1970). Tectonic stress and the spectra of seismic shear waves from earthquakes. *Journal of Geophysical Research*, **75**:4997-5009.

Campbell KW, Bozorgnia Y (2008). NGA ground motion model for the geometric mean horizontal component of PGA, PGV, PGD and 5% damped linear elastic response spectra for periods ranging from 0.01 to 10 s. *Earthquake Spectra,* **24**:139-171.

Causse M, Cotton F, Cornou C, Bard PY (2008). Calibrating median and uncertainty estimates for a practical use of empirical Green's funtions technique. *Bulletin of the Seismological Society of America*, **98**:344-353.

Chang MK, Kwiatkowski JW, Nau RF, Oliver RM, Pister KS (1982). ARMA models for earthquake ground motions. *Earthquake Engineering and Structural Dynamics,* **10**:651-662.

Chiou B, Youngs R (2008). An NGA model for the average horizontal component of peak ground motion and response spectra. *Earthquake Spectra*, **24**:173-215.

Chopra AK (2001). *Dynamics of structures, theory and applications to earthquake engineering, 2nd edition*. Prentice Hall: Upper Saddle River, NJ.

Conte JP, Peng BF (1997). Fully nonstationary analytical earthquake ground-motion model. *Journal of Engineering Mechanics* (ASCE), **12**:15-24.

Conte JP, Pister KS, Mahin SA (1992). Nonstationary ARMA modeling of seismic motions. *Soil Dynamics and Earthquake Engineering,* **11**: 411-426.

Cornell CA (1960). *Stochastic process models in structural engineering*. Technical Report No. 34, Department of Civil Engineering, Stanford University, Stanford, CA.

Der Kiureghian A (2000). The geometry of random vibrations and solutions by FORM and SORM. *Probabilistic Engineering Mechanics,* **15**:81-90.

Der Kiureghian A, Crempien J (1989). An evolutionary model for earthquake ground motion. *Structural Safety*, **6**:235-246.

Der Kiureghian A, Fujimura K (2009). Nonlinear stochastic dynamic analysis for performance-based earthquake engineering. *Earthquake Engineering and Structural Dynamics*, **38**:719-738.

Douglas J, Aochi H (2008). A survey of techniques for predicting earthquake ground motions for engineering purposes. *Surveys in Geophysics*, **29**:187-220.

Franchin P (2004). Reliability of uncertain inelastic structures under earthquake excitation. *Journal of Engineering Mechanics*, **130**: 180-191.

Frankel A (2009). A constant stress-drop model for producing broadband synthetic seismograms: comparison with the Next Generation Attenuation relations. *Bulletin of the Seismological Society of America*, **99**:664-680.

Fujimura K, Der Kiureghian A (2007). Tail-equivalent linearization method for nonlinear random vibration. *Probabilistic Engineering Mechanics*, **22**:63-76.

Hancock J, Watson-Lamprey JA, Abrahamson NA, Bommer JJ, Markatis A, McCoy E, Mendis R (2006). An improved method of matching response spectra of recorded earthquake ground motion using wavelets. *Journal of Earthquake Engineering*, **10**:67-89.

Heredia-Zavoni E, Machicao-Barrionuevo R (2004). Response to orthogonal components of ground motion and assessment of percentage combination rules. *Earthquake Engineering and Structural Dynamics*, **33**:271-284.

Holmes WT, Kircher C, Petak W, Youssef N (2008). *Seismic performance objectives for tall buildings*. PEER Report 2008/01, Pacific Earthquake Engineering Research Center.

Hoshiya M, Hasgur Z (1978). AR and MA models of nonstationary ground motion. *Bulletin of the International Institute of Seismology and Earthquake Engineering,* **16**:55-68.

Housner GW, Jennings PC (1964). Generation of artificial earthquakes. *Journal of Engineering Mechanics Division* (ASCE), **90**:113-150.

Hutchings L, Ioannidou E, Foxall W, Voulgaris N, Savy J, Kalogeras I, Scognamiglio L, Stavrakakis G (2007). A physically based strong ground-motion prediction methodology; application to PSHA and the 1999 Mw=6.0 Athens earthquake. *Geophysical Journal International*, **168**:659-680.

Idriss IM (2008). An NGA empirical model for estimating the horizontal spectral values generated by shallow crustal earthquakes. *Earthquake Spectra*, **24**:217-242.

Iyengar RN, Iyengar KTS (1969). A nonstationary random process model for earthquake accelerograms. *Bulletin of the Seismological Society of America*, **59**:1163-1188.

Jurkevics A, Ulrych TJ (1978). Representing and simulating strong ground motion. *Bulletin of the Seismological Society of America,* **68**:781-801.

Kotz S, Balakrishnan N, Johnson NL (2000). *Continuous multivariate distributions, volumen1, Models and Applications, 2nd edition*. Wiley: New York.

Kozin F (1988). Autoregressive moving average models of earthquake records. *Probabilistic Engineering Mechanics*, **3**:58-63.

Kubo T, Penzien J (1979). Simulation of three-dimensional strong ground motions along principal axes, San Fernando earthquak. *Earthquake Engineering and Structural Dynamics*, **7**:279-294.

Li CC, Der Kiureghian A (1995). Mean out-crossing rate of nonlinear response to stochastic input. *Proceedings of the 9th International Conference on Applications of Statistics and Probability*, CERRA, Lemaire, Favre and Mebarki, eds., Balkema, Rotterdam, The Netherlands, 295-302.

Liao S, Zerva A (2006). Physically compliant, conditionally simulated spatially variable seismic ground motions for performance-based design. *Earthquake Engineering and Structural Dynamics*, **35**:891-919.

Lin YK (1986). On random pulse train and its evolutionary spectral representation. *Probabilistic Engineering Mechanics*, **1**:219-223.

Lin YK (1965). Nonstationary excitation and response in linear systems treated as sequences of random pulses. *Journal of the Acoustical Society of America*, **38**:453-460.

Liu SC (1970). Synthesis of stochastic representations of ground motions. *The Bell Systems Technical Journal*, **49**:521-541.

Liu P, Archuleta RJ, Hartzell SH (2006). Prediction of broadband ground-motion time histories: hybrid low/high-frequency method with correlated random source parameters. *Bulletin of the Seismological Society of America*, **96**:2118-2130.

Liu PL, Der Kiureghian A (1986). Multivariate distribution models with prescribed marginals and covariances. *Probabilistic Engineering Mechanics*, **1**:105-112.

Lutes LD, Sarkani S (2004). *Random vibrations: Analysis of structural and mechanical systems*. Elsevier Butterworth-Heinemann: Burlington, MA.

Marsaglia G, Tsang WW (2000). The Ziggurat method for generating random variables. *Journal of Statistical Software*, **5**(8). Available online at http://www.jstatsoft.org/v05/i08/ [9 May 2010].

Mazzoni S, McKenna F, Scott MH, Fenves GL, et al. (2006). OpenSees command language manual. Available online at http://opensees.berkeley.edu [9 May 2010].

Mobarakeh AA, Rofooei FR, Ahmadi G (2002). Simulation of earthquake records using time-varying ARMA (2,1) model. *Probabilistic Engineering Mechanics*, **17**:15-34.

Papadimitriou K (1990). *Stochastic characterization of strong ground motion and application to structural response*. Report No. EERL 90-03, Earthquake Engineering Research Laboratory, California Institute of Technology, Pasadena, CA.

Penzien J, Watabe M (1975). Characteristics of 3-dimensional earthquake ground motions. *Earthquake Engineering and Structural Dynamics*, **3**:365-373.

Polhemus NW, Cakmak AS (1981). Simulation of earthquake ground motions using autoregressive moving average (ARMA) models. *Earthquake Engineering and Structural Dynamics*, **9**:343-354.

Pousse G, Bonilla LF, Cotton F, Margerin L (2006). Nonstationary stochastic simulation of strong ground motion time histories including natural variability: application to the K-net Japanese database. *Bulletin of the Seismological Society of America*, **96**:2103-2117.

Power M, Chiou B, Abrahamson NA, Roblee C, Bozorgnia Y, Shantz, T (2008). An introduction to NGA. *Earthquake Spectra*, **24**:3-21.

Rezaeian S, Der Kiureghian A (2010). Simulation of synthetic ground motions for specified earthquake and site characteristics. *Earthquake Engineering and Structural Dynamics*. In press.

Rezaeian S, Der Kiureghian A (2008). A stochastic ground motion model with separable temporal and spectral nonstationarities. *Earthquake Engineering and Structural Dynamics*, **37**:1565-1584.

Ruiz P, Penzien J (1971). Stochastic seismic response of structures. *Journal of Engineering Mechanics* (ASCE), **97**:441-456.

Sabetta F, Pugliese A (1996). Estimation of response spectra and simulation of nonstationary earthquake ground motions. *Bulletin of the Seismological Society of America*, **86**:337-352.

Saragoni GR, Hart GC (1974). Simulation of artificial earthquakes. *Earthquake Engineering and Structural Dynamics*, **2**:249-267.

Searle SR (1971). *Linear models*. Wiley: New York, pp. 385.

Shinozuka M, Deodatis G (1988). Stochastic process models for earthquake ground motion. *Probabilistic Engineering Mechanics*, **3**:114-123.

Shinozuka M, Sato Y (1967). Simulation of nonstationary random process. *Journal of Engineering Mechanics* (ASCE), **93**:11-40.

Smeby W, Der Kiureghian A (1985). Modal combination rules for multicomponent earthquake excitation. *Earthquake Engineering and Structural Dynamics*, **13**:1-12.

Stafford PJ, Sgobba S, Marano GC (2009). An energy-based envelope function for the stochastic simulation of earthquake accelerograms. *Soil Dynamics and Earthquake Engineering*, **29**:1123-1133.

Tajimi H (1959). Basic theories on aseismic design of structures. *Institute of Industrial Science*, University of Tokyo, **8**(4).

Travasarou T, Bray JD, Abrahamson NA (2003). Empirical attenuation relationship for Arias Intensity. *Earthquake Engineering and Structural Dynamics*, **32**:1133-1155.

Trifunac MD, Brady AG (1975). A study on the duration of strong earthquake ground motion. *Bulletin of the Seismological Society of America*, **65**:581-626.

Vamvatsikos D, Cornell CA (2002). Incremental dynamic analysis. *Earthquake Engineering and Structural Dynamics*, **31**:491-514.

Watson-Lamprey JA (2007). *Selection and scaling of ground motion time series.* Ph.D. Thesis (in Engineering -- Civil and Environmental Engineering), University of California, Berkeley, CA.

Wen YK, Gu P (2004). Description and simulation of nonstationary processes based on Hilbert spectra. *Journal of Engineering Mechanics* (ASCE), **130**:942-951.

Yeh CH, Wen YK (1990). Modeling of nonstationary ground motion and analysis of inelastic structural response. *Structural Safety*, **8**:281-298.

Yeh CH, Wen YK (1989). *Modeling of nonstationary earthquake ground motion and biaxial and torsional response of inelastic structures*. Civil Engineering Studies, Structural Research Series Report No. 546, University of Illinois.

Zerva A (1988). Seismic source mechanisms and ground motion models, review paper. *Probabilistic Engineering Mechanics*, **3**:64-74.

PEER REPORTS

PEER reports are available individually or by yearly subscription. PEER reports can be ordered at http://peer.berkeley.edu/publications/peer_reports.html or by contacting the Pacific Earthquake Engineering Research Center, 1301 South 46th Street, Richmond, CA 94804-4698. Tel.: (510) 665-3448; Fax: (510) 665-3456; Email: peer_editor@berkeley.edu

PEER 2010/02 *Stochastic Modeling and Simulation of Ground Motions for Performance-Based Earthquake Engineering.* Sanaz Rezaeian and Armen Der Kiureghian. June 2010.

PEER 2010/01 *Structural Response and Cost Characterization of Bridge Construction Using Seismic Performance Enhancement Strategies.* Ady Aviram, Božidar Stojadinović, Gustavo J. Parra-Montesinos, and Kevin R. Mackie. March 2010.

PEER 2009/03 *The Integration of Experimental and Simulation Data in the Study of Reinforced Concrete Bridge Systems Including Soil-Foundation-Structure Interaction.* Matthew Dryden and Gregory L. Fenves. November 2009.

PEER 2009/02 *Improving Earthquake Mitigation through Innovations and Applications in Seismic Science, Engineering, Communication, and Response. Proceedings of a U.S.-Iran Seismic Workshop.* October 2009.

PEER 2009/01 *Evaluation of Ground Motion Selection and Modification Methods: Predicting Median Interstory Drift Response of Buildings.* Curt B. Haselton, Ed. June 2009.

PEER 2008/10 *Technical Manual for Strata.* Albert R. Kottke and Ellen M. Rathje. February 2009.

PEER 2008/09 *NGA Model for Average Horizontal Component of Peak Ground Motion and Response Spectra.* Brian S.-J. Chiou and Robert R. Youngs. November 2008.

PEER 2008/08 *Toward Earthquake-Resistant Design of Concentrically Braced Steel Structures.* Patxi Uriz and Stephen A. Mahin. November 2008.

PEER 2008/07 *Using OpenSees for Performance-Based Evaluation of Bridges on Liquefiable Soils.* Stephen L. Kramer, Pedro Arduino, and HyungSuk Shin. November 2008.

PEER 2008/06 *Shaking Table Tests and Numerical Investigation of Self-Centering Reinforced Concrete Bridge Columns.* Hyung IL Jeong, Junichi Sakai, and Stephen A. Mahin. September 2008.

PEER 2008/05 *Performance-Based Earthquake Engineering Design Evaluation Procedure for Bridge Foundations Undergoing Liquefaction-Induced Lateral Ground Displacement.* Christian A. Ledezma and Jonathan D. Bray. August 2008.

PEER 2008/04 *Benchmarking of Nonlinear Geotechnical Ground Response Analysis Procedures.* Jonathan P. Stewart, Annie On-Lei Kwok, Yousseff M. A. Hashash, Neven Matasovic, Robert Pyke, Zhiliang Wang, and Zhaohui Yang. August 2008.

PEER 2008/03 *Guidelines for Nonlinear Analysis of Bridge Structures in California.* Ady Aviram, Kevin R. Mackie, and Božidar Stojadinović. August 2008.

PEER 2008/02 *Treatment of Uncertainties in Seismic-Risk Analysis of Transportation Systems.* Evangelos Stergiou and Anne S. Kiremidjian. July 2008.

PEER 2008/01 *Seismic Performance Objectives for Tall Buildings.* William T. Holmes, Charles Kircher, William Petak, and Nabih Youssef. August 2008.

PEER 2007/12 *An Assessment to Benchmark the Seismic Performance of a Code-Conforming Reinforced Concrete Moment-Frame Building.* Curt Haselton, Christine A. Goulet, Judith Mitrani-Reiser, James L. Beck, Gregory G. Deierlein, Keith A. Porter, Jonathan P. Stewart, and Ertugrul Taciroglu. August 2008.

PEER 2007/11 *Bar Buckling in Reinforced Concrete Bridge Columns.* Wayne A. Brown, Dawn E. Lehman, and John F. Stanton. February 2008.

PEER 2007/10 *Computational Modeling of Progressive Collapse in Reinforced Concrete Frame Structures.* Mohamed M. Talaat and Khalid M. Mosalam. May 2008.

PEER 2007/09 *Integrated Probabilistic Performance-Based Evaluation of Benchmark Reinforced Concrete Bridges.* Kevin R. Mackie, John-Michael Wong, and Božidar Stojadinović. January 2008.

PEER 2007/08 *Assessing Seismic Collapse Safety of Modern Reinforced Concrete Moment-Frame Buildings.* Curt B. Haselton and Gregory G. Deierlein. February 2008.

PEER 2007/07 *Performance Modeling Strategies for Modern Reinforced Concrete Bridge Columns.* Michael P. Berry and Marc O. Eberhard. April 2008.

PEER 2007/06   *Development of Improved Procedures for Seismic Design of Buried and Partially Buried Structures.* Linda Al Atik and Nicholas Sitar. June 2007.

PEER 2007/05   *Uncertainty and Correlation in Seismic Risk Assessment of Transportation Systems.* Renee G. Lee and Anne S. Kiremidjian. July 2007.

PEER 2007/04   *Numerical Models for Analysis and Performance-Based Design of Shallow Foundations Subjected to Seismic Loading.* Sivapalan Gajan, Tara C. Hutchinson, Bruce L. Kutter, Prishati Raychowdhury, José A. Ugalde, and Jonathan P. Stewart. May 2008.

PEER 2007/03   *Beam-Column Element Model Calibrated for Predicting Flexural Response Leading to Global Collapse of RC Frame Buildings.* Curt B. Haselton, Abbie B. Liel, Sarah Taylor Lange, and Gregory G. Deierlein. May 2008.

PEER 2007/02   *Campbell-Bozorgnia NGA Ground Motion Relations for the Geometric Mean Horizontal Component of Peak and Spectral Ground Motion Parameters.* Kenneth W. Campbell and Yousef Bozorgnia. May 2007.

PEER 2007/01   *Boore-Atkinson NGA Ground Motion Relations for the Geometric Mean Horizontal Component of Peak and Spectral Ground Motion Parameters.* David M. Boore and Gail M. Atkinson. May. May 2007.

PEER 2006/12   *Societal Implications of Performance-Based Earthquake Engineering.* Peter J. May. May 2007.

PEER 2006/11   *Probabilistic Seismic Demand Analysis Using Advanced Ground Motion Intensity Measures, Attenuation Relationships, and Near-Fault Effects.* Polsak Tothong and C. Allin Cornell. March 2007.

PEER 2006/10   *Application of the PEER PBEE Methodology to the I-880 Viaduct.* Sashi Kunnath. February 2007.

PEER 2006/09   *Quantifying Economic Losses from Travel Forgone Following a Large Metropolitan Earthquake.* James Moore, Sungbin Cho, Yue Yue Fan, and Stuart Werner. November 2006.

PEER 2006/08   *Vector-Valued Ground Motion Intensity Measures for Probabilistic Seismic Demand Analysis*. Jack W. Baker and C. Allin Cornell. October 2006.

PEER 2006/07   *Analytical Modeling of Reinforced Concrete Walls for Predicting Flexural and Coupled–Shear-Flexural Responses*. Kutay Orakcal, Leonardo M. Massone, and John W. Wallace. October 2006.

PEER 2006/06   *Nonlinear Analysis of a Soil-Drilled Pier System under Static and Dynamic Axial Loading.* Gang Wang and Nicholas Sitar. November 2006.

PEER 2006/05   *Advanced Seismic Assessment Guidelines.* Paolo Bazzurro, C. Allin Cornell, Charles Menun, Maziar Motahari, and Nicolas Luco. September 2006.

PEER 2006/04   *Probabilistic Seismic Evaluation of Reinforced Concrete Structural Components and Systems.* Tae Hyung Lee and Khalid M. Mosalam. August 2006.

PEER 2006/03   *Performance of Lifelines Subjected to Lateral Spreading.* Scott A. Ashford and Teerawut Juirnarongrit. July 2006.

PEER 2006/02   *Pacific Earthquake Engineering Research Center Highway Demonstration Project.* Anne Kiremidjian, James Moore, Yue Yue Fan, Nesrin Basoz, Ozgur Yazali, and Meredith Williams. April 2006.

PEER 2006/01   *Bracing Berkeley. A Guide to Seismic Safety on the UC Berkeley Campus.* Mary C. Comerio, Stephen Tobriner, and Ariane Fehrenkamp. January 2006.

PEER 2005/16   *Seismic Response and Reliability of Electrical Substation Equipment and Systems.* Junho Song, Armen Der Kiureghian, and Jerome L. Sackman. April 2006.

PEER 2005/15   *CPT-Based Probabilistic Assessment of Seismic Soil Liquefaction Initiation.* R. E. S. Moss, R. B. Seed, R. E. Kayen, J. P. Stewart, and A. Der Kiureghian. April 2006.

PEER 2005/14   *Workshop on Modeling of Nonlinear Cyclic Load-Deformation Behavior of Shallow Foundations.* Bruce L. Kutter, Geoffrey Martin, Tara Hutchinson, Chad Harden, Sivapalan Gajan, and Justin Phalen. March 2006.

PEER 2005/13   *Stochastic Characterization and Decision Bases under Time-Dependent Aftershock Risk in Performance-Based Earthquake Engineering.* Gee Liek Yeo and C. Allin Cornell. July 2005.

PEER 2005/12   *PEER Testbed Study on a Laboratory Building: Exercising Seismic Performance Assessment.* Mary C. Comerio, editor. November 2005.

PEER 2005/11   *Van Nuys Hotel Building Testbed Report: Exercising Seismic Performance Assessment*. Helmut Krawinkler, editor. October 2005.

PEER 2005/10   *First NEES/E-Defense Workshop on Collapse Simulation of Reinforced Concrete Building Structures.* September 2005.

PEER 2005/09   *Test Applications of Advanced Seismic Assessment Guidelines.* Joe Maffei, Karl Telleen, Danya Mohr, William Holmes, and Yuki Nakayama. August 2006.

PEER 2005/08 *Damage Accumulation in Lightly Confined Reinforced Concrete Bridge Columns.* R. Tyler Ranf, Jared M. Nelson, Zach Price, Marc O. Eberhard, and John F. Stanton. April 2006.

PEER 2005/07 *Experimental and Analytical Studies on the Seismic Response of Freestanding and Anchored Laboratory Equipment.* Dimitrios Konstantinidis and Nicos Makris. January 2005.

PEER 2005/06 *Global Collapse of Frame Structures under Seismic Excitations.* Luis F. Ibarra and Helmut Krawinkler. September 2005.

PEER 2005//05 *Performance Characterization of Bench- and Shelf-Mounted Equipment.* Samit Ray Chaudhuri and Tara C. Hutchinson. May 2006.

PEER 2005/04 *Numerical Modeling of the Nonlinear Cyclic Response of Shallow Foundations.* Chad Harden, Tara Hutchinson, Geoffrey R. Martin, and Bruce L. Kutter. August 2005.

PEER 2005/03 *A Taxonomy of Building Components for Performance-Based Earthquake Engineering.* Keith A. Porter. September 2005.

PEER 2005/02 *Fragility Basis for California Highway Overpass Bridge Seismic Decision Making.* Kevin R. Mackie and Božidar Stojadinović. June 2005.

PEER 2005/01 *Empirical Characterization of Site Conditions on Strong Ground Motion.* Jonathan P. Stewart, Yoojoong Choi, and Robert W. Graves. June 2005.

PEER 2004/09 *Electrical Substation Equipment Interaction: Experimental Rigid Conductor Studies.* Christopher Stearns and André Filiatrault. February 2005.

PEER 2004/08 *Seismic Qualification and Fragility Testing of Line Break 550-kV Disconnect Switches.* Shakhzod M. Takhirov, Gregory L. Fenves, and Eric Fujisaki. January 2005.

PEER 2004/07 *Ground Motions for Earthquake Simulator Qualification of Electrical Substation Equipment.* Shakhzod M. Takhirov, Gregory L. Fenves, Eric Fujisaki, and Don Clyde. January 2005.

PEER 2004/06 *Performance-Based Regulation and Regulatory Regimes.* Peter J. May and Chris Koski. September 2004.

PEER 2004/05 *Performance-Based Seismic Design Concepts and Implementation: Proceedings of an International Workshop.* Peter Fajfar and Helmut Krawinkler, editors. September 2004.

PEER 2004/04 *Seismic Performance of an Instrumented Tilt-up Wall Building.* James C. Anderson and Vitelmo V. Bertero. July 2004.

PEER 2004/03 *Evaluation and Application of Concrete Tilt-up Assessment Methodologies.* Timothy Graf and James O. Malley. October 2004.

PEER 2004/02 *Analytical Investigations of New Methods for Reducing Residual Displacements of Reinforced Concrete Bridge Columns.* Junichi Sakai and Stephen A. Mahin. August 2004.

PEER 2004/01 *Seismic Performance of Masonry Buildings and Design Implications.* Kerri Anne Taeko Tokoro, James C. Anderson, and Vitelmo V. Bertero. February 2004.

PEER 2003/18 *Performance Models for Flexural Damage in Reinforced Concrete Columns.* Michael Berry and Marc Eberhard. August 2003.

PEER 2003/17 *Predicting Earthquake Damage in Older Reinforced Concrete Beam-Column Joints.* Catherine Pagni and Laura Lowes. October 2004.

PEER 2003/16 *Seismic Demands for Performance-Based Design of Bridges.* Kevin Mackie and Božidar Stojadinović. August 2003.

PEER 2003/15 *Seismic Demands for Nondeteriorating Frame Structures and Their Dependence on Ground Motions.* Ricardo Antonio Medina and Helmut Krawinkler. May 2004.

PEER 2003/14 *Finite Element Reliability and Sensitivity Methods for Performance-Based Earthquake Engineering.* Terje Haukaas and Armen Der Kiureghian. April 2004.

PEER 2003/13 *Effects of Connection Hysteretic Degradation on the Seismic Behavior of Steel Moment-Resisting Frames.* Janise E. Rodgers and Stephen A. Mahin. March 2004.

PEER 2003/12 *Implementation Manual for the Seismic Protection of Laboratory Contents: Format and Case Studies.* William T. Holmes and Mary C. Comerio. October 2003.

PEER 2003/11 *Fifth U.S.-Japan Workshop on Performance-Based Earthquake Engineering Methodology for Reinforced Concrete Building Structures.* February 2004.

PEER 2003/10 *A Beam-Column Joint Model for Simulating the Earthquake Response of Reinforced Concrete Frames.* Laura N. Lowes, Nilanjan Mitra, and Arash Altoontash. February 2004.

PEER 2003/09 *Sequencing Repairs after an Earthquake: An Economic Approach.* Marco Casari and Simon J. Wilkie. April 2004.

PEER 2003/08 *A Technical Framework for Probability-Based Demand and Capacity Factor Design (DCFD) Seismic Formats.* Fatemeh Jalayer and C. Allin Cornell. November 2003.

PEER 2003/07 *Uncertainty Specification and Propagation for Loss Estimation Using FOSM Methods.* Jack W. Baker and C. Allin Cornell. September 2003.

PEER 2003/06 *Performance of Circular Reinforced Concrete Bridge Columns under Bidirectional Earthquake Loading.* Mahmoud M. Hachem, Stephen A. Mahin, and Jack P. Moehle. February 2003.

PEER 2003/05 *Response Assessment for Building-Specific Loss Estimation.* Eduardo Miranda and Shahram Taghavi. September 2003.

PEER 2003/04 *Experimental Assessment of Columns with Short Lap Splices Subjected to Cyclic Loads.* Murat Melek, John W. Wallace, and Joel Conte. April 2003.

PEER 2003/03 *Probabilistic Response Assessment for Building-Specific Loss Estimation.* Eduardo Miranda and Hesameddin Aslani. September 2003.

PEER 2003/02 *Software Framework for Collaborative Development of Nonlinear Dynamic Analysis Program.* Jun Peng and Kincho H. Law. September 2003.

PEER 2003/01 *Shake Table Tests and Analytical Studies on the Gravity Load Collapse of Reinforced Concrete Frames.* Kenneth John Elwood and Jack P. Moehle. November 2003.

PEER 2002/24 *Performance of Beam to Column Bridge Joints Subjected to a Large Velocity Pulse.* Natalie Gibson, André Filiatrault, and Scott A. Ashford. April 2002.

PEER 2002/23 *Effects of Large Velocity Pulses on Reinforced Concrete Bridge Columns.* Greg L. Orozco and Scott A. Ashford. April 2002.

PEER 2002/22 *Characterization of Large Velocity Pulses for Laboratory Testing.* Kenneth E. Cox and Scott A. Ashford. April 2002.

PEER 2002/21 *Fourth U.S.-Japan Workshop on Performance-Based Earthquake Engineering Methodology for Reinforced Concrete Building Structures.* December 2002.

PEER 2002/20 *Barriers to Adoption and Implementation of PBEE Innovations.* Peter J. May. August 2002.

PEER 2002/19 *Economic-Engineered Integrated Models for Earthquakes: Socioeconomic Impacts.* Peter Gordon, James E. Moore II, and Harry W. Richardson. July 2002.

PEER 2002/18 *Assessment of Reinforced Concrete Building Exterior Joints with Substandard Details.* Chris P. Pantelides, Jon Hansen, Justin Nadauld, and Lawrence D. Reaveley. May 2002.

PEER 2002/17 *Structural Characterization and Seismic Response Analysis of a Highway Overcrossing Equipped with Elastomeric Bearings and Fluid Dampers: A Case Study.* Nicos Makris and Jian Zhang. November 2002.

PEER 2002/16 *Estimation of Uncertainty in Geotechnical Properties for Performance-Based Earthquake Engineering.* Allen L. Jones, Steven L. Kramer, and Pedro Arduino. December 2002.

PEER 2002/15 *Seismic Behavior of Bridge Columns Subjected to Various Loading Patterns.* Asadollah Esmaeily-Gh. and Yan Xiao. December 2002.

PEER 2002/14 *Inelastic Seismic Response of Extended Pile Shaft Supported Bridge Structures.* T.C. Hutchinson, R.W. Boulanger, Y.H. Chai, and I.M. Idriss. December 2002.

PEER 2002/13 *Probabilistic Models and Fragility Estimates for Bridge Components and Systems.* Paolo Gardoni, Armen Der Kiureghian, and Khalid M. Mosalam. June 2002.

PEER 2002/12 *Effects of Fault Dip and Slip Rake on Near-Source Ground Motions: Why Chi-Chi Was a Relatively Mild M7.6 Earthquake.* Brad T. Aagaard, John F. Hall, and Thomas H. Heaton. December 2002.

PEER 2002/11 *Analytical and Experimental Study of Fiber-Reinforced Strip Isolators.* James M. Kelly and Shakhzod M. Takhirov. September 2002.

PEER 2002/10 *Centrifuge Modeling of Settlement and Lateral Spreading with Comparisons to Numerical Analyses.* Sivapalan Gajan and Bruce L. Kutter. January 2003.

PEER 2002/09 *Documentation and Analysis of Field Case Histories of Seismic Compression during the 1994 Northridge, California, Earthquake.* Jonathan P. Stewart, Patrick M. Smith, Daniel H. Whang, and Jonathan D. Bray. October 2002.

PEER 2002/08 *Component Testing, Stability Analysis and Characterization of Buckling-Restrained Unbonded Braces[TM].* Cameron Black, Nicos Makris, and Ian Aiken. September 2002.

PEER 2002/07 *Seismic Performance of Pile-Wharf Connections.* Charles W. Roeder, Robert Graff, Jennifer Soderstrom, and Jun Han Yoo. December 2001.

PEER 2002/06 *The Use of Benefit-Cost Analysis for Evaluation of Performance-Based Earthquake Engineering Decisions.* Richard O. Zerbe and Anthony Falit-Baiamonte. September 2001.

PEER 2002/05 *Guidelines, Specifications, and Seismic Performance Characterization of Nonstructural Building Components and Equipment.* André Filiatrault, Constantin Christopoulos, and Christopher Stearns. September 2001.

PEER 2002/04 *Consortium of Organizations for Strong-Motion Observation Systems and the Pacific Earthquake Engineering Research Center Lifelines Program: Invited Workshop on Archiving and Web Dissemination of Geotechnical Data, 4–5 October 2001.* September 2002.

PEER 2002/03 *Investigation of Sensitivity of Building Loss Estimates to Major Uncertain Variables for the Van Nuys Testbed.* Keith A. Porter, James L. Beck, and Rustem V. Shaikhutdinov. August 2002.

PEER 2002/02 *The Third U.S.-Japan Workshop on Performance-Based Earthquake Engineering Methodology for Reinforced Concrete Building Structures.* July 2002.

PEER 2002/01 *Nonstructural Loss Estimation: The UC Berkeley Case Study.* Mary C. Comerio and John C. Stallmeyer. December 2001.

PEER 2001/16 *Statistics of SDF-System Estimate of Roof Displacement for Pushover Analysis of Buildings.* Anil K. Chopra, Rakesh K. Goel, and Chatpan Chintanapakdee. December 2001.

PEER 2001/15 *Damage to Bridges during the 2001 Nisqually Earthquake.* R. Tyler Ranf, Marc O. Eberhard, and Michael P. Berry. November 2001.

PEER 2001/14 *Rocking Response of Equipment Anchored to a Base Foundation.* Nicos Makris and Cameron J. Black. September 2001.

PEER 2001/13 *Modeling Soil Liquefaction Hazards for Performance-Based Earthquake Engineering.* Steven L. Kramer and Ahmed-W. Elgamal. February 2001.

PEER 2001/12 *Development of Geotechnical Capabilities in OpenSees.* Boris Jeremi . September 2001.

PEER 2001/11 *Analytical and Experimental Study of Fiber-Reinforced Elastomeric Isolators.* James M. Kelly and Shakhzod M. Takhirov. September 2001.

PEER 2001/10 *Amplification Factors for Spectral Acceleration in Active Regions.* Jonathan P. Stewart, Andrew H. Liu, Yoojoong Choi, and Mehmet B. Baturay. December 2001.

PEER 2001/09 *Ground Motion Evaluation Procedures for Performance-Based Design.* Jonathan P. Stewart, Shyh-Jeng Chiou, Jonathan D. Bray, Robert W. Graves, Paul G. Somerville, and Norman A. Abrahamson. September 2001.

PEER 2001/08 *Experimental and Computational Evaluation of Reinforced Concrete Bridge Beam-Column Connections for Seismic Performance.* Clay J. Naito, Jack P. Moehle, and Khalid M. Mosalam. November 2001.

PEER 2001/07 *The Rocking Spectrum and the Shortcomings of Design Guidelines.* Nicos Makris and Dimitrios Konstantinidis. August 2001.

PEER 2001/06 *Development of an Electrical Substation Equipment Performance Database for Evaluation of Equipment Fragilities.* Thalia Agnanos. April 1999.

PEER 2001/05 *Stiffness Analysis of Fiber-Reinforced Elastomeric Isolators.* Hsiang-Chuan Tsai and James M. Kelly. May 2001.

PEER 2001/04 *Organizational and Societal Considerations for Performance-Based Earthquake Engineering.* Peter J. May. April 2001.

PEER 2001/03 *A Modal Pushover Analysis Procedure to Estimate Seismic Demands for Buildings: Theory and Preliminary Evaluation.* Anil K. Chopra and Rakesh K. Goel. January 2001.

PEER 2001/02 *Seismic Response Analysis of Highway Overcrossings Including Soil-Structure Interaction.* Jian Zhang and Nicos Makris. March 2001.

PEER 2001/01 *Experimental Study of Large Seismic Steel Beam-to-Column Connections.* Egor P. Popov and Shakhzod M. Takhirov. November 2000.

PEER 2000/10 *The Second U.S.-Japan Workshop on Performance-Based Earthquake Engineering Methodology for Reinforced Concrete Building Structures.* March 2000.

PEER 2000/09 *Structural Engineering Reconnaissance of the August 17, 1999 Earthquake: Kocaeli (Izmit), Turkey.* Halil Sezen, Kenneth J. Elwood, Andrew S. Whittaker, Khalid Mosalam, John J. Wallace, and John F. Stanton. December 2000.

PEER 2000/08 *Behavior of Reinforced Concrete Bridge Columns Having Varying Aspect Ratios and Varying Lengths of Confinement.* Anthony J. Calderone, Dawn E. Lehman, and Jack P. Moehle. January 2001.

PEER 2000/07 *Cover-Plate and Flange-Plate Reinforced Steel Moment-Resisting Connections.* Taejin Kim, Andrew S. Whittaker, Amir S. Gilani, Vitelmo V. Bertero, and Shakhzod M. Takhirov. September 2000.

PEER 2000/06 *Seismic Evaluation and Analysis of 230-kV Disconnect Switches.* Amir S. J. Gilani, Andrew S. Whittaker, Gregory L. Fenves, Chun-Hao Chen, Henry Ho, and Eric Fujisaki. July 2000.

PEER 2000/05 *Performance-Based Evaluation of Exterior Reinforced Concrete Building Joints for Seismic Excitation.* Chandra Clyde, Chris P. Pantelides, and Lawrence D. Reaveley. July 2000.

PEER 2000/04 *An Evaluation of Seismic Energy Demand: An Attenuation Approach.* Chung-Che Chou and Chia-Ming Uang. July 1999.

PEER 2000/03 *Framing Earthquake Retrofitting Decisions: The Case of Hillside Homes in Los Angeles.* Detlof von Winterfeldt, Nels Roselund, and Alicia Kitsuse. March 2000.

PEER 2000/02 *U.S.-Japan Workshop on the Effects of Near-Field Earthquake Shaking.* Andrew Whittaker, ed. July 2000.

PEER 2000/01 *Further Studies on Seismic Interaction in Interconnected Electrical Substation Equipment.* Armen Der Kiureghian, Kee-Jeung Hong, and Jerome L. Sackman. November 1999.

PEER 1999/14 *Seismic Evaluation and Retrofit of 230-kV Porcelain Transformer Bushings.* Amir S. Gilani, Andrew S. Whittaker, Gregory L. Fenves, and Eric Fujisaki. December 1999.

PEER 1999/13 *Building Vulnerability Studies: Modeling and Evaluation of Tilt-up and Steel Reinforced Concrete Buildings.* John W. Wallace, Jonathan P. Stewart, and Andrew S. Whittaker, editors. December 1999.

PEER 1999/12 *Rehabilitation of Nonductile RC Frame Building Using Encasement Plates and Energy-Dissipating Devices.* Mehrdad Sasani, Vitelmo V. Bertero, James C. Anderson. December 1999.

PEER 1999/11 *Performance Evaluation Database for Concrete Bridge Components and Systems under Simulated Seismic Loads.* Yael D. Hose and Frieder Seible. November 1999.

PEER 1999/10 *U.S.-Japan Workshop on Performance-Based Earthquake Engineering Methodology for Reinforced Concrete Building Structures.* December 1999.

PEER 1999/09 *Performance Improvement of Long Period Building Structures Subjected to Severe Pulse-Type Ground Motions.* James C. Anderson, Vitelmo V. Bertero, and Raul Bertero. October 1999.

PEER 1999/08 *Envelopes for Seismic Response Vectors.* Charles Menun and Armen Der Kiureghian. July 1999.

PEER 1999/07 *Documentation of Strengths and Weaknesses of Current Computer Analysis Methods for Seismic Performance of Reinforced Concrete Members.* William F. Cofer. November 1999.

PEER 1999/06 *Rocking Response and Overturning of Anchored Equipment under Seismic Excitations.* Nicos Makris and Jian Zhang. November 1999.

PEER 1999/05 *Seismic Evaluation of 550 kV Porcelain Transformer Bushings.* Amir S. Gilani, Andrew S. Whittaker, Gregory L. Fenves, and Eric Fujisaki. October 1999.

PEER 1999/04 *Adoption and Enforcement of Earthquake Risk-Reduction Measures.* Peter J. May, Raymond J. Burby, T. Jens Feeley, and Robert Wood.

PEER 1999/03 *Task 3 Characterization of Site Response General Site Categories.* Adrian Rodriguez-Marek, Jonathan D. Bray, and Norman Abrahamson. February 1999.

PEER 1999/02 *Capacity-Demand-Diagram Methods for Estimating Seismic Deformation of Inelastic Structures: SDF Systems.* Anil K. Chopra and Rakesh Goel. April 1999.

PEER 1999/01 *Interaction in Interconnected Electrical Substation Equipment Subjected to Earthquake Ground Motions.* Armen Der Kiureghian, Jerome L. Sackman, and Kee-Jeung Hong. February 1999.

PEER 1998/08 *Behavior and Failure Analysis of a Multiple-Frame Highway Bridge in the 1994 Northridge Earthquake.* Gregory L. Fenves and Michael Ellery. December 1998.

PEER 1998/07 *Empirical Evaluation of Inertial Soil-Structure Interaction Effects.* Jonathan P. Stewart, Raymond B. Seed, and Gregory L. Fenves. November 1998.

PEER 1998/06 *Effect of Damping Mechanisms on the Response of Seismic Isolated Structures.* Nicos Makris and Shih-Po Chang. November 1998.

PEER 1998/05 *Rocking Response and Overturning of Equipment under Horizontal Pulse-Type Motions.* Nicos Makris and Yiannis Roussos. October 1998.

PEER 1998/04   *Pacific Earthquake Engineering Research Invitational Workshop Proceedings, May 14–15, 1998: Defining the Links between Planning, Policy Analysis, Economics and Earthquake Engineering.* Mary Comerio and Peter Gordon. September 1998.

PEER 1998/03   *Repair/Upgrade Procedures for Welded Beam to Column Connections.* James C. Anderson and Xiaojing Duan. May 1998.

PEER 1998/02   *Seismic Evaluation of 196 kV Porcelain Transformer Bushings.* Amir S. Gilani, Juan W. Chavez, Gregory L. Fenves, and Andrew S. Whittaker. May 1998.

PEER 1998/01   *Seismic Performance of Well-Confined Concrete Bridge Columns.* Dawn E. Lehman and Jack P. Moehle. December 2000.

ONLINE REPORTS

The following PEER reports are available by Internet only at http://peer.berkeley.edu/publications/peer_reports.html

PEER 2010/106 *Verification of Probabilistic Seismic Hazard Analysis Computer Programs.* Patricia Thomas, Ivan Wong, and Norman Abrahamson. May 2010.

PEER 2010/105 *Structural Engineering Reconnaissance of the April 6, 2009, Abruzzo, Italy, Earthquake, and Lessons Learned.* M. Selim Günay and Khalid M. Mosalam. April 2010.

PEER 2010/104 *Simulating the Inelastic Seismic Behavior of Steel Braced Frames Including Low-Cycle Fatigue.* Yuli Huang and Stephen A. Mahin. April 2010.

PEER 2010/103 *Post-Earthquake Traffic Capacity of Modern Bridges in California.* Vesna Terzic and Božidar Stojadinović. March 2010.

PEER 2010/102 *Analysis of Cumulative Absolute Velocity (CAV) and JMA Instrumental Seismic Intensity (I_{JMA}) Using the PEER–NGA Strong Motion Database.* Kenneth W. Campbell and Yousef Bozorgnia. February 2010.

PEER 2009/109 *Simulation and Performance-Based Earthquake Engineering Assessment of Self-Centering Post-Tensioned Concrete Bridge Systems.* Won K. Lee and Sarah L. Billington. December 2009.

PEER 2009/108 *PEER Lifelines Geotechnical Virtual Data Center.* J. Carl Stepp, Daniel J. Ponti, Loren L. Turner, Jennifer N. Swift, Sean Devlin, Yang Zhu, Jean Benoit, and John Bobbitt. September 2009.

PEER 2009/107 *Experimental and Computational Evaluation of Current and Innovative In-Span Hinge Details in Reinforced Concrete Box-Girder Bridges: Part 2: Post-Test Analysis and Design Recommendations.* Matias A. Hube and Khalid M. Mosalam. December 2009.

PEER 2009/106 *Shear Strength Models of Exterior Beam-Column Joints without Transverse Reinforcement.* Sangjoon Park and Khalid M. Mosalam. November 2009.

PEER 2009/105 *Reduced Uncertainty of Ground Motion Prediction Equations through Bayesian Variance Analysis.* Robb Eric S. Moss. November 2009.

PEER 2009/104 *Advanced Implementation of Hybrid Simulation.* Andreas H. Schellenberg, Stephen A. Mahin, Gregory L. Fenves. November 2009.

PEER 2009/103 *Performance Evaluation of Innovative Steel Braced Frames.* T. Y. Yang, Jack P. Moehle, and Božidar Stojadinovic. August 2009.

PEER 2009/102 *Reinvestigation of Liquefaction and Nonliquefaction Case Histories from the 1976 Tangshan Earthquake.* Robb Eric Moss, Robert E. Kayen, Liyuan Tong, Songyu Liu, Guojun Cai, and Jiaer Wu. August 2009.

PEER 2009/101 *Report of the First Joint Planning Meeting for the Second Phase of NEES/E-Defense Collaborative Research on Earthquake Engineering.* Stephen A. Mahin et al. July 2009.

PEER 2008/104 *Experimental and Analytical Study of the Seismic Performance of Retaining Structures.* Linda Al Atik and Nicholas Sitar. January 2009.

PEER 2008/103 *Experimental and Computational Evaluation of Current and Innovative In-Span Hinge Details in Reinforced Concrete Box-Girder Bridges. Part 1: Experimental Findings and Pre-Test Analysis.* Matias A. Hube and Khalid M. Mosalam. January 2009.

PEER 2008/102 *Modeling of Unreinforced Masonry Infill Walls Considering In-Plane and Out-of-Plane Interaction.* Stephen Kadysiewski and Khalid M. Mosalam. January 2009.

PEER 2008/101 *Seismic Performance Objectives for Tall Buildings.* William T. Holmes, Charles Kircher, William Petak, and Nabih Youssef. August 2008.

PEER 2007/101 *Generalized Hybrid Simulation Framework for Structural Systems Subjected to Seismic Loading.* Tarek Elkhoraibi and Khalid M. Mosalam. July 2007.

PEER 2007/100 *Seismic Evaluation of Reinforced Concrete Buildings Including Effects of Masonry Infill Walls.* Alidad Hashemi and Khalid M. Mosalam. July 2007.